PFC/RR-96-1

Decomposition of Chlorinated Ethylenes and Ethanes in an Electron Beam Generated Plasma Reactor

Steven A. Vitale

S.M. Thesis
Plasma Fusion Center
Massachusetts Institute of Technology
Cambridge, Massachusetts 02139

February, 1996

Decomposition of Chlorinated Ethylenes and Ethanes in an Electron Beam Generated Plasma Reactor
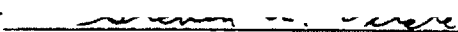
by

Steven A. Vitale

Submitted to the Department of Nuclear Engineering
in Partial Fulfillment of the Requirements for the
Degree of
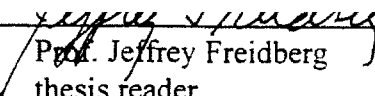
Master of Science
in Nuclear Engineering

at the

Massachusetts Institute of Technology
February 1996

Signature of Author_____
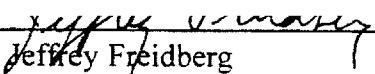
Steven A. Vitale

Certified by_____

Dr. Daniel R. Cohn, Ph.D.
thesis supervisor

Certified by_____

Prof. Jeffrey Freidberg
thesis reader

Certified by_____

Prof. Jeffrey Freidberg
Chairman, Department Committee on Graduate Students

Decomposition of Chlorinated Ethylenes and Ethanes in an Electron Beam Generated Plasma Reactor

by

Steven A. Vitale

Abstract

An electron beam generated plasma reactor (EBGPR) is used to determine the plasma chemistry kinetics, energetics and decomposition pathways of six chlorinated ethylenes and ethanes: 1,1,1-trichloroethane, 1,1-dichloroethane, ethyl chloride, trichloroethylene, 1,1-dichloroethylene, and vinyl chloride. A traditional chemical kinetic and chemical engineering analysis of the data from the EBGPR is performed, and the following hypothesis was verified:

The specific energy required for chlorinated VOC decomposition in the electron beam generated plasma reactor is determined by the electron attachment coefficient of the VOC and the susceptibility of the molecule to radical attack.

Of the chlorinated ethanes, 1,1,1-trichloroethane is shown to decompose with the least energy, followed by 1,1-dichloroethane and ethyl chloride. Of the chlorinated ethylenes, trichloroethylene decomposes using the least energy, followed by dichloroethylene and vinyl chloride. This pattern follows the known electron attachment coefficients of these compounds; molecules with higher dissociative electron attachment coefficients are shown quantitatively to decompose more readily than those with lower attachment rates.

Comparing compounds with the same number of chlorines, e.g., 1,1,1-trichloroethane and trichloroethylene, it is seen that the chlorinated ethylene decomposes more readily than the chlorinated ethane. This is shown to be true for all three ethane/ethylene pairs. Chlorinated ethylenes are more susceptible to radical attack than ethanes, thus the decomposition of the ethylenes is enhanced by radical reactions, and less energy is required for decomposition.

Several theoretical treatments are provided to aid in analyzing the data. A radiation chemistry approach was used to derive an expression to relate the VOC concentration to the electron beam dose through the G-value of the molecule, or equivalently, the beta value. A differential kinetic approach is used to determine the order with respect to time n_t and the order with respect to concentration, n_c, for each of the six chlorinated VOCs. The reaction rate constants for the decomposition reaction are also determined. An integral kinetic model, the INHIBIT model, is derived analytically from a

simplified set of chemical reactions to account for some of the apparent inhibition of the reaction by products.

A traditional chemical engineering analysis is applied to the EBGPR by modeling it as an ideal plug flow reactor. This allows the derivation a modified performance equation relating the VOC outlet concentration from the reactor to the reactor power required, through the reaction rate expression

Nearly 4000 data points were collected with the EBGPR over the 15 month period of this study. These data points are used in conjunction with the differential and integral kinetic models described above to determine several quantities of interest for each of the six VOCs in this study. The rate constants, k, and unimolecular reaction orders, n_t, were determined. Best fits to the INHIBIT model gave values of two fitting parameters, K and β', to allow a calculated analytic expression of the VOC concentration as a function of electron beam dose. The parameter K gives an indication of the importance of inhibition in the reaction mechanism: if K is near zero, then inhibition is unimportant, and the reaction follows first order exponential decay behavior. If K is non-zero, than the reaction appears to have inhibited kinetics, and the reaction follows a non-linear decay pattern.

Measurements are given of all of the identifiable reaction product abundances. This information was used in conjunction with the kinetic analysis to determine possible reaction pathways for decomposition in the reactor. Reaction pathways for all six chlorinated ethylenes and ethanes were proposed. The most important major reaction products in every case were carbon dioxide, carbon monoxide, and hydrogen chloride. Many other minor decomposition products were also observed.

Rosocha β-values and specific energies, ε, were determined for each VOC as a function of concentration. Unlike the efforts of previous research groups, in this study, β and ε are allowed to be functions of concentration. For most compounds, the two values do in fact have a marked dependence on inlet concentration. For cases where previous literature values for β are available at a known concentration, the results agree very well with those from the EBGPR. This result is important to both the EBGPR study and the previous works, because it provides verification of the results of both studies. It also serves to show that the dosimetry calculation performed on the EBGPR have given reasonable values, since the β-values obtained are directly related to the knowledge of the electron beam dose.

Thesis Supervisor: Dr. Daniel R. Cohn
                             Head of the Plasma Technology and Systems Division,
                             MIT Plasma Fusion Center

Table of Contents

List of Figures

List of Tables

1. Introduction

1.1. Background

The electron beam generated plasma reactor (EBGPR) project began at MIT in 1990 to evaluate the utility of using non-equilibrium electron beam generated plasmas for the decomposition of chlorinated VOCs present at government hazardous waste sties. At these hazardous waste sites. tons of chlorinated solvents were to be vapor extracted from the soil. and the resultant VOC-laden air stream would be passed through the EBGPR for treatment. This process was put into practice in January, 1995, when a field scale demonstration unit of the EBGPR was used at Hanford, Washington to decompose carbon tetrachloride (CCl_4) in a soil vapor extracted air stream.

Extensive laboratory study of the decomposition of CCl_4 preceded the field test. A comprehensive review of the design of the laboratory version of the EBGPR and of carbon tetrachloride decomposition can be found in the thesis of Mathias Koch[1] and in several papers[2-4]. Any references to Koch in this work will be to the thesis. unless otherwise stated. After the successful completion of the CCl_4 analysis. it was determined that the EBGPR could be used as a very versatile instrument for the study of the plasma chemistry kinetics of decomposition of many types of compounds. Other research groups have studied the energetics of decomposition of compounds such as trichloroethane and trichloroethylene. but these studies were conducted over limited concentration ranges, and they have concentrated on the determination of the specific energy, ε. required for decomposition of the chlorinated compounds. The specific energy was assumed to be independent of inlet concentration and other parameters, and little work has been done to attempt to explain the results of chlorinated ethane or ethylene decomposition quantitatively. The present work will explore quantitatively and qualitatively the plasma chemistry and energetics of chlorinated ethane and ethylene decomposition in the EBGPR.

1.2 The Electron Beam Generated Plasma Reactor

The energy efficient nature of the EBGPR as compared to thermal plasma or thermal oxidation methods has been discussed elsewhere.[2,3,5] A very brief summary of this argument is that the energy from the electron beam is directed preferentially towards the decomposition of the chlorinated organics in an air stream, due to their high dissociative electron attachment cross-section. This results in little energy being transferred to the carrier gas molecules and ions. and thus not much energy is wasted in vibrational and rotational mode heating of the carrier gas.

A previously unexamined feature of the EBGPR is that its ease of operation makes it well suited to the examination of the plasma chemistry and radiation chemistry

of many different compounds. In this work, the term plasma chemistry will refer to the kinetics and reaction pathways of the reactions in the plasma, and the term radiation chemistry or energetics will refer to the energy requirements for decomposition of the molecules under irradiation by electrons in the EBGPR specifically. The EBGPR has several advantages over other types of plasma processes for these studies. which will be discussed in detail below:

- Atmospheric pressure operation
- Easily controlled radiation dose
- Widely variable flow rate
- Steady state operation
- Plasma can be created in nearly any type of carrier gas
- Additives or contaminants will not quench or inhibit plasma formation
- Reaction products such as particulates will not damage system

Most industrially relevant processes would be run optimally at atmospheric pressure to allow maximum flowrates and to reduce capital costs. Therefore the study of plasma and radiation chemistry at atmospheric pressure is essential for accurate modeling of the process for scale up to industrial size reactors. Other types of plasmas. e.g. corona discharges and microwave cavity experiments, can operate only with relatively small plasma volumes at atmospheric pressure. This results in a heterogeneous reactor volume on a macroscopic scale. and thus makes it difficult to perform accurate analyses of the plasma chemistry. Electron beam generated plasmas do not have this difficulty, however, since energetic electrons have a relatively large penetration distance in air. In the laboratory reactor. the penetration depth of the electrons in air is approximately 5 cm; the field unit has a penetration depth of approximately twice that.

The electron beam dose to the plasma in radiation and plasma chemistry is the analog to residence time in the reactor for traditional chemical kinetics. In order to perform steady state kinetic studies. traditionally one must be able to vary the residence time in the reactor over a wide range. This is usually done by varying the flowrate of the reactants through a traditional chemical reactor. In plasma chemistry studies. the effective residence time is the energy dose, which may be varied through either the reactant flowrate or the power coupled to the plasma. However, in corona discharges and microwave plasmas. these parameters are not independently variable. Breakdown in a microwave plasma will only occur if the power coupled to the plasma exceeds some threshold value. Thus studies at low energy densities cannot be easily conducted. In corona reactors. the power discharged to the plasma is often fixed by capacitors and is not easily varied. The EBGPR. does not have any of these drawbacks, since a plasma may be produced at any flowrate. and the power coupled to the plasma is easily controlled from zero up to the maximum power of the reactor through control of the electron beam current.

Kinetic studies of gas phase reactions are typically easier to perform in a steady state reactor rather than in batch operations, if the nature of the chemical species allow it. This is because it is easier to change the parameters of a flowing system. i.e.. it is simpler

to change a flowrate and sample the exit stream in a steady state process than to clean, recharge, wait. and sample a batch reactor. Steady state operation also helps to insure the homogeneity and reproducibility of the process.

Electron beam generated plasmas can be created in any type of carrier gas. The energetic electrons from the beam possess enough energy to ionize any species, and charge transfer processes will result in the transfer of this energy to the chlorinated molecules in the stream. This is discussed more thoroughly in Section 4.2. Although all of the experiments in this work were conducted using air as the carrier gas, further reaction pathway and kinetic studies would benefit from studies of the VOC reactions in pure nitrogen. pure oxygen, pure hydrogen, and other gases. Energy requirements for breakdown in microwave and corona plasmas are dependent upon the nature of the carrier gas. however plasmas of any desired energy density can be created in the EBGPR independently of the carrier gas used. Similarly, other reactants such as hydrogen peroxide or water can be added to catalyze or inhibit the reactions without any adverse affects on the plasma. Reaction byproducts such as particulates or corrosive radicals will not cause quenching of the plasma. or significantly change its characteristics.

Thus the EBGPR has great value as a tool with which to study plasma chemistry effects of many compounds under a wide variety of experimental conditions. Specifically, this work will examine the reaction pathways, kinetics, and energetics of chlorinated ethane and ethylene decomposition.

This study of the plasma chemistry of chlorinated ethylenes and ethanes will aid in the understanding of halogenated VOC decomposition in the EBGPR. This will allow the design of more efficient reactors for both commercial and remediation use. Furthermore. this study will allow a better understanding of the limitations of the EBGPR in processing of certain types of compounds. as well as the advantages that the EBGPR has over conventional and other emerging technologies. The work of Koch has established the viability of the EBGPR for carbon tetrachloride decomposition, and the Hanford. Washington field test showed that the reactor could perform reliably under "real-world" conditions. This study will build upon the previous work, by showing that the energy efficient reactor is capable of decomposing a variety of chlorinated compounds. and as such it can be a valuable tool as a commercial unit operation in the chemical process industry and at many remediation sites.

1.3 Review of Plasma Processing of Chlorinated Compounds

Plasma processing of chemicals is an expanding field, and many research groups around the world are currently investigating innovative approaches. A brief listing of some of these research efforts is given it table 1.1 to put the current work into perspective. Note that the listing is limited only to publications which include chlorinated methanes. ethanes. or ethylenes: and even in that limited scope it is not comprehensive. This list does not include the extensive work performed on the plasma processing of NO_x, SO_x, methane. acetylene. ammonia, fluorinated compounds, or plasma chemical synthesis methods.

Chemicals of Interest	Type of Plasma	Reference
VC	Electron Beam	5
TCE	Microwave	6
	Corona Discharge	7
	Dielectric Barrier	8
	Dielectric Barrier	9
	Dielectric Barrier	10
	Dielectric Barrier	11
	Dielectric Barrier	12
CCl_4, TCE	Electron Beam	13
TCE	Electron Beam	14
CHF_2Cl, $C_2Cl_3F_3$	Dielectric Barrier	15
	Corona Discharge	16
	Corona Discharge	17
	Corona Discharge and Ferroelectric Packed Bed	18
	Corona Discharge	19
VC	Electron Beam	20
VC	Pulse Ionization Chamber	21
TCE	Dielectric Barrier and Pulsed Corona	22
TCE	Electron Beam	23
TCE	Electron Beam	24
	Pulsed Corona and Ferroelectric Packed Bed	25
	Dielectric Barrier	26
	Dielectric Barrier	27
	Dielectric Barrier	28
	Dielectric Barrier	29
	Dielectric Barrier	30
	Dielectric Barrier	31
	Dielectric Barrier	32
	Surface Discharge	33
	Surface Discharge	34
	Gliding Arc	35
	Gliding Arc	36
	Microwave	37
CCl_4	Electron Beam and Pulsed Corona	38
CH_2Cl_2	Pulsed Corona	39
CCl_4, TCE, CH_2Cl_2	Electron Beam and Pulsed Corona	40
$CHFCl_2$, CHF_2Cl, TCA, TCE, C_2Cl_4	Microwave	41
TCE, TCA	Microwave	42

CHCl$_3$, TCE. C$_6$H$_5$Cl	Microwave	43
TCE, C$_2$Cl$_4$	Dielectric Barrier	44
CCl$_4$	Pulsed Microwave	45
CCl$_2$F$_2$	DC Arc	46
CHCl$_3$, CCl$_4$, CH$_3$Cl	Dielectric Barrier	47
CH$_3$Cl,CH$_2$Cl, CHCl$_3$. CCl$_4$	r.f. Discharge	48
CCl$_2$F$_2$, CClF$_3$	Dielectric Barrier	49
C$_6$Cl$_6$	Dielectric Barrier	50
C$_6$H$_5$Cl	Glow Discharge	51
C$_6$Cl$_6$	Dielectric Barrier	52
C$_6$Cl$_6$	Dielectric Barrier	53
MeSiCl$_3$	Dielectric Barrier	54
MeSiCl$_3$	Dielectric Barrier	55
C$_6$H$_5$Cl	Glow Discharge	56
C$_6$H$_5$Cl	Corona Discharge	57
Me$_2$Cl$_2$Si	Dielectric Barrier	58
C$_6$H$_5$Cl	Glow Discharge	59
CCl$_4$	Dielectric Barrier	60
SiCl$_4$	Glow Discharge	61
CCl$_4$	r.f. Glow Discharge	62
chlorobenzenes	r.f. Glow Discharge	63
chlorobenzenes	r.f. Glow Discharge	64
VC	Dielectric Barrier	65
chlorinated hydrocarbons	Plasma Jet	66
CCl$_4$	r.f. Discharge	67
	r.f. Discharge	68
C$_2$Cl$_4$, C$_2$Cl$_4$O$_2$	r.f. Discharge	69
TCA, TCE, CCl$_4$	Dielectric Barrier	70
1,2-DCA, TCE	Plasmatron	71
TCE	Corona Discharge	72
1,2-DCA	Capacitively Coupled r.f.	73

Table 1.1: TCA=1.1.1-trichloroethane, DCA=1,1-dichloroethane. EC=ethyl chloride, TCE=trichloroethylene. DCE=1,1-dichloroethylene, and VC=vinyl chloride. Available literature references on chlorinated VOC processing in plasma reactors. Where a chemical compound is not given in the table, the reference was not available to the author at the time of publication.

1.4 Objectives

The objective of this study will be to perform an analysis of the decomposition pathways, the kinetics, and the energetics of the reactions of six chlorinated compounds: 1,1,1-trichloroethane (TCA), 1,1-dichloroethane (DCA), ethyl chloride (EC), trichloroethylene (TCE), 1,1-dichloroethylene (DCE), and vinyl chloride (VC). The analysis of these compounds will be used in conjunction with the known physical and chemical properties of these compounds to attempt to formulate a basis for understanding the trends observed in the energy requirements for decomposition in the reactor. It is believed that a relationship exists between the energy required for the decomposition of a particular molecule and the chemical structure that molecule, and that this relationship can be characterized by a study of specific series of chemicals. This idea is put in the form of a hypothesis in the following subsection.

1.4.1 Hypothesis of Chlorinated Compound Decomposition in the EBGPR

One major objective of this study will be to relate the specific energy required for decomposition of the molecules to the plasma chemistry of those molecules in the reactor. By analyzing the reaction kinetics, this study will seek to verify or disprove the following hypothesis:

The specific energy required for chlorinated VOC decomposition in the electron beam generated plasma reactor is determined by the electron attachment coefficient of the VOC and the susceptibility of the molecule to radical attack.

Knowledge of these two factors for a particular compound will allow reasonable predictions of the specific energy required for the decomposition of a molecule in the EBGPR.

The electron attachment coefficient of a molecule is a measure of the affinity of the molecule for the capture of a free electron. This, in turn, is primarily determined by the individual atoms which compose the molecule; bond order and group functionality is only of secondary importance. For halogenated molecules the electron attachment coefficient is determined primarily by the number of halogen atoms on the molecule, since halogen atoms have a very high electron affinity compared to carbon, oxygen, or nitrogen. In the case of chlorinated molecules, which are the focus of this study, molecules which possess more chlorines per carbon will have a higher electron attachment coefficient. Assuming that dissociative electron attachment is the primary decomposition mechanism in the reactor, the higher the electron attachment coefficient, the more easily a molecule is decomposed in the reactor. Thus a molecule such as trichloroethane (which has 3 chlorines) will require less energy for decomposition than dichloroethane (which 2 chlorines). The quantitative verification that the specific energy

15

required for decomposition is related directly to the electron affinity of the molecule is the first requirement to verify the above stated hypothesis.

Trichloroethylene and 1.1.1-trichloroethane both have three chlorine atoms per molecule, and thus using the above argument both molecules should decompose with similar specific energy requirements. However, it will been shown in Chapter 5 that trichloroethane requires 15 to 75 times more energy for decomposition than trichloroethylene. Thus a second factor is also needed to account for the energetics of VOC decomposition. This factor is the susceptibility of a molecule to radical attack, as explained below.

The decomposition pathways of a molecule and its susceptibility to radical attack are determined by the chemical structure of the molecule. For example. simple chlorinated methanes such as carbon tetrachloride have only a limited number of possible decomposition pathways available. Carbon tetrachloride is not very susceptible to oxygen radical attack. and chlorine radical attack will at most result in chlorine-chlorine substitution. Thus CCl_4 is difficult to decompose compared to chloroform ($CHCl_3$) which is susceptible to both kinds of radical attack, as well as hydrogen atom abstraction. Chlorinated ethanes are more complicated molecules, and thus have more possible decomposition pathways. Chlorinated ethylenes possess a carbon-carbon double bond and have decomposition pathways available to them which are forbidden to chlorinated ethanes or methanes. In order to understand how the pathways of VOC decomposition affects the energy required for decomposition, one must first know what those pathways are. The elucidation of decomposition mechanisms for chlorinated ethanes and ethylenes is within the scope of this work. and detailed pathways are proposed in Chapter 4. Note that full reaction mechanism studies are complicated, and require many experiments under different reaction conditions to determine specific mechanisms. This is beyond the scope of the present work. and only reasonable reaction pathways are proposed in Chapter 4 to account for the formation of product species and the observed reaction kinetics. Reaction pathways have been proposed previously in which trichloroethylene decomposes by a chlorine radical addition chain reaction mechanism which is not available to trichloroethane. This chain reaction mechanism results in the decomposition of a large number of molecules from a single electron attachment event. and may explain the result that trichloroethylene decomposes much more easily than trichloroethane. Similar results are expected for other chlorinated ethylenes and ethanes which have not previously been studied. The quantitative verification that the carbon-carbon double bond and other chemical properties of these molecules influence the susceptibility of the molecule to radical attack. and by consequence, the specific energy required for decomposition. is the second requirement to verify the above stated hypothesis.

1.4.2 Method for Verification of Hypothesis

By studying the decomposition of six molecules in the reactor. it is believed that a quantitative analysis of the above hypothesis can be performed. Three chlorinated ethanes will be studied: 1,1,1-trichloroethane (TCA), 1,1-dichloroethane (DCA). and monochloroethane (commonly called ethyl chloride, EC). The chemical structure of these

16

molecules is shown in figure 1.1. Although not obvious from the brief summary above, the decomposition mechanisms of these molecules is believed to be quite similar under the conditions in this study. By studying this series of chlorinated ethanes, the second factor influencing specific energy requirements for decomposition, i.e., the susceptibility to radical attack, can be held "constant" while the first variable, i.e., the number of chlorines on the molecule, is varied. In addition, three chlorinated ethylenes will also be studied: trichloroethylene (TCE), dichloroethylene (DCE), and monochloroethylene (commonly called vinyl chloride, VC). The chemical structure of these molecules is also shown in figure 1.1. The same analysis can be performed on this series of chlorinated ethylenes: the second variable can be held "constant" while the first variable is varied. Looking at these two series of molecules will allow the study of the specific energy required for decomposition as a function of electron affinity.

The decomposition mechanisms of chlorinated ethylenes are very different from chlorinated ethanes, as described briefly in the TCA/TCE example above. By comparing the specific energy for decomposition of TCA and TCE, the electron affinity of the molecules can be held "constant" (since they each possess three chlorines) and the effect of the different reaction mechanisms can be studied. The same is true for DCA and DCE, as well as for EC and VC. Through the study of the decomposition of these three pairs, a quantitative analysis of the effect of the susceptibility to radical attack on the energetics of VOC decomposition in the reactor can be performed.
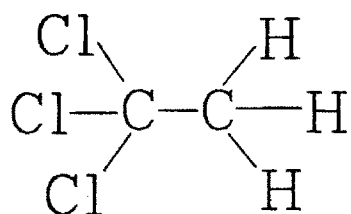
1,1,1 −Trichloroethane (TCA)
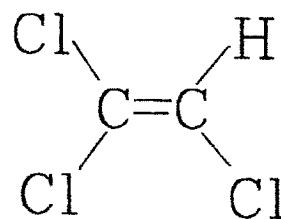
Trichloroethylene (TCE)
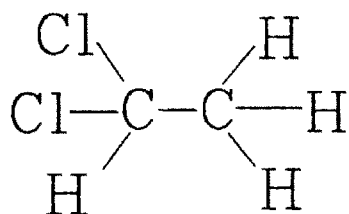
1,1−Dichloroethane (DCA)
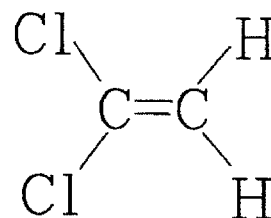
1,1−Dichloroethylene (DCE)
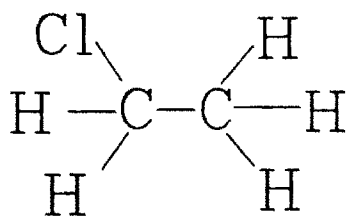
Ethyl Chloride (EC)
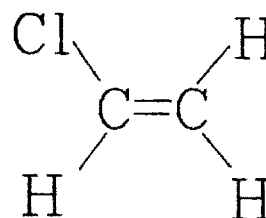
Vinyl Chloride (VC)

Figure 1.1: Chemical structure of chlorinated ethylenes and ethanes

1.5 Overview

1.5.1 Organization of the Present Work

This thesis is organized into seven sections: an *Introduction*, a chapter on *Reactor Chemistry*, a chapter on *Experimental Procedures*, a chapter giving the *Results and Discussion*, and chapters on the *Discussion of the Hypothesis*, a *Conclusion*, and *Appendices*.

The *Introduction* serves to: explain the background of the project, provide a listing of available literature references, state clearly the objectives of the project, and emphasize the contribution of this work compared to previous studies.

The *Reactor Chemistry* chapter summarizes some of the important aspects of the field required to understand the results and discussion. Derivation of the electron beam dose, G-value, and β-values are given. Chemical kinetics are described by both an inhibitor model and a differential method, which allow complementary treatments of the data.

The *Experimental Procedures* chapter briefly describes the EBGPR, the inlet gas system, and the gas analysis system. The redesign of the reaction chamber is also described, as well as the results of new dosimetry calculations in this reaction chamber.

The *Results and Discussion* chapter is divided into eight sections: a brief overview, one section for each of the chlorinated ethylenes and ethanes compound studied, plus a final section for the results from miscellaneous other compounds. This section will extract the β-values and kinetic constants from the data. Reaction pathways for decomposition will also be proposed.

The *Discussion of the Hypothesis* chapter will summarize the data from the previous chapter into a unified discussion relating the specific energy requirements for decomposition to the electron attachment coefficients and decomposition mechanisms of the molecules.

The *Conclusion* will summarize all of the results and suggest future areas for research. The *Appendices* will give the derivations of some of the equations.

1.5.2 Contribution of the Present Work

As discussed in Section 1.3, a large amount of literature information is available on the decomposition of VOC's in plasma reactors. The present work contributes to this body of knowledge by presenting a detailed study of chlorinated ethane and ethylene

decomposition in an electron beam generated plasma reactor. The following aspects of this project are. to the author's knowledge, unexplored in the available literature:

1. While detailed analysis of TCA, TCE, and VC decomposition in plasma reactors has been performed previously, such analyses for DCA, DCE. and EC are not available. In this work. reaction pathways and energetic analysis of all of these compounds are proposed.

2. Traditional kinetic analyses are performed on the data. to extract reaction rate constants. reaction orders, and to provide insight into inhibition of the reactions by decomposition products.

3. Previous studies have assumed that the specific energy required for decomposition is independent of inlet concentration. The present work determines this specific energy over an inlet concentration range from 100 to 3000 ppm, and it is seen to be dependent upon the inlet concentration over this range. Note that in this work all concentrations expressed as ppm are on a mol/mol basis.

4. A direct correlation between the electron attachment coefficient of the molecule and the energy required for decomposition has not been presented previously.

5. The susceptibility of a molecule to radical attack has not been proposed explicitly as a predictive indicator of the relative difficulty of the decomposition of the molecule.

6. A traditional chemical engineering analysis of the EBGPR is performed. The reactor is modeled as an ideal plug-flow reactor, and the reaction rate equations from the kinetic analysis are coupled with the plug flow reactor performance equations. The equations are modified to be applicable to the EBGPR, and an industrially viable scaling law results to determine the reactor power needed as a function of desired flowrate, outlet concentration. and the chemical kinetics of a particular VOC.

7. The EBGPR will be shown to be an energy efficient method of decomposing many different compounds. and thus to be a versatile device with many applications in the chemical process industries and in remediation efforts. The reactor achieved 99% decomposition of all of the compounds in this study, with the primary decomposition products in most cases being carbon dioxide. carbon monoxide, and hydrogen chloride.

2. Chemistry in the Reactor

2.1 Radiation Chemistry

As mentioned in the Introduction, in this work radiation chemistry or energetics will be used to describe processes relating directly to the specific energy required for decomposition of the compounds. This distinction from plasma chemistry and kinetics is arbitrary and only applies to this work. Nevertheless, it seems useful to distinguish between "electron radiation interactions," which are specific to the EBGPR, and "plasma chemistry kinetics," which are radical and ion reactions and should apply generally to any plasma reactor operating under similar conditions.

The theory for determining the energy required for the decomposition of CCl_4 in the EBGPR has been treated by Koch (1,4). A modified summary of this treatment is presented here to derive three quantities of interest: the *G-value* of a molecule, the β *value*, and the *specific energy required for decomposition*, ε.

If the absorption of energy by some molecule k results in the decomposition of some molecule j, then the *G-value* of species j may be used as a measure of the energy required for the decomposition of a molecule of species j. The G-value is defined as:

$$G_{jk} = \frac{dN_j}{dQ_k} \qquad (2.1)$$

where dN_j molecules of species j are removed due to energy dQ_k absorbed by species k. This completely general definition can be applied to the situation of interest in the present work, where the energy required for the decomposition of species j is absorbed by species j itself. Thus,

$$G_{jj} = \frac{dN_j}{dQ_j} \qquad (2.2)$$

In the derivation by Koch, it was assumed that G_{jj} was constant and independent of the concentration of species j. In this work, that assumption is relaxed, and it is shown experimentally that G_{jj} is a function of concentration. G_{jj} is still assumed to be independent of temperature, dose rate, and any parameter other than concentration of species j.

The energy absorbed by the molecules in this work comes from the electron beam irradiation of the gas stream in the reactor. This energy absorption results in electronic excitation, ionization, electron attachment, and molecular fragmentation. Koch proposed that this energy was partitioned among various species in the plasma according to the number of electrons each species possesses. Assume that there are N_i molecules of species i, each of which has Z_i electrons, present in a gas stream in which has a total of N

molecules, with an average of Z electrons each. If the energy absorbed by dN of these molecules is dQ, and if the energy is partitioned according to the total number of electrons of species i.

$$\frac{dQ_j}{dQ} = \frac{Z_j}{Z} \frac{N_j}{N}$$

(2.3)

and therefore.

$$dN_j = G_{ij} \frac{Z_j}{Z} \frac{N_j}{N} dQ$$

(2.4)

However. this assumption that energy deposited in the plasma is partitioned according to the number of electrons on each molecule is not in agreement with the mechanisms of decomposition proposed. As mentioned by Koch, and will be explained in more detail in Section 4.2. the energy is preferentially directed toward halogenated organic compounds due to their high electron attachment cross section and their low ionization potential. These physical properties are not necessarily related to the number of electrons on the molecule. A more appropriate partitioning parameter might be the ratio of the electron attachment cross section of species i to the average electron attachment cross section of the gas. However, this partitioning parameter is nearly as arbitrary as the ratio of molecular electrons. and undoubtedly fails to capture some of the important physics of the very complicated mechanism of decomposition. For now, the ratio Z_i/Z will be replaced by a factor K. a parameter giving the ratio of the rate constant for the decomposition reaction to that of a competitive inhibition reaction. The origin of this factor will be derived in Section 2.2.3; the reader is asked to accept it for now.

The electron beam dose, D, is defined as the energy Q deposited in a mass m of the gas.

$$D = \frac{Q}{m} = \frac{1}{M_c} \frac{Q}{n} = \frac{N_A}{M_c} \frac{Q}{N}$$

(2.5)

where M_c is the average molecular weight of the gas, n is the number of moles given by mass m. and N_A is Avagadro's number. If it is assumed that the species to be decomposed is in low concentration in the carrier gas, then $N \approx$ constant and $M_c \approx$ constant, and equation (2.5) can be differentiated,

$$dD = \frac{N_A}{M_c} \frac{1}{N} dQ$$

(2.6)

Substituting the equation for the G-value,

$$dN_j = \frac{M_C}{N_A} K \cdot N_j G_{jj} dD \qquad (2.7)$$

Now defining the mole fraction of species j as x_j,

$$x_j = \frac{N_j}{N} \qquad (2.8)$$

equation (2.7) becomes.

$$dx_j = \frac{M_C}{N_A} KG_{jj} dD \qquad (2.9)$$

This equation gives the differential amount of species j decomposed by applying a dose dD to the gas. Integrating this equation will give the concentration of species j as a function of electron beam dose. which is one of the primary goals of this study. Unfortunately. G_{jj} is assumed in this study to be a function of concentration, which is currently unknown. Also. nothing has been said of the factor K; this may also be a function of concentration. Thus this equation cannot be integrated yet to give a theoretical curve for reactant concentration versus electron beam dose. In Chapter 4, these parameters will be used as fitting parameters to match the experimental data.

It will be useful to look at two simplified situations which will allow the analytic integration of equation (2.9). First, we assume that $K \approx$ constant. and that the G-value can be expressed as a monomial function of x_j, i.e.,

$$G = G_0 \left(x_j \right)^\alpha \qquad (2.10)$$

Where G_0 and α are constants. Note that the subscripts have been dropped from G. From this point on, G will be assumed to be G_{jj}. Equation (2.9) can be integrated using the initial condition that $x_j = x_{jo}$ at D=0,

$$x_j = \left((1 - \alpha) \frac{M_C}{N_A} G_0 K \cdot D + x_{jo}^{1-\alpha} \right)^{1/1-\alpha} \qquad (2.11)$$

This gives the desired theoretical relation of concentration of species j to electron beam dose.

The second simplified situation is to assume that $K \approx$ constant. and that the G-value can be expressed as a monomial function of the inlet concentration of x_j, i.e.,

$$G = G_o \left(x_{jo} \right)^{\alpha} \qquad (2.12)$$

With this assumption. G is constant with respect to the integration. and equation (2.9) can be integrated using the same initial condition,

$$x_j = x_{jo} \exp\left(-\frac{M_c}{N_A} K \cdot G_o \left(x_o \right)^{\alpha} D \right) \qquad (2.13)$$

Equations (2.11) and (2.13) are models which can be fit to experimental data. This is performed in Chapter 4. to give best fit values of the parameters for all of the compounds studied. Note that in these equations. the parameters K and G_o appear together. Thus, unless there is some independent method of finding one or the other. only their product can be determined from fitting data to equation (2.11) or (2.13).

Equation (2.13) shows a pure exponential dependence of the concentration on electron beam dose. This is the same functional form which would be derived using a simple. uninhibited. first-order kinetic model. First-order kinetics for decomposition were assumed by Rosocha[27] and led to the definition of the β-*value*. β is defined by the equation:

$$x_j = x_{jo} \exp\left(-D/\beta \right) \qquad (2.14)$$

Rosocha assumed that β was a constant, independent of inlet concentration. To allow comparison with literature data. β values were determined in this study for the six compounds of interest. In this study, however, β was not assumed to be constant. By comparing equations (2.13) and (2.14),

$$\beta = \frac{1}{\dfrac{M_c}{N_A} K \cdot G_o \left(x_o \right)^{\alpha}} \qquad (2.15)$$

In order for β to have any meaning, the concentration, x, must fall off purely exponentially with electron beam dose. Equation (2.11), which is more general than equation (2.13). does not predict this exponential behavior. As will be shown in Section 2.2.3. an inhibited. kinetic model also will not predict exponential decay. However, at low fractional decomposition. i.e.. $x_j/x_{jo} \approx 1$, these models are approximately exponential. The experimental data in fact does show exponential decay behavior at relatively low fractional decomposition. and thus in this regime an estimation of β will be performed. For higher fractional decomposition. the more complicated models must be used.

The *fractional decomposition* of species j, η_j, can be defined as

$$\eta_j = \frac{N_{jo} - Nj}{N_{jo}} = 1 - \frac{x_j}{x_{jo}} \qquad (2.16)$$

This quantity was referred to as the destruction and removal efficiency by Koch, however the term fractional decomposition will be used here since the term "efficiency" could be misleading. Using this definition. the *specific energy* or *energy expense* per molecule decomposed. ε, can be related to the electron beam dose,

$$\varepsilon = \frac{Q}{N_{jo} - N_j} = \frac{1}{\eta_j} \frac{Q}{x_{jo} N} = \frac{1}{\eta_j x_{jo}} \frac{M_c}{N_A} D \qquad (2.17)$$

If equations (2.11) or (2.13) are coupled with equation (2.17), a predictive model results for the specific energy required for decomposition at any desired fractional decomposition. This is given in the summary to this chapter. Section 2.4.

2.2 Chemical Kinetics

The field of plasma chemistry is quite extensive, and there are several excellent texts and literature reviews of the subject. In general the reaction mechanisms in high temperature gas phase reactions are extremely complicated, and only representative reaction pathways can be proposed to account for the formation of observed products. Plasma chemistry is even more difficult to analyze, since it contains all of the complex mechanisms of high temperature chemistry, plus additional complexities resulting from ionization, recombination. and electron energy distribution effects. Koch attempted a simple kinetic model of the plasma chemistry of CCl_4 decomposition using the nonlinear partial differential equations which govern electron attachment and oxygen radical formation. This simple model is still very ambitious, and in general very difficult to solve.

A more common approach is to use an integrated chemical kinetics package such as CHEMKIN II to model the reaction kinetics. These packages require the input of all the elementary reactions which are thought to contribute to the reaction mechanism, and the rate constants of these reactions. The elementary reactions which can be used in the integrated packages are limited only by the user's imagination. Rate constants for these elementary reactions are either found in the literature, or they are estimated by various methods such as transition state theory. Chang[79] used such a model with 385 reactions to study TCE decomposition. Evans[26] expanded upon Chang's work by coupling this high temperature oxidation model to a standard Boltzmann equation solver routine to calculate the electron energy distribution function. In this way, the electron energy distribution function was applied to the calculation of rate constants for electron impact dissociation mechanisms. These models generally agreed quite well with the experimental data.

Kinetic modeling with CHEMKIN II or some other kinetics package was not performed in this study due to a lack of time. Instead. simple reaction pathways are

proposed in Chapter 4 to account for observed products, and a kinetic analysis of the simple reaction:

$$e\text{-} + VOC \rightarrow products \tag{2.18}$$

is presented in this chapter.

2.2.1. Idealized Chemical Reactors

In order to perform an analysis of the experimental data, one must understand how to interpret the data in terms of the type of chemical reactor used. In general. there are three types of idealized chemical reactors used for kinetic studies.

1. Batch Reactors
2. Plug Flow Reactors (PFR)
3. Continuously Stirred Tank Reactors (CSTR)

and the analysis of the data must be performed in the context of the assumptions which govern each type of reactor. The three types of reactor are illustrated in figure 2.1.

In chemical engineering practice. one generally expresses the extent of a chemical reaction in terms of the conversion. X, defined for a particular reactant k as,

$$X_k = moles\ reacted\ /\ moles\ fed\ = \frac{N_k - N_{ko}}{N_{ko}} \tag{2.19}$$

Note that the extent of reaction. X_k, is the same as the fractional decomposition. η_k. The extent of reaction is used here simply to confirm to standard notation for the derivation of the performance equations. and should not be confused with the mole fraction of species k. x_k. Equation (2.19) can be solved for N_k and differentiated,

$$dN_k = - N_{ko}\ dx_k \tag{2.20}$$

For gas phase reactions. it is often necessary to consider the volume change which takes place as the reaction proceeds. Assuming ideal gas behavior, the volume change is linearly proportional to the conversion.

$$V = V_0\ (\ 1 + \varepsilon_A\ X_A) \tag{2.21}$$

where,

$$\varepsilon_A = \frac{N_f - N_O}{N_O} = \frac{F_f - F_O}{F_O}$$ (2.22)

Ca = Ca(t)

BATCH REACTOR

z   z+dz

IN   →   Fo (1−X)   Fo (1−X−dX)   OUT   PLUG FLOW REACTOR

Fo   dV F_f

IN

C_o, F_o

CSTR

OUT

C_f, F_f

C=C_f
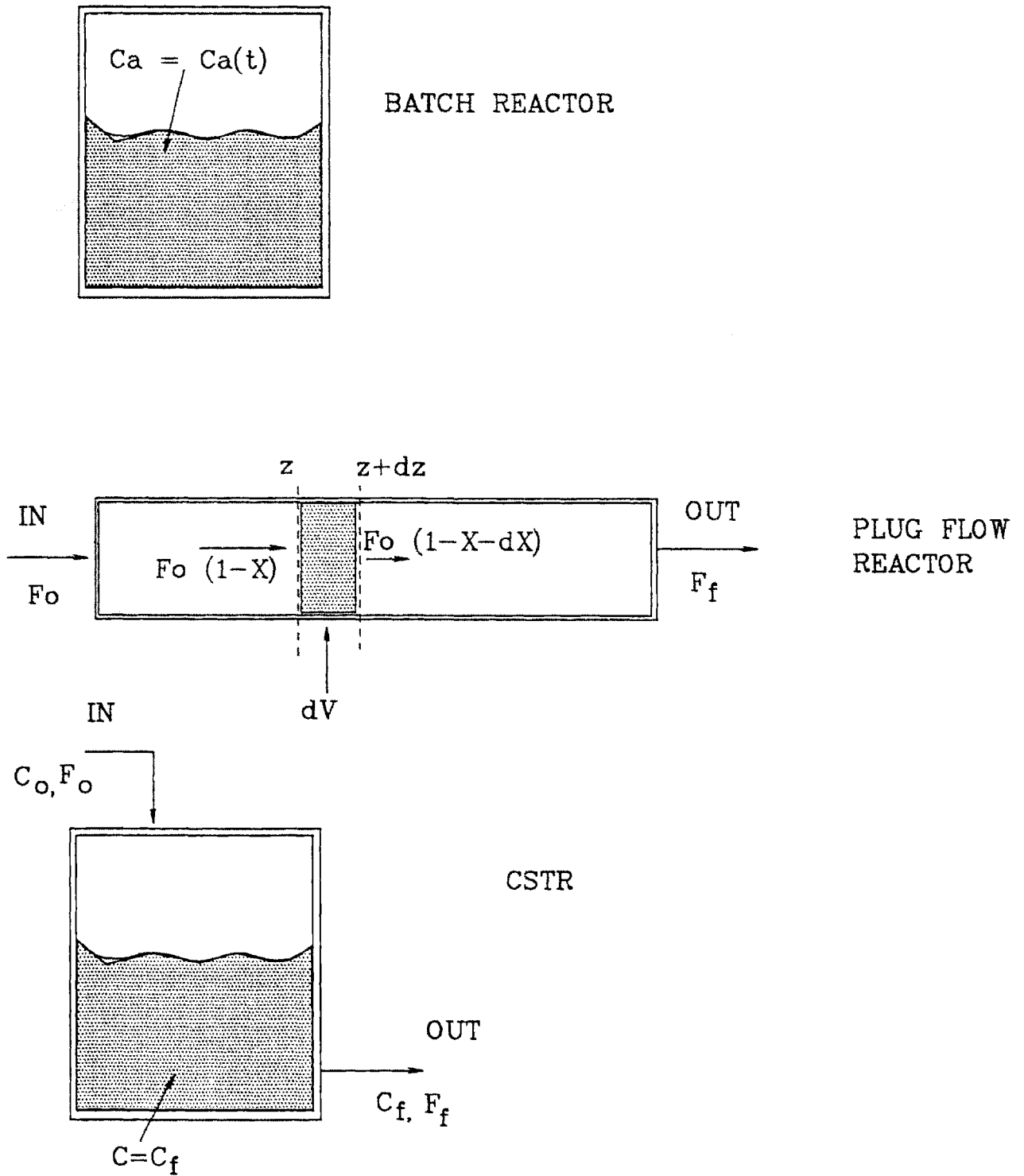
Figure 2.1: Ideal chemical reactor designs

and F is the total molar flow rate in a continuous flow reactor. The subscript f indicates the final number of moles or the final molar flow rate assuming the reaction had gone to completion. The performance equations are derived from mass balances on the reactors, of the form:

In - Out + Generation - Accumulation = 0 $\qquad$ (2.23)

Batch reactors are most commonly used for bench-scale liquid-phase reactions. The reactants are initially charged into a vessel, and the reaction is allowed to proceed. The contents of the vessel are typically stirred to ensure homogeneity. Samples are removed from the reactor, and the composition of the mixture is determined as a function of time. In applying equation (2.23), the *in* and *out* terms are zero, since it is a closed system, and the generation term is the volumetric reaction rate, r, times the reactor volume.

$$rV = \frac{dN_k}{dt} \qquad (2.24)$$

$$rV_0\left(1 + \varepsilon_k X_k\right) = \frac{d\left(N_{ko}\left(1 - X_k\right)\right)}{dt} \qquad (2.25)$$

$$dt = \frac{C_{ko}}{1 + \varepsilon_k X_k} \frac{dX_k}{-r} \qquad (2.26)$$

The initial molar concentration of k is represented here by C_{ko} to avoid confusion with the conversion. This expression may be integrated.

$$t = \int_0^{X_k} \frac{C_{ko}}{(1 + \varepsilon_k X_k)} \frac{dX_k}{-r} \qquad (2.27)$$

If $\varepsilon_k = 0$, $V = V_0$, and equation (2.20) becomes.

$$dC_k = - C_{ko}\, dX_k \qquad (2.28)$$

Using this in equation (2.27)

$$t = \int_{C_{kf}}^{C_{ko}} \frac{dC_k}{-r} \qquad (2.29)$$

Equation (2.29) is the performance equation for a constant volume batch reactor. If the functional form of the reaction rate equation is known, equation (2.29) can be integrated, and the resulting expression fit to experimental data to determine the reaction rate constants.

The assumption that volume is constant is well justified in the EBGPR, since the reactants (the halogenated organic molecules) are present in low concentrations. Greater than 99% of the flow stream is made up of "inert" molecules, such as nitrogen, oxygen, and argon. Thus even if all of the reactants are completely converted to products, the change in the number of moles in the system is less than 1%. Thus the volume of the system remains essentially constant. From this point on, it will be assumed that ε_k is zero.

Plug flow reactors are most often used for gas phase reactions. The plug flow reactor is a steady state reactor, in which the reactants flow continuously through a long tube. As the reactants move along the tube, they react, producing product. The longer the tube, the longer the reactants are in contact, and the greater the extent of reaction. In a PFR, the flow is assumed to be turbulent, so that there are no concentration gradients in the radial direction. To derive the performance equation, consider a differential volume of the reactor of length dz as shown in figure 2.1. Using equation (2.23),

$$F_{ko}(1-X_k) - F_{ko}(1-X_k-dX_k) + r\, dV - 0 = 0 \qquad (2.30)$$

The accumulation term in equation (2.30) has been set to zero since it is assumed that the reactor is operating at steady state. Rearranging,

$$\frac{dX_k}{-r} = \frac{dV}{F_{ko}} \qquad (2.31)$$

$$\int_0^{X_k} \frac{dX_k}{-r} = \int_0^{V_o} \frac{dV}{F_{ko}} \qquad (2.32)$$

substituting equation (2.28), and integrating the right hand side.

$$\int_{c_{kf}}^{C_{ko}} \frac{dC_k}{-r} = \frac{V_o C_{ko}}{F_{ko}} \equiv \tau \qquad (2.33)$$

where τ is the space time (similar to residence time in the reactor). This is the performance equation for the plug flow reactor. Upon comparison with equation (2.29), it is evident that this is the same as the performance equation for a batch reactor, if the space time is exchanged for the time the reaction is allowed to proceed. Again, as in the batch case, if a functional form of the reaction rate is known, equation (2.33) can be integrated and the reaction rate constants determined from data.

30

Continuously stirred tank reactors are similar to batch reactors. except that they are operated in steady state. The reactants enter the reactor continuously, and they are well mixed to ensure homogeneity. In a CSTR, the composition of the contents of the vessel are assumed to be the same as the composition of the outlet stream. Applying the mass balance once more.

$$F_{ko} - F_{ko}(1-X_{kf}) + rV = 0 \qquad (2.34)$$

$$X_k F_{ko} = -r V \qquad (2.35)$$

multiplying by C_{ko}.

$$\frac{C_k}{-r} = \frac{VC_{ko}}{F_{ko}} = \tau \qquad (2.36)$$

$$\frac{C_{ko} - C_k}{-r} = \tau \qquad (2.37)$$

This is the performance equation for a CSTR. Note that unlike the batch reactor and PFR, the performance equation is an algebraic equation, and no assumed form of the reaction rate expression is necessary to evaluate experimental data. This makes the CSTR performance equation quite versatile, as the reaction rate can be found as an function of C_k or X_k explicitly. Note that if a series of differentially small CSTRs are operated in series, the integral sum of their behavior is the same as the performance equation for the PFR. Physically this relates to the fact that a PFR is modeled using a differentially small slice of the reactor. which is well mixed, but does not mix at all with the slice in front of or behind itself. The fact that all of the performance equations are fundamentally the same should be the case. because for ideal reactors, the kinetics of the reaction mechanism cannot be a function of the reactor geometry.

To study the kinetics of decomposition in the EBGPR. one must decide which type of idealized reactor the EBGPR most closely resembles. Since it is a steady state, gas phase reactor. the PFR is natural choice. However. kinetic analysis of the data using a PFR performance equation is complicated, difficult since the integral equation cannot be evaluated analytically without some equation for r; thus the analysis must be performed using the kinetic rate expressions directly. The CSTR model would allow the rate expression to be determined algebraically from equation (2.37). But the assumption that the EBGPR behaves as a CSTR is a poor one, and will not be used here. Most kinetic studies implicitly assume ideal PFR or batch reactor behavior. but to be complete, one should state what type of reactor model is being used. The PFR model will be used in the data analysis for the EBGPR. and thus it is necessary to work with the differential equations which govern the kinetics of the process.

This is important. since the data taken in the EBGPR experiments is usually the outlet concentration of the species being decomposed. as a function of electron beam dose

to the plasma. However, traditional chemical kinetics defines the rate of reaction as the change in concentration of a species (say A) with time, or

$$r = \frac{d[A]}{dt} \qquad (2.38)$$

The relation between this definition and the experimental data taken as a function of electron beam dose must be determined in order to perform a kinetic analysis.

Starting with the differential performance equation for a PFR, equation (2.31), and using equation (2.28),

$$\frac{d[A]}{-r} = \frac{[A]_o \, dV}{F_{Ao}} \qquad (2.39)$$

Now differentiating equation (2.33),

$$d\tau = \frac{[A]_o}{F_{Ao}} \, dV \qquad (2.40)$$

Combining these last two equations, we see that,

$$-r = \frac{d[A]}{d\tau} \qquad (2.41)$$

This is the steady state reactor equivalent of equation (2.38), which is obviously transient in nature and is used to model batch reactors. Now using a chain rule expansion of equation (2.41),

$$\frac{d[A]}{d\tau} = \frac{\partial D}{\partial t} \frac{d[A]}{dD} \qquad (2.42)$$

where D is the electron beam dose. The dose to the gas being irradiated is given by

$$D = C_o \frac{I}{\rho Q} \qquad (2.43)$$

where I is the electron beam current, Q is the volumetric flow rate of the gas, ρ is the density of the gas, and C_o is a constant related to the energy deposited in the reactor (see Section 3.3.2). The definition of residence time is,

$$\tau = \frac{V_o}{Q} \qquad (2.44)$$

where V_o is the volume of the reactor. Substituting for Q in equation (2.43),

$$D = \frac{C_o}{\rho} I \frac{\tau}{V_o} \qquad (2.45)$$

and taking the derivative with respect to τ,

$$\frac{dD}{d\tau} = \frac{C_o}{\rho} \frac{I}{V_o} \qquad (2.46)$$

This differential may now be substituted into equation (2.42)

$$\frac{d[A]}{d\tau} = \frac{d[A]}{dD} \frac{C_o}{\rho} \frac{I}{V_o} \qquad (2.47)$$

and thus the reaction rate becomes,

$$r = \frac{d[A]}{d\tau} = \frac{d[A]}{dD} \frac{C_o}{\rho} \frac{I_o}{V_o} \qquad (2.48)$$

Now in the actual experiments, τ is held constant while the electron beam current is varied. This does not materially change the analysis in any way, since.

$$\left(\frac{d[A]}{dI} \right)_\tau = \left(\frac{\partial D}{\partial I} \right)_\tau \left(\frac{d[A]}{dD} \right)_\tau = \left(\frac{d[A]}{dD} \right)_\tau C_o \tau V_o \qquad (2.49)$$

where the subscript τ means that the residence time is being held constant. Thus the change in [A] with respect to electron beam current is different from the change in [A] with respect to electron beam dose only by a multiplicative constant. Similarly, rate of reaction r is equivalent to $d[A]/dD$ apart from a multiplicative constant. These constants are immaterial, as they will actually be absorbed into the reaction rate constant as shown in Section (2.4). Thus.

$$\frac{d[A]}{dt} = r \Leftrightarrow r = \frac{d[A]}{dD} \qquad (2.50)$$

and the data taken as a function of electron beam dose is equivalent to data taken as a function of time in a traditional chemical reactor.

2.2.2 Modification of the Performance Equation for the EBGPR

33

In order to use the performance equation for a PFR to design an EBGPR, it is necessary to modify the equation slightly in order to account for the differences between a plasma reactor and a traditional reactor. First, as demonstrated above, in the EBGPR the electron beam dose is the relevant measure of reaction progression, not time as in a traditional reactor. Second, the reaction rate expressions which will be determined in Chapter 4 will have units of concentration/dose rather than the traditional concentration/time units. A modified performance equation will be derived from first principles, starting with a mass balance, as in equation (2.30)

$$F_{ko}(1 - X_k) - F_{ko}(1 - X_k - dX_k) - \dot{D} \cdot r dV = 0 \qquad (2.51)$$

Where the mass balance has been modified by the addition of the electron beam dose rate, $\dot{D}$. This equation can easily be verified to have the proper units, since,

F_{ko} [=] mol/sec
$\dot{D}$ [=] dose/sec
r [=] mols/volume-dose
dV [=] volume

Rearranging,

$$\frac{dX_k}{-r} = \frac{\dot{D} \cdot dV}{F_{ko}} \qquad (2.52)$$

if we assume that the dose rate is uniform throughout the irradiation volume, the right hand side can be integrated,

$$\int_0^{X_k} \frac{dX_k}{-r} = \frac{\dot{D} \cdot V}{F_{ko}} \qquad (2.53)$$

substituting equation (2.28), and using

$$F_{ko} = C_{ko} F_o \qquad (2.54)$$

where F_o is the total volumetric flow rate, equation (2.54) becomes,

$$\int_{C_{ko}}^{C_k} \frac{dC_k}{-r} = -\frac{\dot{D} \cdot V}{F_o} \qquad (2.55)$$

34

now the right hand side may be simplified somewhat by noting that the total electron beam power to the plasma is given by,

$$P = \rho_0 \dot{D} V \qquad (2.56)$$

where ρ_0 is the density of the gas stream. Finally, the EBGPR performance equation is obtained,

$$\int_{C_{ko}}^{C_{kf}} \frac{dC_k}{-r} = -\frac{P}{\rho_0 F_0} \qquad (2.57)$$

This important equation allows the design of an electron beam generated plasma reactor, once an accurate rate expression is known. For a given inlet VOC concentration, carrier gas density, and volumetric flow rate. the power to the plasma needed for a desired outlet concentration is given by equation (2.57) In Chapter 4, a kinetic analysis of the laboratory reaction data will be analyzed to determine the rate equation, r, for use in the EBGPR performance equation.

One must be aware of the assumptions which were used in deriving the EBGPR performance equation. Most importantly, it was assumed that the reactor can be modeled as an ideal PFR. For this to be true. the flow through the reaction channel must be turbulent to allows no radial concentration gradients. The electron beam energy deposition must be as uniform as possible throughout the reaction region. PFR analysis assumes that the reaction takes place in a long tube. simulated as a series of well mixed differential volumes. Thus the reactor should be designed to allow uniform irradiation along the flow direction. Unfortunately, both the current design of the field unit does not follow this contacting pattern: instead all of the energy is deposited in a thin volumetric section. This is known as the "electron curtain" design. It is well known in chemical engineering practice that the PFR-type contacting pattern gives better conversion for most chemical reactions of industrial interest. This will not be shown in detail here. but there are many texts which deal with this subject. The subject of optimized EBGPR design will be revisited in Chapter 6. *Conclusion*.

2.2.3. Inhibitor Model and Integral Analysis

A chemical kinetic method of arriving at a relation between electron beam dose and reactant concentration will be derived on the basis of an inhibitor species model in which other species in the plasma compete with the VOC molecules for the energy deposited by the electron beam.[5,74] This will be derived for a generic inhibitor species, and then the results applied to the decomposition mechanism of each VOC of interest in Chapter 4. The model assumes that chlorine and oxygen radicals formed in the plasma

initiate the halogenated VOC decomposition reaction, and will be referred to as the VOC removal agent X_1. This reaction proceeds with rate constant k_1,

$$X_1 + T \rightarrow P_1 + X_2 \qquad\qquad k_1 \qquad\qquad (2.58)$$

where T represents a generic VOC, P_1 is some stable decomposition product, and X_2 is a byproduct, either a radical or a molecule. For example, X_2 could be a chlorine radical, which will further react with other VOC molecules, and thus enhance the decomposition rate,

$$X_2 + T \rightarrow P_2 \qquad\qquad k_2 \qquad\qquad (2.59)$$

or X_2 could be scavenged by some other species in the plasma, M, which could be an oxygen molecule or radical, or a decomposition product of the VOC,

$$X_2 + M \rightarrow P_3 \qquad\qquad k_3 \qquad\qquad (2.60)$$

Reaction (2.60) is called an *inhibition* reaction, because it scavenges the species X_2 which could otherwise be used to decompose more of the VOC. If the rate constant k_3 is large compared to k_2. the decomposition is greatly hindered by this process, and the reaction is said to be *inhibited*.

The rate equations for reactions (2.58-2.60) are given by,

$$\frac{d[T]}{dt} = - k_1 [X_1] [T] - k_2 [X_2][T] \qquad\qquad (2.61)$$

$$\frac{d[X_2]}{dt} = - k_1 [X_1][T] - k_2 [X_2][T] - k_3 [M][X_2] \qquad\qquad (2.62)$$

To solve these equations analytically, several assumptions must be made. First, it is assumed that the concentration initial VOC removal species X_1 is constant. This is probably a good assumption. since the initiating species is likely either oxygen radicals or electrons. both of which are present in great excess. Second, a pseudo-steady state assumption is placed on species X_2. This is common practice for a chemical kinetic analysis in which a transient species can be assumed to be in low concentration since it is removed by some mechanism very soon after it is formed. Finally the assumption is made that the inhibitor species concentration, [M], is constant. This is arguably not a very good assumption for the reactions of interest in this work. It is more likely that M is a reaction product of VOC decomposition. and thus as more VOC is decomposed, the concentration of species M increases. and the inhibition becomes more important. Unfortunately, if M is assumed to be a product of VOC decomposition. (e.g., P_1. P_2, or P_3, above) these

equations cannot be solved analytically. Though numerical solutions are common in chemical kinetic analyses, time constraints do not allow a formal numerical treatment to be performed in this study. In this work [M] will be assumed to be constant. This has the effect of removing some of the non-linear nature of the problem, resulting in a model which is accurate at predicting low levels of inhibition. For reactions which are strongly inhibited. the model fails to capture the non-linear nature of the problem, and the equations must be numerically evaluated.

With the above assumptions, equations (2.61-2.62) can be integrated, as shown in Appendix B:

$$\frac{[T]}{[T_o]} \cdot \sqrt{\frac{K+1}{K+\frac{[T]}{[T_o]}}} = \exp(-k_1[X_1] \cdot t) \qquad (2.63)$$

where.

$$K = \frac{k_3[M]}{2 \cdot k_2 \cdot [T_o]} = \text{constant} \qquad (2.64)$$

K is a measure of the degree of inhibition of the reaction. It is the ratio of the rate at which the removal agent X2 is scavenged by M to the rate at which it decomposes the VOC. T. If k3 is small. and thus K→0. equation 2.63 becomes.

$$[T] = [T_o]\exp(-2 \cdot k_1 \cdot [X_1] \cdot t) \qquad (2.65)$$

Thus first order decay is recovered. This is makes sense. considering reactions (2.58-2.60). If k_3 is small. and reaction (2.60) is negligible. then reactions (2.58) and (2.59) ensure that two VOC molecules are removed for each initiation step. Thus the reaction rate is exactly first order. which the pseudo rate constant of the initiation reaction. $k_1[X_1]$ multiplied by a factor of 2. If one now defines a parameter β, such that,

$$\beta = \frac{1}{2 \cdot k_1[X_1]} \qquad (2.66)$$

and equation (2.64) becomes.

$$[T] = [T_o]\exp\left(-\frac{t}{\beta}\right) \qquad (2.67)$$

In Section 2.2.1, it was shown that the electron beam dose to the plasma, D, was the EBGPR equivalent to residence time t in a traditional chemical reactor. Thus D can be substituted for t in equation (2.67) without any loss of generality; only the units of β need to be changed.

$$[T] = [T_0]\exp\left(-\frac{D}{\beta}\right) \qquad (2.68)$$

This pure exponential dependence is characteristic for simple, uninhibited, first-order kinetics, and is the form used by Rosocha[10,12,26,27,70] to model the decomposition of chlorinated VOCs in a dielectric barrier discharge, and by Penetrante [22,38,29,41] to model the decomposition of chlorinated VOCs in an electron beam generated plasma and in a pulsed corona discharge. β will occasionally be referred to in this work as the Rosocha β. This is to distinguish it from the use of the same parameter in equation (2.64) yielding,

$$\frac{[T]}{[T_0]} \cdot \sqrt{\frac{K+1}{K+\dfrac{[T]}{[T_0]}}} = \exp\left(-\frac{D}{2\cdot\beta'}\right) \qquad (2.69)$$

The pseudobeta value, β', differs from the Rosocha β since equations (2.69) and (2.67) have different functional forms. Data fit to these two equations will yield different values of β and β'.

The first-order Rosocha model is only valid when the exhaust concentration versus dose data is linear on a semilog plot. This is the same relation derived in Section 2.1 using a radiation chemistry approach, in contrast to the kinetic approach used here. Note that for high fractional decomposition, inhibition of the decomposition reactions becomes important, and the concentration versus electron beam dose curves are no longer linear. For fractional decomposition greater than approximately 90%, the more complicated model represented by equation (2.69) must be used. The two parameters, β' and K, can be determined by a non-linear regression of the data.. Note again that the β'-value obtained from equation (2.69) is not the same as the β-value obtained from equation (2.68). To compare β-values to previously published values, equation (2.68) must be used.

The factor K indicates of the importance of inhibition by decomposition products in TCA reaction kinetics. If one compares equations (2.68) and (2.65) to equation (2.15) the origin of the factor K in equation (2.15) becomes clear. The ratio of kinetic constants for the forward reaction and inhibition reactions is a good measure of the way in which the energy from the reactor is partitioned among species in the plasma. If this ratio is large, most of the energy is being directed toward the VOCs, and thus the decomposition reaction will be fast. However, if this ratio is low, most of the energy will be directed toward the carrier gas molecules or the production of inhibitor species, and the decomposition of the VOC will be slow. Unfortunately, unless some previous measure of

these rate constants has been made, this ratio (represented by K) is unknown. In this study, K will be used as a fitting parameter, and its value derived from the experimental data for each VOC.

There is another derivation of an inhibitor species model, proposed by Slater(5), which predicts an explicit dependence of β on inlet concentration. Chlorine and oxygen radicals formed in the plasma initiate the TCA decomposition reaction, and will be referred to as the TCA removal agent X•. This reaction proceeds with rate constant k_1,

$$X\bullet \;+\; TCA \;\rightarrow\; Y \;+\; \text{other products} \qquad k_1 \qquad (2.70)$$
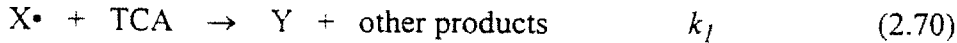
where Y is some decomposition product, either a radical or a molecule.

Now assume that Y is itself an inhibitor of reaction (2.70) since it also can react with X• and thus compete with TCA for the removal agent. This reaction proceeds with rate constant k_2.

$$X\bullet \;+\; Y \;\rightarrow\; Z \;+\; \text{other products} \qquad k_2 \qquad (2.71)$$
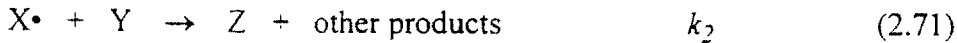
where Z is another reaction byproduct. The rate equations for reactions (2.70-2.71) are given by,

$$\frac{d[X]}{dt} = S - k_1 [X][T] - k_2[X][Y] \qquad (2.72)$$

$$\frac{d[T]}{dt} = -k_1[X][T] \qquad (2.73)$$

where S is the X• formation rate, [X] is the concentration of the reactive radical, and [T] is the concentration of TCA. Conservation of species requires $[T_0] = [Y] + [Z] + [T]$. If the TCA removal is small. or if reaction (2.71) is slow. then the approximation can be made that $[T_0] \approx T + Y$. If the production and removal of X is at steady state, and $k_1 \approx k_2$, equations (2.72-2.73) can be integrated to give,

$$[T] = [T_0]\exp\left(-m\frac{D}{[T_0]}\right) \qquad (2.74)$$

The production rate of species X• is related to the electron beam dose to the plasma, D,

$$D = \frac{St_r}{m} \qquad (2.75)$$

$$m = \frac{0.0367G}{\rho_c} \qquad (2.76)$$

where G is the G value for the VOC, t_r is the residence time in the reactor (sec), and ρ_c is the density of the carrier gas (g/cm^3). The constant 0.0367 is a conversion fact for obtaining G in units of molecules per 100 eV, when m is expressed in ppm/Mrad. It is easily seen that equation (2.74) reduces to equation (2.68) if the following substitution is made.

$$\beta = \frac{\rho_c [T_o]}{0.0367\,G} \qquad (2.77)$$

This expression shows clearly that for this inhibitor model, β is a linear function of inlet VOC concentration. For the chemicals which exhibit his behavior, equation (2.77) will be used to calculate the G value from β in Chapter 4.

To find the energy expense per molecule required for decomposition, ε, equation (2.69) can be solved for D as a function of η, the fractional decomposition. This equation for D can then be inserted in equation (2.17),

$$\varepsilon = \frac{1}{\eta T_o} \frac{M_c}{N_A} 2 \cdot \beta' \left[\ln\left(\frac{1}{1-\eta} \cdot \sqrt{1 - \frac{\eta}{K+1}} \right) \right] \qquad (2.78)$$

Equations (2.68) and (2.69) are a examples of an integral model for kinetic analysis. The kinetics of the decomposition were first assumed, then the model derived. The data is then fit to the model to determine the kinetic constants. Of course, in order for equation (2.69) to have any meaning, the assumed kinetic description must be correct. Without previous literature on the subject, this is a risky procedure at best. In the next section, another method of determining kinetic constants from data without these assumptions is presented, and the two methods are compared.

2.2.3. Differential Analysis

For the differential analysis, one must only assume that the reaction has an order with respect to the concentration of some species of interest. By saying that the reaction has an order n with respect to the concentration [A] of a reactant, it is implied that the reaction rate equation can be written as.

$$r = -\frac{d[A]}{dt} = k[A]^n \qquad (2.79)$$

40

Equation (2.79) is an example of a reaction with order n with respect the concentration [A] of a reactant, and with order zero with respect to the concentrations of all other species. In general, a reaction can have an order with respect to any number of species,

$$r = -\frac{d[A]}{dt} = k[A]^n [B]^m [C]^p \ldots \ldots \tag{2.80}$$

For the decomposition reactions considered in the present work, the rate of decomposition is not expected to depend on the concentrations of any species in the plasma other that that of the reactant itself. Oxygen radicals, which are necessary for the decomposition mechanisms, are assumed to be in great excess with respect to the concentration of the VOC. In any case, the concentration of oxygen radicals produced (for a given electron beam dose) is always held constant in this system, since air is always used as the carrier gas and the concentration of the VOC is always low. Therefore, the effect of oxygen radicals on the reaction rate is constant will be absorbed into the rate constant k of the pseudo n-th order reaction. The "concentration" of electrons will be dealt with in a different manner: the electron beam dose D will be substituted for time in the above equations, as was justified in Section 2.2.1. Since the reaction was assumed to be a function only of one species (that being decomposed), equation (2.79) is sufficient,

$$r = -\frac{d[A]}{dD} = k[A]^n \tag{2.81}$$

From equation (2.81), it can be seen that a plot of $\ln r$ versus $\ln [A]$ gives a straight line of slope n and, the intercept of this line is $\ln k$,

$$\ln r = \ln k + n \ln [A] \tag{2.82}$$

If a straight-line plot is not obtained, the rate cannot be expressed in terms of equation (2.81), and thus the reaction does not have an order with respect to that particular reactant. For example, the reaction,

$$H_2 + Br_2 \rightarrow 2HBr \tag{2.83}$$

has a reaction rate which is fit well by the expression,[75]

$$r = \frac{k[H_2][Br_2]^{1/2}}{1 + \frac{[HBr]}{m[Br_2]}} \tag{2.84}$$

41

This reaction does not have an order with respect to [Br$_2$]. However, at low extents of reaction. i.e.. [HBr]/[Br$_2$] << 1, the reaction rate expression reduces to:

$$r = k[H_2][Br_2]^{\frac{1}{2}}$$

(2.85)

Thus for short times after the reaction begins the rate has a definite order with respect to both hydrogen and bromine. but after this induction period, the rate has no order with respect to bromine. This result is seen in many complex reaction mechanisms. in which complicated rate expressions like equation (2.84) reduce to simple rate expressions at some limiting value of the extent of reaction, pressure, catalyst coverage, etc.

Note that the order with respect to bromine in equation (2.85) is non-integer. This is allowed for multistep reaction mechanisms: the details of the derivation of equation (2.76) are beyond the scope of this work. However, it is useful to note this non-integer order here. as all of the decomposition reactions of interest in this study proceed by very complicated. multistep mechanisms. and may have apparent non-integer orders. This will be discussed further in Chapters 4 and 5.

Returning to equation (2.82). to determine the order, n. and the rate constant, k, the rate of reaction d[A]/dD must be determined from the data. This may be done in two different ways. as illustrated in figure 2.2. Using the first method, runs are carried out at different initial concentrations. and the initial rates are determined by measuring the initial slopes. A double logarithmic plot then gives the order of the reaction. and the rate constant. Because the initial rates are used. this procedure avoids the possible complications due to interference by products. This order is called the order with respect to concentration, and is denoted by n_c.

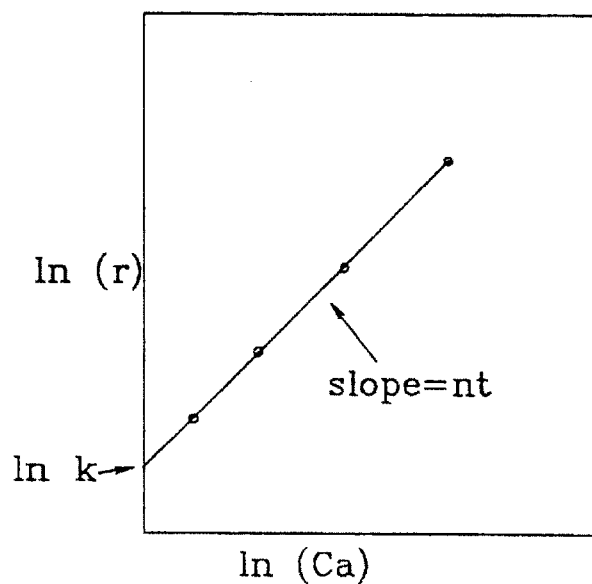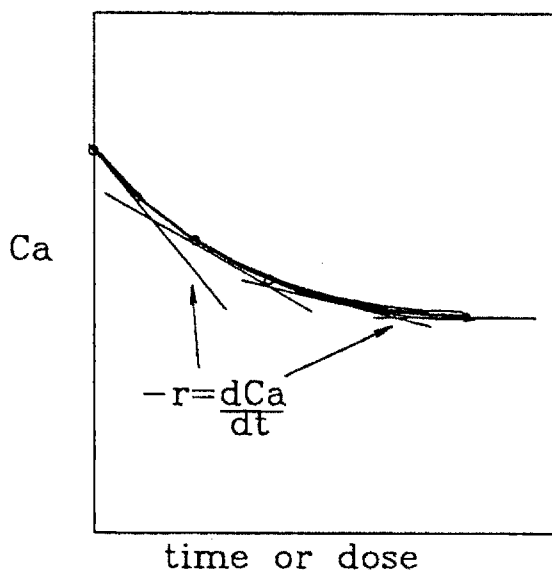# ORDER WITH RESPECT TO CONCENTRATION
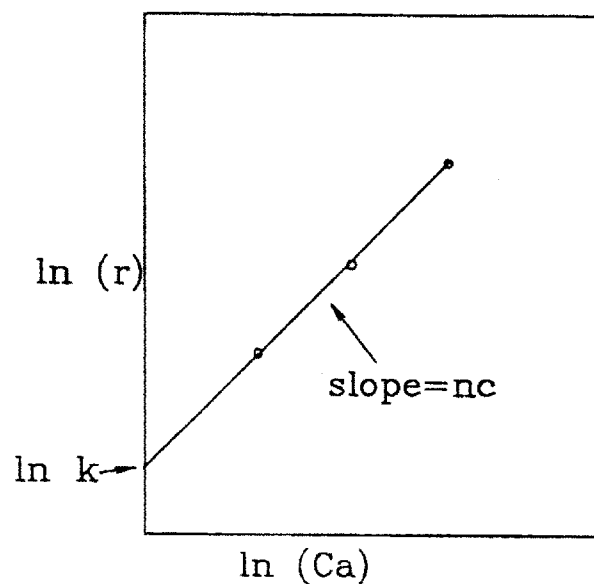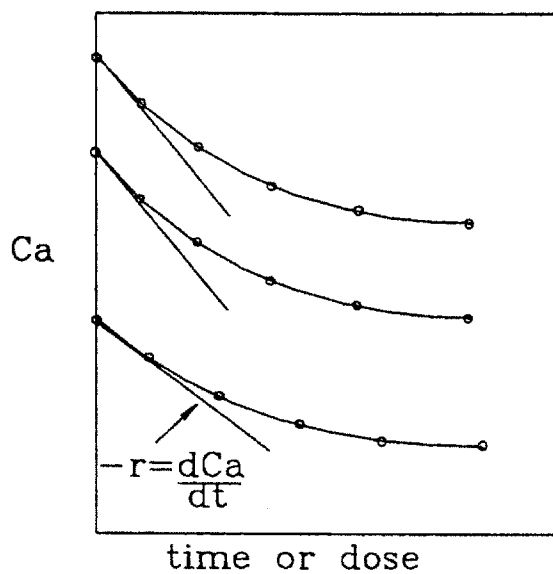
ORDER WITH RESPECT TO TIME

Figure 2.2: Differential kinetic method of finding the order with respect to concentration. n_c

The second procedure is to use the data from one run, and to measure the slope at various points. corresponding to a number of values of the reactant concentration. This is the second method illustrated in figure 2.2, and is usually referred to as the order with respect to time. In the present case, the dose is actually changing rather than the time, but for simplicity the same standard nomenclature will be used, and this order will be denoted by n_t.

The two orders are not always the same for a given reaction. If the order with respect to time is greater than the order with respect to concentration, then as the reaction proceeds the rate falls off more rapidly than would be expected if the order with respect to concentration applied to the entire time course of the reaction. This abnormally large decrease in the rate with time (or dose) most likely means that some species being produced in the reaction is inhibiting further reaction of the original reactant. As the reaction proceeds. more inhibitor is formed, and the reaction rate continues to fall off.

Conversely. if the order with respect to time is smaller than the order with respect to concentration. the rate of reaction is falling off less rapidly than if n_c were to apply during the entire time course of the reaction. This would mean that some reaction product is causing the rate of reaction of the initial reactant to increase. This activation by the products of the reaction is known as autocatalysis. and the reaction is said to be autocatalytic.

The differential method clearly illustrates inhibition or autocatalysis of the reaction.[75] This method is the most reliable for investigating the kinetics of a reaction about which there is little previous information. since it does not require an assumption about what the order of the reaction should be. Miller[76] referred to the method of integration as the ·method of guess and try"; the differential method he called the "method of systematic exploration." If the double logarithmic plots from the differential methods are linear. the reaction has an order with respect to a particular reactant. Information about the influence of reaction products is clearly revealed from the orders of reaction n_t and n_c.

The method of integration has some advantages in its simplicity. Data is easily fit to a predictive model. and an accurate value of rate constants can be determined. However, the method creates prejudice in favor of integer or half integer orders, since the data will often fit into these orders within the experimental error. The differential method is more likely to indicate deviations from integral or half integral orders.

Another problem with the integral method is that very different kinetic mechanisms can gave integrated forms with very similar graphical appearance. For example, the time course of a simple-second order reaction mechanism is similar to that of a first-order reaction inhibited by products. The method of integration generally leads to difficulties when the two orders n_c and n_t are different. In Chapter 4, the differential method will be used to identify apparent orders of reaction. and to examine the influence of products. If the kinetics appear to be inhibited. the integral model given in equation (2.69) will be used to fit the data, and the values of K and pseudo-β's will be determined. If the kinetics do not appear to be inhibited, equations (2.11) and/or (2.13) will be fit to the data. In either case. equation (2.14) will be fit to the data for low fractional

decomposition where inhibition is unlikely to be important, in order to generate β values to compare to literature results.

2.4 Summary

The four integral models are summarized in table 2.1, along with the various assumptions used to derive them. Computer programs were written to perform the fitting to the integral models. since there is a large amount of data to be evaluated. Another computer program. DERIVS, was written to perform the differential analysis of the data. As mentioned in the last section. the differential analysis will be used to determine whether the ALPHAPLUS. ALPHAFIT or INHIBIT model should be used to examine the reaction kinetics. The BETAFIT model will be used on all of the data to generate β values. Table 2.2 gives the corresponding equations for the specific energy requirements, when each model is solved for D and substituted into equation (2.17).

Computer Code	x = f (D, parameters)	assumptions	parameters
ALPHAPLUS	$x = \left((1 - \alpha) \dfrac{M_C}{N_A} G_0 K \cdot D + x_0^{1-\alpha} \right)^{1/1 - \alpha}$	$G = a\,(x)^{\alpha}$	$\alpha, (G_0\,K)$
ALPHAFIT	$x = x_0 \exp\left(-\dfrac{M_C}{N_A} K \cdot G_0 (x_0)^{\alpha} D \right)$	$G = a\,(x_0)^{\alpha}$	$\alpha, (G_0\,K)$
INHIBIT	$\dfrac{[T]}{[T_0]} \cdot \sqrt{\dfrac{K + 1}{K + \dfrac{[T]}{[T_0]}}} = \exp\left(-\dfrac{D}{2 \cdot \beta'} \right)$	inhibited kinetics, $K \neq f(x)$. K can be $K = f(x_0)$	β', K
BETAFIT	$x = x_0 \exp\left(-D/\beta \right)$	$\beta \neq f(x)$, only accurate for first-order kinetics	β

Table 2.1: Integral kinetic models for EBGPR analysis. The concentration versus electron beam dose curves are fit to these model to determine the parameters.

Model	Specific Energy $\quad \varepsilon = f(\eta, x_0, \text{parameters})$
ALPHAPLUS	$$\varepsilon = \frac{\left((1-\eta)^{1-\alpha}-1\right)}{\eta} \frac{x_0^{-\alpha}}{(1-\alpha)G_0 \cdot K}$$
ALPHAFIT	$$\varepsilon = \frac{1}{\eta x_0} \frac{1}{K} \frac{1}{G_0 x_0^{\alpha}} \ln\left(\frac{1}{1-\eta}\right)$$
INHIBIT	$$\varepsilon = \frac{1}{\eta T_0} \frac{M_C}{N_A} 2 \cdot \beta' \left[\ln\left(\frac{1}{1-\eta} \cdot \sqrt{1-\frac{\eta}{K+1}}\right)\right]$$
BETAFIT	$$\varepsilon = \frac{1}{\eta x_0} \frac{M_C}{N_A} \beta \ln\left(\frac{1}{1-\eta}\right)$$

Table 2.2: Energy expense or specific energy per molecule required for decomposition calculated using the integral models in table 2.1

3. Experimental Methods

The EBGPR has been described in detail by Koch. This work will give a brief description of the components, and will emphasize those components which have been changed to improve reactor performance, such as the flow meters and the reaction chamber design.

3.1. Gas Mixing System

The gas manifold system allows the mixing of up to six streams to create complex mixtures for experiments. Calibrated gas cylinders are used for DCA, DCE, EC, and VC reactions; liquid bubblers are used for TCE and TCA experiments. The gas flow rates for the experiments are typically between 2 and 10 liters per minute. For the TCE and TCA experiments. calibrated rotameters were used to measure the gas flow rates. Unfortunately, rotameter readings are unstable, and it is difficult to read the exact position of the glass ball in the flow tube. This limits the accuracy of the readings to ± 10%. For the other experiments, digital mass flow meters were installed downstream from the rotameters. These meters are reported to be accurate to ± 2%. The meters do not need to be calibrated. and they operate independently of temperature, pressure, or gas composition. The inaccuracy and instability of the flowmeters were believed to be a major source of experimental uncertainty; the new flow meters improve the reproducibility of the results.

3.2 Electron Beam Generated Plasma Reactor

In the EBGPR. the electrons are generated in a vacuum chamber by thermionic emission from a directly heated tungsten filament. The electrons pass through a control grid. which may be negatively biased up to 100 V with respect to the filament. The bias on the grid allows control over how many electrons pass through the grid, thus allowing control of the beam current. The electrons are then accelerated by an applied voltage of 100 kV from the control grid. through a 25 μm aluminum foil window. into the reaction chamber through which the VOC contaminated air stream flows at atmospheric pressure. The electrons deposit a fraction of their energy in the air stream before being dumped onto a titanium plate opposite the electron beam window. The electron beam deposition in the gas will be treated in Section 3.3.2. The maximum electron beam power to the plasma is approximately 25 W. The EBGPR operates at steady state, and the reaction chamber is at atmospheric pressure. The fast electrons from the beam ionize the nitrogen and oxygen molecules in the carrier gas, creating many secondary electrons for each fast

electron. The secondary electrons slow down by collisions with the VOC and carrier gas molecules, and initiate the decomposition of the VOC molecules.

3.3. Reaction Chamber Design

The reaction chamber design used for the experiments on TCE, TCA, and VC decomposition was the same as that used by Koch for his later studies. This design is illustrated schematically in figure 3.1. This reaction chamber is a straight-flow-through design in which the gas flows perpendicularly to the electron beam propagation direction. The chamber consists of a Pyrex frame sandwiched between two titanium plates. The electron beam enters through a 1" square hole in one of the plates, irradiates the gas stream flowing perpendicularly to the beam, and is dumped on to the back titanium plate. The plates are bolted together with plastic screws, sandwiching the Pyrex frame between them. The back titanium plate is water cooled since the majority of the energy from the beam is dumped on to this plate. The spacing between the plates, which is the same as the thickness of the Pyrex frame, is approximately 1.5 cm.

Unfortunately, this design has several problems. The Pyrex frame is subject to radiation damage and thermal stresses, which often cause it to crack. The fact that it is sandwiched in between two plates also causes stresses, since the plates must be held together tightly to prevent leaks. As a result, a new frame would break after only two weeks of use, on average. No glue was successful in repairing the frame, since most glues are susceptible to radiation damage as well. Further, even if the glue did hold, the frame would simply crack in another place. The cracked reaction chamber would allow a significant amount of sample to leak out of the reaction chamber. Thus, it was not certain that gas stream analyzed after the reactor was at all representative of the composition in the reactor.

In addition, the Pyrex frames were custom made, and required six weeks for delivery. The frames cost $600 each, so it was not possible to replace a frame each time it broke. The o-ring design used to seal the frame against the titanium was also troublesome, since it was also non-standard and difficult to make each time the reaction chamber had to be opened. Finally, the short path length of the beam in the reaction chamber (1.5 cm) meant that most of the energy from the reactor was being wasted by being dumped into the back plate of the chamber.
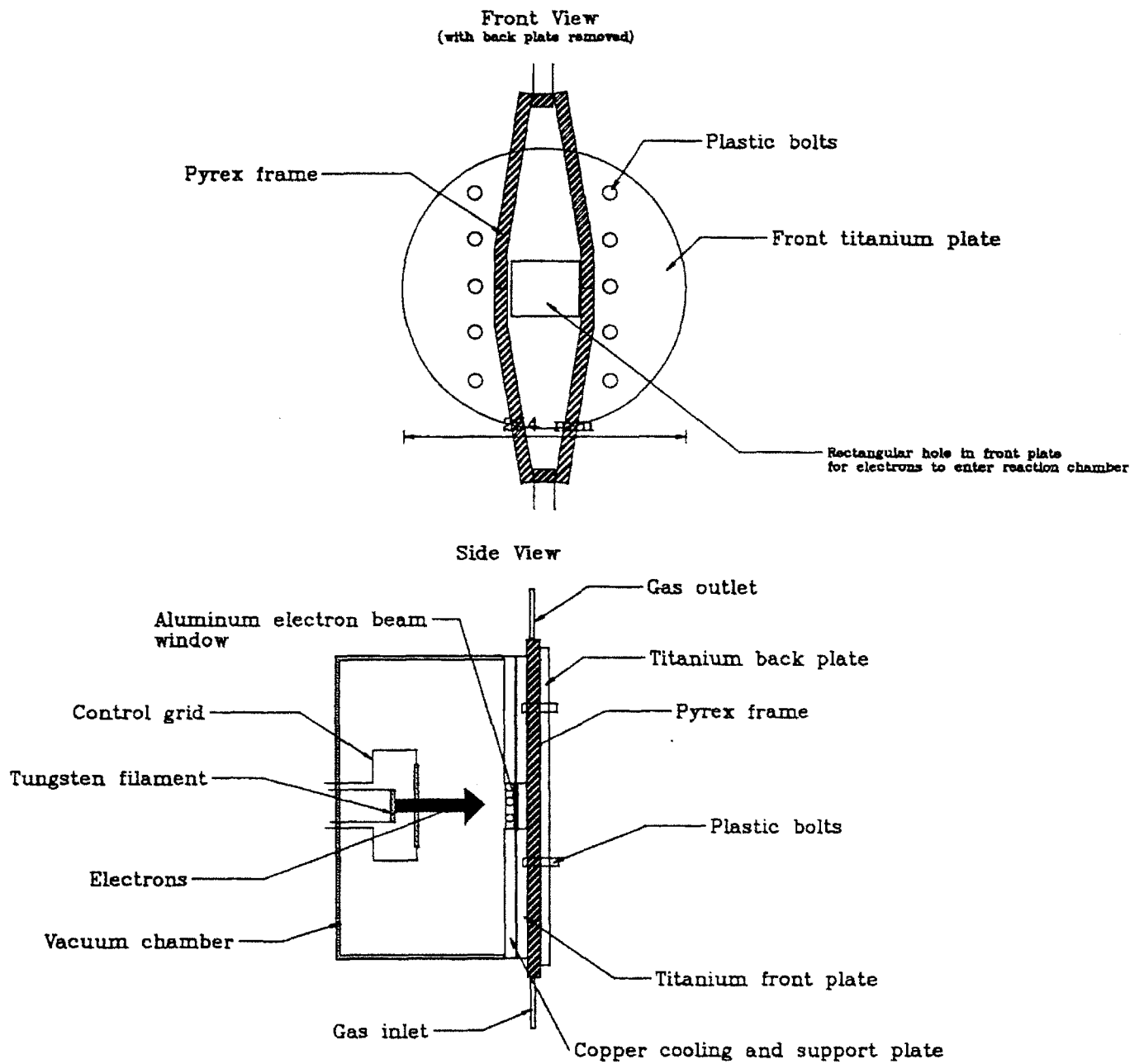
48

Front View
(with back plate removed)

Plastic bolts

Pyrex frame

Front titanium plate

554 mm

Rectangular hole in front plate
for electrons to enter reaction chamber

Side View

Gas outlet

Aluminum electron beam
window

Titanium back plate

Control grid

Pyrex frame

Tungsten filament

Plastic bolts

Electrons

Vacuum chamber

Titanium front plate

Gas inlet

Copper cooling and support plate

Figure 3.1: Old rectangular reaction chamber design

49

Front View

(with back plate removed)

Front titanium plate

50 mm

Alumina reaction chamber

25.4 mm

Plastic bolts

264 mm

Rectangular hole in front plate
for electrons to enter reaction chamber

Side View

Aluminum electron beam window

Gas outlet

Alumina reaction chamber

Control grid

Titanium back plate

Tungsten filament

Gas inlet

Electrons

100 mm

Vacuum chamber

Plastic bolts

Titanium front plate

Copper cooling and support plate

Figure 3.2: New cylindrical reaction chamber design

50

For all of these reasons, an alternative reaction chamber was designed. This design is shown schematically in figure 3.2. This design will be referred to as the Cylindrical Reaction Chamber, to avoid confusion with Koch's two previous reaction chamber designs. The rectangular Pyrex frame of the previous design is replaced by an alumina right circular cylinder 5 cm O.D., 4.4 cm I.D., and 10 cm in length. The cylinder is sandwiched between two titanium plates using plastic bolts as in the previous design. The electron beam enters the chamber through a 1" square hole in the front titanium plate, passes through the length of the reaction chamber, and is dumped onto a titanium back plate. The gas stream enters though a hole in the back plate and flows through the length of the chamber parallel to and counter-current to the electron beam propagation direction. The stream exits the reaction chamber through a small hole in the front titanium plate. This exit hole is placed as close to the aluminum foil electron beam window as possible, to minimize dead volume in the reaction chamber. This improved reactor design has several advantages:

1. The alumina cylinder is much stronger than Pyrex.
2. The alumina cylinder does not appear to suffer any heat or radiation damage under the experimental conditions used.
3. The cylinders are standardly available components. costing $100 each.
4. The o-rings which seal the cylinder against the front and back plates are standard.
5. The path length in the direction of the electron beam is long.

In four months of experimental use. the cylindrical reactor has not cracked or shown any signs of wear. The reactor is leak free to less than 10 ml/min air at a pressure of 10 psig. The previous reactor design had a leakage rate of greater than 200 ml/min air at 10 psig.

3.3.1. Temperature Studies in the Cylindrical Reaction Chamber

It was initially uncertain what sort of cooling requirements would be necessary for the cylindrical reaction chamber design. A thermocouple was used to measure the adiabatic temperature rise both inside and on the outside wall of the reactor. The temperature as a function of position is shown in figure 3.3. Note that there was no active cooling of either the rear of the reaction chamber or on the outside of the cylinder, and no air was flowing through the reaction chamber. The alumina cylinder seemed to suffer no ill effects from the 329°C temperature. The maximum operating temperature of the material is given as 1950°C by the manufacturer.[77] From the sharp increase in the temperature profile just below 5 cm from the foil. and from rapid fluctuations in the thermocouple meter readings at this distance. it is believed that 5 cm marks the penetration distance of the electrons in air. This gives an effective plasma volume inside the reaction chamber of 76 ml. The fact that the plasma extends for 5 cm from the foil is

consistent with both the visual examination of the plasma without the reactor present, and from the calculation of the Monte Carlo code in the next section.
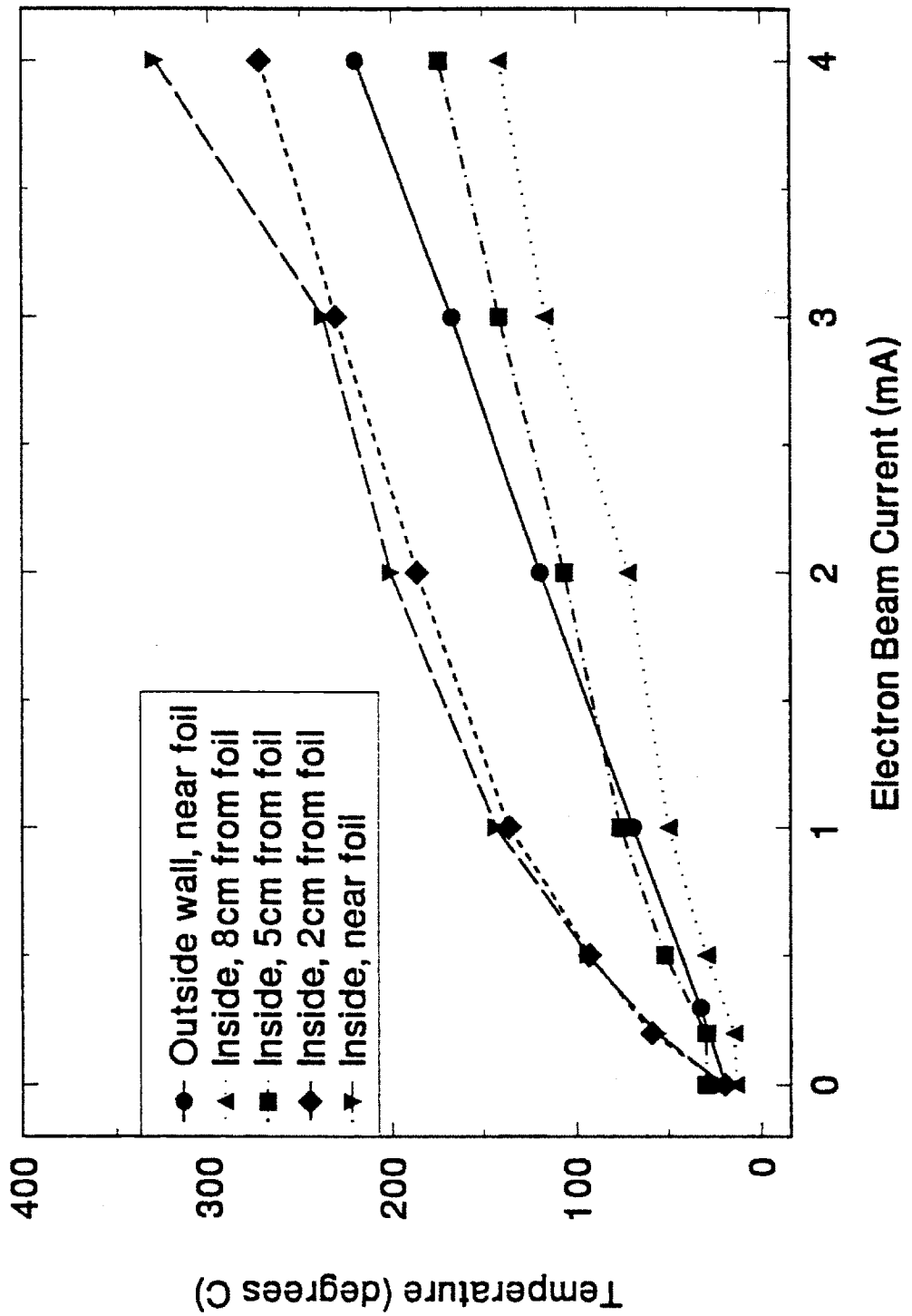
Figure 3.3: Temperature as a function of position inside and outside the cylindrical reaction chamber
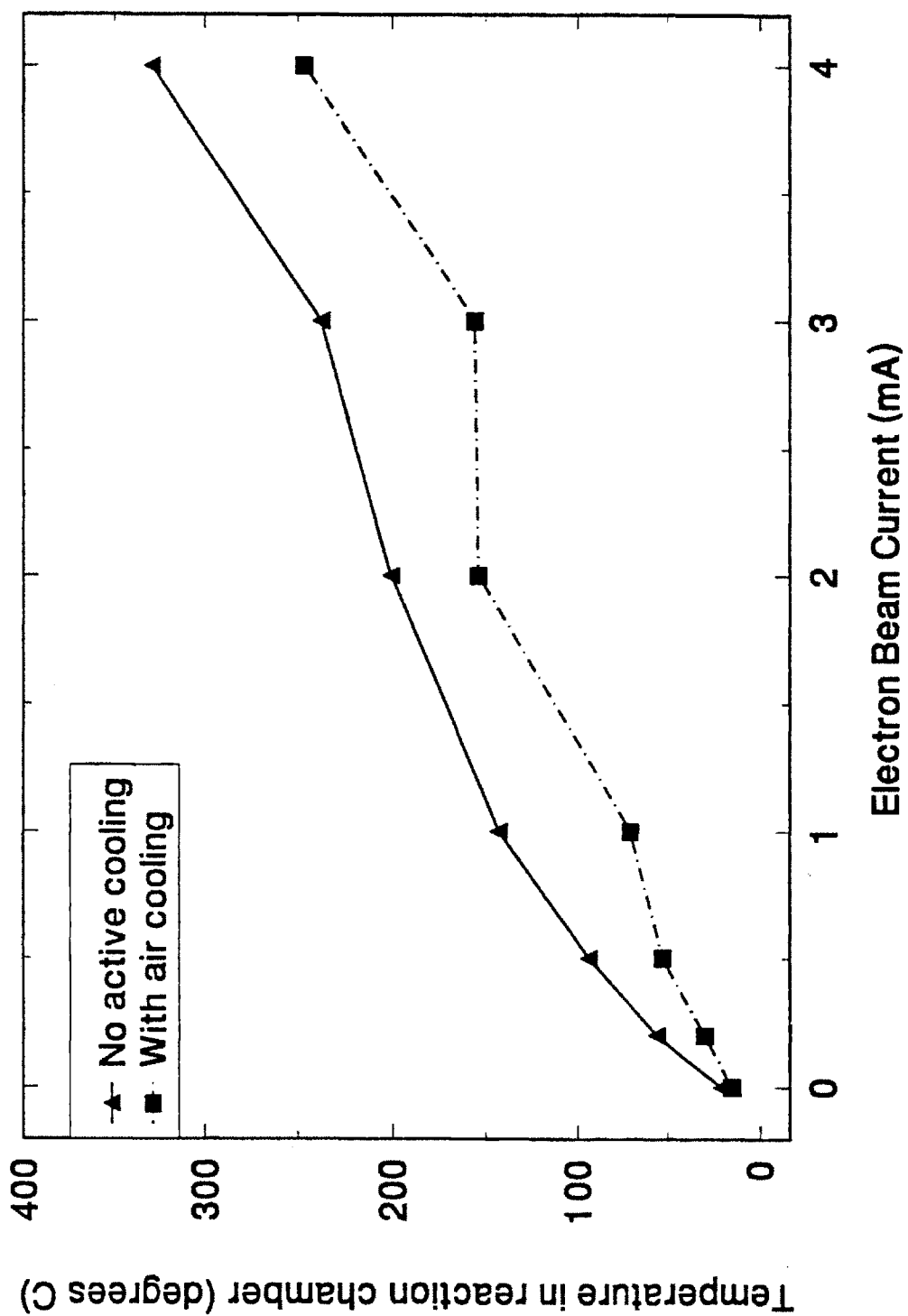
Figure 3.4: Temperature as a function of position inside the cylindrical reaction chamber, with auxiliary air cooling

Although the reactor did not suffer any apparent problems from the high temperature operation. it was decided that the reaction chamber should be cooled to prevent thermal decomposition effects from interfering with the plasma decomposition effects. A small blower and hose was connected to the reaction chamber to provide active air cooling. The temperature experiment was repeated inside the reaction chamber, and these results are shown in figure 3.4. The air cooling results in a 100°C temperature decrease inside the reaction chamber. Note that when a gas stream is flowing through the reactor, the temperature inside the reaction chamber should be much lower. Measurements of the outlet stream show no increase in temperature from ambient temperature once the stream has completely exited the reactor. Thus the air cooling system was determined to be sufficient.

3.3.2. Dosimetry in the Cylindrical Reaction Chamber

It is necessary to determine an accurate value for the electron beam dose to the plasma in order to perform any kinetic or energetic analysis of the data. Since the dose is not a quantity which can be measured directly in real time. it must be determined as a function of measurable quantities, such as electron beam current and gas stream flow rate. Koch performed extensive studies of the electron beam dose in the two previous reaction chambers using Monte Carlo simulation, aluminum plate calorimetry, nitrous oxide dosimetry, and facsimile paper radiography.

The dose is defined as the energy absorbed per mass of air:

$$D = \frac{Q}{m} \tag{3.1}$$

Since the reactor operates at steady state, the dose is equivalently given by the power deposited by the electron beam. divided by the mass flow rate of the gas stream,

$$D = \frac{\dot{Q}}{\dot{m}} = \frac{P}{\dot{m}} = \frac{P}{\rho \dot{F}} \tag{3.2}$$

Where P is the power deposited in the gas, and F is the volumetric flow rate. The mass flow rate of the gas stream entering the reactor is known: it remains to determine the power deposited in the plasma. This power is equal to the electron beam current which enters the reaction chamber. multiplied by the energy loss per electron in the air stream,

$$P = I_0 \, \Delta E \tag{3.3}$$

Note that the total power of the reactor is the measured current multiplied by the measured potential through which the electrons are accelerated. Using a maximum electron beam current of 4 mA. and a typical operating voltage of 100kV. the maximum total power of the reactor is 400 W. Only a small fraction of this power is actually deposited in the plasma. and it is this fraction which must be used to define the electron beam dose. The remainder of the energy is lost in the foil support grid, the foil itself, and the walls of the reaction chamber.

Koch proposed that the current which enters the reaction chamber is equal to the total measured current, multiplied by a factor τ,

$$I_0 = I \tau \qquad\qquad (3.4)$$

τ is a factor less than unity which accounts for the fraction of the electrons produced by the electron beam which are intercepted by the copper foil support grid. The total area irradiated by the electron beam is larger than the area of the emission source due to electron beam spreading inside the electron emission vacuum chamber. The electrons are emitted from a tungsten source which can be approximated as a 1" square. The window in the copper support plate through which the electrons pass is also approximately 1" square. Thus if the electron beam spreads in diameter after it is emitted and before it passes through the foil. some of the electrons will be intercepted by the copper plate and will not enter the reaction chamber. Further, the foil support grid itself consists of copper strips which are impermeable to electrons. These strips serve to support the thin aluminum foil and prevent it from breaking due to the one atmosphere pressure differential between the reaction chamber and the vacuum electron emission chamber. The total area irradiated by the electron beam inside the vacuum chamber was determined by Koch to be approximately 2 square inches using facsimile paper radiography. However, the total open area through which the electrons may pass is only 36.5% of this. Thus $\tau = 0.365$ and,

$$I_0 = 0.365 \, I \qquad\qquad (3.5)$$

The rest of the electron beam current is assumed to be completely intercepted by the copper support plate. This intercepted current is collected by the current meter however, and thus the electron beam current measured is actually the sum of this intercepted current and the current which enters the reaction chamber.

The energy deposited by the electrons in the reaction chamber is very difficult to determine. Koch used nitrous oxide dosimetry to quantify the energy deposition, but these results were eventually discarded since the data did not match the functional form of the theoretical predictions. Eventually, a one-dimensional Monte Carlo TIGER code was used to model the energy deposition in the reactor. An average energy deposition of 15 keV per electron was found for isothermal conditions at 398 K and 19 keV per electron was found at 298 K. The final number used by Koch for electron energy

deposition in the rectangular reaction chambers was the average of the two, or 17 keV. Using this value in equation (3.4),

$$D = 3.14 \cdot 10^{10} \frac{I}{\overset{.}{F}} \qquad (3.6)$$

with D in rads, I in mA. and F in ml/minute. The origin of the constant is given in Appendix B.

To determine the energy deposition in the cylindrical reaction chamber, the three dimensional ACCEPT code from the ITS series was used to perform Monte Carlo simulations. The ACCEPT code allows the reaction chamber geometry to be modeled exactly, without the one-dimensional simplifications of the TIGER code. Details of the physics used by the codes to determine energy deposition have been treated by Koch, and will not be repeated here.

Both the rectangular reaction chamber and the cylindrical reaction chamber were modeled. For both cases. the energy deposition was calculated in the aluminum foil, the side walls, the rear wall. and the gas itself. Electrons are counted as escaped if they are backscattered from the foil. lost in the front titanium plate, or if they penetrate through the reaction chamber. One million primary electrons were used in the simulations, each with 100 keV of initial energy. The run time on a Power PC workstation was approximately 5 hours for each trial. The results are summarized in table 3.1.

Chamber	Foil	Frame or Cylinder	Rear Plate	Escaped	Gas
Rectangular	54.9	11.4	13.8	8.0	**11.9**
Cylindrical	54.2	19.2	0.0	7.8	**18.8**

Table 3.1: Results of Monte Carlo Dosimetry calculations in the old and new reaction chambers. The results are given in keV per electron.

From table 3.1. it can be seen that the electron deposition in the gas for the rectangular reaction chamber was calculated to be 11.9 keV, or 30% less than that used by Koch. This is probably due to the fact that the ACCEPT code includes the effect of the side walls of the Pyrex frame in the model, whereas the 1-D TIGER code cannot include this. Nevertheless. for consistency with the results of Koch, the value of 17 keV per electron was used in the calculations of the electron beam dose for the experiments in the rectangular reaction chamber was used (TCA and TCE data).

The calculated energy deposition in the cylindrical reaction chamber was 19.2 keV per electron. or 70% more than in the rectangular chamber. This is primarily due to the fact that the length of the cylindrical reactor is six times longer in the direction of the electron beam than the previous reaction chamber. This means that most of the electrons will lose all of their energy in the air before being stopped by the back plate. From table 3.1. the energy deposited in the back plate for the previous design was 13.8 keV, which is

comparable to that deposited in the air. Thus half of the available energy was simply dumped into the plate. The new reaction chamber design allows the use of more of this energy, so higher flow rates or higher reactant concentrations can be used. The results of the ACCEPT simulations show that more energy was deposited in the cylindrical reaction vessel than in the parallel walls of the rectangular design. This is because the rectangular design is completely open to flow at the top and bottom; there are no walls there to intercept the electrons. In the cylindrical design, the top and bottom are blocked, with only a small hole at the top for the outlet flow. The inlet is through the back of the reactor. Thus the cylinder stops more of the electrons than the two parallel Pyrex plates. Graphical representations of the energy deposition in both reaction chamber geometries are shown in figure 3.5.

Using the value of 19.2 keV per electron energy deposition in equation (3.5) gives

$$D = 3.47 \cdot 10^{10} \frac{I}{\dot{F}} \tag{3.7}$$

This is the formula used to calculate the electron beam dose with the cylindrical reaction chamber design.

3.4 Gas Analysis System

The outlet gas stream from the EBGPR is analyzed on-line using a Hewlett Packard 5890 gas chromatograph and a HP-5971-A mass spectrometer. All quantitative analysis is performed using the MS; the GC is used only for chromatographic separation of the components of the gas stream. The mass spectrometer is calibrated using the certified calibration cylinders of the various VOCs. The GC/MS system is computer controlled from Hewlett-Packard Chemstation software.
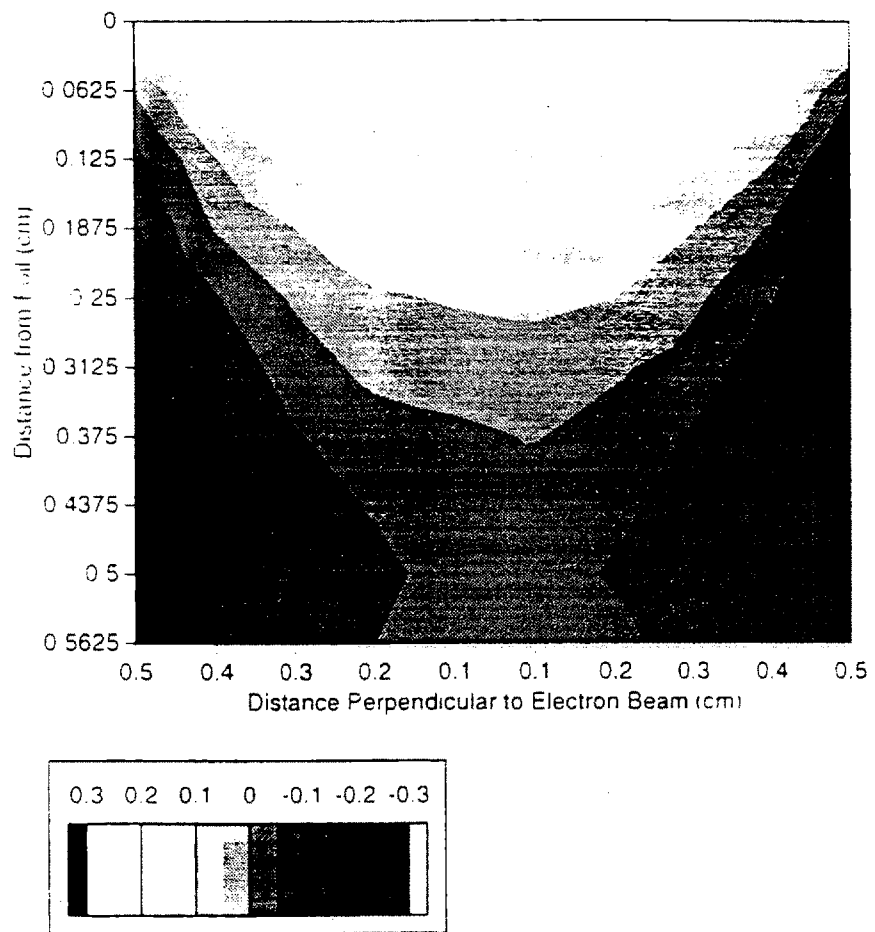
Figure 3.5a: Energy deposition in the old rectangular reaction chamber. Light areas correspond to high energy density, dark areas correspond to low energy density. The integral total of the energy deposited in the reaction volume in this configuration is 11.9 keV
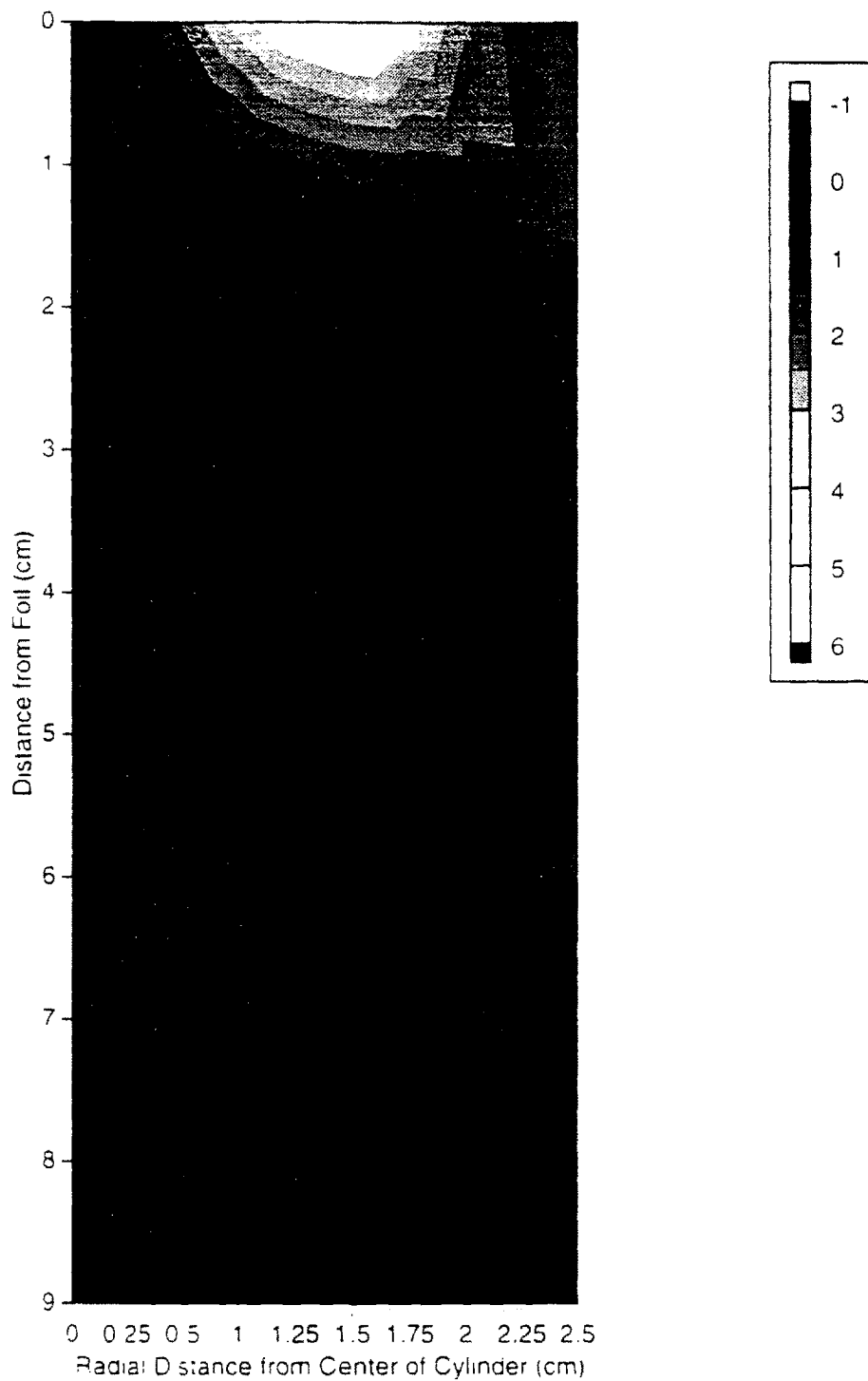
59

Figure 3.5b: Energy deposition in the new cylindrical reaction chamber. Light areas correspond to high energy density, dark areas correspond to low energy density. The integral total of the energy deposited in the reaction volume in this configuration is 18.8 keV

4. Results and Discussion

4.1. General Remarks

Over 4000 data points were taken in the period from September 1994, to December 1995, using the EBGPR. Over 2000 of these contributed materially to the present study, and thus represent the utility of the EBGPR in performing rapid and accurate experiments to determine the plasma chemistry kinetics of halogenated VOC reactions. The results of these experiments will be presented in this chapter, along with qualitative and quantitative interpretation. Section 4.2 will explain some of the aspects of plasma chemistry applicable to all of the reactions.

Sections 4.3-4.8 will present detailed results for the six chemicals of interest in this study. For consistency and ease of interpretation, the same format will be used in each of these sections. First, an example of the outlet concentration as a function of electron beam dose data is given. This data is then analyzed using the differential approach as described in Section 2.3 to determine approximate orders of reaction, approximate rate constants, and to see if inhibition effects or other factors are important. If the reaction kinetics appear to be inhibited, equation (2.69) will be fit to the data to obtain an estimate of the magnitude of the inhibition and the β'-value for the decomposition. If the data does not appear inhibited, equations (2.11) and/or (2.13) will be fit to the data to obtain values for α and $(G_0 K)$. In either case, Rosocha β-values are then be determined using equation (2.14) and compared with literature values, if available. For convenience, β-values will be converted to G-values using equation (2.77), if appropriate. The reaction products identified in the study are discussed, along with the relation between the reaction products and the kinetic results. Finally, reaction pathways are proposed to account for the reaction products formed and the kinetic behavior observed.
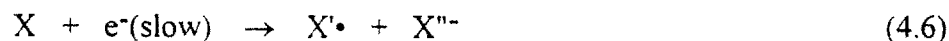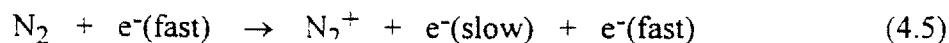
4.2 General Plasma Chemistry

The reactions which take place in the EBGPR are different from traditional gas phase chemical reactions, due to the abundance of ions, electrons, and radicals present in the plasma. The plasma in the EBGPR is assumed in this study to be non-equilibrium; that is, the electron temperature is higher than the ion temperature everywhere in the plasma. This is not justified quantitatively here, since a discussion of this has been given by Koch. Qualitatively, one can say that since the plasma is being driven by a high energy electron beam, there is an abundant source of high energy electrons in the plasma. These fast electrons produce secondary electrons by impact ionization, which also leads to fast electrons and relatively immobile ions. So the non-equilibrium plasma assumption is probably well justified. Also, non-equilibrium plasmas are predicted to be much more energy efficient at decomposing compounds which have high electron capture cross

61

sections; the experimentally demonstrated energy efficiency of the EBGPR as compared to thermal decomposition processes is also a justification of the non-equilibrium plasma assumption.

This assumption allows one to rule out chemical reaction mechanisms which occur due to energetic ions. or mechanisms which have high activation energy steps and thus require high temperatures to proceed to an appreciable extent. This is not to say that ions do not play a role in the decomposition processes, only that processes which require very energetic ions or molecules are probably not important. Focusing then on electron initiated decomposition mechanisms, the energy from the beam is directed toward the production of reactive radical species from the VOC molecules by two possible processes. In the first process, proposed by Slater,[5] energy is transferred to the species in the gas with the lowest ionization potential through rapid charge transfer with the carrier gas ions,

$$N_2 + e^-(\text{fast}) \rightarrow N_2^+ + e^-(\text{slow}) + e^-(\text{fast}) \qquad (4.1)$$

$$N_2^+ + N_2 \rightarrow N_4^+ \qquad (4.2)$$

$$N_4^+ + X \rightarrow X^+ - 2\,N_2 \qquad (4.3)$$

$$X^+ + e^-(\text{slow}) \rightarrow X'\bullet + X''\bullet \qquad (4.4)$$
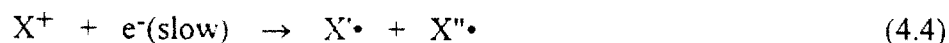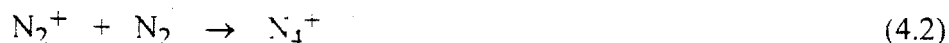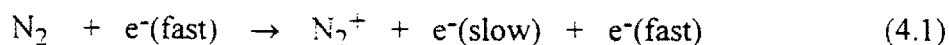
Here. X is a species in the gas with lower ionization potential than the carrier gas (such as most chlorinated VOCs). and $X'\bullet$ and $X''\bullet$ are reactive radicals produced by dissociative recombination. reaction (4.4). The second possible process, illustrated by Koch, is one by which the reactive radicals are produced through dissociative electron attachment followed by charge exchange,
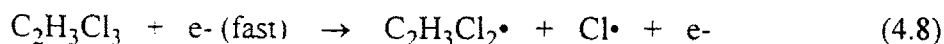
$$N_2 + e^-(\text{fast}) \rightarrow N_2^+ + e^-(\text{slow}) + e^-(\text{fast}) \qquad (4.5)$$

$$X + e^-(\text{slow}) \rightarrow X'\bullet + X''^- \qquad (4.6)$$

$$X''^- + M \rightarrow M^- + X''\bullet \qquad (4.7)$$

Both dissociative recombination and dissociative electron attachment may produce the same reactive radicals. so either process may initiate the decomposition reaction.
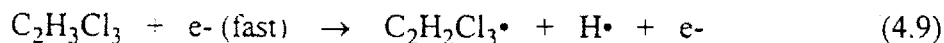
Since most VOCs have lower ionization potentials than nitrogen or oxygen molecules, and since their cross sections for dissociative electron attachment are higher than for nitrogen or oxygen molecules, the energy from the electron beam is directed preferentially towards dissociation of the VOC molecules into reactive radicals such as $Cl\bullet$. By directing the energy toward the VOC molecules, the cold electron beam generated plasma is more energy efficient for chlorinated VOC decomposition than thermal processes.

The two processes above, dissociative recombination and electron attachment, may produce reactive radicals such as Cl• or O•. These radicals may be produced directly from a molecule of the VOC in the air stream, in the case of Cl•, or from oxygen molecules, in the case of O•. These radicals then attack other VOC molecules, and cause further decomposition reactions.

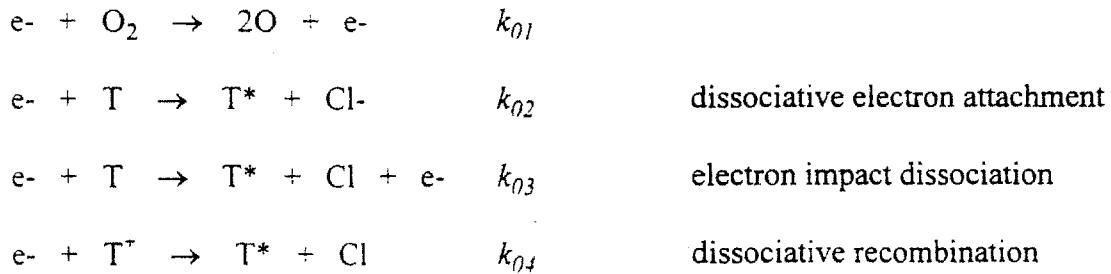An alternative method of decomposition in a non-equilibrium plasma is electron impact dissociation, illustrated here for TCA,

$$C_2H_3Cl_3 + e\text{-(fast)} \rightarrow C_2H_3Cl_2\bullet + Cl\bullet + e\text{-} \qquad (4.8)$$

or

$$C_2H_3Cl_3 + e\text{-(fast)} \rightarrow C_2H_2Cl_3\bullet + H\bullet + e\text{-} \qquad (4.9)$$

These reactions may seem qualitatively similar to dissociative electron attachment, but there is an important difference in the physics of the two processes. In dissociative electron attachment, the electron becomes strongly bound to an atom on the molecule; typically a chlorine atom for the chemicals of interest here. The energy from the electron is deposited in the bond structure of the molecule, causing loosening and extended vibrations of the molecule. The most energetically accessible route to dissipate this energy, in the absence of a collision, is for the carbon-chlorine bond to rupture, resulting in an organic radical and a stable chlorine ion.

In the case of electron impact dissociation, an energetic electron collides with a VOC molecule, giving a portion of its energy to the molecule. The electron does not attach to an atom. The energy in the molecule is again dissipated by a rupture of the least stable bond in the molecule, which in the cases of interest here is usually a carbon-chlorine bond. The fact that these processes are distinct has been proven experimentally; reaction cross sections are shown to have two resonance peaks as a function of electron energy: one for dissociative electron attachment, and a peak at higher electron energy for electron impact dissociation.[78]

Now that the initiation steps have been considered, the propagation and inhibition of the reaction mechanism can be explored. In general, a VOC molecule can be decomposed by an electron, by an oxygen radical, or by a chlorine radical. Oxygen radicals can be formed from electron impact dissociation in the plasma. Chlorine radicals can be formed by dissociative electron attachment, the decomposition of activated species formed by electron-VOC interactions, or from oxygen or chlorine atom induced VOC decomposition. Inhibitor species (denoted as I below) can be formed from any of the above mechanisms. Inhibitors can scavenge chlorine or oxygen radials which are useful in aiding VOC decomposition. This complicated set of reactions is illustrated below to describe the decomposition of any generic VOC, T:
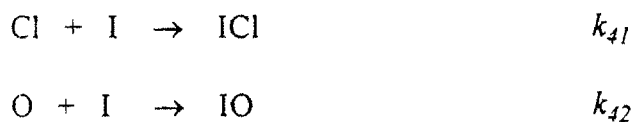
<u>initiation steps:</u>

$$e\text{-} + O_2 \rightarrow 2O + e\text{-} \qquad k_{01}$$

$$e\text{-} + T \rightarrow T^* + Cl\text{-} \qquad k_{02} \qquad \text{dissociative electron attachment}$$

$$e\text{-} + T \rightarrow T^* + Cl + e\text{-} \qquad k_{03} \qquad \text{electron impact dissociation}$$

$$e\text{-} + T^+ \rightarrow T^* + Cl \qquad k_{04} \qquad \text{dissociative recombination}$$

<u>decomposition steps</u>

$$T^* \rightarrow P_{11} \qquad k_{11}$$

$$\rightarrow P_{12} + I \qquad k_{12}$$

$$\rightarrow P_{13} + Cl \qquad k_{13}$$

$$Cl + T \rightarrow P_{21} \qquad k_{21}$$

$$\rightarrow P_{22} + I \qquad k_{22}$$

$$\rightarrow P_{23} + Cl \qquad k_{23}$$

$$O + T \rightarrow P_{31} \qquad k_{31}$$

$$\rightarrow P_{32} + I \qquad k_{32}$$

$$\rightarrow P_{33} + Cl \qquad k_{33}$$

<u>inhibition steps</u>

$$Cl + I \rightarrow ICl \qquad k_{41}$$

$$O + I \rightarrow IO \qquad k_{42}$$
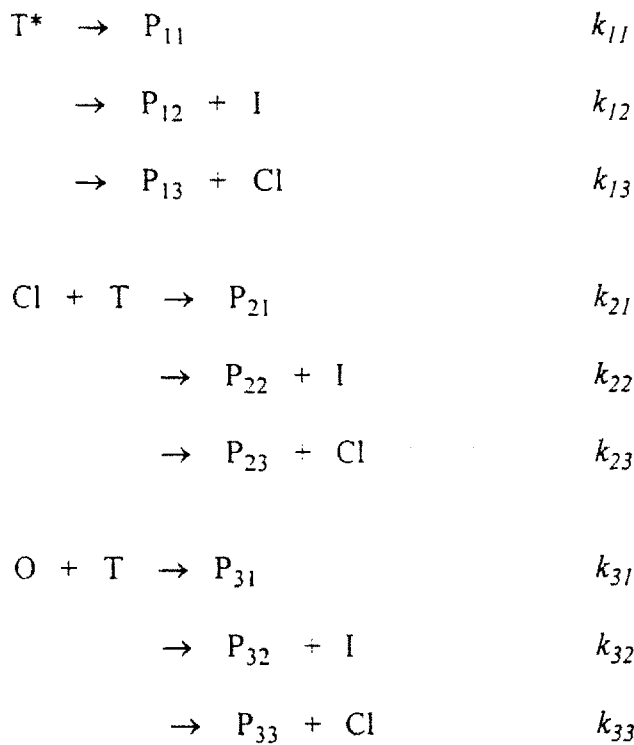
This general kinetic formulation of course cannot be solved analytically. The numerical simulation of a system of reactions on a commercial code such as CHEMKIN II requires accurate values of the rate constants for these reactions, for each VOC of interest.

Numerical methods are not employed in this study; instead an analytical result was derived in Section 2.2.3. for a very simplified form of the reaction system above. The effect of oxygen radical and chlorine radical decomposition were lumped together in that model, and were assumed not to influence one another. In effect, the INHIBIT model derived in that section assumed all of the reaction rates in the above system of equations were negligible. except for:

- $k_{01}, k_{02}, k_{03}, k_{04}$ (collectively lumped together to produce X_1 in section 2.2.3)
- k_{23} and k_{33} (collectively called k_1 in section 2.2.3)
- k_{21} and k_{31} (collectively called k_2 in section 2.2.3)
- k_{42} and k_{41} (collectively called k_3 in section 2.2.3)

Though this simplified model may be a good approximation in some cases. through the results presented in the rest of this chapter it will be seen that at high fractional decomposition. the kinetics of the decomposition are highly inhibited. This strongly non-linear behavior is not well represented by the simple INHIBIT model. and a formal treatment should include a numerical analysis of the complete reaction system given above.

However, for fractional decompositions below 90%, the inhibition is not extremely strong. and the observed kinetics are not far removed from first order. The slight non-linearity allowed by the INHIBIT model fits the data quite well. and is certainly an improvement over the first-order uninhibited reaction kinetics assumed by previous researchers.

4.2.1 Plasma Chemistry of Ethanes and Ethylenes

The mechanisms proposed in the following section are a combination of those found in the literature for high temperature and radiation induced oxidation, and new reaction pathways proposed by the author. In general, deviations from literature mechanisms are presented for several reasons: 1) when not all of the observed reaction products are accounted for by the literature mechanisms. 2) when products predicted by the literature mechanisms are not observed in his study, and 3) when the peculiarities of the EBGPR make a traditional reaction sequence unlikely.

For the chlorinated ethanes. extensive previous work has been performed on the mechanisms of TCA decomposition, but few literature references are available for 1,1-dichloroethane and ethyl chloride. For the latter two compounds. the mechanisms proposed are original in this work.

For the chlorinated ethylenes. a comprehensive review of the oxidation of these compounds was published by Sanheuzea.[88] There are several aspects of that review of interest to the present study. including two different methods of halogenated ethylene oxidation: 1) Cl atom sensitized oxidation in the presence of molecular oxygen. and 2) O^3P induced oxidation in the presence of molecular oxygen. In the context of EBGPR studies. the first mechanism corresponds to dissociative electron attachment to a chlorinated ethylene. followed by reaction of this chlorine atom of other molecules on the

chlorinated ethylene. The second mechanism corresponds to the productions of oxygen radicals by the electron beam, which react with the chlorinated ethylenes without any electron attachment event occurring. The relative reactivities of TCE, DCE, and VC to both of these types of decomposition were listed by Sanheuza, as well as for several other compounds and mechanisms not of interest here. In brief, it was noted that DCE and VC have almost equal reactivities with both O^3P and Cl radicals. TCE, on the other hand, reacts much more readily with Cl radicals than with O^3P. Therefore, for TCE the reaction mechanism presented will concentrate on Cl sensitized oxidation occurring through electron attachment, whereas DCE and VC mechanisms will include both decomposition pathways.

4.3. 1,1,1-Trichloroethane

4.3.1 Kinetic Analysis

A graph of outlet stream TCA concentration versus electron beam dose is shown in figure 4.1 for several inlet stream concentrations. Greater than 99% decomposition of TCA is achieved for the lower concentration streams at flow rates up to 3 liters/min. The higher concentration streams do not achieve 99% decomposition at this flow rate because of the limited power that the electron beam deposits in the plasma. At lower flow rates, streams up to 3000 ppm can realize 99% decomposition.

Thirty-two curves similar to those shown in figure 4.1 were generated for TCA inlet concentrations from 100 to 3000 ppm. These curves were analyzed by the differential kinetic method, as described in Section 2.3. Both the order with respect to time approach and the order with respect to concentration approaches were used. As stated in Section 2.3, the two orders are not always the same for a given reaction. If the order with respect to time is greater than the order with respect to concentration, then most likely some species being produced in the reaction is inhibiting further reaction of the original reactant. Conversely, if the order with respect to time is smaller than the order with respect to concentration, then some reaction product is causing the rate of reaction to increase. This activation by the products of the reaction is known as autocatalysis, and the reaction is said to be autocatalytic.

A computer program DERIVS was written to evaluate the slope of each of the thirty-two curves at each of the data points. The initial slope from each line was used to calculate the order with respect to concentration. The slopes along a given line were used to calculate the order with respect to time, and the results from all thirty-two curves were averaged. Figure 4.2 shows the initial rates calculated from the curves as a function of initial concentration of TCA. If the reaction rate has an order with respect to TCA, this plot should be linear. This result comes from the reaction rate expression, equations (2.73-2.74):

$$r = -\frac{d[A]}{dD} = k[A]^n \qquad (4.10)$$

66

$$\ln r = \ln k + n \ln [A] \qquad (4.11)$$

Although the fit to a straight line in this case is not great, a definite trend is apparent in figure 4.2, which can be approximated as a straight line. In this case, the slope of the line gives the order with respect to concentration, n_c, which is calculated to be 0.46, with a correlation coefficient of 0.82. This correlation coefficient is reasonable, considering the difficulty in accurately measuring the initial slope of the curve. However, since half-integer or integer reaction rate orders are the only common orders reported, this result will be rounded to $n_c = 0.5$. The intercept of this line with the reaction rate axis gives the rate constant, k.

$$\ln k = 1.89 \quad \Rightarrow \quad k = 6.62 \, \text{Mrad}^{-1} \, \text{ppm}^{1/2}$$

Note that one half-order rate coefficients typically have units of $\sec^{-1}$ concentration$^{1/2}$, however in this case the electron beam dose is the relevant quantity and not time. The data taken in this study was calculated using the Mrad as the unit of electron beam dose to be consistent with the results of Koch. Other research groups use Joules/kg or Joules/liter as a measure of energy dose, so it will be noted here that:

$$1 \, \text{Mrad} = 10^4 \, \text{J/kg} = 12.89 \, \text{J/liter air} \quad \text{at} \quad \text{STP}$$

The order with respect to time analysis was performed on each curve of TCA concentration versus electron beam dose. A representative plot is shown in figure 4.3. The order with respect to time, n_t, and the rate constant, k, were calculated for each curve and the results averaged, to give:

$$n_t = 1.36 \pm 0.11$$

$$\ln k = -4.1 \pm 1.02 \quad \Rightarrow \quad k = 5.97 * 10^{-3} - 4.60 * 10^{-2} \, \text{Mrad}^{-1} \, \text{ppm}^{-1/2}$$

Two results of the differential analysis are immediately apparent: n_t is significantly greater than n_c, and the values of the rate constants determined by the two methods are quite different. Recall that if n_t is greater than n_c, the reaction rate is falling off more rapidly than the initial rate, and thus the reaction is inhibited. This result is justified by the reaction mechanism outlined below.

But which rate constant should be used, the one found from the n_c plot, or the n_t plot? First, it should be noted that in kinetic analyses rate constants are often known only to within an order of magnitude, and sometimes only to within several orders of magnitude. Rate constants can vary over forty orders of magnitude, from very slow organic reactions to very fast ionic reactions. Thus a difference of two or three orders of magnitude between the techniques is not at all remarkable. Nevertheless, for practical

design calculations. it is the order with respect to time analysis which is more relevant. The n_t calculation describes more accurately the time evolution of a reaction, which is important when designing a chemical reactor. This rate expression is used in conjunction with the ideal performance equation for the EBGPR derived in Section 2.2.2 to determine the reactor power needed to achieve a desired conversion of the reactant. The final rate expression is thus:

$$C_2H_3Cl_3 \rightarrow \text{products}$$

$$r = -1.7 * 10^{-2} [C_2H_3Cl_3]^{3/2} \quad \text{ppm/Mrad} \hspace{3cm} (4.12)$$

Though the n_t calculation is more relevant to engineering calculations, the n_c calculation is also important. In addition to giving information about the influence of reaction products on reaction rate (inhibition or autocatalysis), the order with respect to concentration gives information about what the reaction rate should be in the absence of products. If this order is non-integer, then the reaction pathways are likely complex and cannot be reduced to a simple reaction. Whether this order is greater or less than unity also helps in the analysis of a reaction mechanism. A high order means that more than one TCA molecule may play a role in the decomposition of a molecule, whereas an order less than one indicates that the decomposition of one molecule may aid the decomposition of another molecule, assuming no reaction products were to build up and influence the mechanism. These results will be taken into account when reaction pathways for TCA decomposition are proposed below.

Since n_c is less than n_t in this case, and the reaction thus appears to be inhibited, the INHIBIT model. equation (2.69) was fit to the 32 concentration versus dose curves. The best fit parameter for K (the ratio of the reaction rates for the forward and inhibition reactions) is:

$$K = 0.18 \pm 0.1$$

This ratio shows the importance of inhibition by products on the reaction rate. It should be noted here that in the INHIBIT model, the value of K which leads to greatest non-linearity in the plots is approximately K=0.30. For K much higher than 0.50 or less than 0.10. the kinetics again appear to be inhibited. This small range for K is due to the fact that the simplified reaction rate equations do not allow strongly non-linear behavior.

A value for K in this non-linear region indicates that inhibition is important in this mechanism. This is consistent with the large difference between n_t and n_c found in the differential kinetic analysis. also indicating that inhibition was an important factor. A discussion of how this inhibition can occur is given below in the discussion of reaction pathways.

The second parameter in the inhibitor analysis is the value of β' in equation (2.69). The value of β' was determined from each TCA concentration versus electron beam dose curve using K=0.18. A graph of β' (or pseudobeta) is shown in figure 4.4a as a function of inlet TCA concentration. β' appears to have an approximately linear dependence on TCA

68

concentration. though there is a lot of scatter in the data. Nevertheless, as a first approximation, β' can be given by:

$$\beta' = 0.00438 * T_0 + 2.11 \qquad \text{Mrad} \qquad (4.13)$$

with T_0 in ppm. Using this expression for β' and the constant value of K, equation (2.69) can be used to calculate the dose required for TCA decomposition as a function of inlet concentration:

$$\frac{[T]}{[T_0]} \cdot \frac{\overline{K+1}}{\left(K + \frac{[T]}{[T_0]} \right)} = \exp\left(-\frac{D}{2 \cdot \beta'} \right) \qquad (4.14)$$

This analytic function was used to calculate the continuous curves given in figure 4.4b. The same inlet concentrations used for the experimental data points in figure 4.1 were used to create figure 4.4b. and comparing the two shows that equation (4.14) generally fits the data rather well.

Using these same parameters again in equation (2.70). the energy expense. ε. was calculated as a function of the inlet concentration T_0. and the desired fractional decomposition η:

$$\varepsilon = \frac{1}{\eta T_0} \frac{M_c}{N_A} 2 \cdot \beta' \left[\ln\left(\frac{1}{1-\eta} \cdot \sqrt{1 - \frac{\eta}{K+1}} \right) \right] \qquad (4.15)$$

The results are given in figure 4.8.

For comparison with previous literature results. Rosocha β-values were calculated from the data using equation (2.14)

$$x_j = x_{jo} \exp\left(-D \big/ \beta \right) \qquad (4.16)$$

In figure 4.1. one can see that the simple exponential dependence of TCA concentration on electron beam dose is only valid for low fractional decomposition. typically less than 90%. For decomposition greater than 90%. the inhibition of the reaction by decomposition products is important. and equation (4.16) gives a poor fit to the data. So to generate β-values. equation (4.16) was fit to all of the TCA curves. but only using data up to 90% decomposition. where an exponential dependence fits the data well. This is consistent with the procedures of Rosocha[10,12,26,27,70] and Penetrante [22,38,39,41]. since in their experiments the fractional decomposition typically did not exceed 90%. The resulting value of β for each curve is shown in figure 4.5 as a function of the inlet TCA concentration. A linear fit to this data was performed. with the result:

$$\beta = .00787 \, [T_o] + 1.76 \qquad\qquad (4.18)$$

with T_o in ppm. Thus unlike in the previous literature studies, in this case beta is not a constant; in fact it has nearly a linear dependence on inlet concentration, given by the above equations. Rosocha[13] reports $\beta = 16.1$ Mrad for decomposition of TCA, in a dielectric barrier discharge, over a similar range of concentrations. Note that the reported β-value was given in J/L, and was converted to Mrad using the above conversion factor. In this work, β shows a linearly increasing dependence on inlet concentration, which intersects the value found by Rosocha at $[T_o] \approx 2100$ ppm. Thus below 2100 ppm, the electron beam generated plasma reactor is more energy efficient than the dielectric barrier discharge for TCA decomposition.

Using equation (2.77) to calculate the G-value for TCA,

$$G_{TCA} = 4.4 \text{ molecules} / 100 \text{ eV} \qquad\qquad (4.19)$$
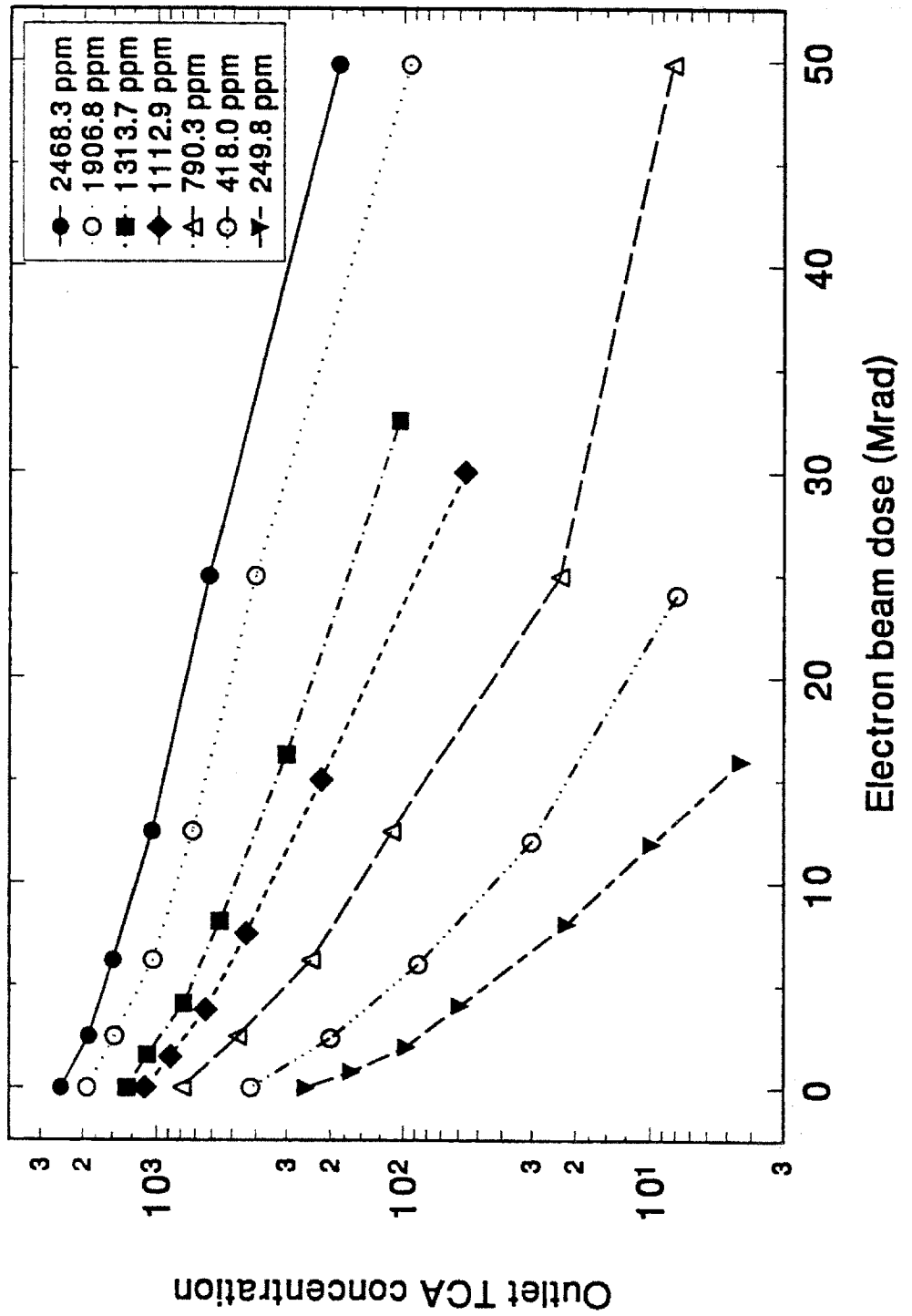
Figure 4.1: 1.1.1 Trichloroethane outlet concentration as a function of electron beam dose.
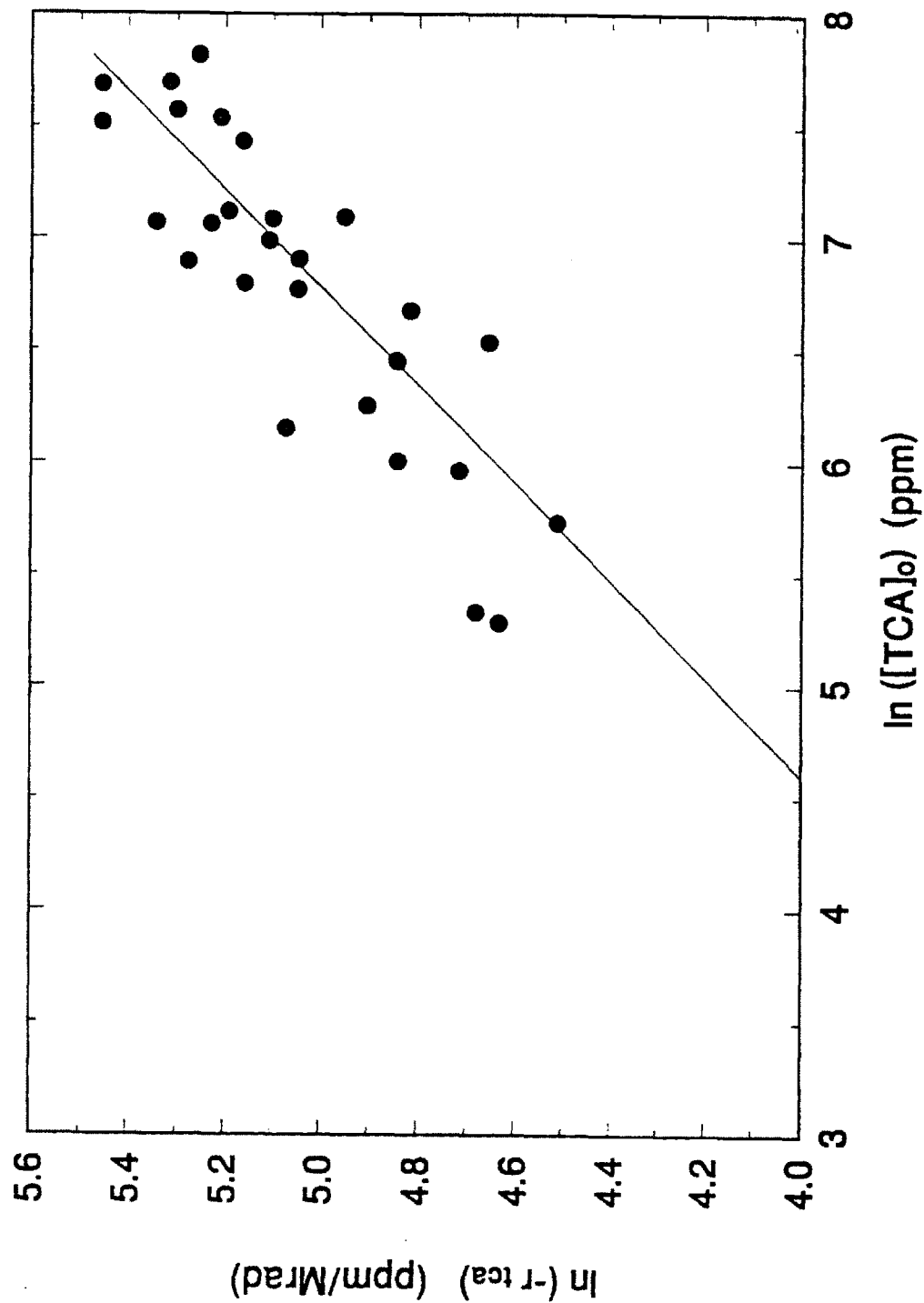
Figure 4.2: Differential kinetic analysis of TCA decomposition. This graph shows the initial reaction rate, $-r = \dfrac{d[TCA]}{dD}$, as a function of initial TCA concentration. The slope of this line gives the order with respect to concentration, n_c, and the intercept with the Y-axis gives the rate constant, k.
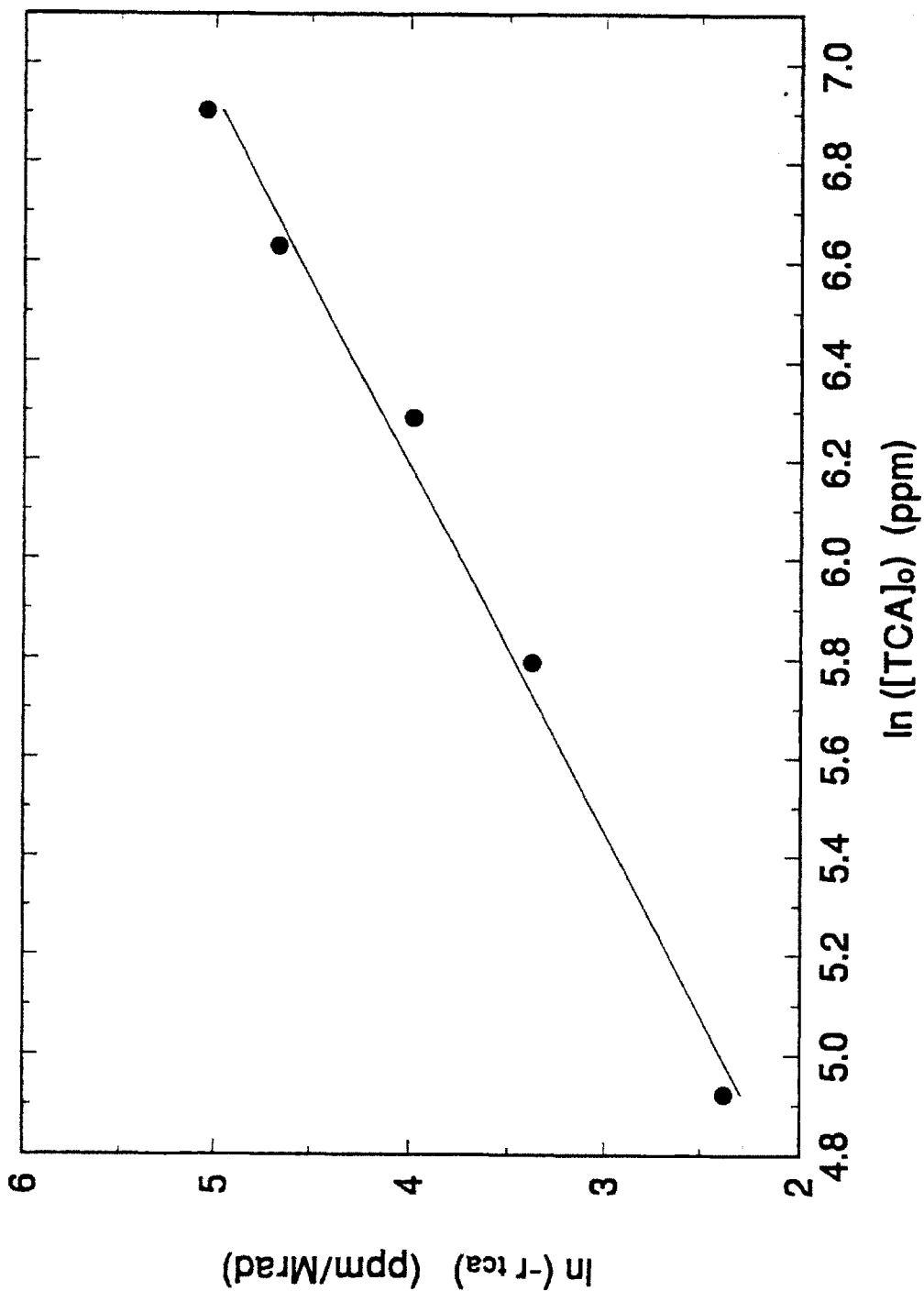
Figure 4.3: A representative graph of one run of TCA, showing the actual reaction rate as a function of TCA concentration, as the reaction proceeds. The slope of this line gives the order with respect to time, n_t, and the intercept with the Y-axis gives the rate constant, k.
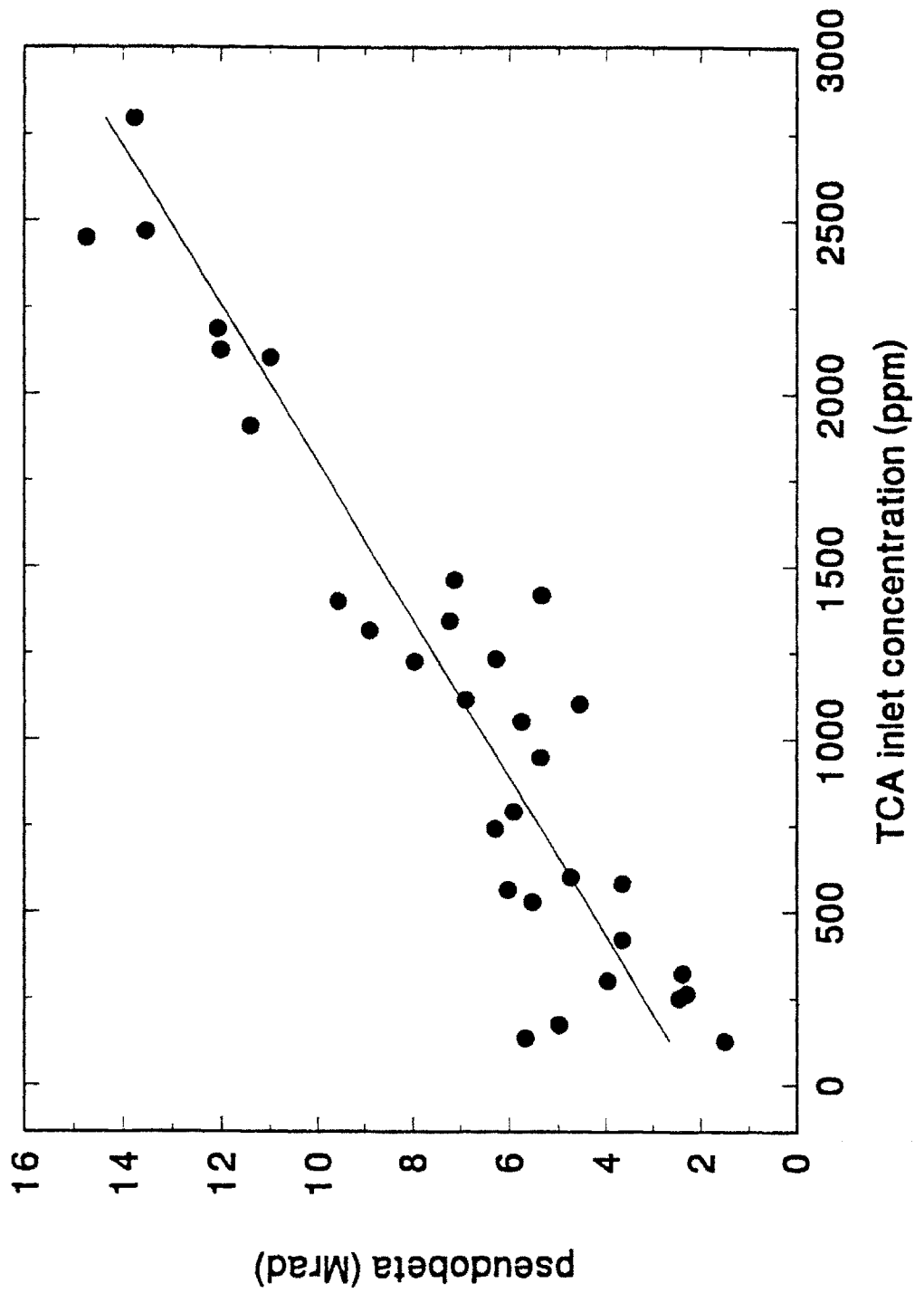
Figure 4.4a: Graph of pseudo-β or β', versus TCA inlet concentration from INHIBIT model fit.
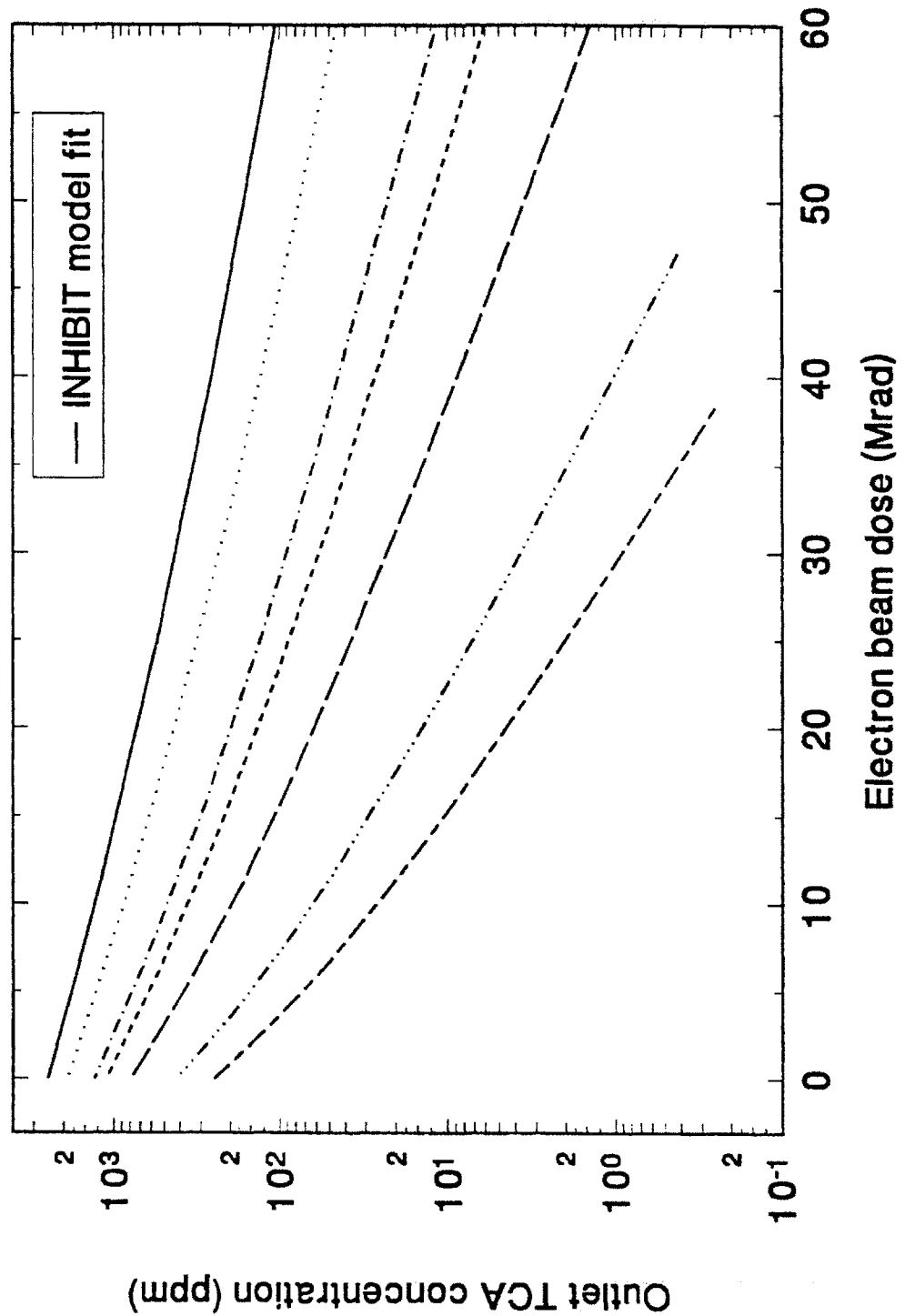
Figure 4.4b: Graph of calculated TCA concentration versus electron beam dose curves from best fit INHIBIT model. The initial concentrations are the same as the experimental data given in figure 4.1 so the two graphs may be compared.
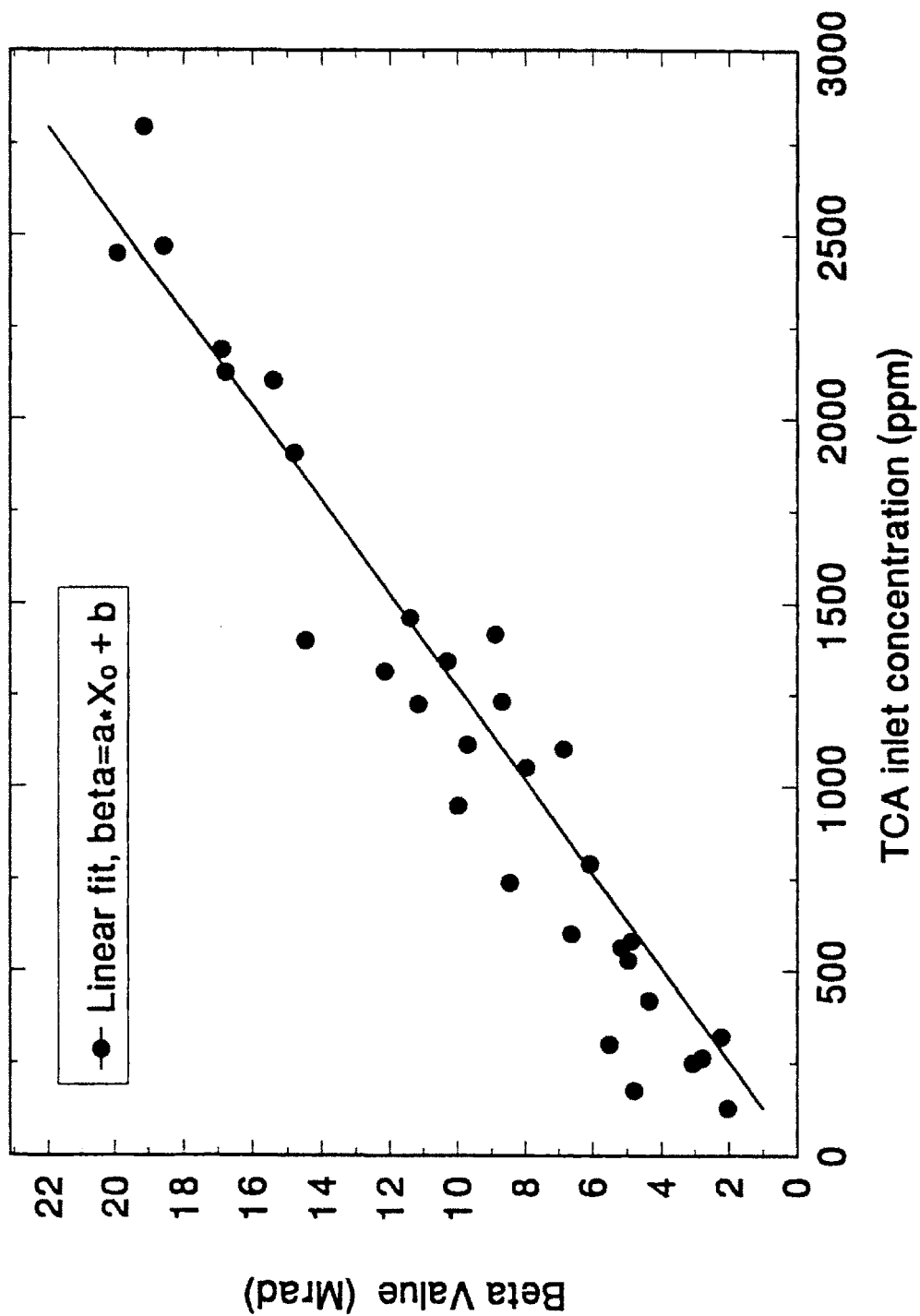
Figure 4.5: Graph of the Rosocha β-value versus inlet TCA concentration
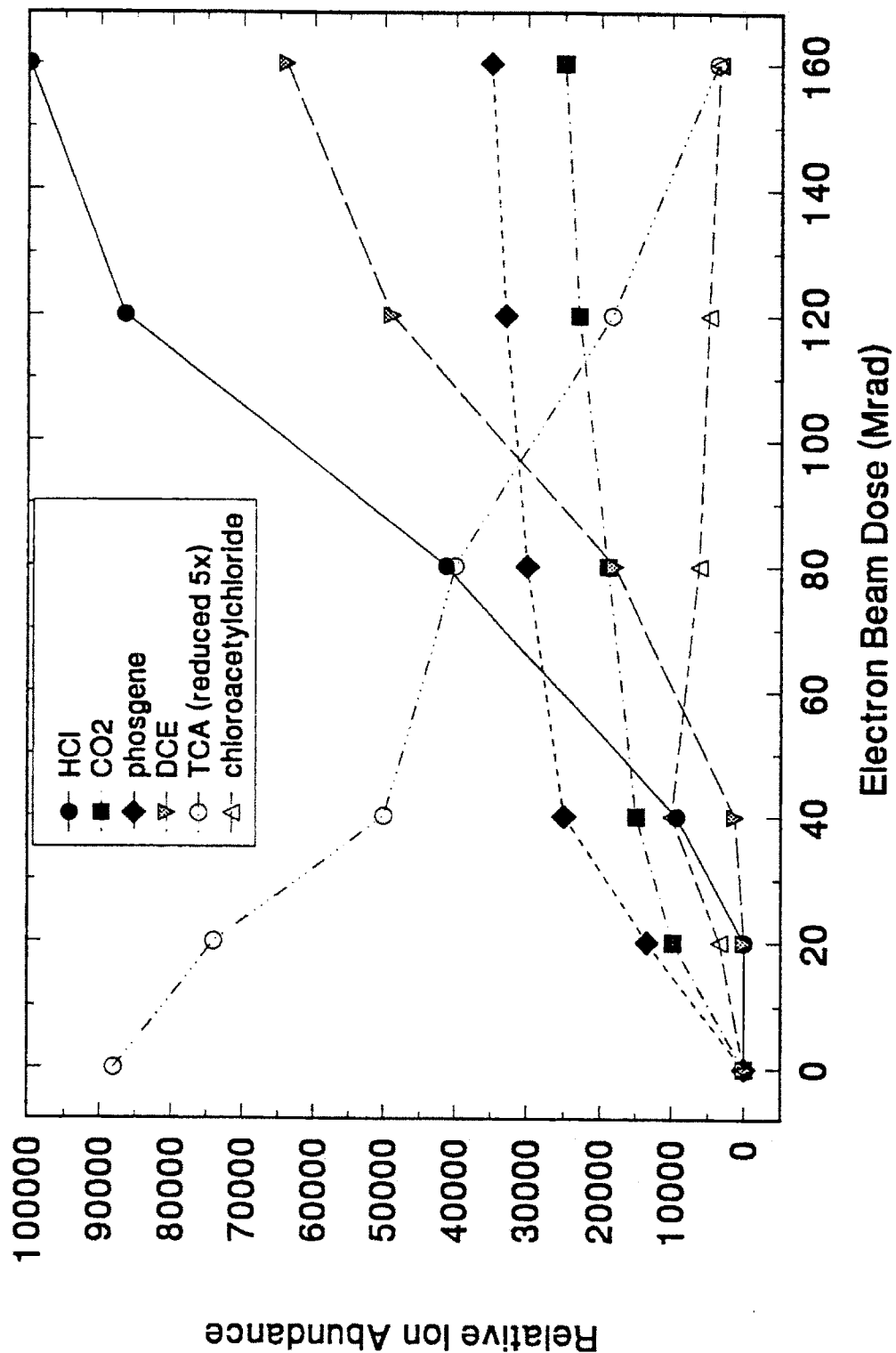
Figure 4.6: Major reaction products of TCA decomposition. The ion abundances from the mass spectrometer peaks are given as a function of electron beam dose. The ion abundance is approximately linearly proportional to the concentration.
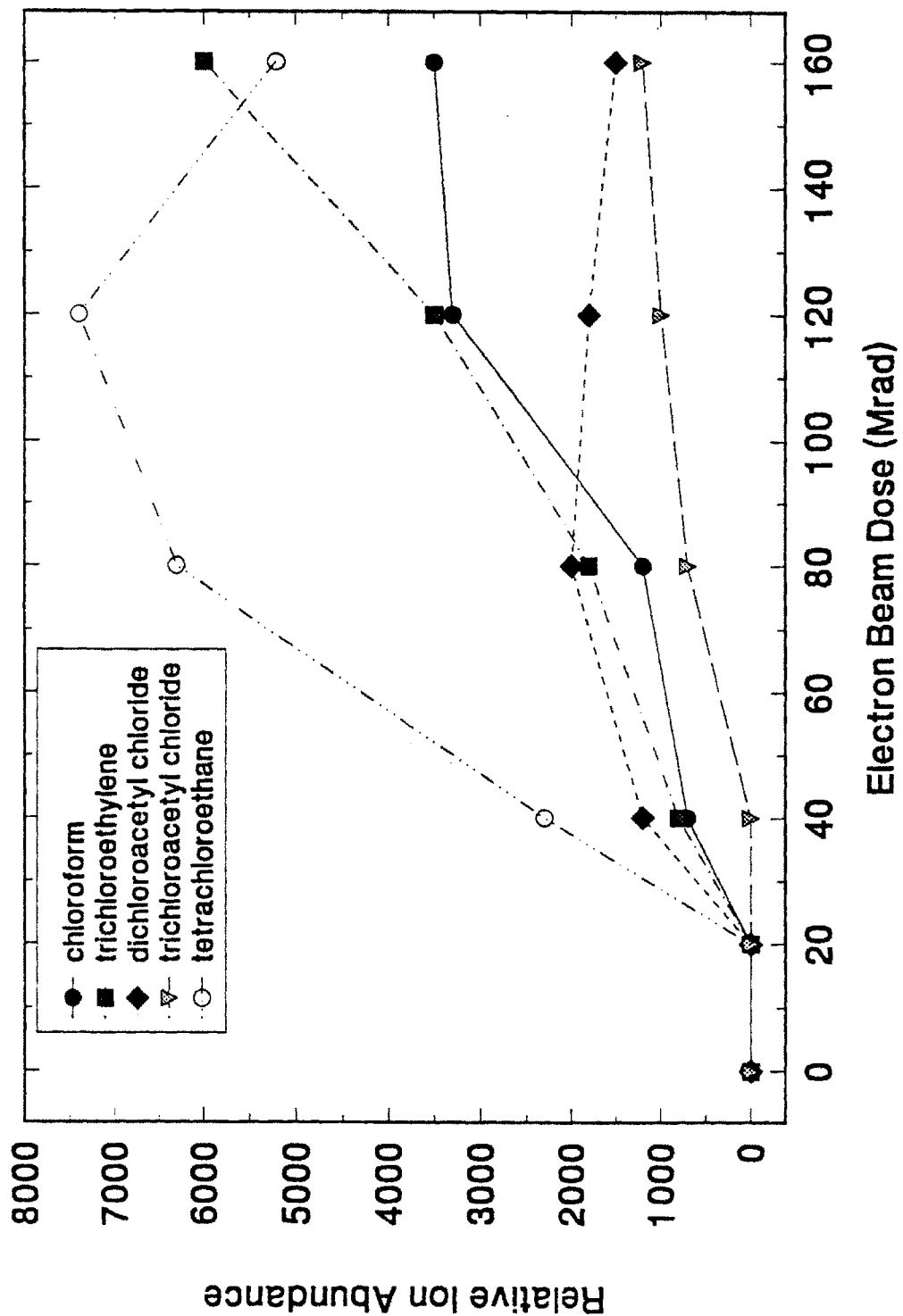
Figure 4.7: Minor reaction products of TCA decomposition. The ion abundances from the mass spectrometer peaks are given as a function of electron beam dose. The ion abundance is approximately linearly proportional to the concentration.
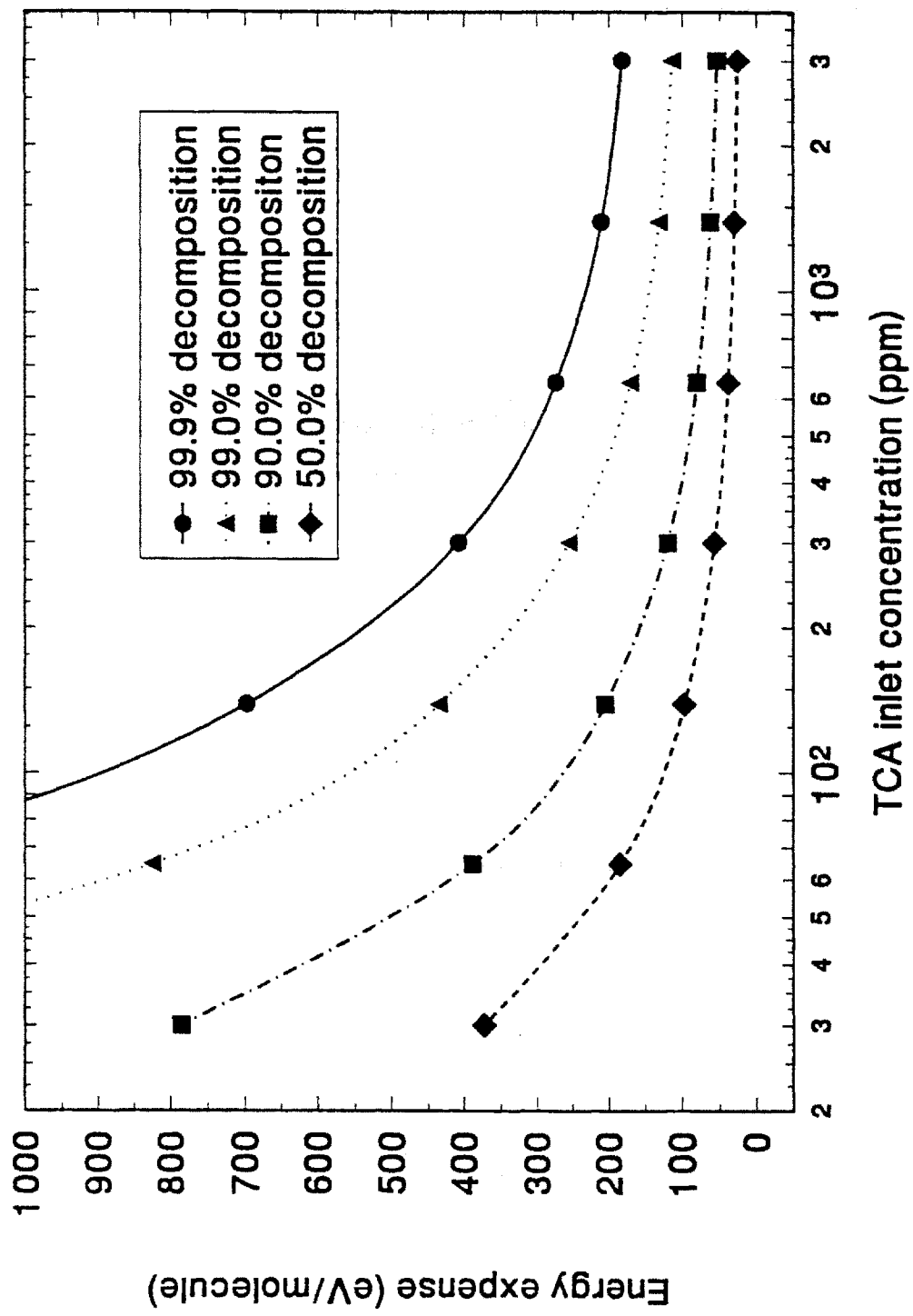
Figure 4.8: Energy expense, ε, required for TCA decomposition, as a function of TCA inlet concentration and desired fractional decomposition, η.
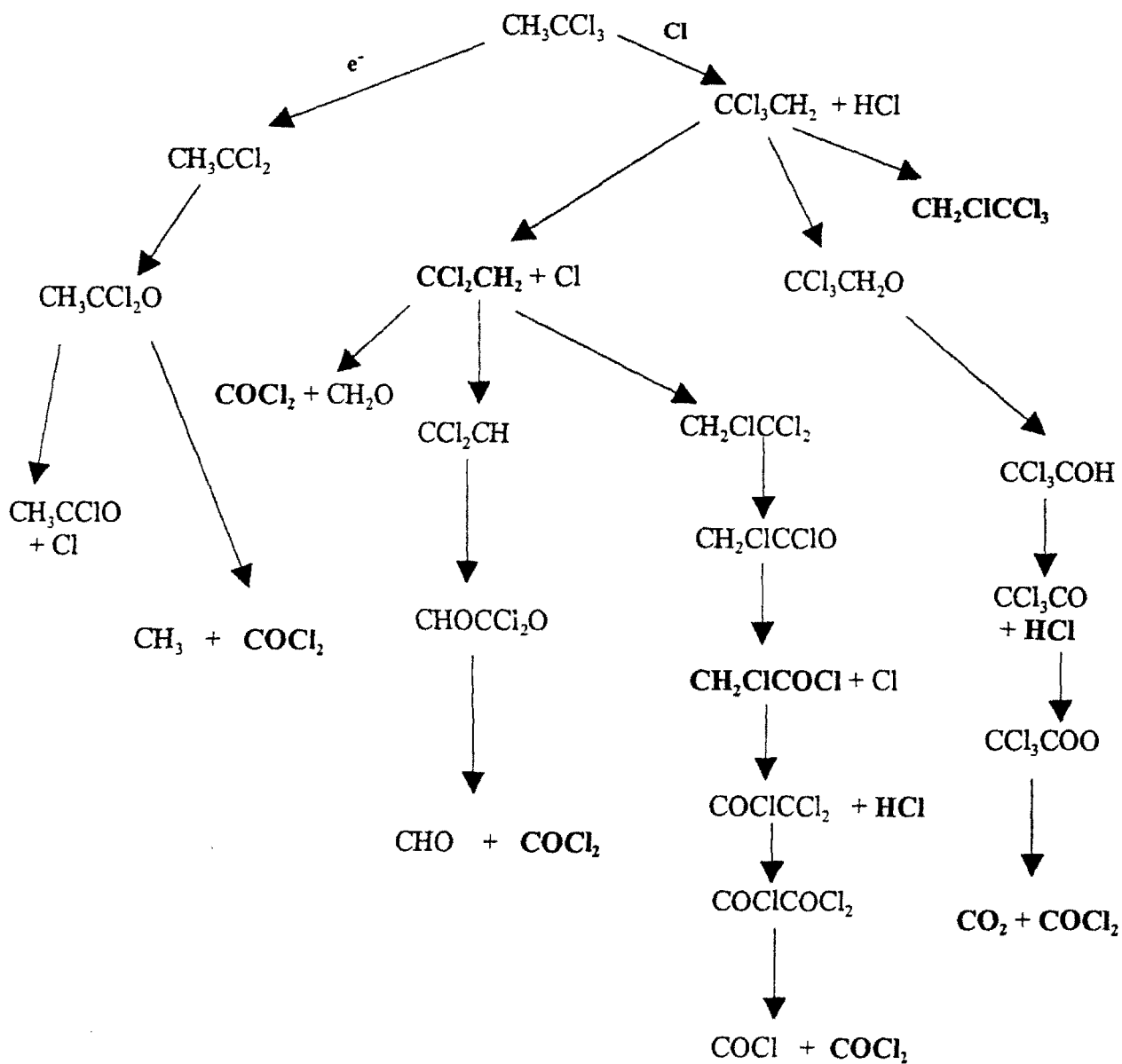
Figure 4.9: Schematic of reaction pathways of TCA decomposition in the EBGPR.

4.3.2. Reaction Pathways

Several decomposition products of TCA were observed experimentally. The primary chlorine containing product of TCA decomposition is HCl. The primary carbon containing products of TCA decomposition in the plasma reactor are carbon dioxide, 1,1 dichloroethylene, phosgene. and chloroacetyl chloride. Several minor reaction products were also detected: chloroform, trichloroethylene, dichloroacetyl chloride. trichloroacetyl chloride, and tetrachloroethane (both 1,1,1,2- and 1,1,2,2- isomers). The reaction mechanism proposed below accounts for the experimental observation of all of the major reaction products. and most of the minor products. The absolute concentrations of the intermediate species were not determined due to a lack of accurate calibration standards, but the relative ion abundances from the mass spectrometer peaks are presented for the major and minor reaction products as a function of electron beam dose in figures 4.6 and 4.7.

Several reaction mechanisms for the decomposition 1.1.1-trichloroethane have been proposed in the literature.[80-84] None of these individually account for all of the decomposition products observed. but if several reaction pathways are considered, it is possible to account for most of the observed products. The reaction pathways proposed below are illustrated schematically in figure 4.8, which is similar to that given by Thompson[80] for the high temperature oxidation of 1,1,1-trichloroethane. TCA decomposition in the electron beam generated plasma reactor is initiated by the formation of reactive species through electron induced dissociation of the TCA molecule as shown in reactions (4.1-4.7). The reactive radicals thus produced will then react with other TCA molecules through hydrogen abstraction.

The initiation step for the reaction is dissociative recombination or dissociative electron attachment with a TCA molecule, producing a chlorine radical.
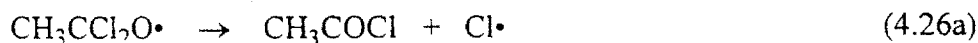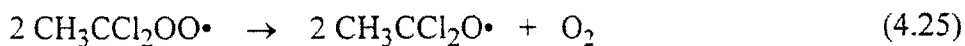
$$e^- + CH_3CCl_3^+ \rightarrow CH_3CCl_2\bullet + Cl\bullet \quad k \leq 10^{-6} \text{ cm}^3/\text{sec}^{(78)} \quad (4.20a)$$

$$e^- + CH_3CCl_3 \rightarrow CH_3CCl_2\bullet + Cl^- \quad k = 5 \times 10^{-9} \text{ cm}^3/\text{sec}^{(78)} \quad (4.20b)$$
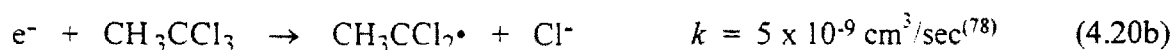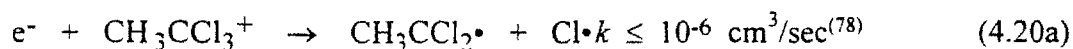
or with an oxygen molecule. producing an excited O^{3p} or O^{1d} radical.

$$e^- + O_2^+ \rightarrow 2\,O\bullet \quad k \leq 10^{-7} \text{ cm}^3/\text{sec}^{(89)} \quad (4.21a)$$

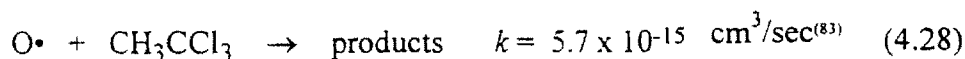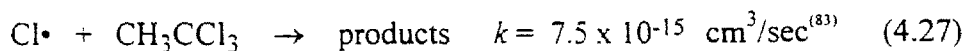$$e^- + O_2 \rightarrow 2\,O^- \quad k \approx 10^{-11} \text{ cm}^3/\text{sec}^{(89)} \quad (4.21b)$$
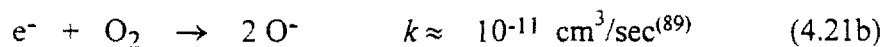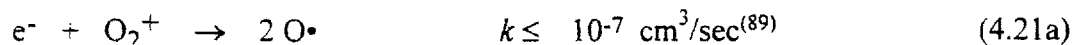
The dichloroethyl radical produced in reaction (4.20) may decompose by direct oxidation.[80]

$$CH_3CCl_2\bullet + O_2 \rightarrow CH_3CCl_2OO\bullet \quad (4.24)$$

-81

$$2\ CH_3CCl_2OO\cdot \rightarrow 2\ CH_3CCl_2O\cdot + O_2 \qquad (4.25)$$

$$CH_3CCl_2O\cdot \rightarrow CH_3COCl + Cl\cdot \qquad (4.26a)$$
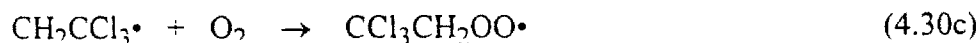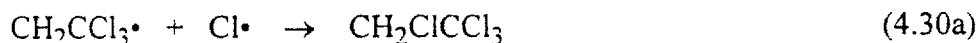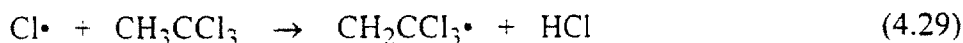
$$CH_3CCl_2O\cdot \rightarrow CH_3\cdot + COCl_2 \qquad (4.26b)$$
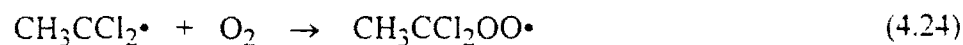
It is then possible for the $Cl\cdot$ or $O\cdot$ radical produced in reaction (4.20) or (4.21) to abstract a hydrogen atom from another molecule of TCA and begin the radical induced decomposition process, (note that rate constants are at 298K),
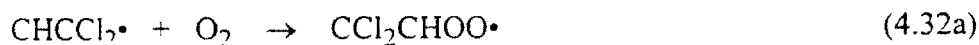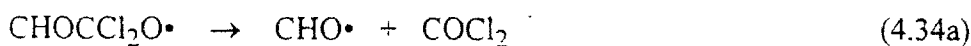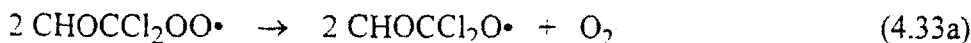
$$Cl\cdot + CH_3CCl_3 \rightarrow products \quad k = 7.5 \times 10^{-15}\ cm^3/sec^{[83]} \qquad (4.27)$$

$$O\cdot + CH_3CCl_3 \rightarrow products \quad k = 5.7 \times 10^{-15}\ cm^3/sec^{[83]} \qquad (4.28)$$

Hydrogen abstraction by hydroxyl radicals. which is the primary mechanism for chlorinated VOC removal in atmospheric chemistry,[80-81] is not a likely mechanism in the electron beam generated plasma reactor due to the very low concentration of hydroxyl radicals generated in dry air. as shown by Koch. Also, chlorine abstraction by hydrogen molecules as studied by Barat[85] is not a likely mechanism since no molecular hydrogen or water vapor was added to the system. In the following mechanism, hydrogen abstraction by $Cl\cdot$ will be illustrated as proposed by Jiang[81] and Nelson;[82] $O\cdot$ initiated decomposition is analogous.

$$Cl\cdot + CH_3CCl_3 \rightarrow CH_2CCl_3\cdot + HCl \qquad (4.29)$$

$$CH_2CCl_3\cdot + Cl\cdot \rightarrow CH_2ClCCl_3 \qquad (4.30a)$$

$$CH_2CCl_3\cdot \rightarrow CH_2CCl_2 + Cl\cdot \qquad (4.30b)$$

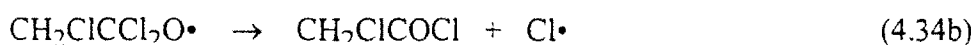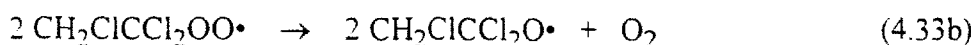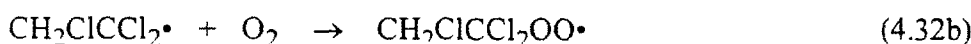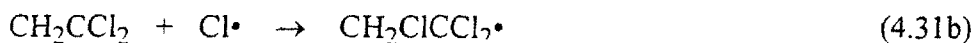$$CH_2CCl_3\cdot + O_2 \rightarrow CCl_3CH_2OO\cdot \qquad (4.30c)$$

Reaction (4.30a) produces the experimentally observed byproduct 1,1,1,2 tetrachloroethane. and reaction (4.30b) produces the primary decomposition product 1,1 dichloroethylene. Reaction (4.30c) is also a possible branch and will be illustrated following the primary reaction pathway. which is through (4.30b). The 1.1 dichloroethylene produced in reaction (4.30b) can decompose by three different mechanisms:

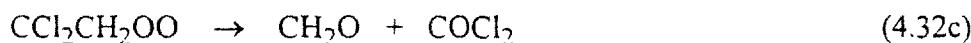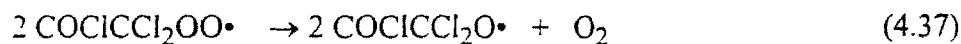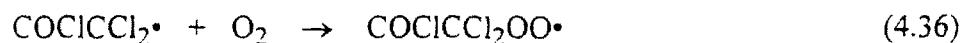1. hydrogen abstraction. forming phosgene.

$$CH_2CCl_2 + Cl\cdot \rightarrow CHCCl_2\cdot + HCl \qquad (4.31a)$$

$$CHCCl_2\cdot + O_2 \rightarrow CCl_2CHOO\cdot \qquad (4.32a)$$

$$2 \, CHOCCl_2OO\bullet \quad \rightarrow \quad 2 \, CHOCCl_2O\bullet \; + \; O_2 \qquad (4.33a)$$

$$CHOCCl_2O\bullet \quad \rightarrow \quad CHO\bullet \; + \; COCl_2 \qquad (4.34a)$$

2. chlorine radical addition, forming chloroacetyl chloride,

$$CH_2CCl_2 \; + \; Cl\bullet \quad \rightarrow \quad CH_2ClCCl_2\bullet \qquad (4.31b)$$

$$CH_2ClCCl_2\bullet \; + \; O_2 \quad \rightarrow \quad CH_2ClCCl_2OO\bullet \qquad (4.32b)$$

$$2 \, CH_2ClCCl_2OO\bullet \quad \rightarrow \quad 2 \, CH_2ClCCl_2O\bullet \; + \; O_2 \qquad (4.33b)$$

$$CH_2ClCCl_2O\bullet \quad \rightarrow \quad CH_2ClCOCl \; + \; Cl\bullet \qquad (4.34b)$$

or 3. direct oxidation, forming formaldehyde and phosgene

$$CH_2CCl_2 \; + \; O_2 \quad \rightarrow \quad CCl_2CH_2OO \qquad (4.31c)$$

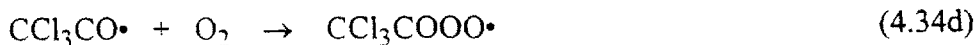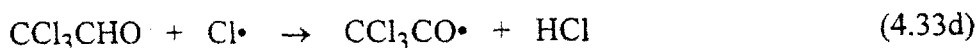$$CCl_2CH_2OO \quad \rightarrow \quad CH_2O \; + \; COCl_2 \qquad (4.32c)$$

Note that reactions (4.34a) and (4.32c) are elementary reactions which proceed through a four center complex. The formation of dichloroacetyl chloride and trichloroacetyl chloride probably occurs by the same mechanism as that proposed for chloroacetyl chloride, with the addition of one or two chloride ion substitution steps. The acetyl chlorides further decompose into chloral. phosgene and chlorinated radicals, following mechanisms analogous to that for dichloroacetyl chloride:

$$COClCHCl_2 \; + \; Cl\bullet \, (or \, O_2) \quad \rightarrow \quad COClCCl_2\bullet \; + \; HCl \; (or \, HO_2\bullet) \qquad (4.35)$$

$$COClCCl_2\bullet \; + \; O_2 \quad \rightarrow \quad COClCCl_2OO\bullet \qquad (4.36)$$

$$2 \, COClCCl_2OO\bullet \quad \rightarrow 2 \, COClCCl_2O\bullet \; + \; O_2 \qquad (4.37)$$

$$COClCCl_2O\bullet \quad \rightarrow \quad COCl\bullet \; + \; COCl_2 \qquad (4.38)$$

The phosgene thus formed will decompose through Cl• abstraction in the plasma to form carbon monoxide and molecular chlorine or chlorine radicals.[83]

Another reaction pathway following reaction (4.30c) has been proposed in the literature for TCA oxidation.[82] which leads to the formation of phosgene and trichloroacetaldehyde.

$$2 \, CCl_3CH_2OO\bullet \quad \rightarrow \quad 2 \, CCl_3CH_2O\bullet \; + \; O_2 \qquad (4.31d)$$

$$2 \, CCl_3CH_2O\bullet \; + \; O_2 \, (or \, Cl\bullet) \quad \rightarrow \quad CCl_3CHO \; + \; HO_2\bullet \; (or \, HCl) \qquad (4.32d)$$

$$CCl_3CHO + Cl\bullet \rightarrow CCl_3CO\bullet + HCl \qquad (4.33d)$$

$$CCl_3CO\bullet + O_2 \rightarrow CCl_3COOO\bullet \qquad (4.34d)$$

$$2\,CCl_3COOO\bullet \rightarrow 2\,CCl_3COO\bullet + O_2 \qquad (4.35d)$$

$$CCl_3COO\bullet \rightarrow CCl_3\bullet + CO_2 \qquad (4.36d)$$

$$CCl_3\bullet + O_2 \rightarrow CCl_3OO\bullet \qquad (4.37d)$$

$$2\,CCl_3OO\bullet \rightarrow 2CCl_3O\bullet + O_2 \qquad (4.38d)$$

$$CCl_3O\bullet \rightarrow Cl\bullet + COCl_2 \qquad (4.39d)$$
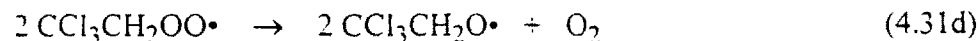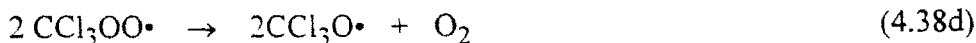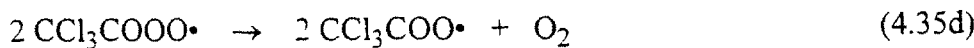
No trichloroacetaldehyde was observed experimentally as a stable reaction product. This would indicate that either the trichloroacetaldehyde decomposes very rapidly in the plasma, or that the branching ratio of reaction (4.30c) is negligible. Further analysis would require detailed experimental study of the reaction kinetics in the plasma, which is beyond the scope of this work. The reaction pathways proposed above account for the formation of all the major and most of the minor decomposition products observed.

4.4 Trichloroethylene

4.4.1 Kinetic Analysis

A graph of outlet stream TCE concentration versus electron beam dose is shown in figure 4.10 for several inlet stream concentrations. Greater than 99% decomposition of TCE is achieved for the lower concentration streams at flow rates up to 5 liters/min. Thirty-eight curves similar to those shown in figure 4.10 were generated at TCE inlet concentrations from 100 to 6000 ppm. These curves were analyzed by the differential kinetic method. to determine the order with respect to time n_t and the order with respect to concentration. n_c.

Figure 4.11 shows the initial rates calculated from the curves as a function of initial concentration of TCE. In this case, the slope of the best fit line to this data gives the order with respect to concentration, $n_c = 0.59$, with a correlation coefficient of 0.91. This correlation coefficient shows a better fit to the data than for TCA. The reaction rate constant. k. is calculated to be:

$$\ln k = 3.03 \qquad \Rightarrow \qquad k = 20.70 \text{ Mrad}^{-1} \text{ ppm}^{1/2}$$

The order with respect to time analysis was performed on each curve of TCE concentration versus electron beam dose. A representative plot is shown in figure 4.12. The order with respect to time. n_t, and the rate constant. k, were calculated for each curve and the results averaged, to give:

$$n_t = 0.99 \pm 0.20$$

$$\ln k = 0.26 \pm 1.96 \quad \Rightarrow \quad k = 0.183 - 2.22 \text{ Mrad}^{-1}$$

As with TCA. n_t is greater than n_c, showing that the kinetics are inhibited. However, this difference is not as great as with TCA; this result will be dealt with in Chapter 5. The inhibition is accounted for in the reaction mechanism outlined below.

Again rounding n_t to the nearest third or quarter integer, the final rate expression is:

$$C_2HCl_3 \quad \rightarrow \quad \text{products}$$

$$r = -1.3 \; [C_2HCl_3] \quad \text{ppm/Mrad} \tag{4.40}$$

This rate expression is used in conjunction with the ideal performance equation for the EBGPR derived in Section 2.2.2 to determine the reactor power needed to achieve a desired conversion of TCE.

Since n_c is less than n_t in this case, and the reaction thus appears to be inhibited. the INHIBIT model. equation (2.69), was fit to the 38 concentration versus dose curves. As for TCA. β' and K values were generated. The best fits gave $K \approx 0$. indicating that inhibition is not very important in this mechanism. Figure 4.13a shows β' for TCE as a function of inlet concentration. with a best fit of:

$$\beta' = 0.000121 \; T_o + 0.266$$

Figure 4.13b shows the continuous curves calculated for the INHIBIT model with these parameters. The fact that inhibition is much less important for TCE than for TCA is consistent with the large smaller difference between n_t and n_c found in the differential kinetic analysis. also indicating that inhibition was a less important factor.

Using the K and β' parameters again in equation (2.70), the energy expense. ε, was calculated as a function of the inlet concentration T_o, and the desired fractional decomposition η:

$$\varepsilon = \frac{1}{\eta T_o} \frac{M_C}{N_A} 2 \cdot \beta' \left[\ln\left(\frac{1}{1 - \eta} \cdot \sqrt{1 - \frac{\eta}{K + 1}} \right) \right] \tag{4.41}$$

The results are given in figure 4.14.

For comparison with previous literature results, beta values were calculated from the TCE data using equation (2.14),

$$x_j = x_{jo} \exp\left(-\frac{D}{\beta}\right) \qquad (4.42)$$

but only considering data up to 90% decomposition, where an exponential dependence fits the data well. The resulting value of beta for each curve is shown in figure 4.14 as a function of the inlet TCE concentration. A best fit to this data gives:

$$\beta = .00033\ [T_o] + 0.22 \qquad \text{Mrad} \qquad (4.43)$$

with T_o in ppm. Penetrante[40] reports $\beta = 0.23$ Mrad for decomposition of 100 ppm TCE in an electron beam reactor, which agrees very well with the value of $\beta = 0.253$ Mrad calculated by equation (4.43). In contrast, for TCE decomposition in a pulsed corona reactor, Penetrante[4] reports $\beta = 1.24$ Mrad at 100 ppm inlet concentration. From the data of Lerner[72] for TCE decomposition in a dielectric barrier discharge, at 300 ppm inlet concentration, $\beta = 7.1$ Mrad. This shows that the electron beam generated plasma reactor is more energy efficient than the pulsed corona or the dielectric barrier discharge for TCE decomposition. Rosocha[26] reports $\beta = 0.9$ Mrad in a dielectric barrier discharge, though the inlet concentration was not specified, so it is difficult to make a comparision between these results and the results of this study.

If one ignores the offset for zero in the best fit curve for β, equation (2.77) can be used to calculate the G value for TCE:

$$G_{TCE} = 78.8 \text{ molecules} / 100 \text{ eV} \qquad (4.44)$$
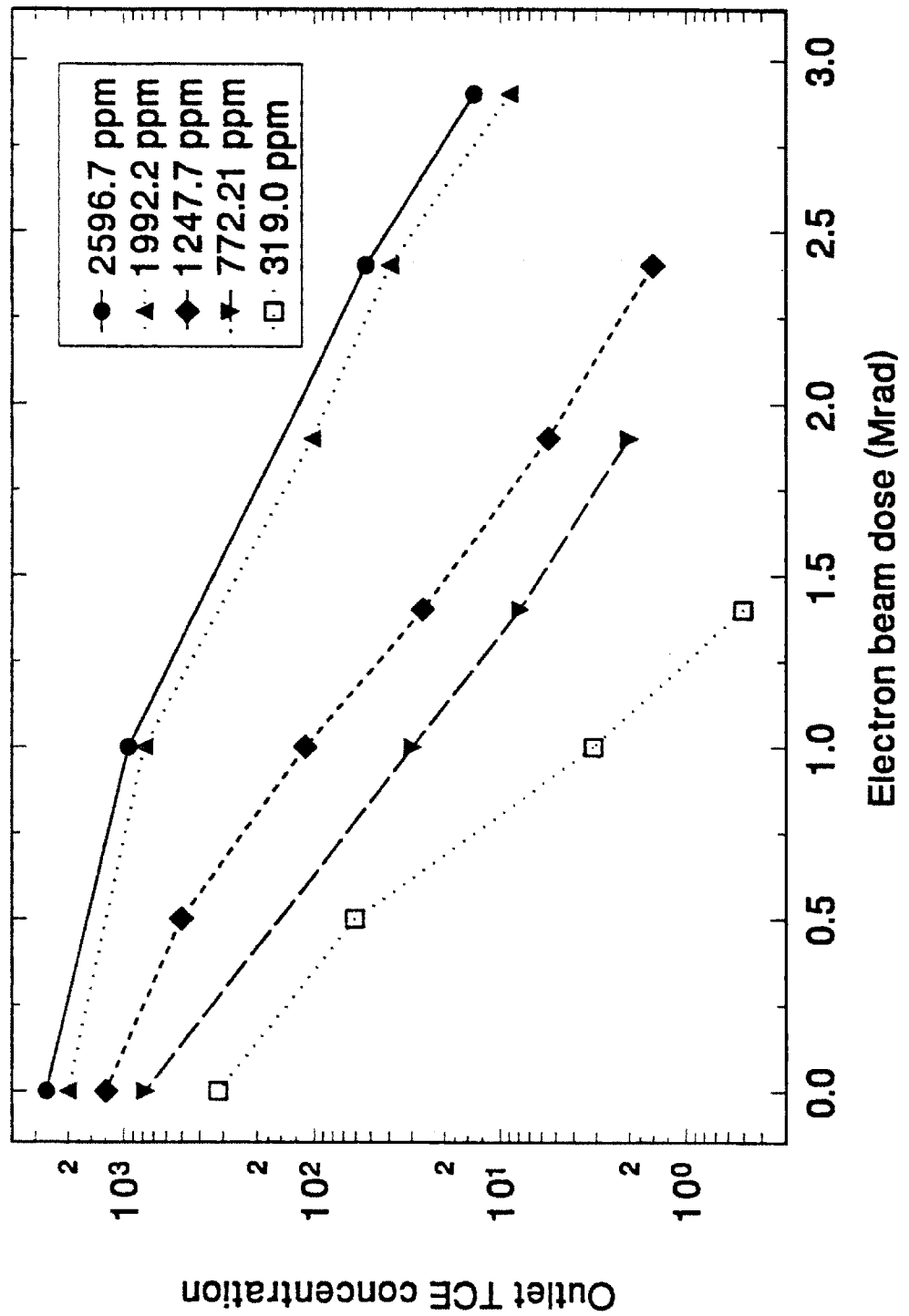
Figure 4.10: Trichloroethylene outlet concentration as a function of electron beam dose.
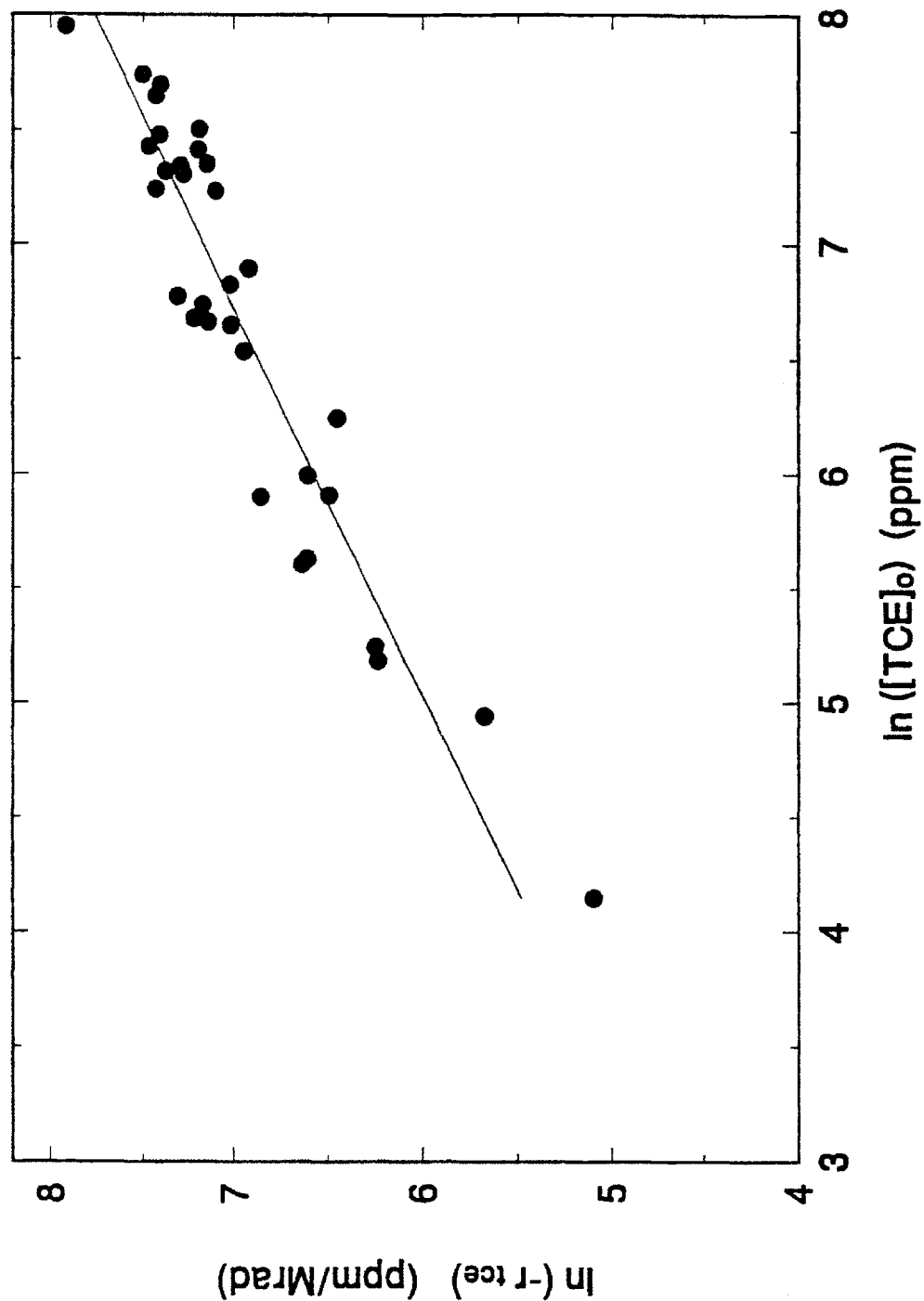
Figure 4.11: Differential kinetic analysis of TCE decomposition. This graph shows the

initial reaction rate. $-r = \dfrac{d[TCE]}{dD}$. as a function of initial TCE concentration. The slope

of this line gives the order with respect to concentration, n_c, and the intercept with the Y-axis gives the rate constant. k.
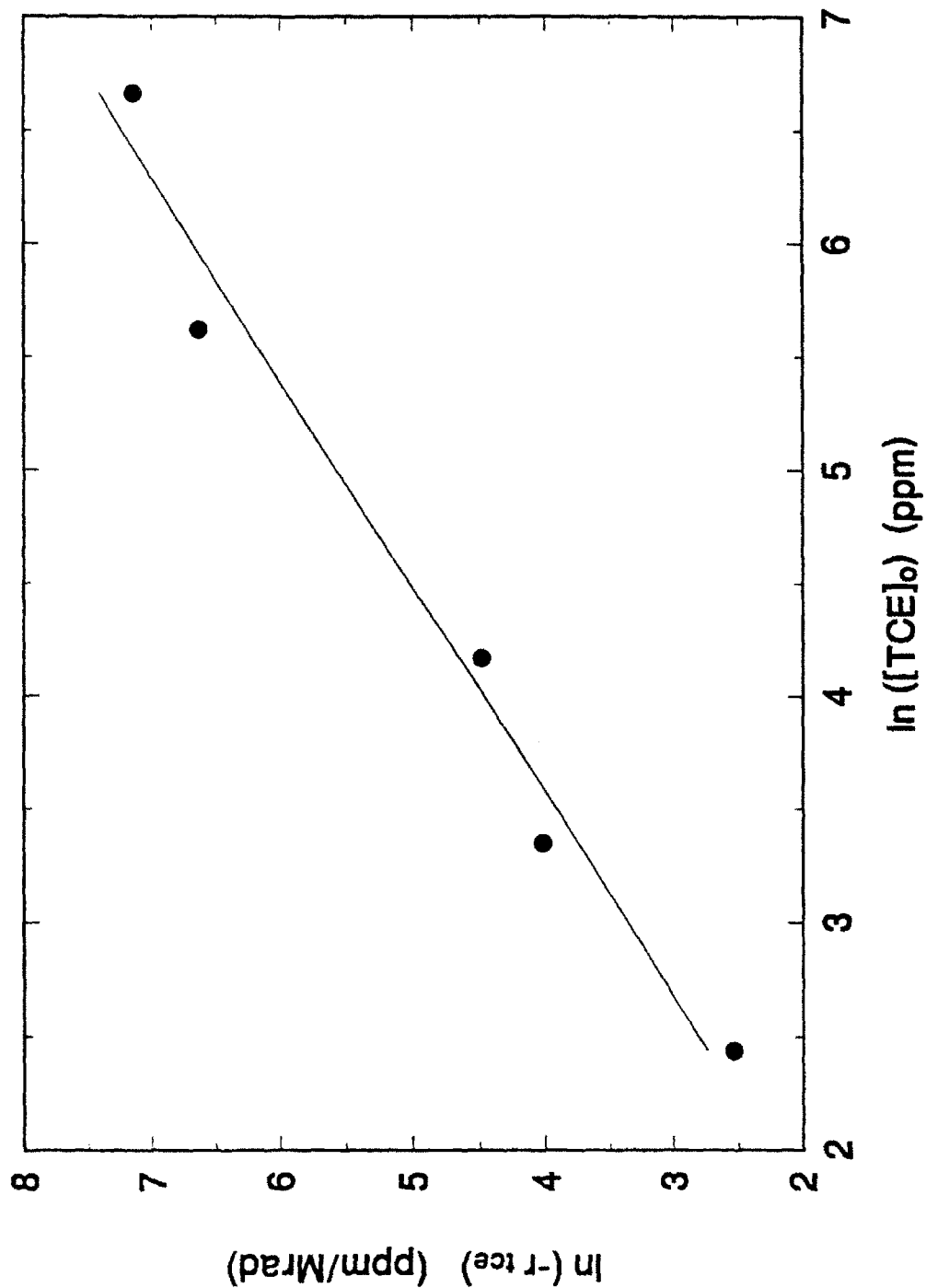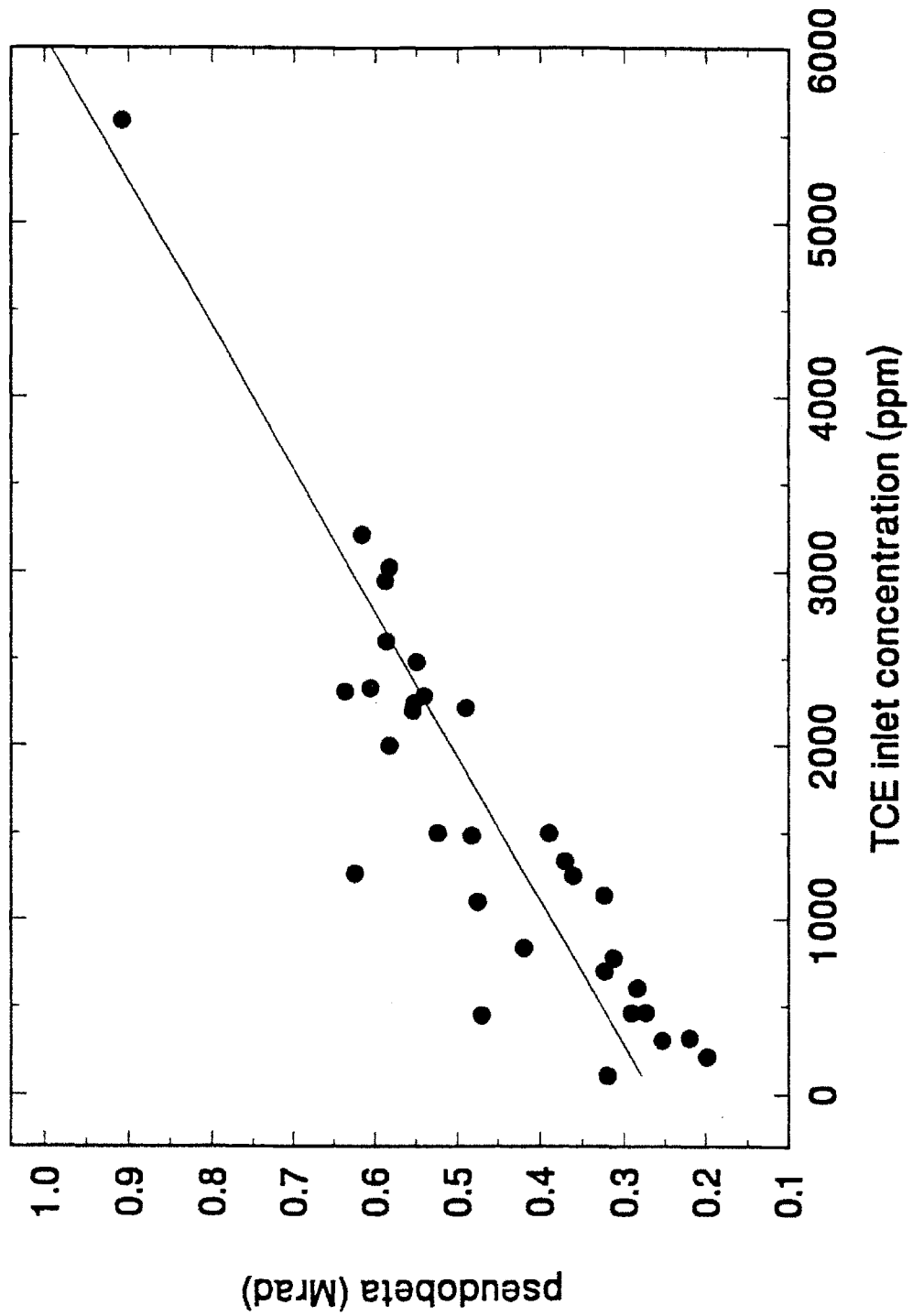
Figure 4.12: A representative graph of one run of TCE, showing the actual reaction rate as a function of TCE concentration. as the reaction proceeds. The slope of this line gives the order with respect to time. n_t. and the intercept with the Y-axis gives the rate constant, k.

Figure 4.13a: Graph of pseudo-β. versus TCE inlet concentration from INHIBIT model fit.
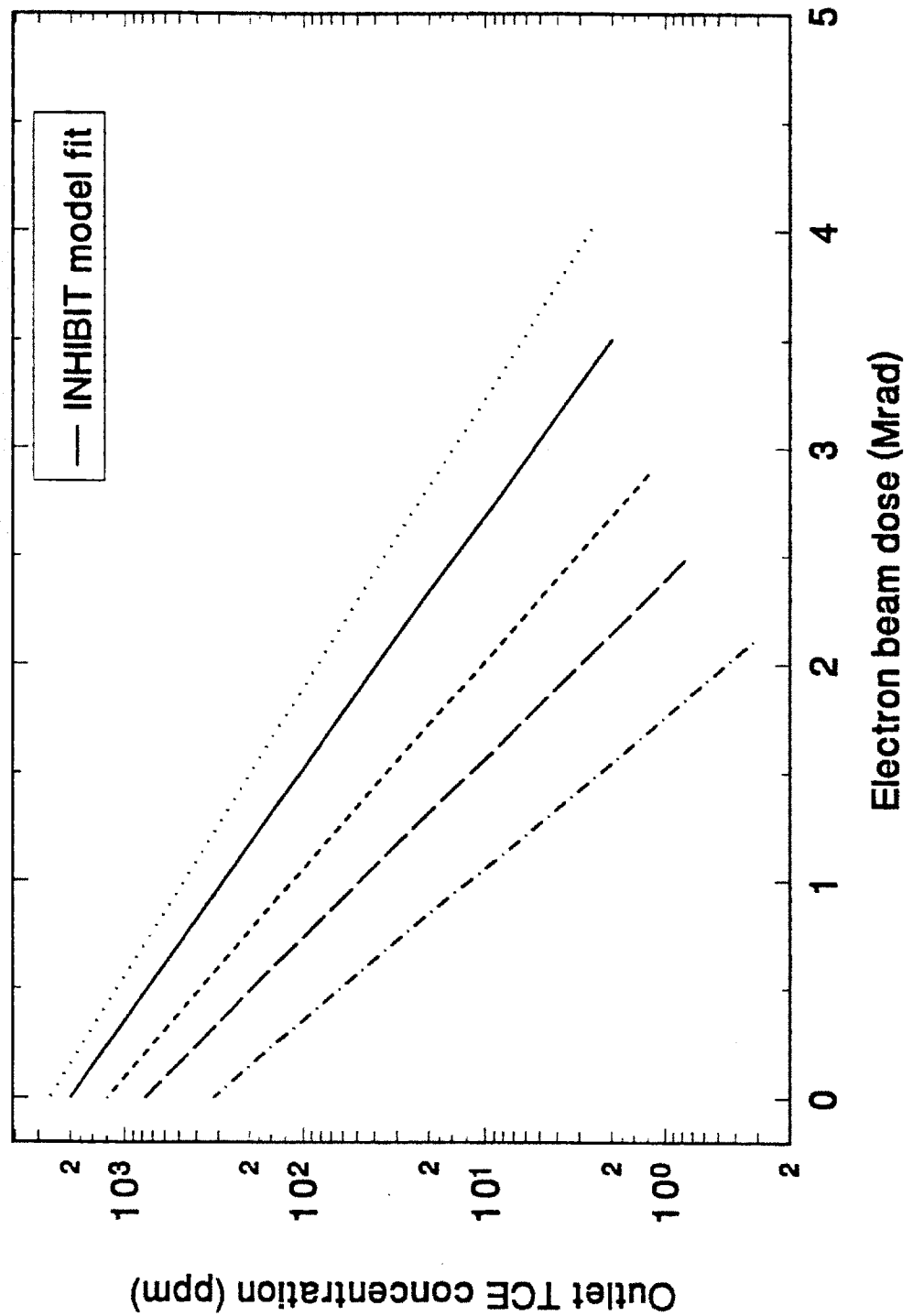
Figure 4.13b: Graph of calculated TCE concentration versus electron beam dose curves from best fit INHIBIT model. The initial concentrations are the same as the experimental data given in figure 4.10 so the two graphs may be compared.
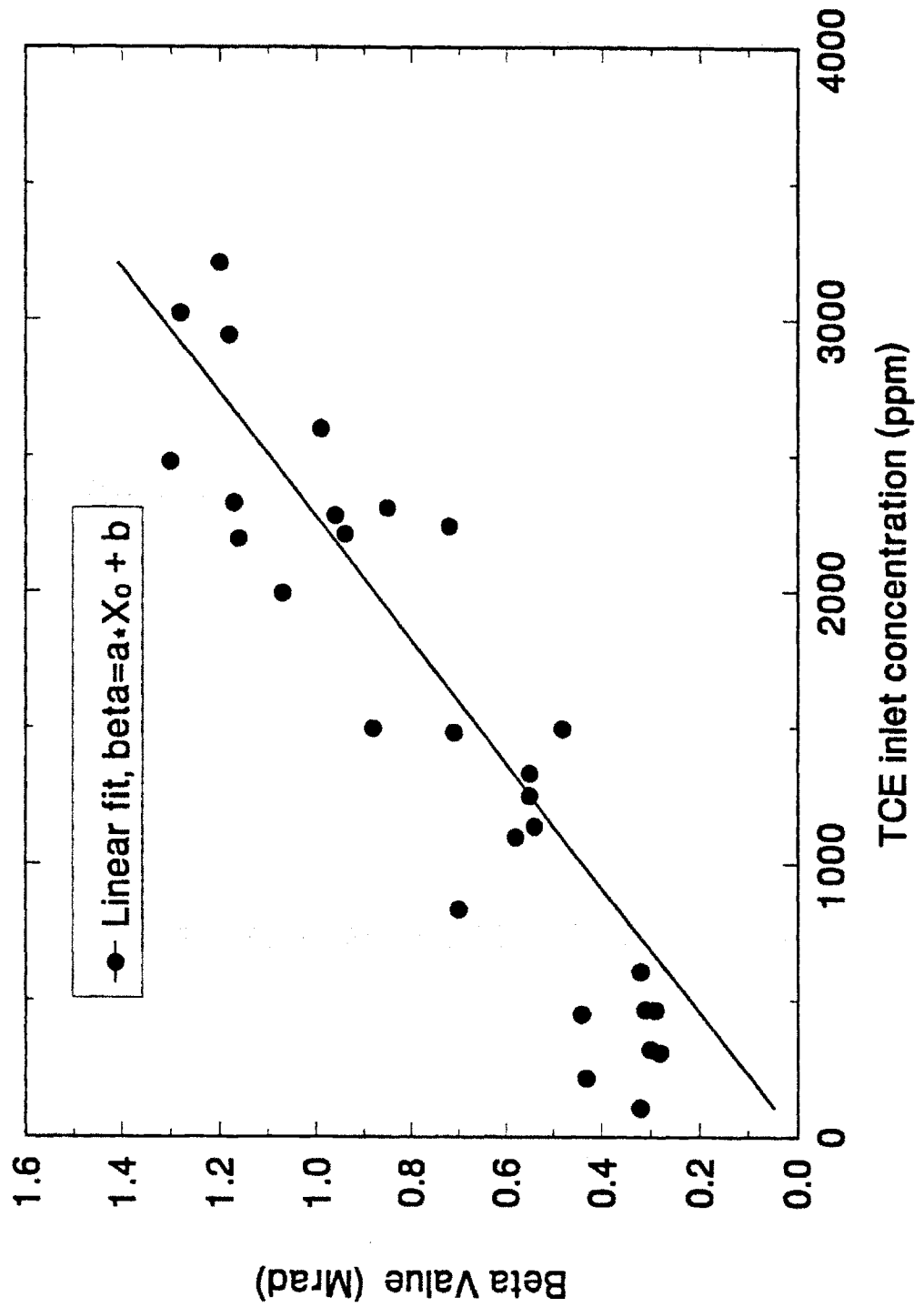
Figure 4.14: Graph of the Rosocha β-value versus inlet TCE concentration.
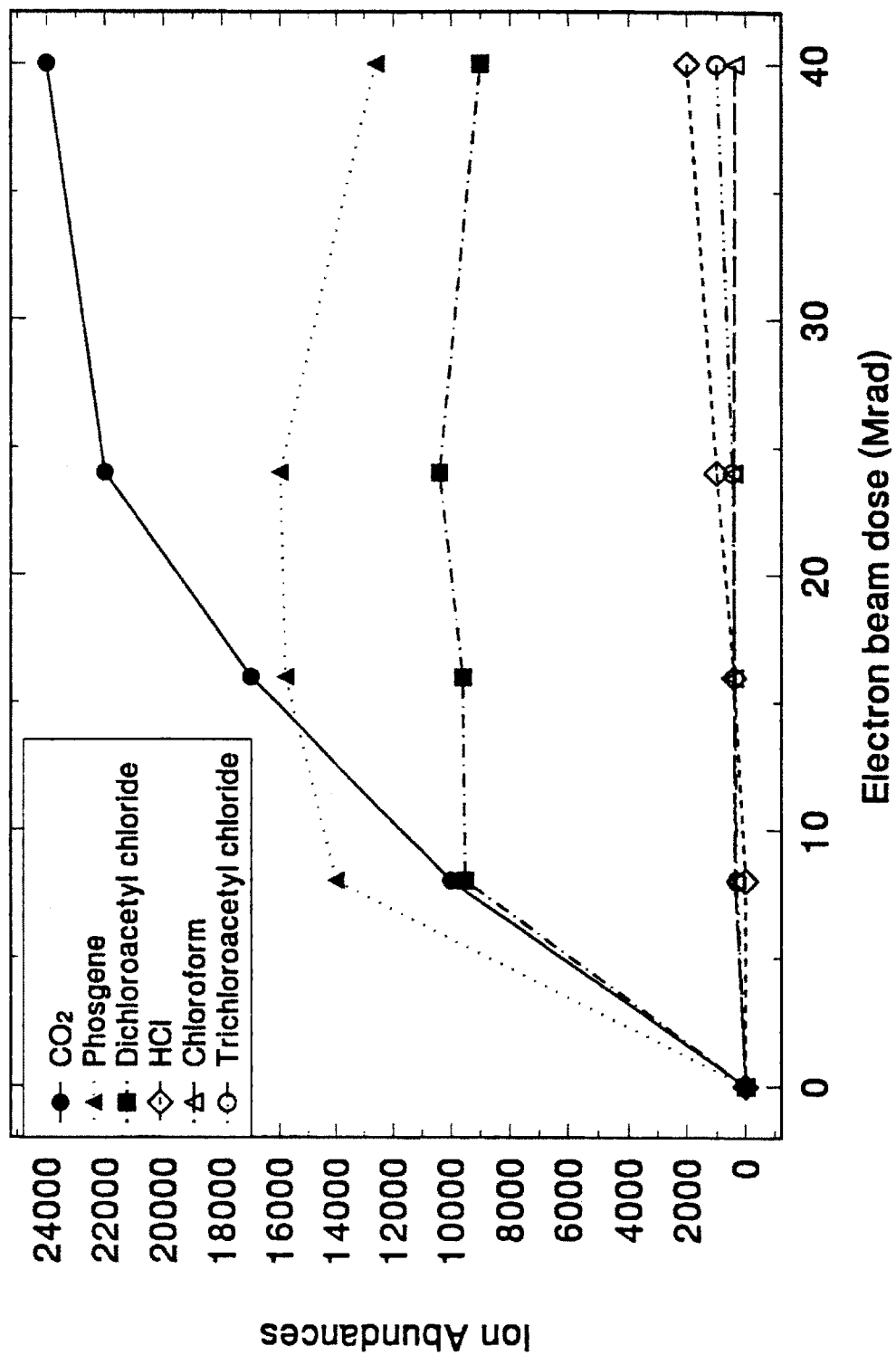
Figure 4.15a: Major reaction products of TCE decomposition. The ion abundances from the mass spectrometer peaks are given as a function of electron beam dose. The ion abundance is approximately linearly proportional to the concentration.
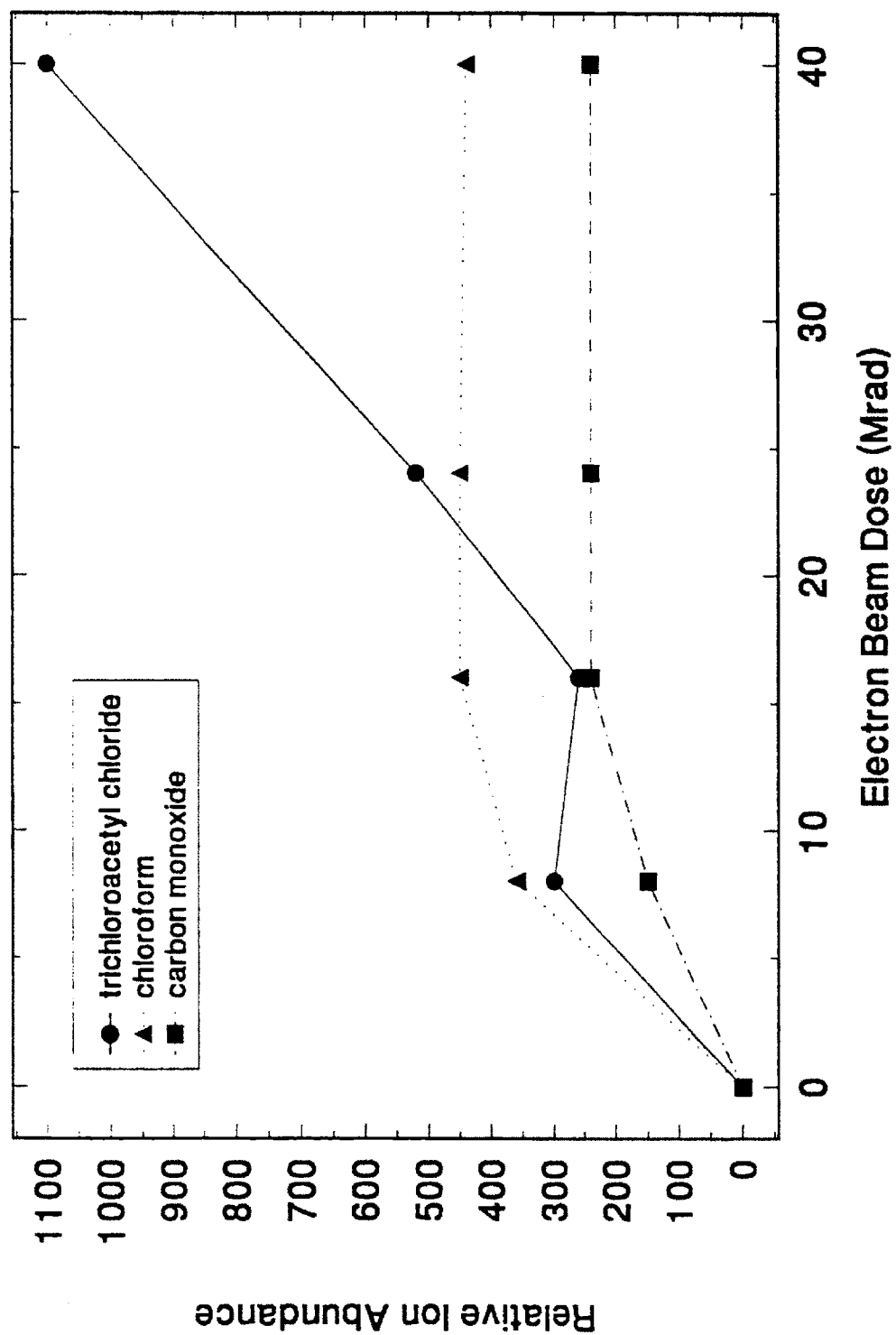
Figure 4.15b: Minor reaction products of TCE decomposition. The ion abundances from the mass spectrometer peaks are given as a function of electron beam dose. The ion abundance is approximately linearly proportional to the concentration.
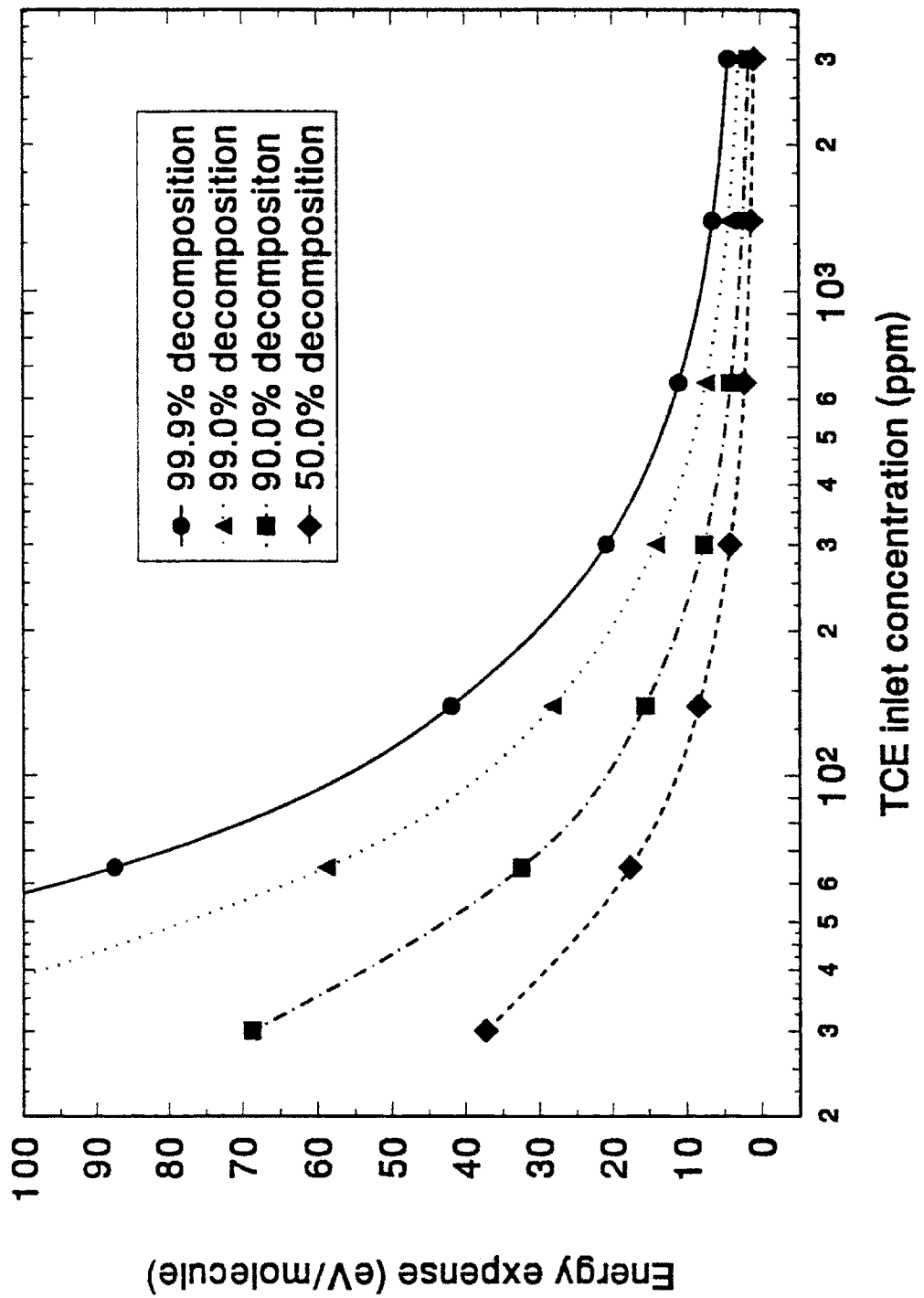
Figure 4.16: Specific energy, ε, required for TCE decomposition, as a function of TCE inlet concentration and desired fractional decomposition, η.

CHClCHCl$_2$

e^-

CHClCHCl + Cl

Cl

CHCl$_2$CCl$_2$

O$_2$

(CHCl$_2$CCl$_2$O)$_2$

CHCl$_2$CCl$_2$OO

CHCl$_2$CCl$_2$O

(CHCl$_2$CCl$_2$O)$_2$

COCl$_2$ + CHCl$_2$

Cl + CHCl$_2$COCl

CHClO + Cl

COClCCl$_2$ + HCl

COClCCl$_3$

COClCCl$_2$OO

COClCCl$_2$O

COCl$_2$ + COCl

COCl$_2$
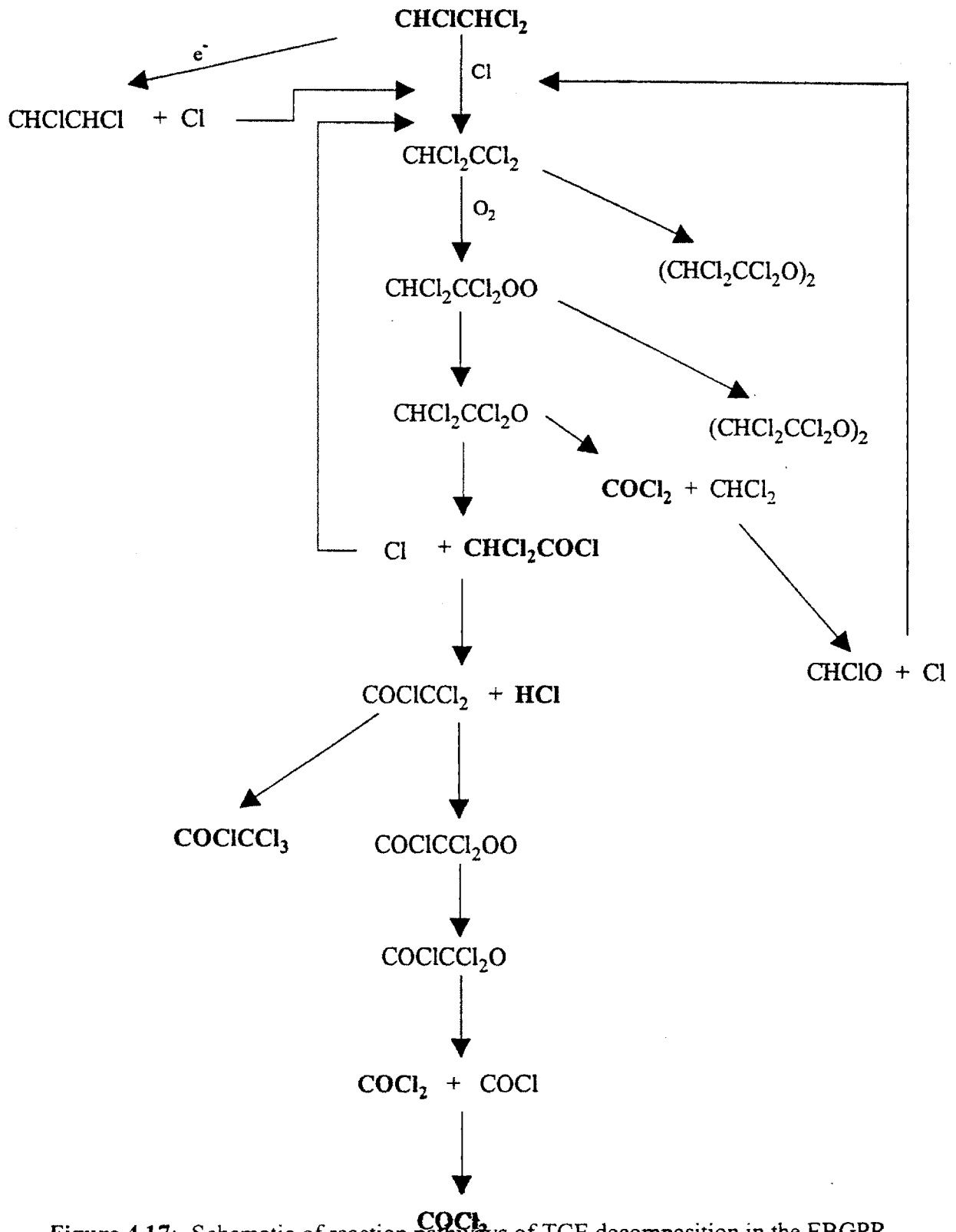
Figure 4.17: Schematic of reaction pathways of TCE decomposition in the EBGPR.

4.4.2. Reaction Pathways

A several decomposition products of TCE were observed experimentally. The primary decomposition products from TCE decomposition are found in this study to be: carbon dioxide. phosgene. dichloroacetyl chloride and hydrogen chloride, in agreement with the results found by Koch. The minor decomposition products are: trichloroacetyl chloride, chloroform. and carbon monoxide. The reaction mechanism proposed below accounts for the experimental observation of all of the major and minor reaction products. Figure 4.15 shows the ion abundance of reaction products as a function of electron beam dose.

The decomposition of both TCA and TCE occurs through radical mechanisms. The reactive radicals needed for TCE decomposition, such as Cl• and O•. are formed through dissociative electron attachment or dissociative recombination of free electrons in the plasma with oxygen or VOC molecules, as described in Section 4.2. Reaction mechanisms for the decomposition of chlorinated ethylenes such as TCE have been proposed extensively in the literature. by Koch and others,[84.86.87] and through a combination of these reaction pathways, all of the decomposition products found in this study can be accounted for. The reaction mechanism presented in this study is illustrated schematically in figure 4.17.

The fast electrons from the electron beam create many secondary electrons which collide with VOC and carrier gas molecules, causing detachment of a reactive radical. This radical will then react with other TCE molecules. There are three likely radical species which may initiate the decomposition mechanism,

1. OH• radicals formed from water molecules,

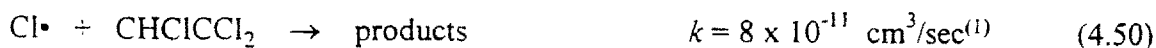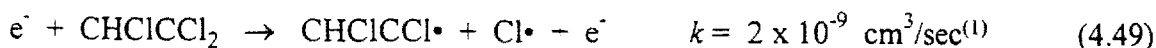$$H_2O + e^- \rightarrow OH\bullet + H\bullet + e^- \tag{4.45}$$

$$OH\bullet + CHClCCl_2 \rightarrow products \qquad k = 1 \times 10^{-12} \ cm^3/sec^{[87]} \tag{4.46}$$
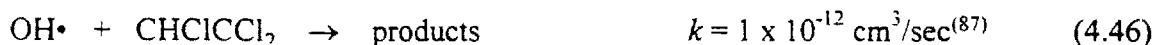
2. Excited O^{3p} or O^{1d} radicals produced from molecular oxygen.

$$O_2 + e^- \rightarrow 2\,O\bullet + e^- \qquad k \leq 1 \times 10^{-11} \ cm^3/sec^{[89]} \tag{4.47}$$

$$O\bullet + CHClCCl_2 \rightarrow products \qquad k = 1 \times 10^{-13} \ cm^3/sec^{[1]} \tag{4.48}$$
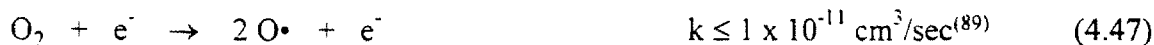
or.

3. Cl• radicals produced from TCE molecules,

$$e^- + CHClCCl_2 \rightarrow CHClCCl\cdot + Cl\cdot - e^- \qquad k = 2 \times 10^{-9} \ cm^3/sec^{(1)} \qquad (4.49)$$

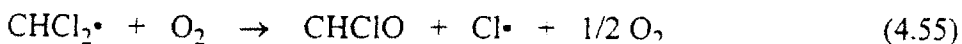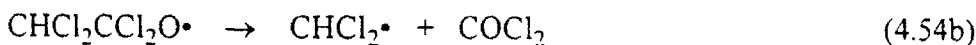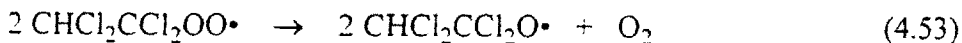$$Cl\cdot + CHClCCl_2 \rightarrow products \qquad k = 8 \times 10^{-11} \ cm^3/sec^{(1)} \qquad (4.50)$$

By using the concentrations of water vapor, oxygen, and TCE, in addition to the average electron density in the plasma reactor, and the rate constants above, Koch has shown that the fastest reaction rate is for chlorine radical induced decomposition, illustrated here as reaction (4.50). Hydroxyl radical reactions, which are the primary mechanisms for chlorinated VOC removal in atmospheric chemistry,[84,86,87] are not likely in the electron beam generated plasma reactor due to the very low concentration of hydroxyl radicals created in dry air. The reaction rate constants for oxygen radical production and reaction are lower than that for Cl· radical reactions, and thus this pathway is not likely to be dominant, though it a possible mechanism. The most likely decomposition pathway is through chlorine radical reactions.

TCE decomposes by chlorine radical addition to the carbon-carbon double bond,

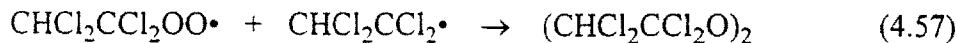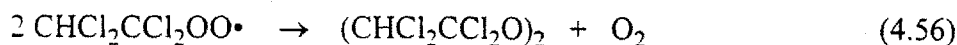$$CHClCCl_2 + Cl\cdot \rightarrow CHCl_2CCl_2\cdot \qquad (4.51)$$

This reaction pathway is not available to TCA, since the carbon-carbon single bond is not susceptible to chlorine radical addition. Note that in reaction (4.51) the chlorine radical adds preferentially to the least substituted carbon atom. Addition to the more chlorinated carbon atom is also possible, but this is less likely to occur. Further, addition at the more chlorinated carbon would lead to the formation of trichloroacetaldehyde, which is not observed experimentally. Sanheuza[88] suggests that addition at the least chlorinated site is favored over addition at the more chlorinated site by a factor of 8. The favored addition reaction proceeds as follows:
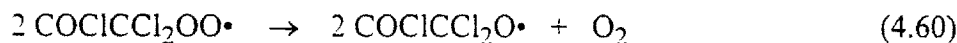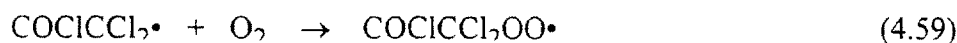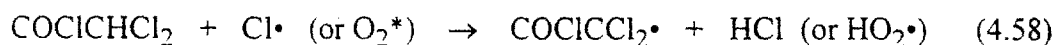
$$CHCl_2CCl_2\cdot + O_2 \rightarrow CHCl_2CCl_2OO\cdot \qquad (4.52)$$

$$2\ CHCl_2CCl_2OO\cdot \rightarrow 2\ CHCl_2CCl_2O\cdot + O_2 \qquad (4.53)$$

$$CHCl_2CCl_2O\cdot \rightarrow CHCl_2COCl + Cl\cdot \qquad (4.54a)$$

$$CHCl_2CCl_2O\cdot \rightarrow CHCl_2\cdot + COCl_2 \qquad (4.54b)$$

$$CHCl_2\cdot + O_2 \rightarrow CHClO + Cl\cdot + 1/2\ O_2 \qquad (4.55)$$

The chlorine radical used in reaction (4.51) is regenerated in reactions (4.54a) or (4.55), and a chain reaction may occur. Chang[84] estimated that the chain length of the TCE reaction is greater than 150. The same reference estimated that reaction (4.54a) is favored over reaction (4.54b) by a factor of 6. This is consistent with the large amount of dichloroacetyl chloride formed as a reaction product.

Chain termination can occur in at least two ways:

$$2\ CHCl_2CCl_2OO\bullet \quad \rightarrow \quad (CHCl_2CCl_2O)_2 \ + \ O_2 \qquad\qquad (4.56)$$

$$CHCl_2CCl_2OO\bullet \ + \ CHCl_2CCl_2\bullet \quad \rightarrow \quad (CHCl_2CCl_2O)_2 \qquad\qquad (4.57)$$

This product, di(tetrachloroethane) peroxide, was not seen experimentally. The long chain length would indicate that this termination step product is present only in very low concentrations.

The dichloroacetyl chloride formed in reaction (4.54a) decomposes in the plasma to form HCl, phosgene, and chlorinated radicals:

$$COClCHCl_2 \ + \ Cl\bullet \ (or\ O_2{}^*) \quad \rightarrow \quad COClCCl_2\bullet \ + \ HCl \ (or\ HO_2\bullet) \quad (4.58)$$

$$COClCCl_2\bullet \ + \ O_2 \quad \rightarrow \quad COClCCl_2OO\bullet \qquad\qquad (4.59)$$

$$2\ COClCCl_2OO\bullet \quad \rightarrow \quad 2\ COClCCl_2O\bullet \ + \ O_2 \qquad\qquad (4.60)$$

$$COClCCl_2O\bullet \quad \rightarrow \quad COCl\bullet \ + \ COCl_2 \qquad\qquad (4.61)$$

The phosgene thus formed may decompose through Cl$\bullet$ abstraction in the plasma to form carbon monoxide and molecular chlorine or chlorine radicals.[83] This reaction mechanism accounts for the formation of all of the observed reaction products.

4.5 1,1-Dichloroethane

4.5.1 Kinetic Analysis

A graph of outlet stream DCA concentration versus electron beam dose is shown in figure 4.18 for several inlet stream concentrations. Greater than 99% decomposition of DCA is achieved for the lower concentration streams at flow rates up to 3 liters/min. Twenty-six curves similar to those shown in figure 4.18 were generated at DCA inlet concentrations from 100 to 3000 ppm.

Figure 4.19 shows the initial rates calculated from the curves as a function of initial concentration of DCA. The order with respect to concentration and rate constant are calculated to be:

$$n_c = 0.41$$

$\ln k = 2.28 \quad \Rightarrow \quad k = 9.78 \ \text{Mrad}^{-1} \ \text{ppm}^{1/2}$

The order with respect to time analysis was performed on each curve of DCA concentration versus electron beam dose. A representative plot is shown in figure 4.20. The results are:

$n_t = 1.29 \pm 0.27$

$\ln k = -4.60 \pm 1.61 \quad \Rightarrow \quad k = 2.01 * 10^{-3} - 5.03 * 10^{-2} \ \text{Mrad}^{-1} \ \text{ppm}^{-1/2}$

As with TCA, n_t is greater than n_c, showing that the kinetics are inhibited. However, for DCA decomposition. difference is even more pronounced than for TCA decomposition; this is the opposite of the TCE and DCE results.

Again rounding n_t to the nearest half integer, the final rate expression is:

$$C_2H_4Cl_2 \quad \rightarrow \quad \text{products}$$

$$r = -1.01 * 10^{-2} \ [C_2H_4Cl_2]^{1/2} \text{ppm/Mrad} \quad\quad\quad (4.62)$$

This rate expression is used in conjunction with the ideal performance equation for the EBGPR derived in Section 2.2.2 to determine the reactor power needed to achieve a desired conversion of DCA.

Since n_c is less than n_t in this case, and the reaction thus appears to be inhibited, the inhibitor model. equation (2.69) was fit to the 26 concentration versus dose curves. Figure 4.21a gives the calculated pseudobeta values, and figure 4.21b shows the calculated curves corresponding to the data presented in figure 4.18. The best fit parameters are given by:

$K = 0.21$

$\beta' = 0.00413 \ [T_o] - 3.02 \quad \text{Mrad}$

Using the K and β' parameters again in equation (2.70), the energy expense, ε, was calculated as a function of the inlet concentration T_o, and the desired fractional decomposition η. The calculated curves are given in figure 4.24.

Rosocha β values were calculated from the DCA data up to 90% fractional decomposition. and the results are given in figure 4.22. Linear fitting of the data gives:

$\beta = 0.00712 \ [T_o] - 2.48 \quad \text{Mrad} \quad\quad\quad (4.63)$
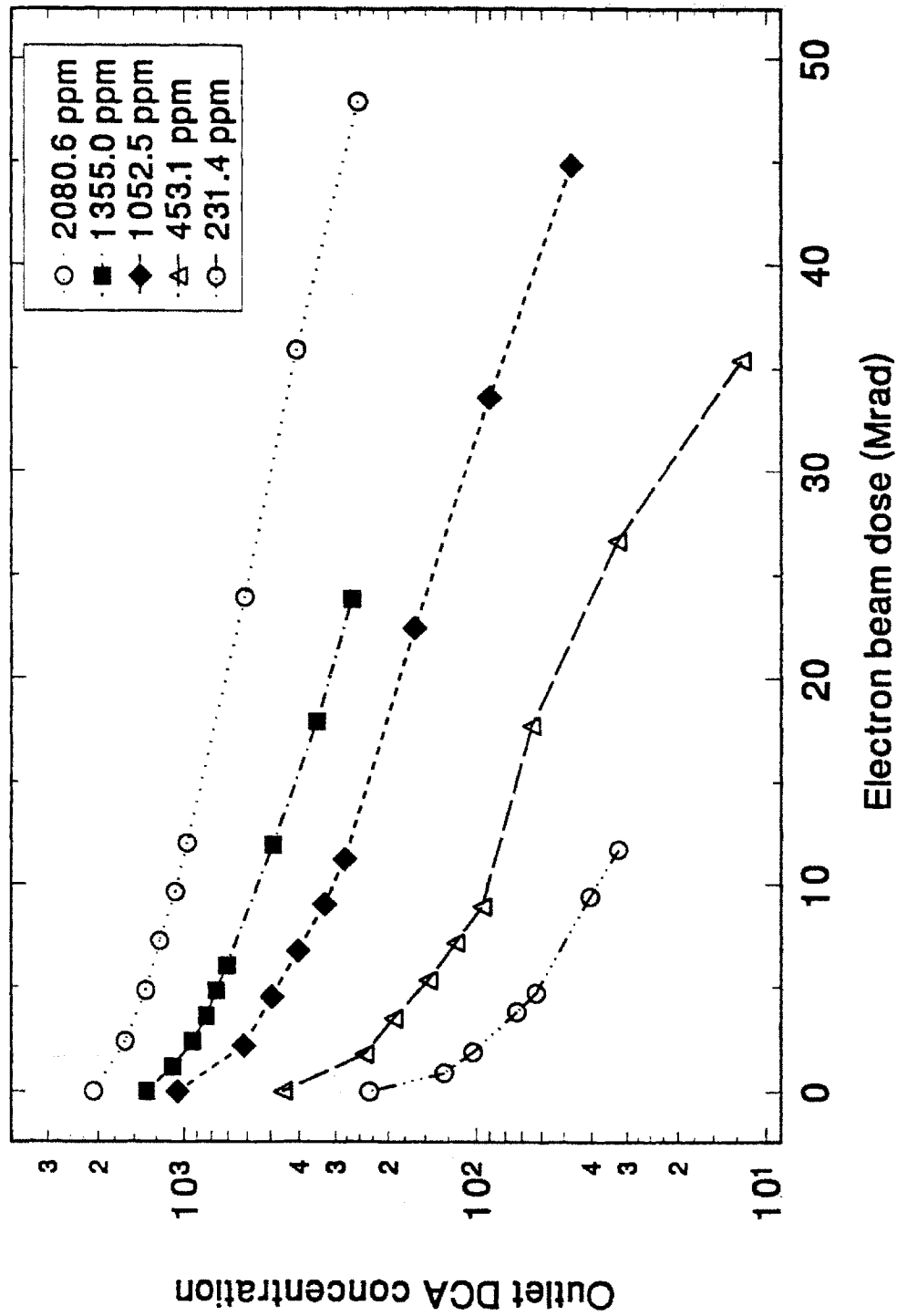
100

Figure 4.18: 1,1-Dichloroethane outlet concentration as a function of electron beam dose.
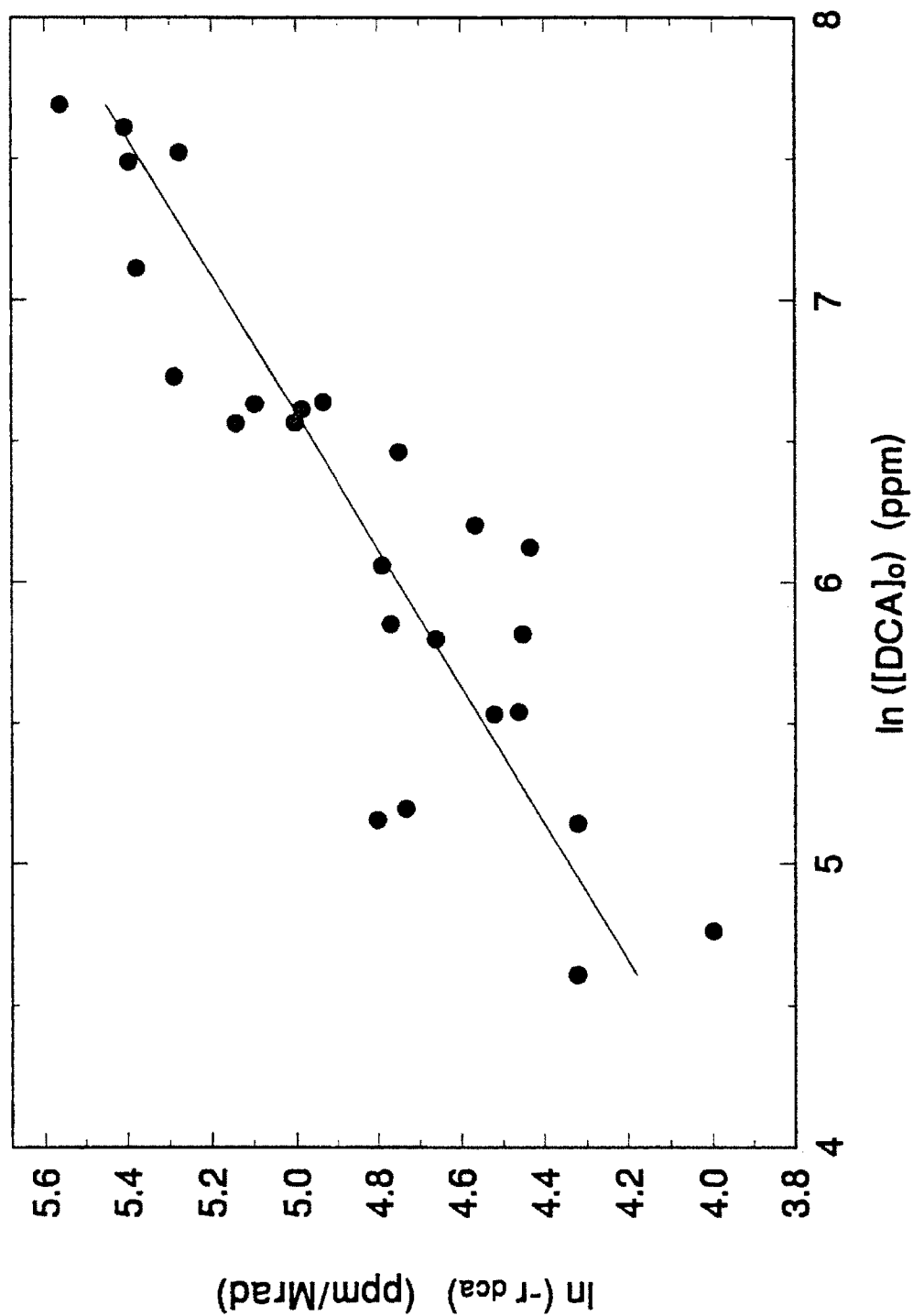
Figure 4.19: Differential kinetic analysis of DCA decomposition. This graph shows the initial reaction rate, $-r = \dfrac{d[DCA]}{dD}$, as a function of initial DCA concentration. The slope of this line gives the order with respect to concentration, n_c, and the intercept with the Y-axis gives the rate constant, k.
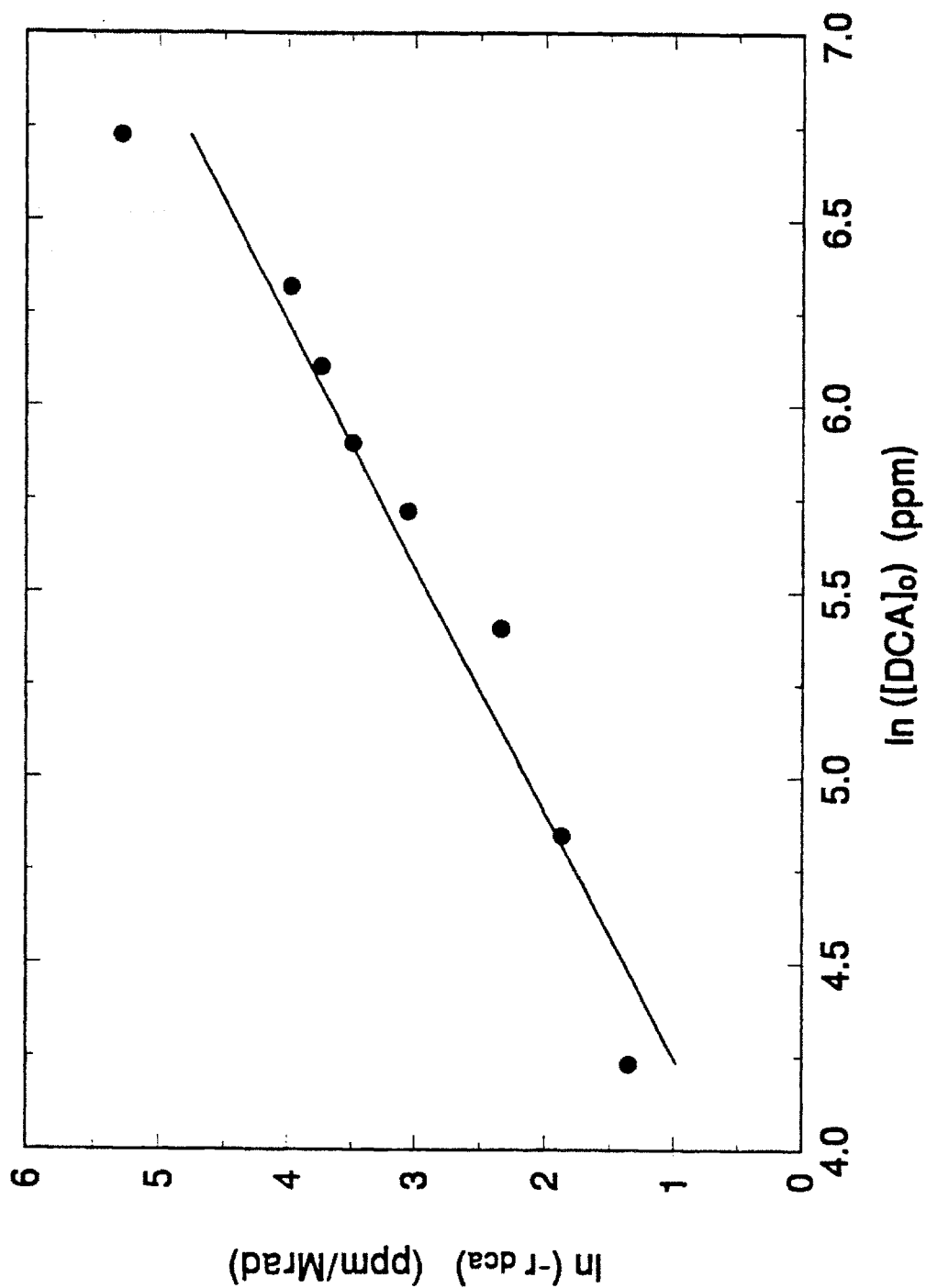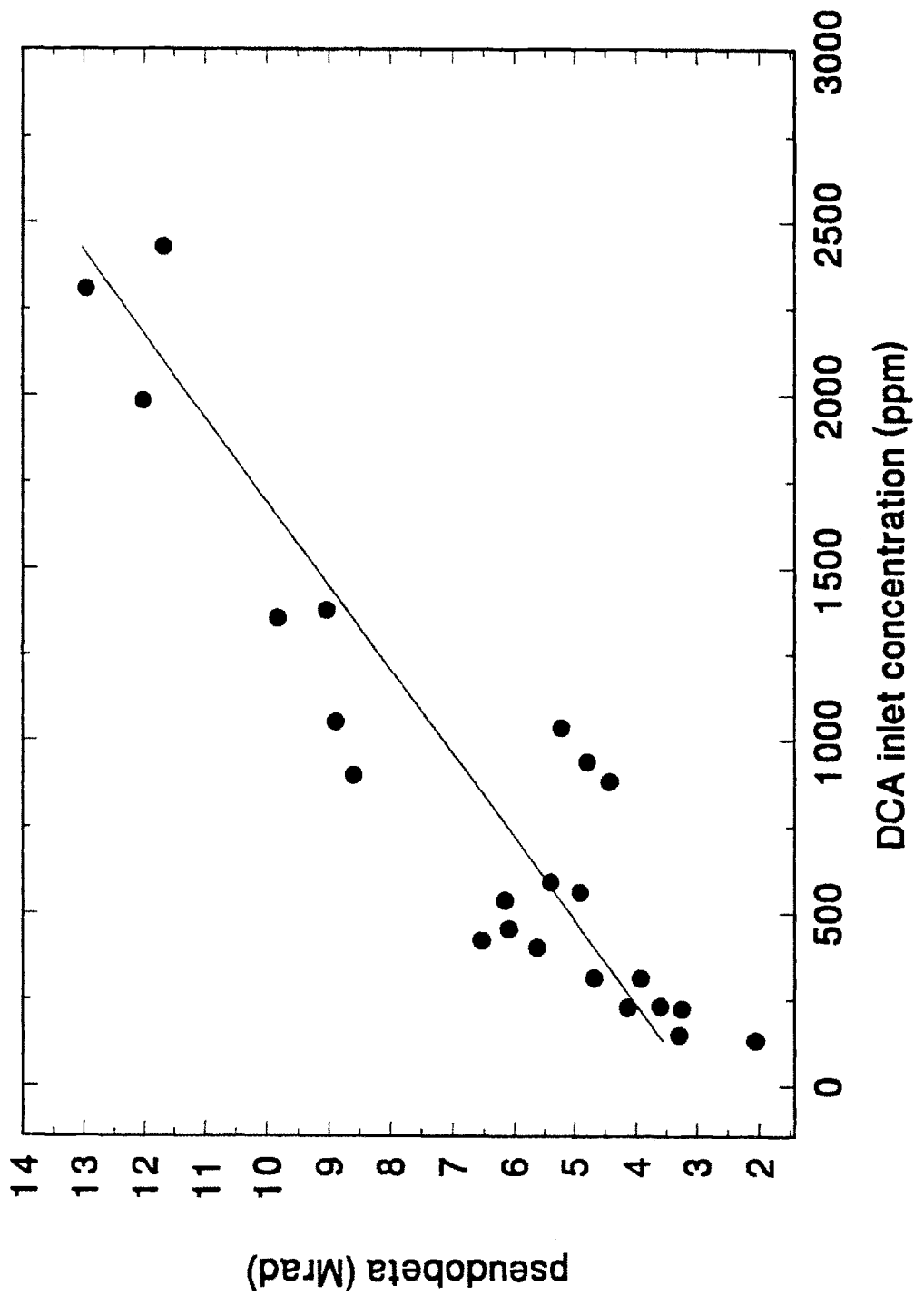
102

Figure 4.20: A representative graph of one run of DCA, showing the actual reaction rate as a function of DCA concentration, as the reaction proceeds. The slope of this line gives the order with respect to time, n_t, and the intercept with the Y-axis gives the rate constant, k.

Figure 4.21a: Graph of pseudo-β, versus DCA inlet concentration from INHIBIT model fit.
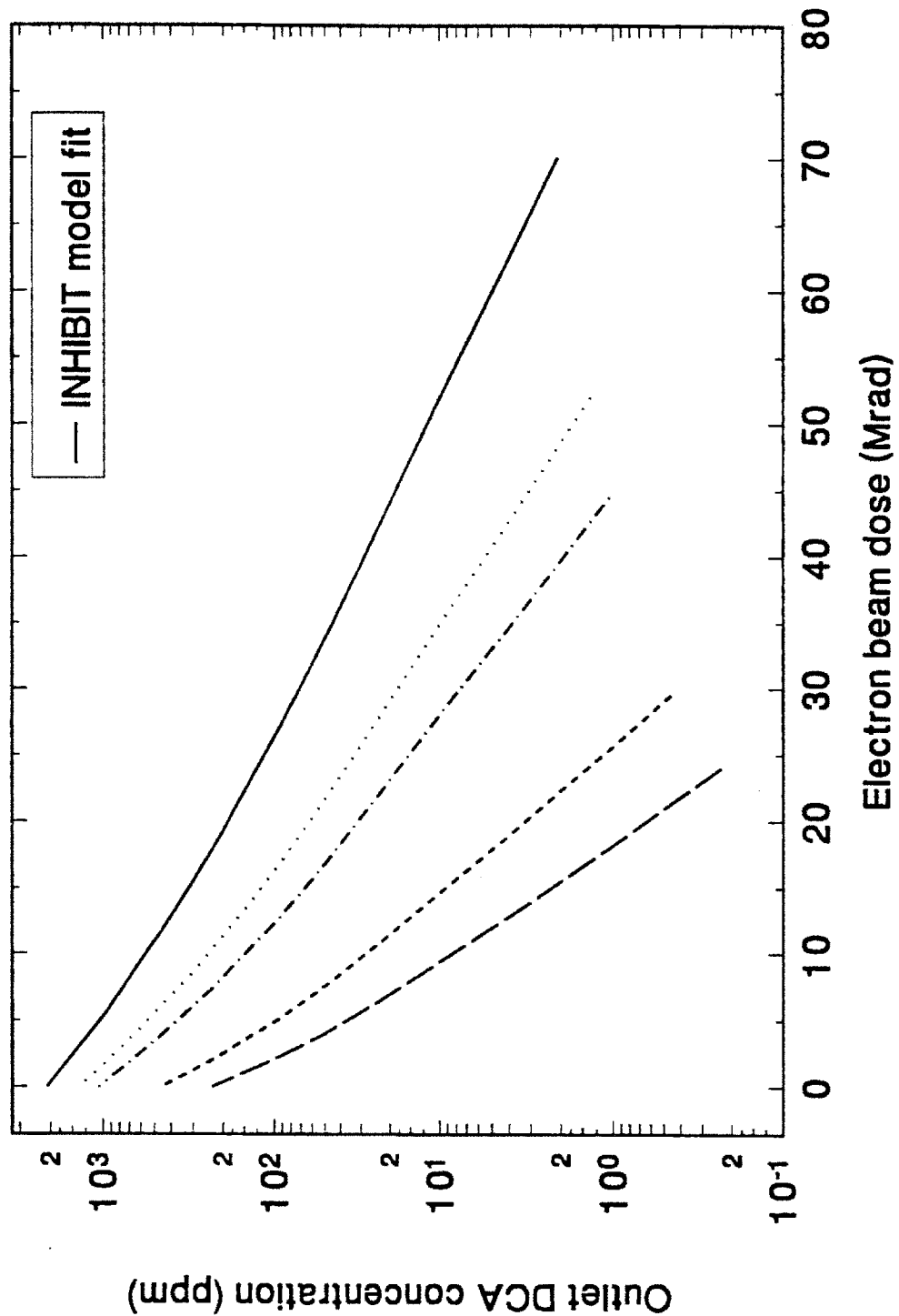
Figure 4.21b: Graph of calculated DCA concentration versus electron beam dose curves from best fit INHIBIT model. The initial concentrations are the same as the experimental data given in figure 4.18 so the two graphs may be compared.
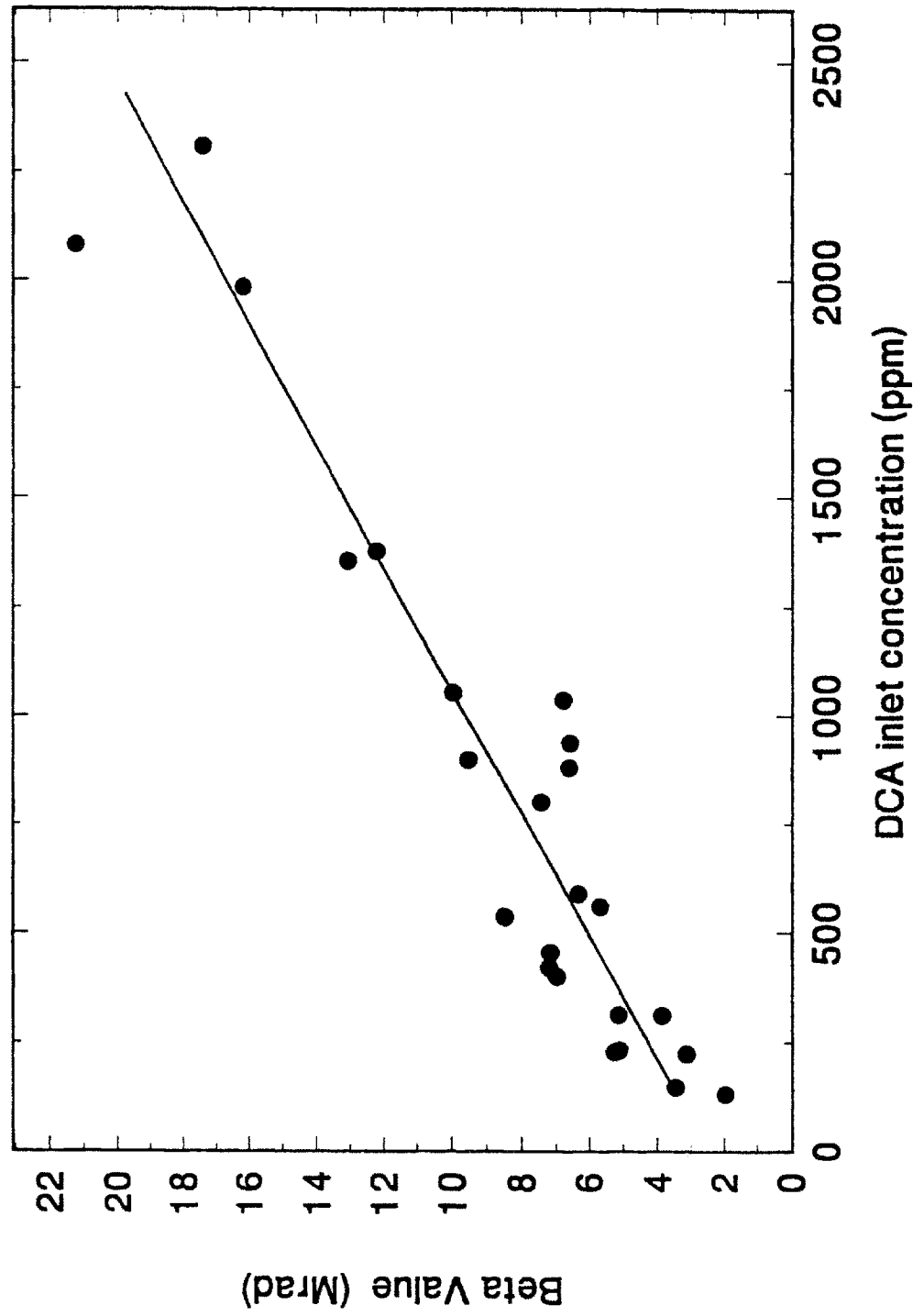
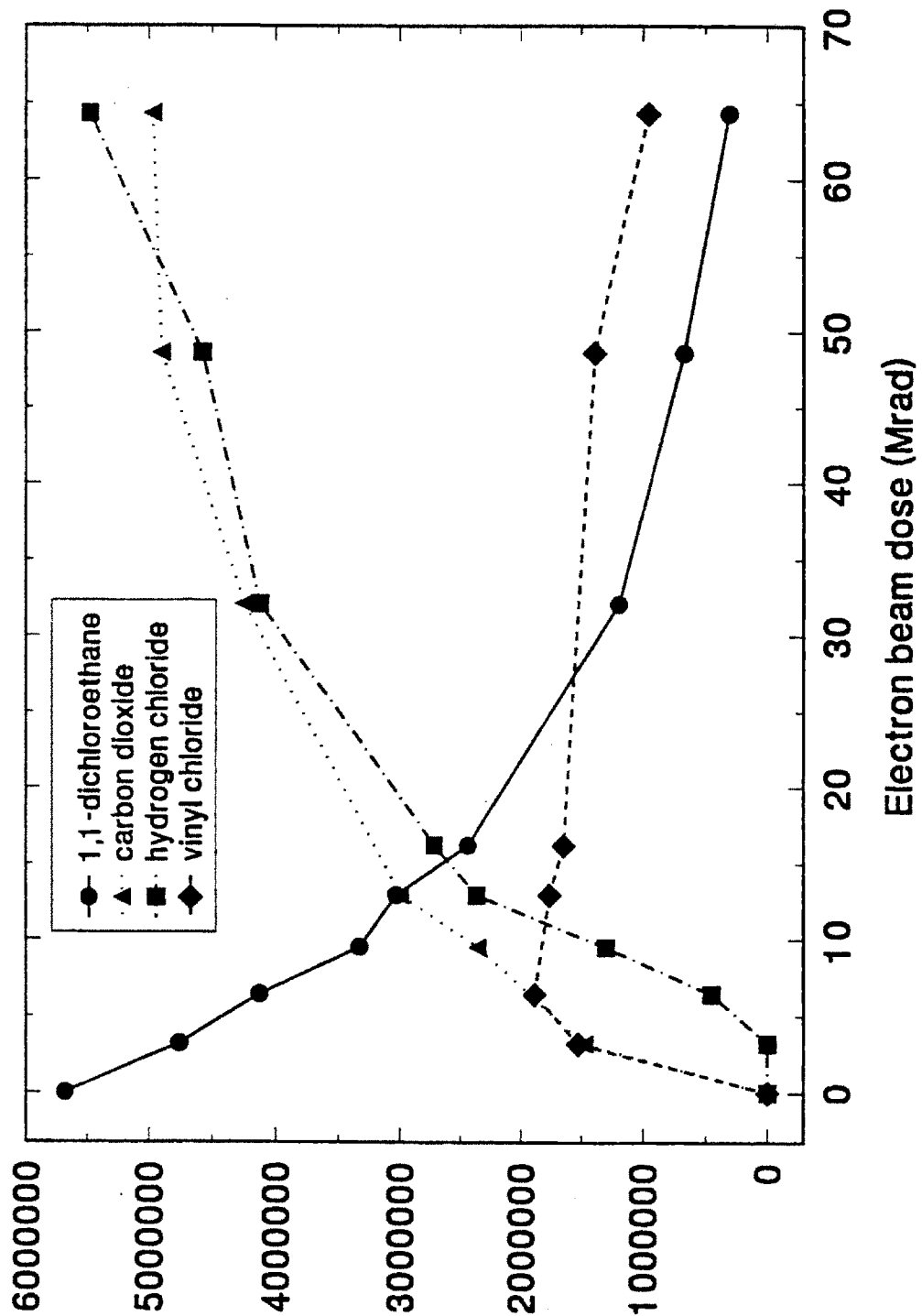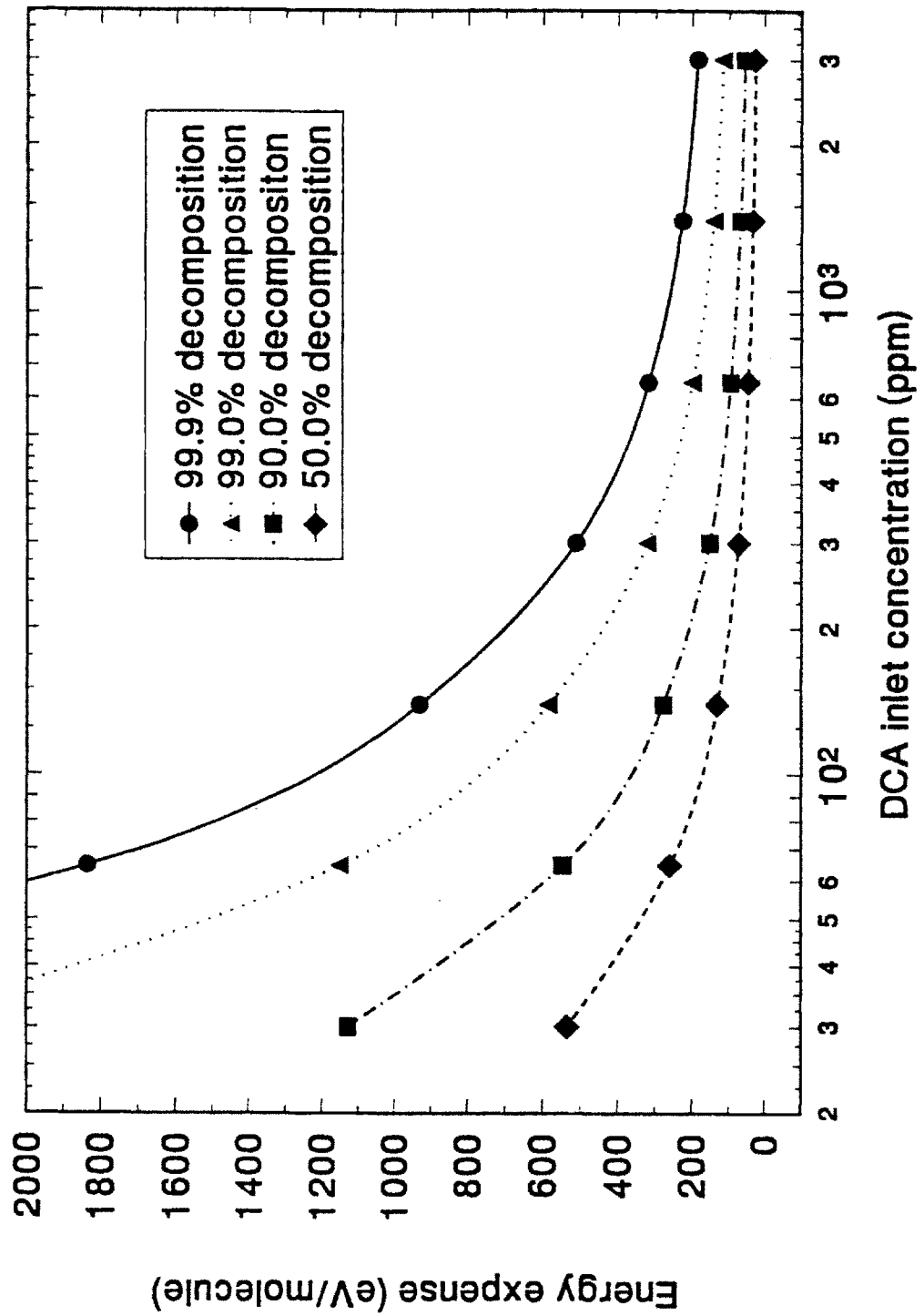**Figure 4.22:** Graph of the Rosocha β-value versus inlet DCA concentration.

Figure 4.23: Major reaction products of DCA decomposition. The ion abundances from the mass spectrometer peaks are given as a function of electron beam dose. The ion abundance is approximately linearly proportional to the concentration.
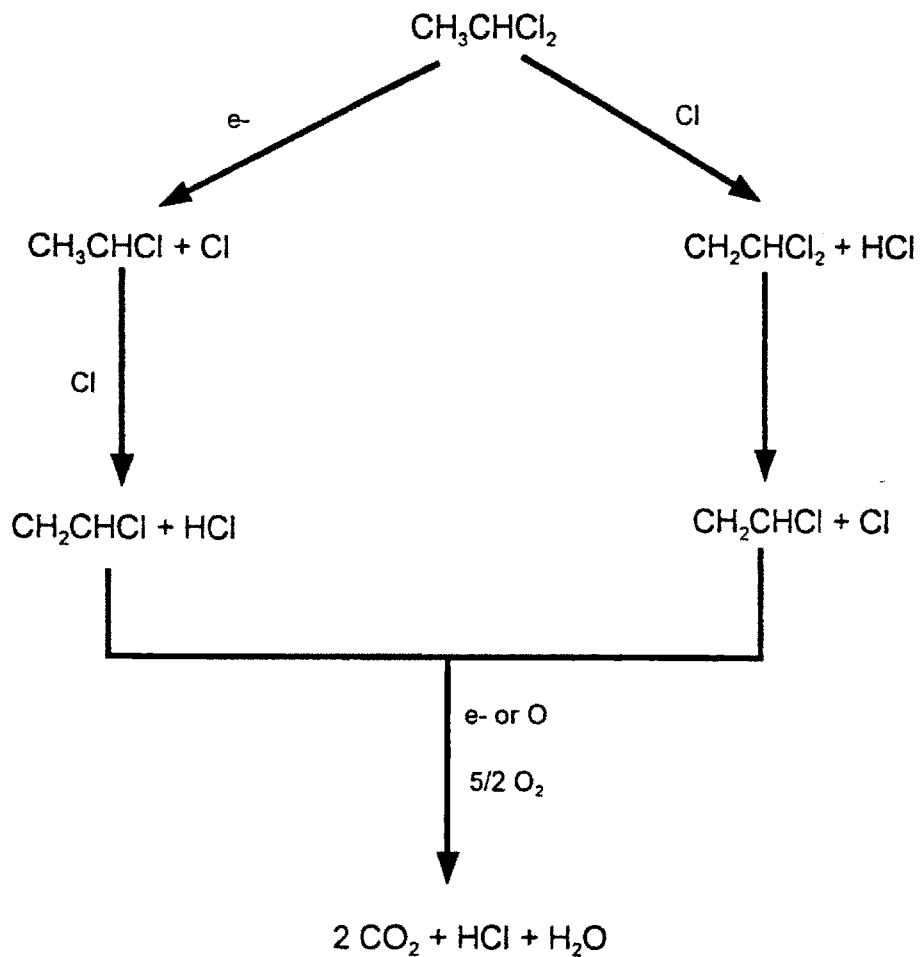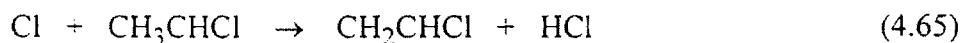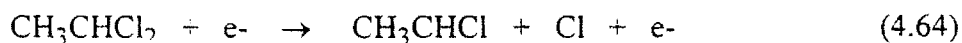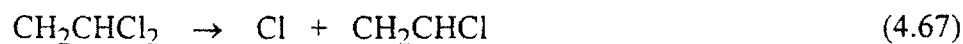
Figure 4.24: Specific energy, ε, required for DCA decomposition, as a function of TCE inlet concentration and desired fractional decomposition, η.

CH_3CHCl_2

e-   Cl

$CH_3CHCl + Cl$ $CH_2CHCl_2 + HCl$

Cl

$CH_2CHCl + HCl$ $CH_2CHCl + Cl$

e- or O

$5/2\ O_2$
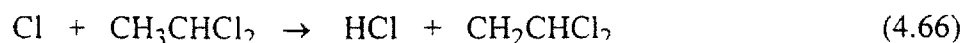
$2\ CO_2 + HCl + H_2O$

Figure 4.25: Schematic of reaction pathways of DCA decomposition in the EBGPR.

4.5.2 Reaction Pathways

The abundances of the observed reaction products of DCA decomposition as a function of electron beam dose are given in figure 4.23. Note that the Y-scale on this graph is arbitrary; that is the relative abundance of the four species is not drawn to scale on this graph. The only observed products of DCA decomposition were hydrogen chloride, carbon dioxide, and small amounts of vinyl chloride. The vinyl is formed from DCA through dehydrochlorination, which is similar to a commercial high temperature process in which DCA is converted to vinyl chloride monomer.[95] Other studies of DCA reactions have also found HCl, CO_2, and VC as the major reaction products.[96-97] In the present work, the reaction is initiated by dissociative electron attachment rather than thermal processes:

$$CH_3CHCl_2 + e- \rightarrow CH_3CHCl + Cl + e- \hspace{2cm} (4.64)$$

$$Cl + CH_3CHCl \rightarrow CH_2CHCl + HCl \hspace{2cm} (4.65)$$

In reaction (4.65), the hydrogen abstraction can either take place at the α or β carbon. It is more likely to take place at the β carbon since there are three hydrogens at this site. Abstraction at the α carbon would most likely be followed by a hydrogen migration anyway, so the two processes lead to the same product, vinyl chloride. The chlorine radical produced in reaction (4.64) may abstract a hydrogen atom from another DCA molecule rather than a radical,

$$Cl + CH_3CHCl_2 \rightarrow HCl + CH_2CHCl_2 \hspace{2cm} (4.66)$$

$$CH_2CHCl_2 \rightarrow Cl + CH_2CHCl \hspace{2cm} (4.67)$$

and the product is again vinyl chloride.

The VC produced by either of these mechanisms will decompose in the plasma by reaction with electrons or activated oxygen atoms in the plasma.

$$CH_2CHCl + 5/2 O_2 \rightarrow 2CO_2 + H_2O + HCl \hspace{2cm} (4.68)$$
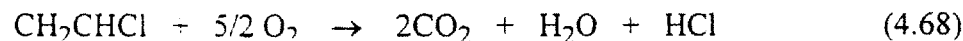
The details of this process are given in Section 4.8.

4.6 1,1-Dichloroethylene

4.6.1 Kinetic Analysis

A graph of outlet stream DCE concentration versus electron beam dose is shown in figure 4.26 for several inlet stream concentrations. Greater than 99% decomposition of

DCE is achieved for the lower concentration streams at flow rates up to 5 liters/min. Twenty-nine curves similar to those shown in figure 4.26 were generated at DCE inlet concentrations from 100 to 4000 ppm. These curves were analyzed by the differential kinetic methods as before.

Figure 4.27 shows the initial rates calculated from the curves as a function of initial concentration of DCE. In this case, the order with respect to concentration is given by: $n_c = 0.96$, with a correlation coefficient of 0.98. This excellent correlation to first order behavior is remarkable. The improvements to the experimental system such as the digital flow meters and the new leak-free reaction chamber are possibly responsible for these excellent results, compared to the less accurate data points taken for TCA and TCE decomposition. The reaction rate constant, k, is calculated to be:

$$\ln k = 0.74 \quad \Rightarrow \quad k = 2.06 \text{ Mrad}^{-1}$$

The order with respect to time analysis was performed on each curve of DCE concentration versus electron beam dose. A representative plot is shown in figure 4.28. The order with respect to time, n_t, and the rate constant, k, were calculated for each curve and the results averaged, to give:

$$n_t = 1.38 \pm 0.14$$

$$\ln k = -1.94 \pm 0.73 \quad \Rightarrow \quad k = 0.069 - 0.29 \text{ Mrad}^{-1} \text{ ppm}^{-1/2}$$

Once again, since $n_t > n_c$, the kinetics appear to be inhibited. However, the difference between the two orders is comparable to that seen for TCE decomposition, as opposed to the large difference seen in TCA decomposition. The inhibition is accounted for in the reaction mechanism outlined below.

Again rounding n_t to the nearest half integer, the final rate expression is:

$$C_2H_2Cl_2 \quad \rightarrow \quad \text{products}$$

$$r = -0.14 \ [C_2H_2Cl_2]^{3/2} \quad \text{ppm/Mrad} \tag{4.69}$$

This rate expression is used in conjunction with the ideal performance equation for the EBGPR derived in Section 2.2.2 to determine the reactor power needed to achieve a desired conversion of DCE.

The INHIBIT model, was fit to the 29 concentration versus dose curves to generate β' and K values. The best fits gave K = 0.04. This would indicate that inhibition is not very important in this mechanism, however from the data in figure 4.26, it is seen that the decomposition follows highly non-linear behavior. The INHIBIT model does not represent this sort of behavior well at all, for the reasons given in Section 2.2.3. To illustrate this, the β' values were calculated for DCE as a function of inlet concentration shown in figure 4.29a. The pseudo-beta values are seen to be approximately constant with concentration, at $\beta' \approx 0.8$, which is quite unlike the previous cases. Figure 4.29b shows

the continuous curves calculated for the INHIBIT model with these parameters. By comparing the calculated best fit and the experimental data, it is seen that the model cannot capture the strong nonlinear behavior of DCE kinetics. Reasons for this behavior are given in the discussion of the mechanism of DCE decomposition.

In spite of the poor qualitative fit of the data to the INHIBIT model, the numerical difference between the data and the calculated curves is not very large at high fractional decompositions. In any event, the small curvature in the plots allowed by the INHIBIT model is better than the first order kinetic assumption used to derive the BETAFIT model and β-values. The uninhibited model ALPHAFITPLUS may in fact give a better fit to the data, though their use cannot be justified as anything other than an attempt to fit the data since the kinetics were shown to be inhibited by the differential analysis.

For comparison to the other compounds, the energy expense was calculated using the INHIBIT parameters and equation (2.70). The results are shown in figure 4.32.

Rosocha β values were calculated from the DCE data up to 90% fractional decomposition, and the results are given in figure 4.30. Linear fitting of the data gives:

$$\beta = .0001\ (T_0) + 0.42 \qquad \text{Mrad} \qquad\qquad (4.70)$$

with T_0 in ppm. Here, the β-values do not show a very strong dependence on concentration, and assuming that β is a constant is reasonable. However, from the data presented in figure 4.26, it is evident that DCE decomposition does not follow first order kinetic behavior very well, and thus β-values are probably not an accurate measure of the decomposition kinetic rate constant. Further the offset from zero is large for this data for the β-values, so equation (2.77) is not an appropriate method to determine the G-value for DCE.
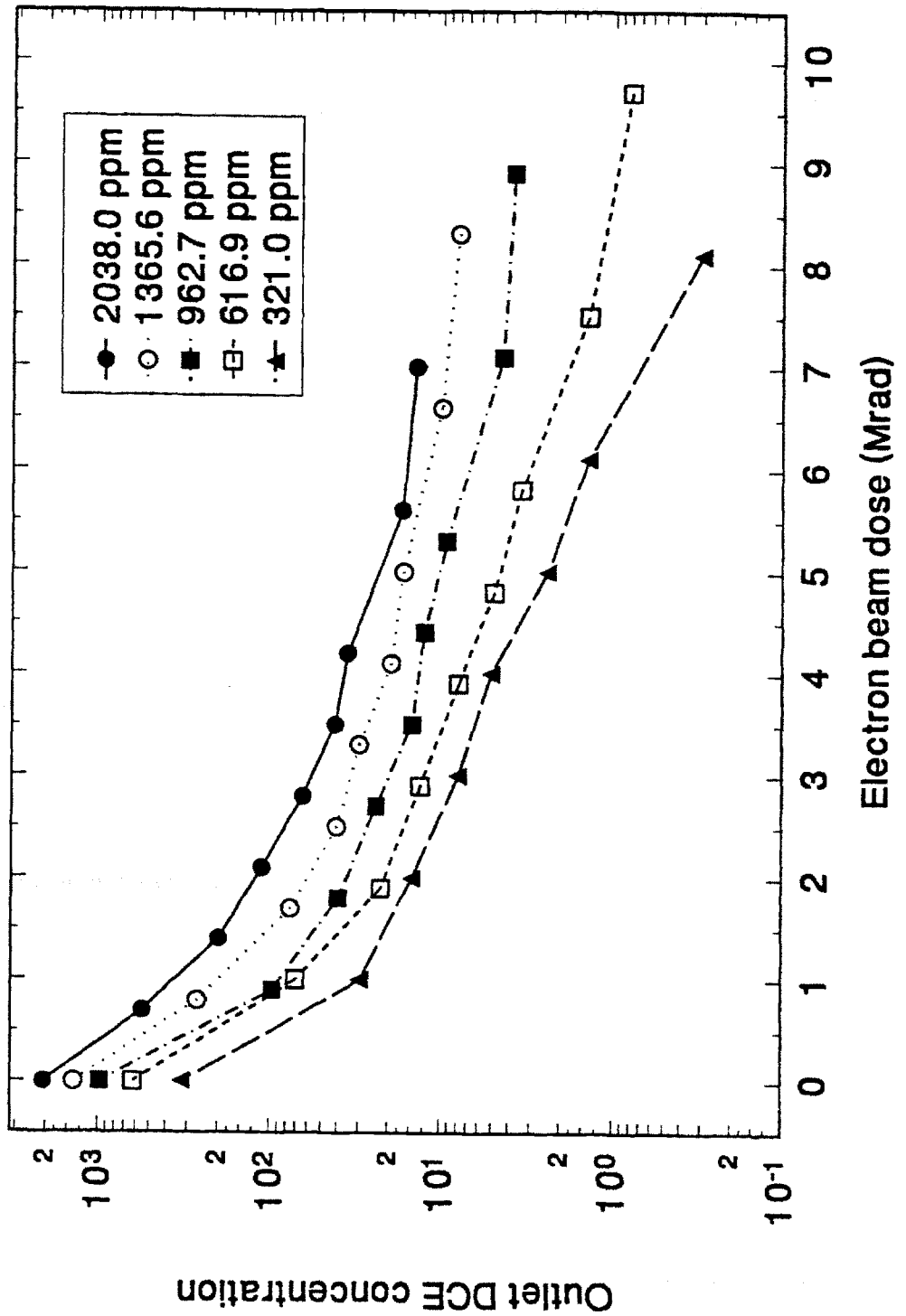
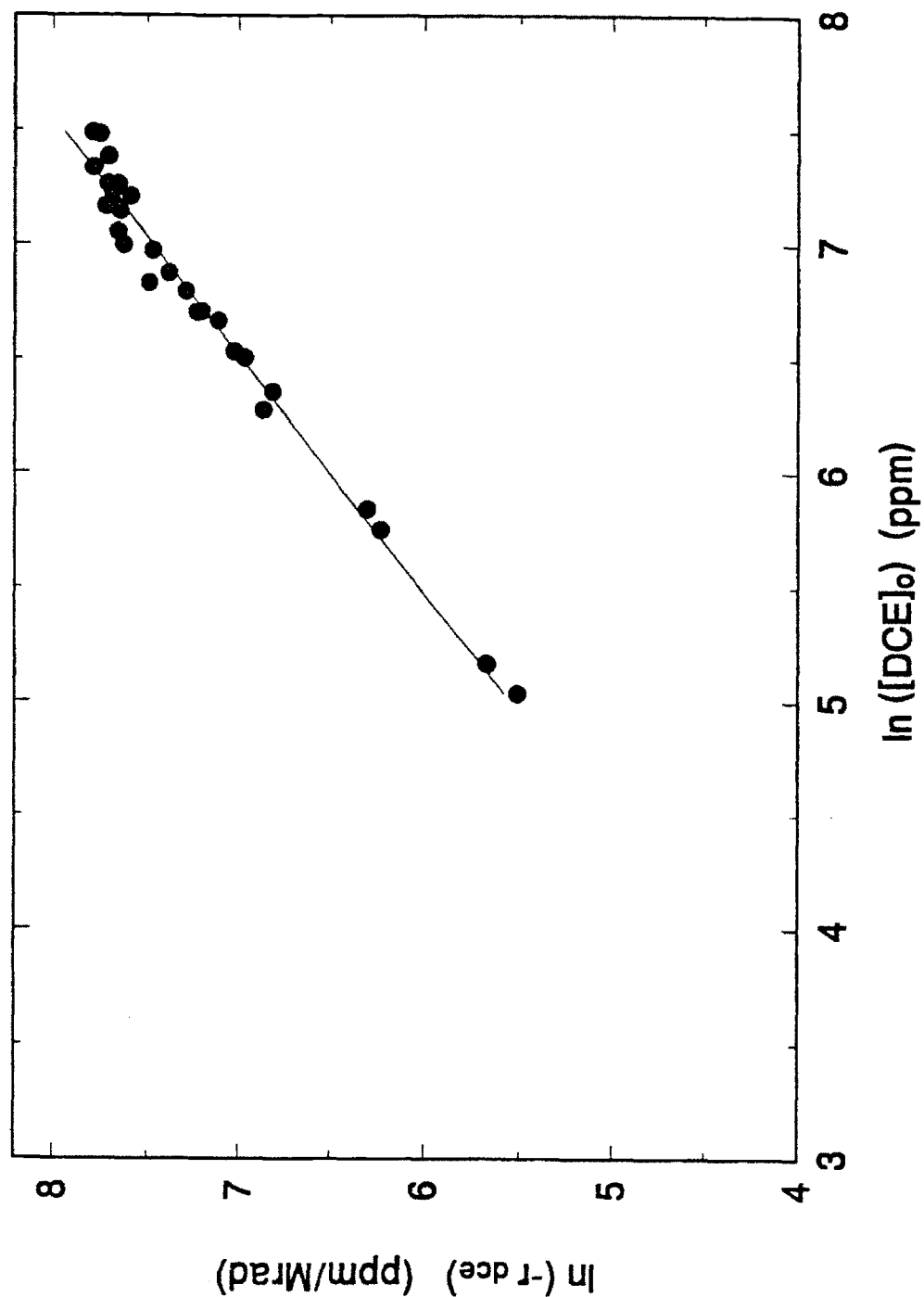**Figure 4.26:** 1.1-Dichloroethylene outlet concentration as a function of electron beam dose.

Figure 4.27: Differential kinetic analysis of DCE decomposition. This graph shows the initial reaction rate, $-r = \dfrac{d[DCE]}{dD}$, as a function of initial DCE concentration. The slope of this line gives the order with respect to concentration, n_c, and the intercept with the Y-axis gives the rate constant, k.
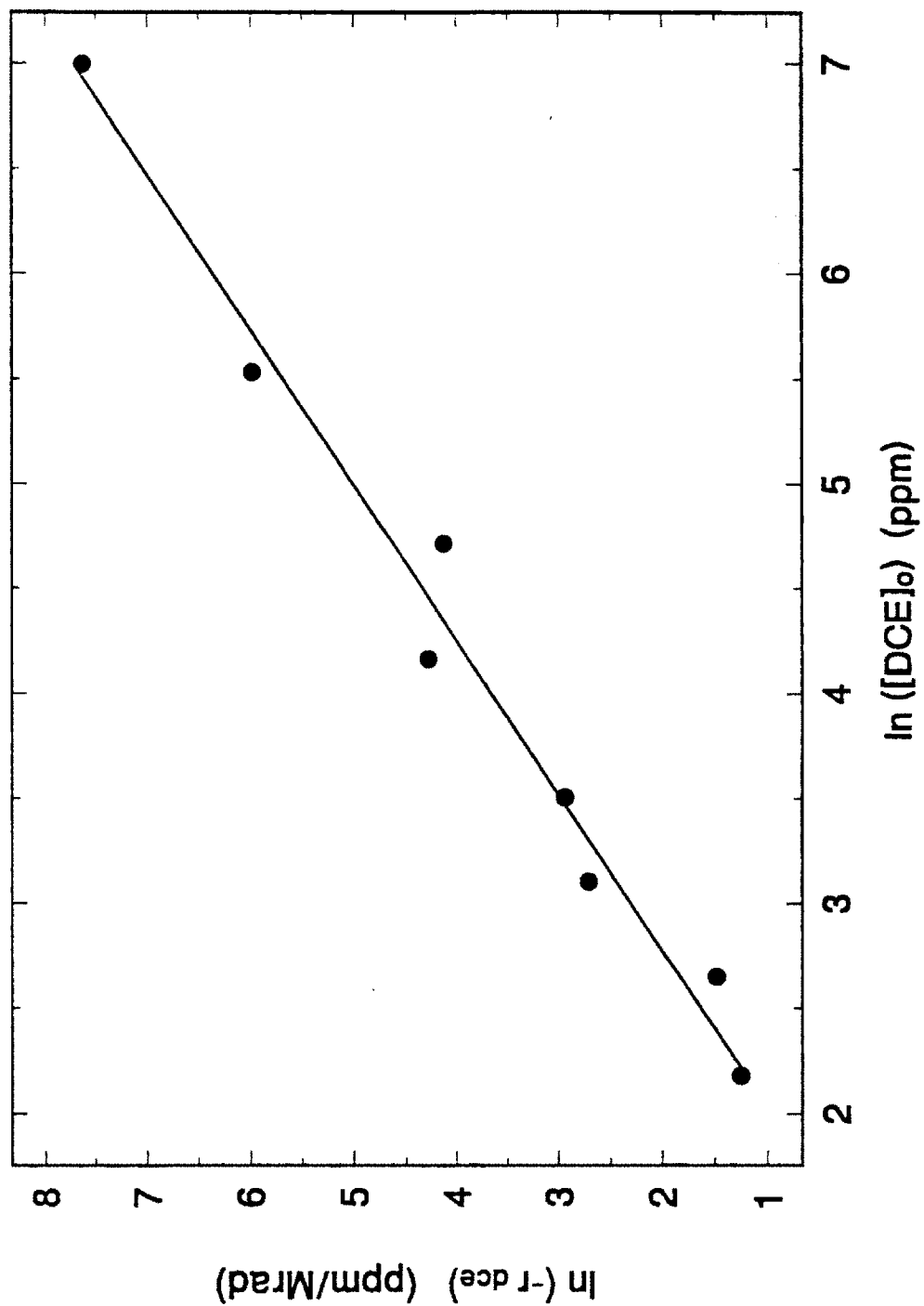
Figure 4.28: A representative graph of one run of DCE, showing the actual reaction rate as a function of DCE concentration, as the reaction proceeds. The slope of this line gives the order with respect to time, n_t, and the intercept with the Y-axis gives the rate constant, k.
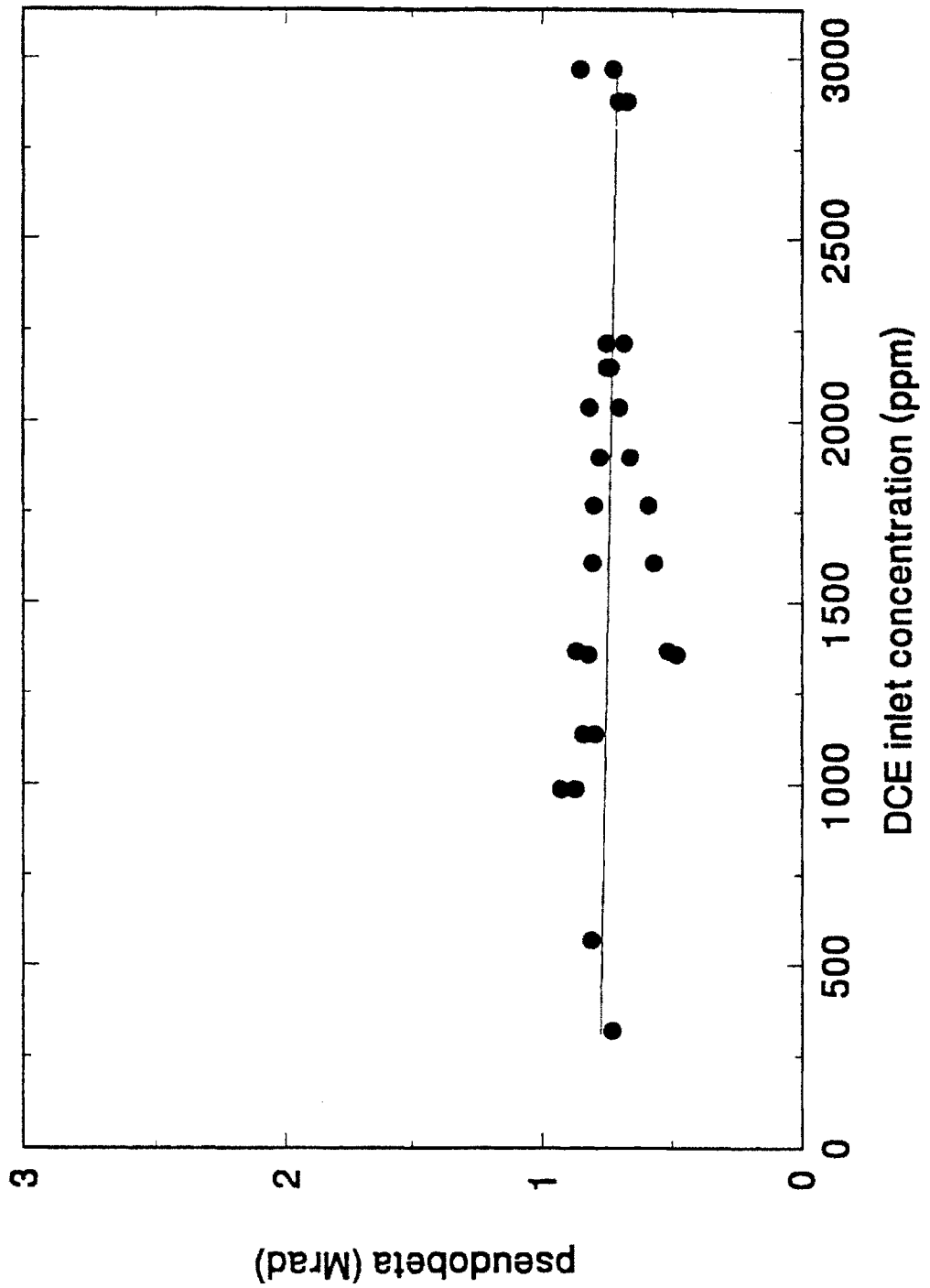
Figure 4.29a: Graph of pseudo-β, versus DCE inlet concentration from INHIBIT model fit.
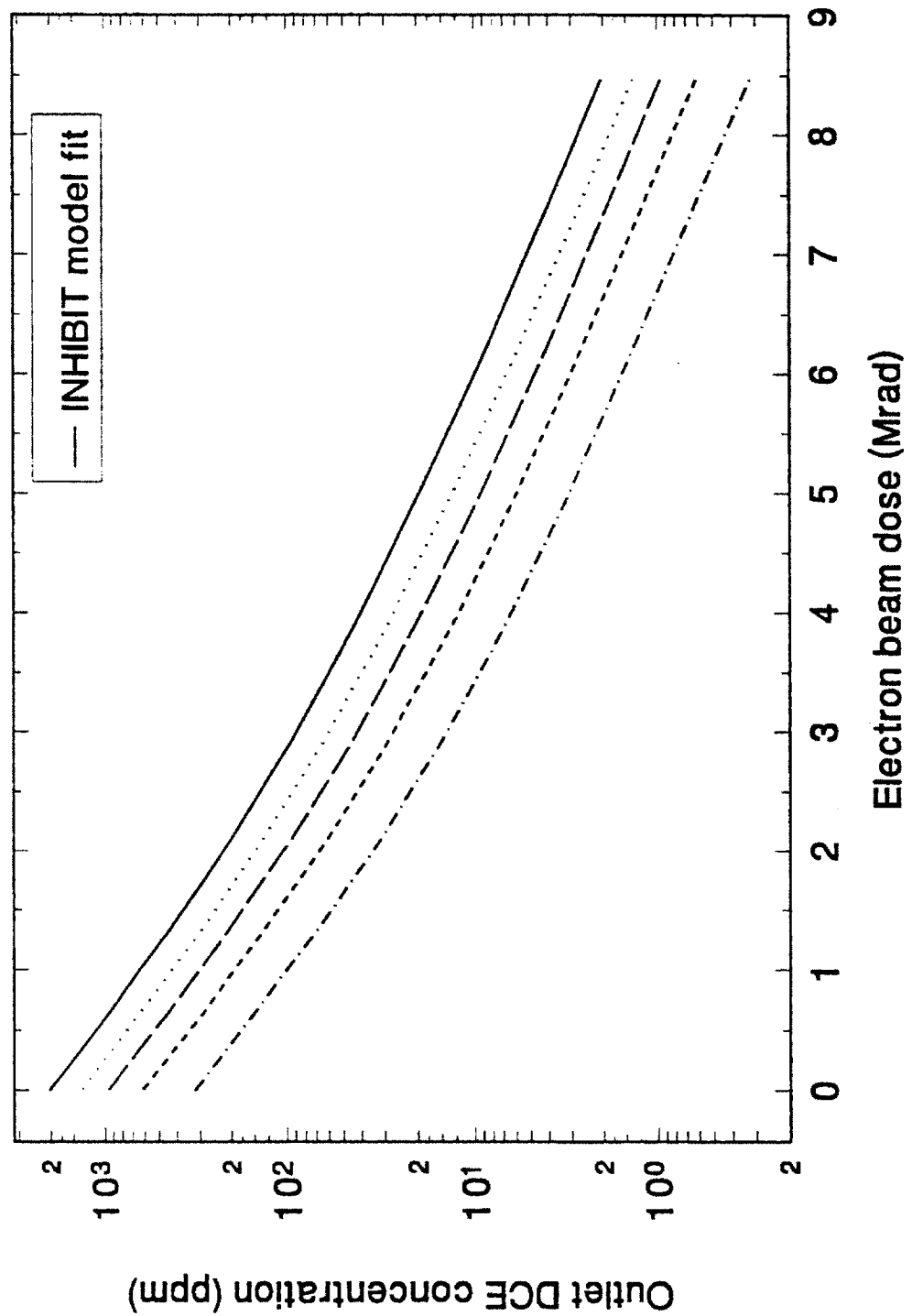
116

Figure 4.29b: Graph of calculated DCE concentration versus electron beam dose curves from best fit INHIBIT model. The initial concentrations are the same as the experimental data given in figure 4.26 so the two graphs may be compared.
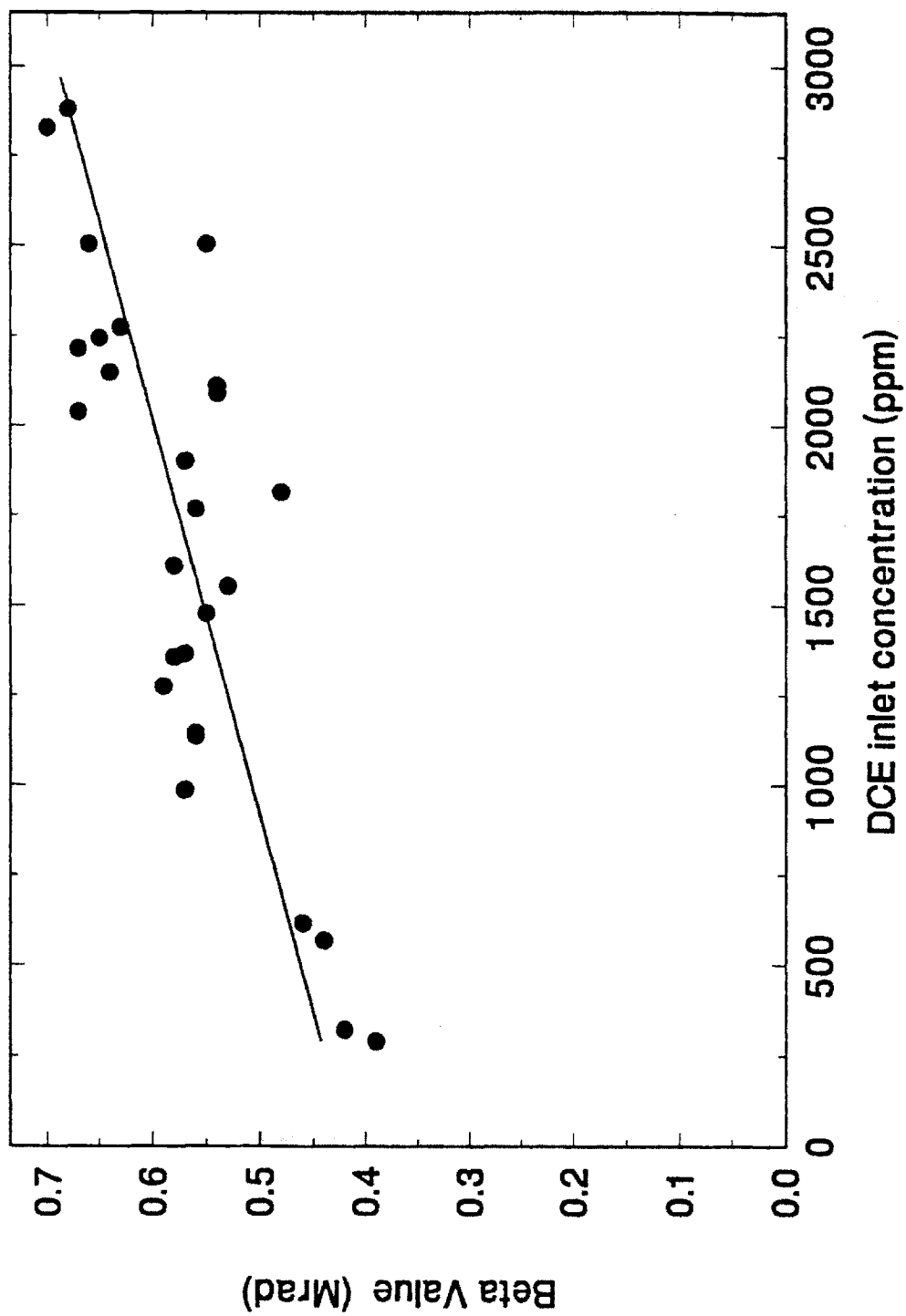
117

Figure 4.30: Graph of the Rosocha β-value versus inlet DCE concentration.
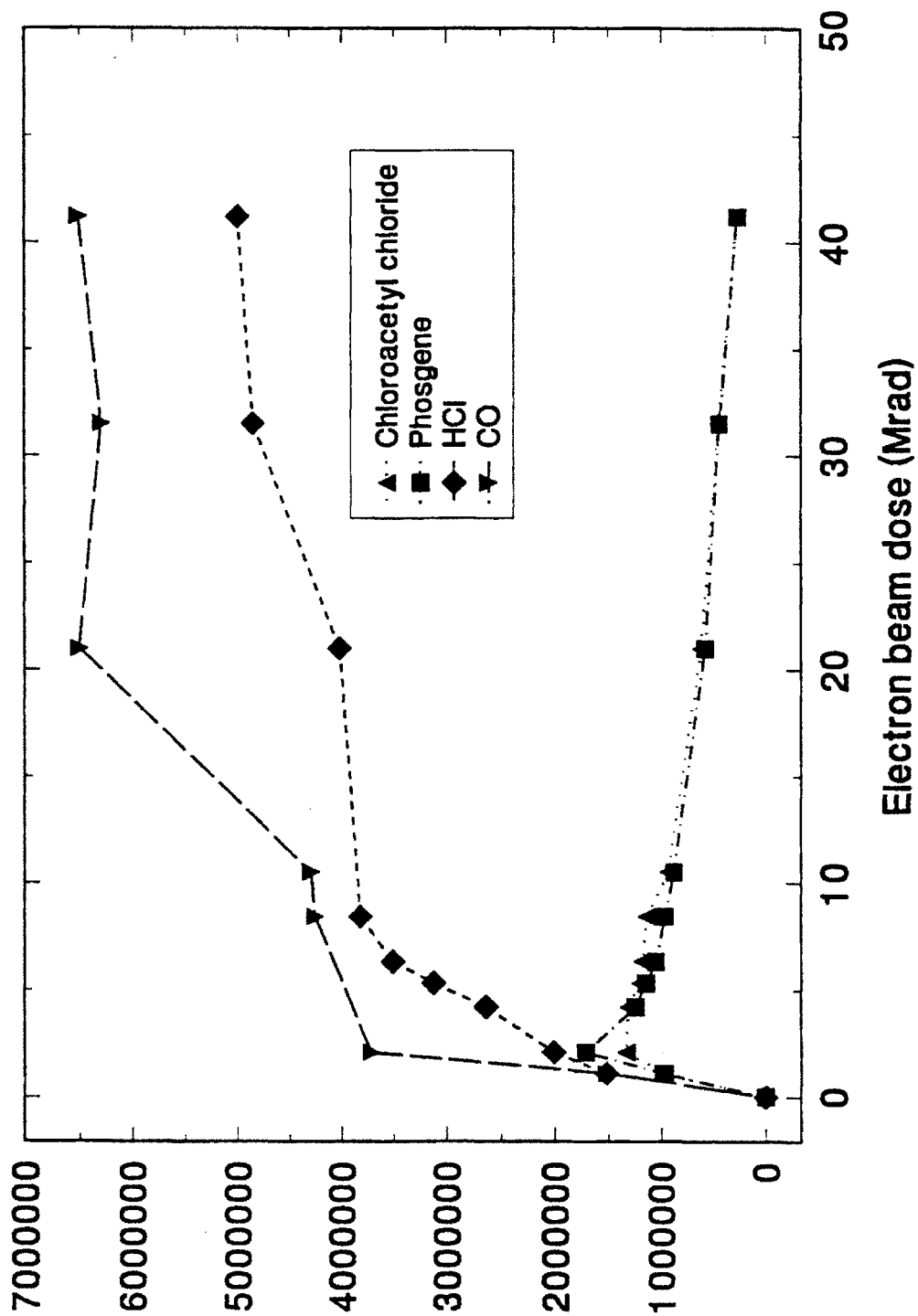
Figure 4.31: Major reaction products of DCE decomposition. The ion abundances from the mass spectrometer peaks are given as a function of electron beam dose. The ion abundance is approximately linearly proportional to the concentration.
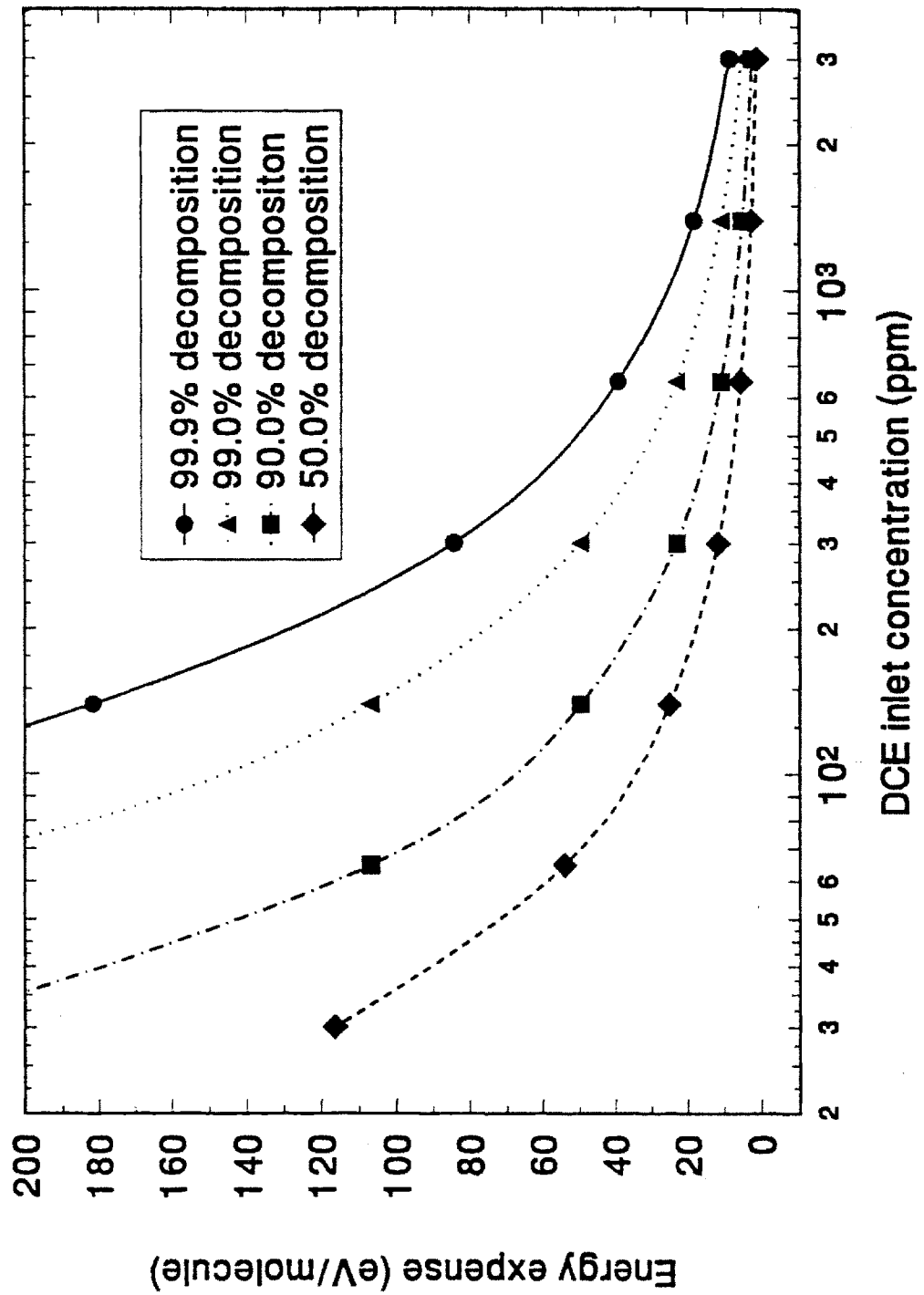
119

Figure 4.32: Specific energy, ε, required for DCE decomposition. as a function of DCE inlet concentration and desired fractional decomposition, η.

CH$_2$CCl$_2$

e - → CH$_2$CCl + Cl → polymer

Cl → CH$_2$ClCCl$_2$

O (^{3}P) → CO + HCl + CHCl

O$_2$ → OH + ClCO → Cl + CO

CCl$_2$CH$_2$O* → polymer

CH$_2$ClCCl$_2$ + O$_2$ → CH$_2$ClCCl$_2$OO

CH$_2$ClCCl$_2$OO

CH$_2$ClCCl$_2$ → (CH$_2$ClCCl$_2$O)$_2$

2 CH$_3$ClCCl$_2$O + O$_2$

CH$_2$ClCCl$_2$OO → (CH$_2$ClCCl$_2$O)$_2$ + O$_2$

COCl$_2$ + CH$_2$Cl

CClH$_2$CClO + Cl

Cl → COClCHCl + HCl

O$_2$ → COClCHCl + HO$_2$

O$_2$ → COClCHClOO

COClCHClOO → 2COClCHClO
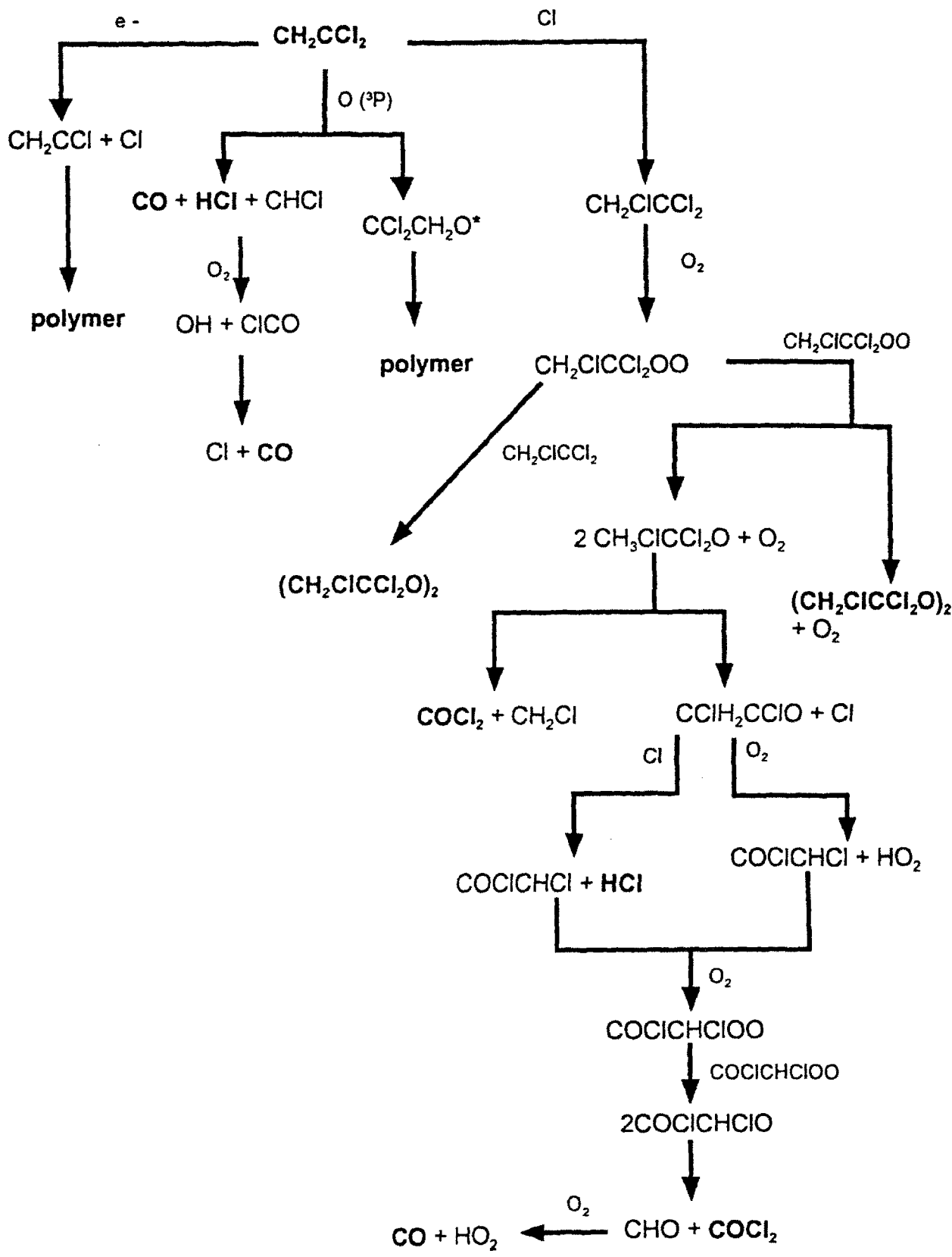
O$_2$ → CHO + COCl$_2$ → CO + HO$_2$

Figure 4.33: Schematic of reaction pathways of DCE decomposition in the EBGPR.

4.6.2 Reaction Mechanism

The observed reaction products of DCE decomposition were carbon monoxide, HCl, chloroacetyl chloride. and phosgene. The ion abundances of these products are shown as a function of electron beam dose figure 4.31. Two mechanisms of DCE decomposition will be illustrated below.
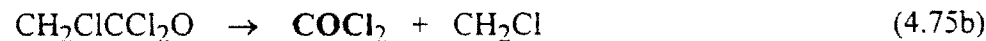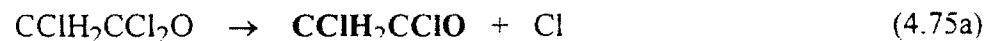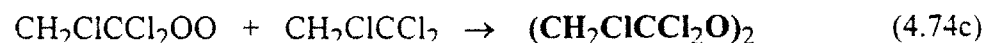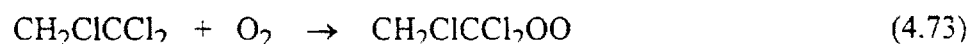
First and electron attachment induced dissociation mechanisms will be considered. This mechanisms follows closely that outlined by Sanheuza.[88]

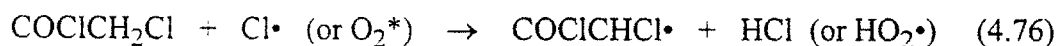$$e^- + CH_2CCl_2 \rightarrow CH_2CCl + Cl \qquad (4.71)$$
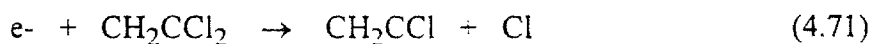
The C_2 radical formed may lose a chlorine atom to forma carbene radical. which can polymerize or oxidize in some way. The chlorine radical then goes on to attack another DCE molecule:

$$Cl + CH_2CCl_2 \rightarrow CH_2ClCCl_2 \qquad (4.72)$$

Here reaction occurs only at the less substituted carbon, since chlorine addition a carbon which already has two chlorines is sterically unfavorable. This species can be decomposed by reaction with oxygen molecules in the carrier gas,

$$CH_2ClCCl_2 + O_2 \rightarrow CH_2ClCCl_2OO \qquad (4.73)$$

$$2CH_2ClCCl_2OO \rightarrow 2\, \mathbf{CH_2ClCCl_2O} + O_2 \qquad (4.74a)$$

$$2CH_2ClCCl2OO \rightarrow \mathbf{(CH_2ClCCl_2O)_2} + O_2 \qquad (4.74b)$$

$$CH_2ClCCl_2OO + CH_2ClCCl_2 \rightarrow \mathbf{(CH_2ClCCl_2O)_2} \qquad (4.74c)$$

$$CClH_2CCl_2O \rightarrow \mathbf{CClH_2CClO} + Cl \qquad (4.75a)$$

$$CH_2ClCCl_2O \rightarrow \mathbf{COCl_2} + CH_2Cl \qquad (4.75b)$$

The reactions (4.75a) and (4.75b) produce chloroacetyl chloride and phosgene respectively. Further. the chloroacetyl chloride can decompose further in the plasma to form carbon monoxide. hydrogen chloride. and more phosgene and carbon monoxide, as shown in the TCE decomposition mechanism.

$$COClCH_2Cl + Cl \cdot \ (or \ O_2^*) \rightarrow COClCHCl \cdot + HCl \ (or \ HO_2 \cdot) \quad (4.76)$$

$$COClCHCl \cdot + O_2 \rightarrow COClCHClOO \cdot \quad (4.77)$$

$$2\,COClCHClOO \cdot \rightarrow 2\,COClCHClO \cdot + O_2 \quad (4.78)$$

$$COClCHClO \cdot \rightarrow CHO \cdot + COCl_2 \quad (4.79)$$

$$CHO \cdot + O_2 \rightarrow CO + HO_2 \cdot \quad (4.80)$$

Reaction (4.79) proceeds through a chlorine migration. That fact that the decomposition of chloroacetyl chloride is occurs in the plasma is reinforced by the observation that HCl and phosgene account for more of the product chlorine than chloroacetyl chloride.

The second mechanism is based on O^3P sensitized oxidation. Sanhueza[88] examined this reaction . and determined that the following two pathways are the most important:

$$O(^3P) + CCl_2CH_2 \rightarrow CO + HCl + CHCl \quad (4.81a)$$

$$O(^3P) + CCl_2CH_2 \rightarrow CCl_2CH_2O^* \quad (4.81b)$$
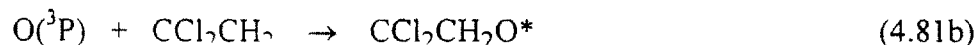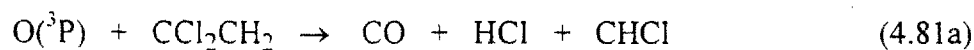
where the asterix represents an excited species. The product of reaction (4.81b) leads to polymer. Although solid polymer was not actually observed in the reactor, if it was formed it is likely to have bee swept out of the continuously flowing system without passing through the GC, or to have been caught in one of two filters on the system. The radical produced in reaction (4.81a) reacts with molecular oxygen,

$$CHCl + O_2 \rightarrow HO + ClCO \quad (4.82)$$

$$ClCO \rightarrow Cl + CO \quad (4.83)$$

Reaction (4.83) produces a free chlorine radical. This radical may then react with a DCE molecule by the first mechanism. Cl sensitized oxidation. This will produce more chlorine radicals. and thus a chain reaction is observed. as was shown to be the case with TCE. Thus both mechanisms produce chlorine radicals to allow a chlorine radical chain reaction. Note that neither chloroacteyl chloride nor phosgene are produced directly by $O(^3P)$ sensitized oxidation. Thus, in order to account for the formation of these products, the chlorine radical produced in reaction (4.83) must react with a DCE molecule as described in mechanism 1. Cl radical sensitization. It cannot be determine from the study of DCE in isolation whether the chlorine radicals are produced through dissociative electron attachment as was assumed in mechanism 1, or through the O(3P) sensitized

oxidation mechanism. The proposal that dissociative electron attachment is the more likely mechanisms will be explained in Chapter 5.

4.7 Ethyl Chloride

4.7.1 Kinetic Analysis

A graph of outlet stream EC concentration versus electron beam dose is shown in figure 4.34 for several inlet stream concentrations. Greater than 99% decomposition of EC is achieved for the lower concentration streams at flow rates up to 3 liters/min. Thirty-four curves similar to those shown in figure 4.34 were generated at EC inlet concentrations from 100 to 3000 ppm.

Figure 4.35 shows the initial rates calculated from the curves as a function of initial concentration of EC. The order with respect to concentration and rate constant are calculated to be:

$$n_c = 0.43$$

$$\ln k = 2.67 \quad \Rightarrow \quad k = 14.43 \text{ Mrad}^{-1} \text{ ppm}^{1/2}$$

The order with respect to time analysis was performed on each curve of EC concentration versus electron beam dose. A representative plot is shown in figure 4.36. The results are:

$$n_t = 1.64 \pm 0.32$$

$$\ln k = -6.16 \pm 1.68 \quad \Rightarrow \quad k = 3.93 * 10^{-4} - 1.13 * 10^{-2} \text{ Mrad}^{-1} \text{ ppm}^{-1/2}$$

As with TCA, n_t is greater than n_c, showing that the kinetics are inhibited. However, for EC decomposition, difference is even more pronounced than for TCA decomposition; this is the opposite of the TCE and DCE results.

Again rounding n_t to the nearest half integer, the final rate expression is:

$$C_2H_5Cl \quad \rightarrow \quad \text{products}$$

$$r = -2.11 * 10^{-3} [C_2H_5Cl]^{1/2} \quad \text{ppm/Mrad} \tag{4.84}$$
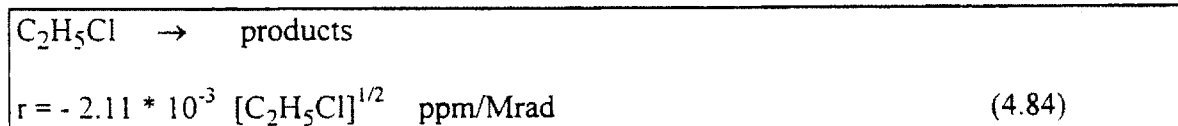
This rate expression is used in conjunction with the ideal performance equation for the EBGPR derived in Section 2.2.2 to determine the reactor power needed to achieve a desired conversion of EC.

Since n_c is less than n_t in this case, and the reaction thus appears to be inhibited, the inhibitor model, equation (2.69) was fit to the 34 concentration versus dose curves.

Figure 4.45a gives the calculated pseudobeta values, and figure 4.46b shows the calculated curves corresponding to the data presented in figure 4.34. The best fit parameters are given by:

$K = 0.22$

$\beta' = .00250 \, T_0 + 4.29 \quad \text{Mrad}$

Using the K and β' parameters again in equation (2.70), the energy expense, ε, was calculated as a function of the inlet concentration T_0, and the desired fractional decomposition η. The calculated curves are given in figure 4.40.

Rosocha β values were calculated from the EC data up to 95% fractional decomposition, and the results are given in figure 4.38. Linear fitting of the data gives:

$$\beta = .00216 \, (T_0) + 6.88 \qquad \text{Mrad} \qquad\qquad (4.85)$$

with T_0 in ppm. Once again, the large offset from zero precludes calculation of the G-value by equation (2.77).
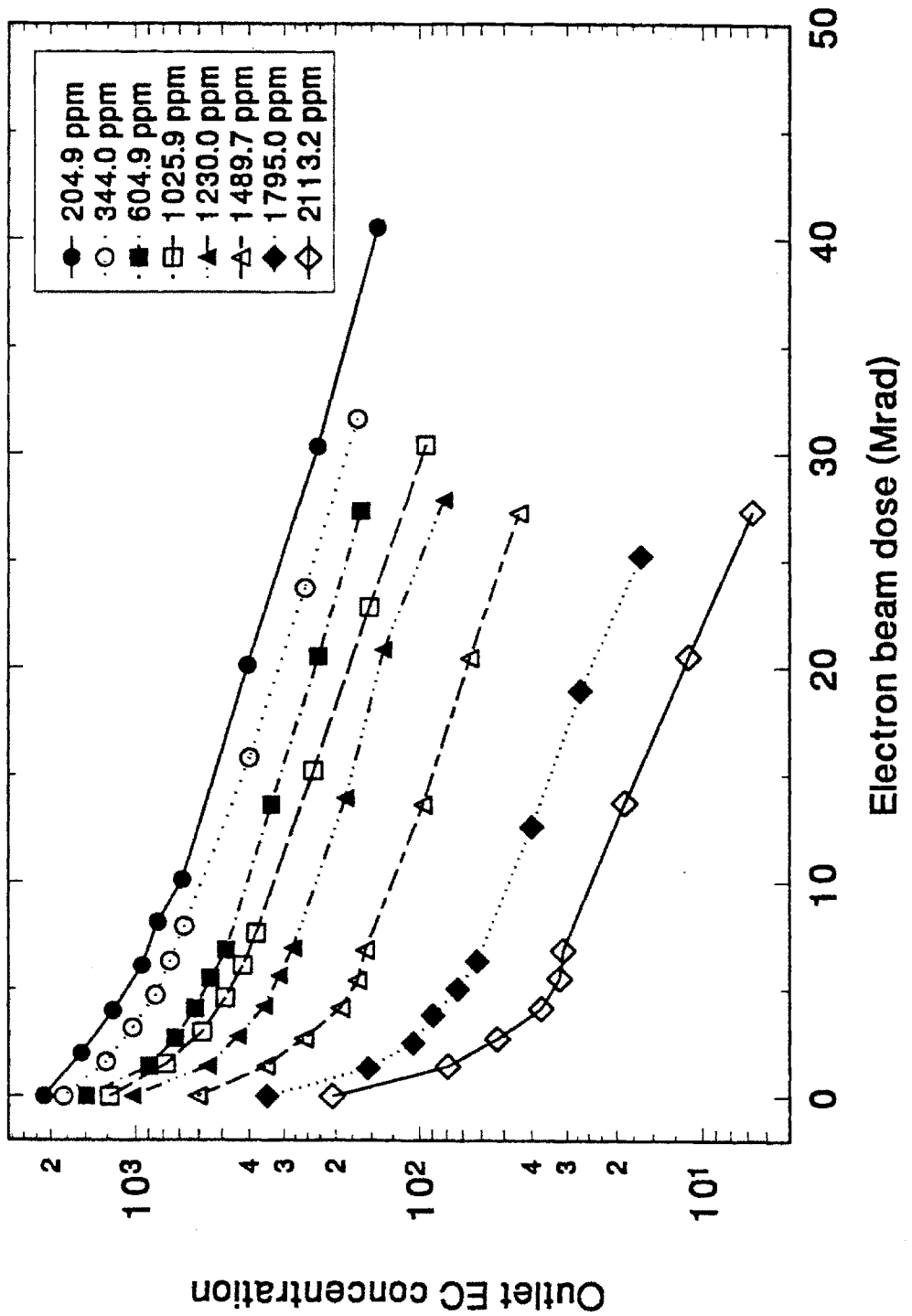
Figure 4.34: Ethyl Chloride outlet concentration as a function of electron beam dose.
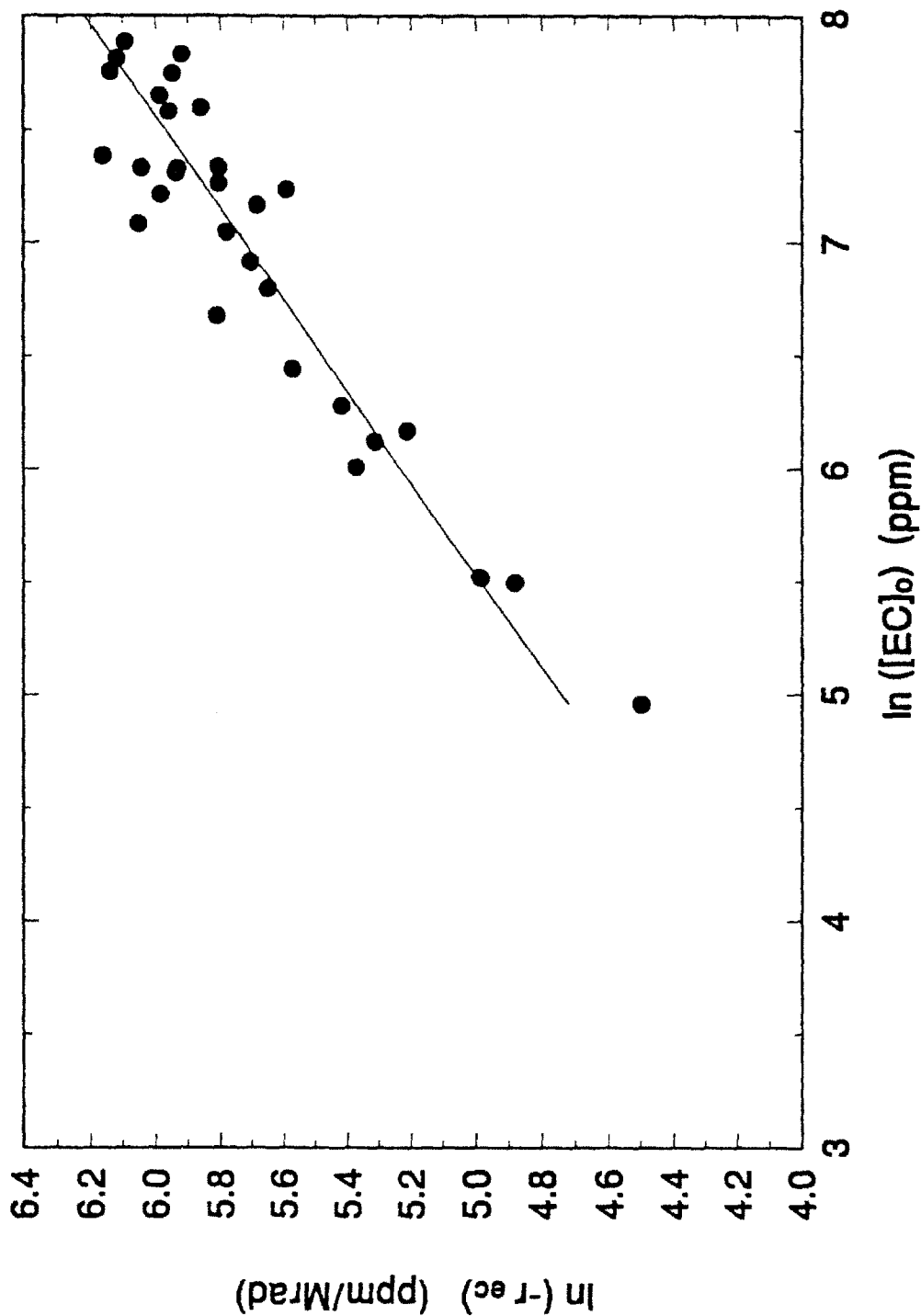
Figure 4.35: Differential kinetic analysis of EC decomposition. This graph shows the

initial reaction rate, $-r = \dfrac{d[EC]}{dD}$, as a function of initial EC concentration. The slope of

this line gives the order with respect to concentration, n_c, and the intercept with the Y-axis gives the rate constant, k.
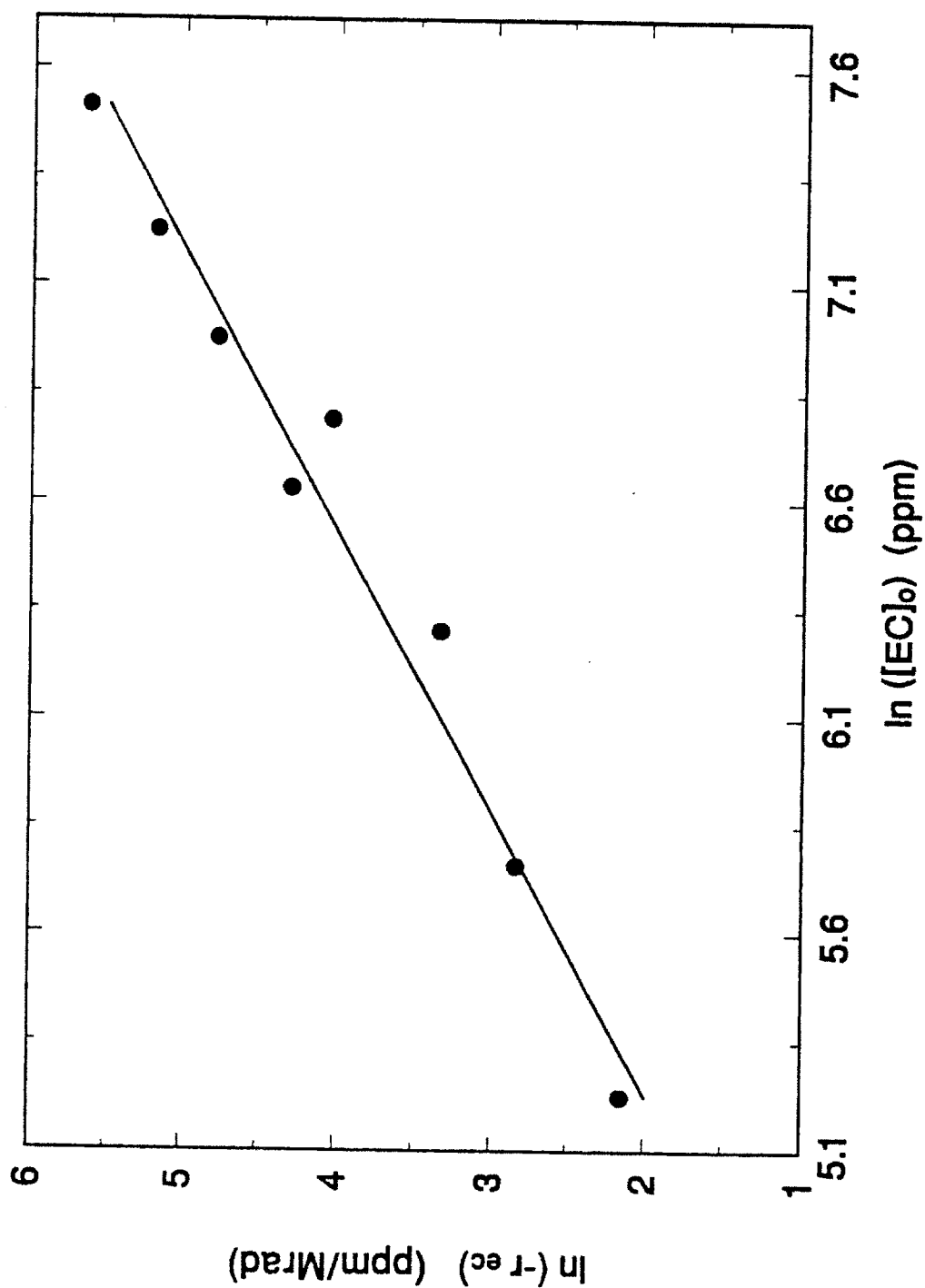
Figure 4.36: A representative graph of one run of EC, showing the actual reaction rate as a function of EC concentration, as the reaction proceeds, The slope of this line gives the order with respect to time, n_t, and the intercept with the Y-axis gives the rate constant, k.
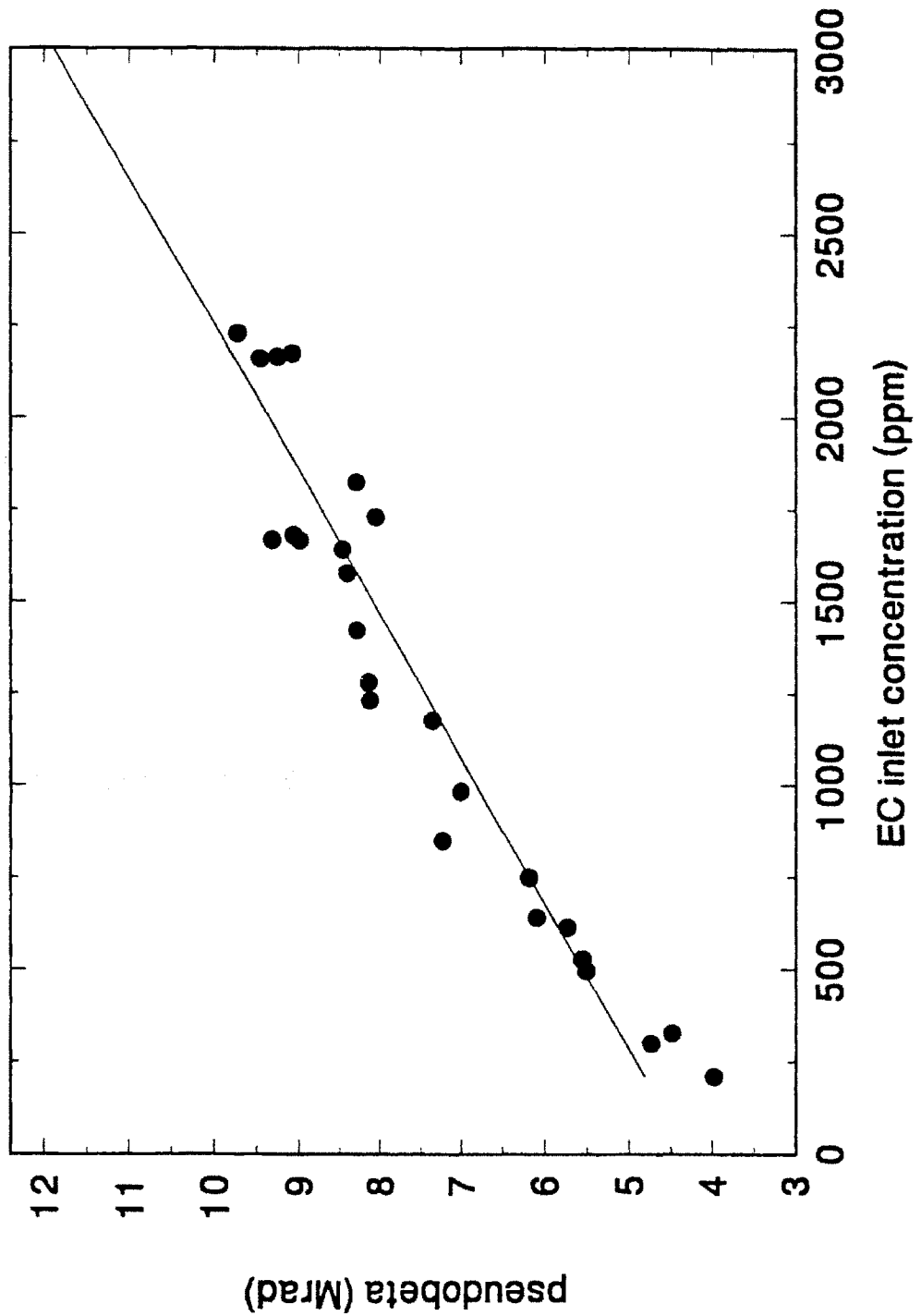
128

Figure 4.37a: Graph of pseudo-β, versus EC inlet concentration from INHIBIT model
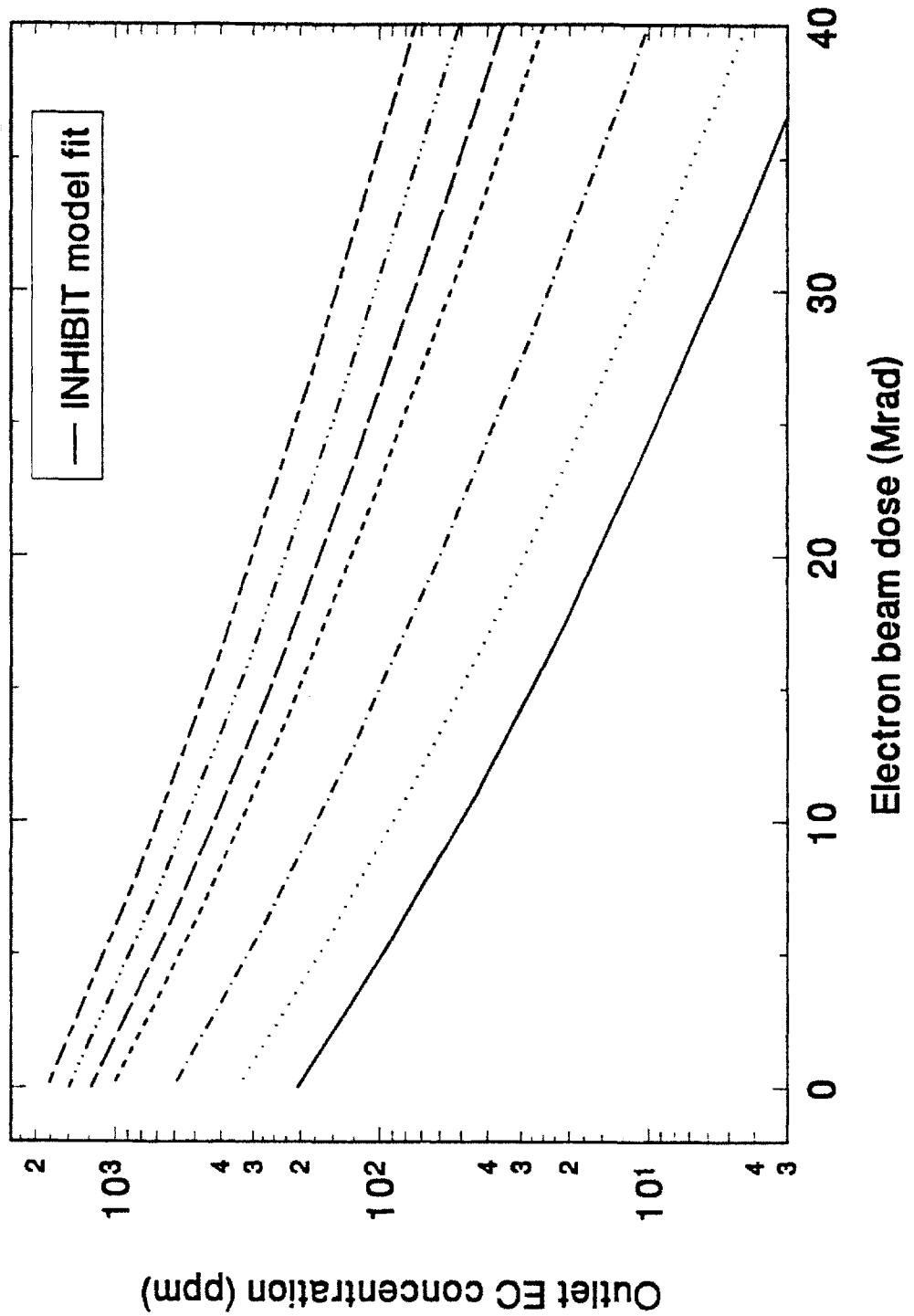fit.

Figure 4.37b: Graph of calculated EC concentration versus electron beam dose curves from best fit INHIBIT model. The initial concentrations are the same as the experimental data given in figure 4.34 so the two graphs may be compared.
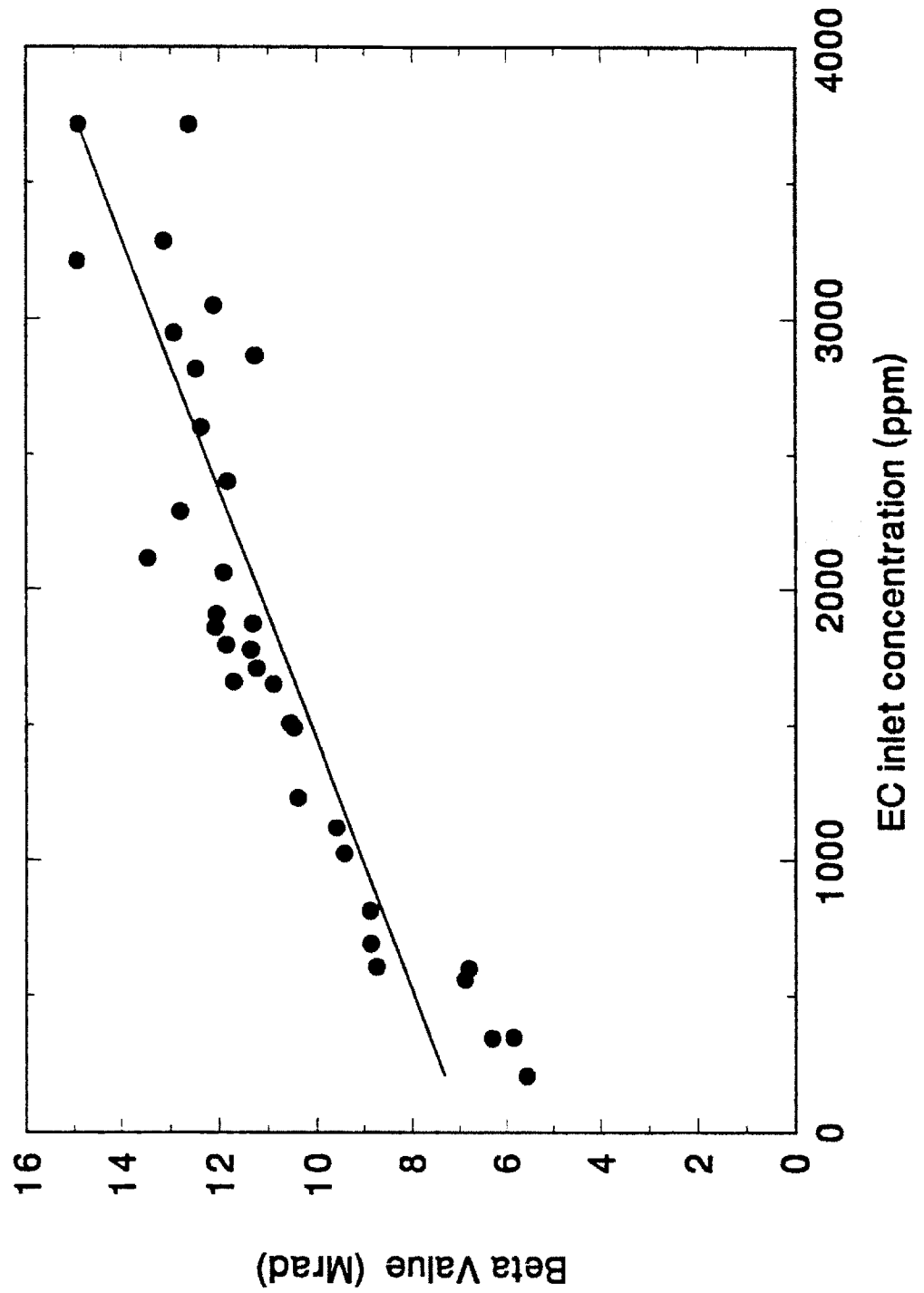
130

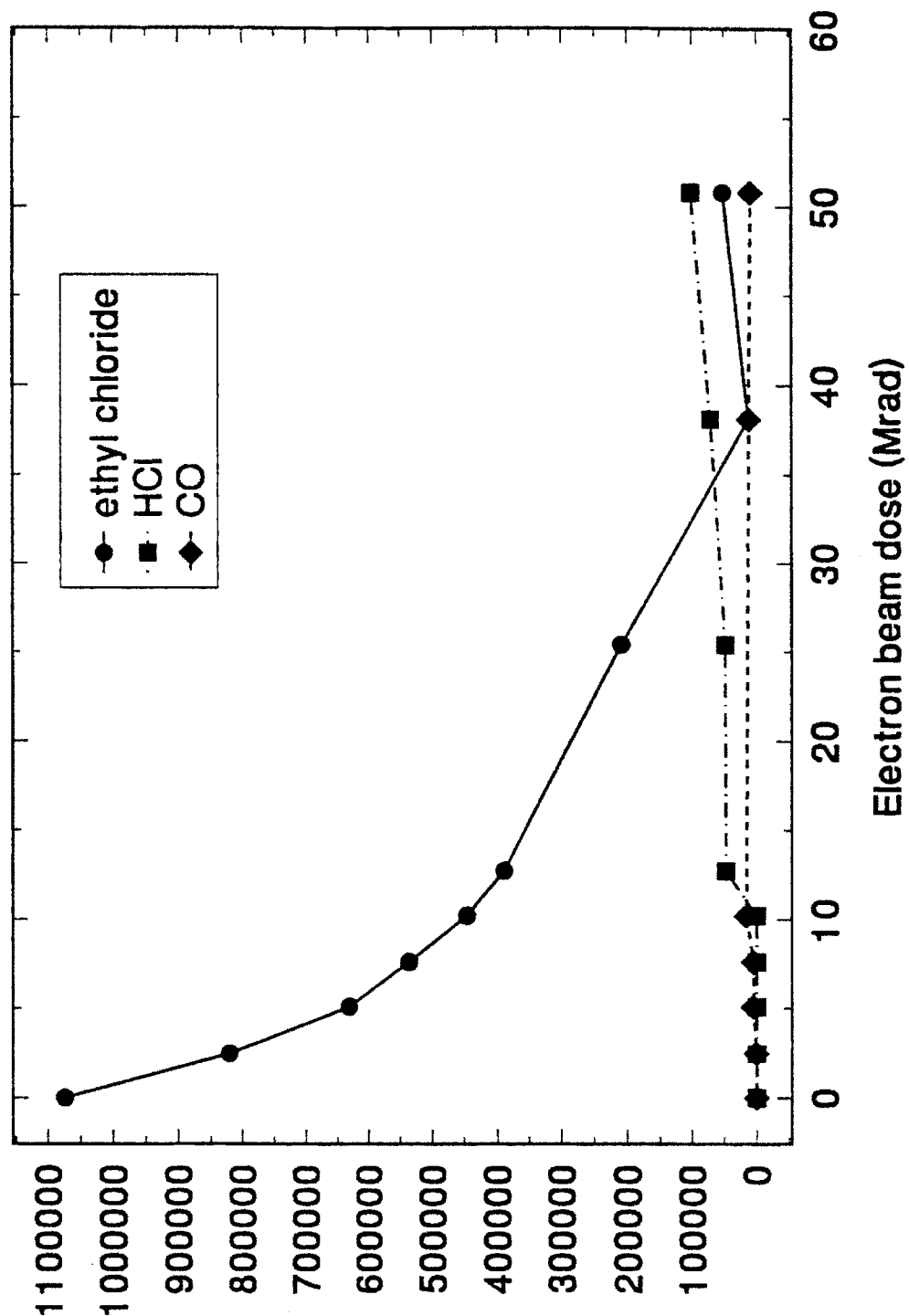**Figure 4.38:** Graph of the Rosocha β-value versus inlet EC concentration.

Figure 4.39: Major reaction products of EC decomposition. The ion abundances mass spectrometer peaks are given as a function of electron beam dose. The ion abundance is approximately linearly proportional to the concentration.
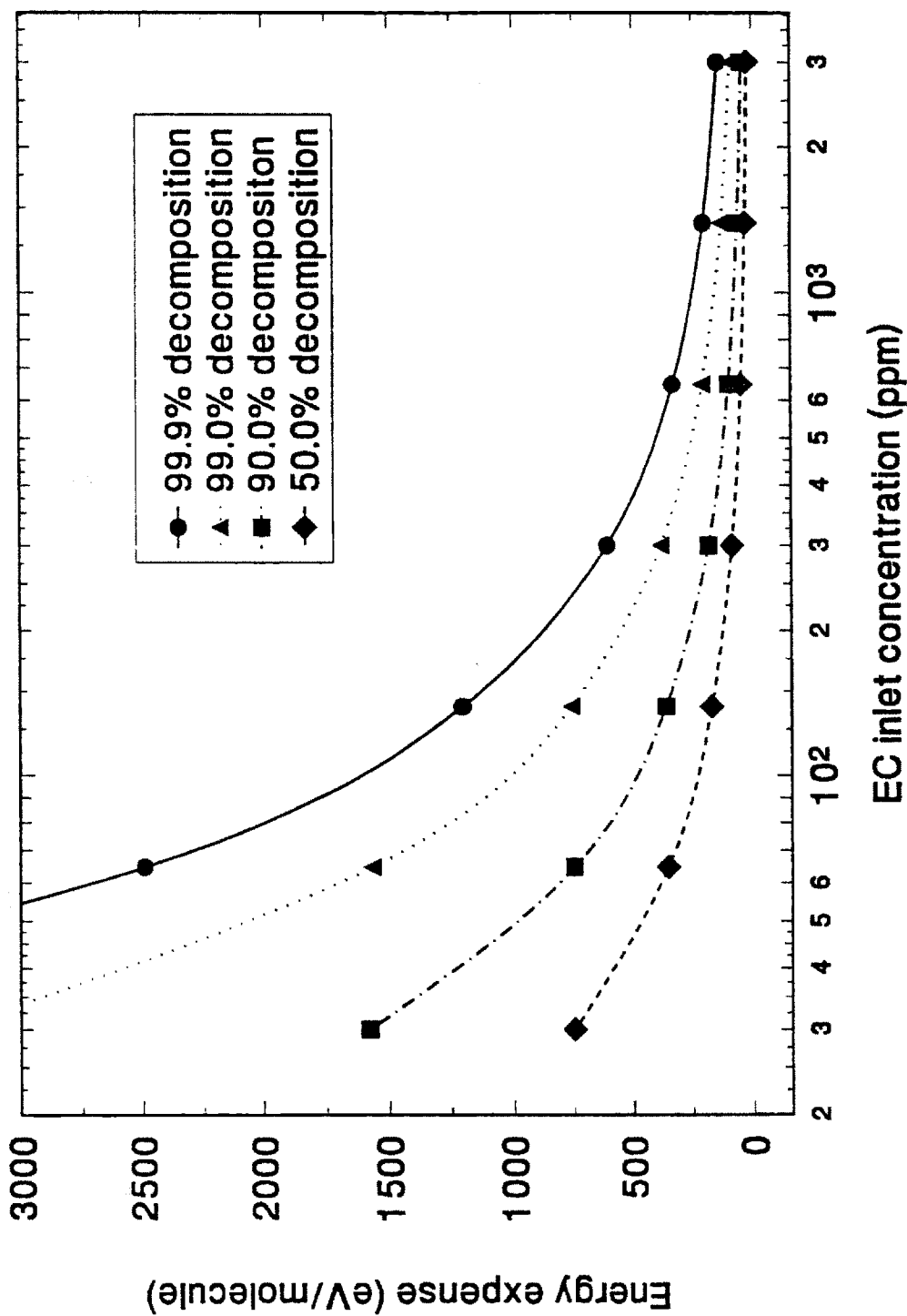
Figure 4.40: Specific energy, ε. required for EC decomposition, as a function of EC inlet concentration and desired fractional decomposition, η.
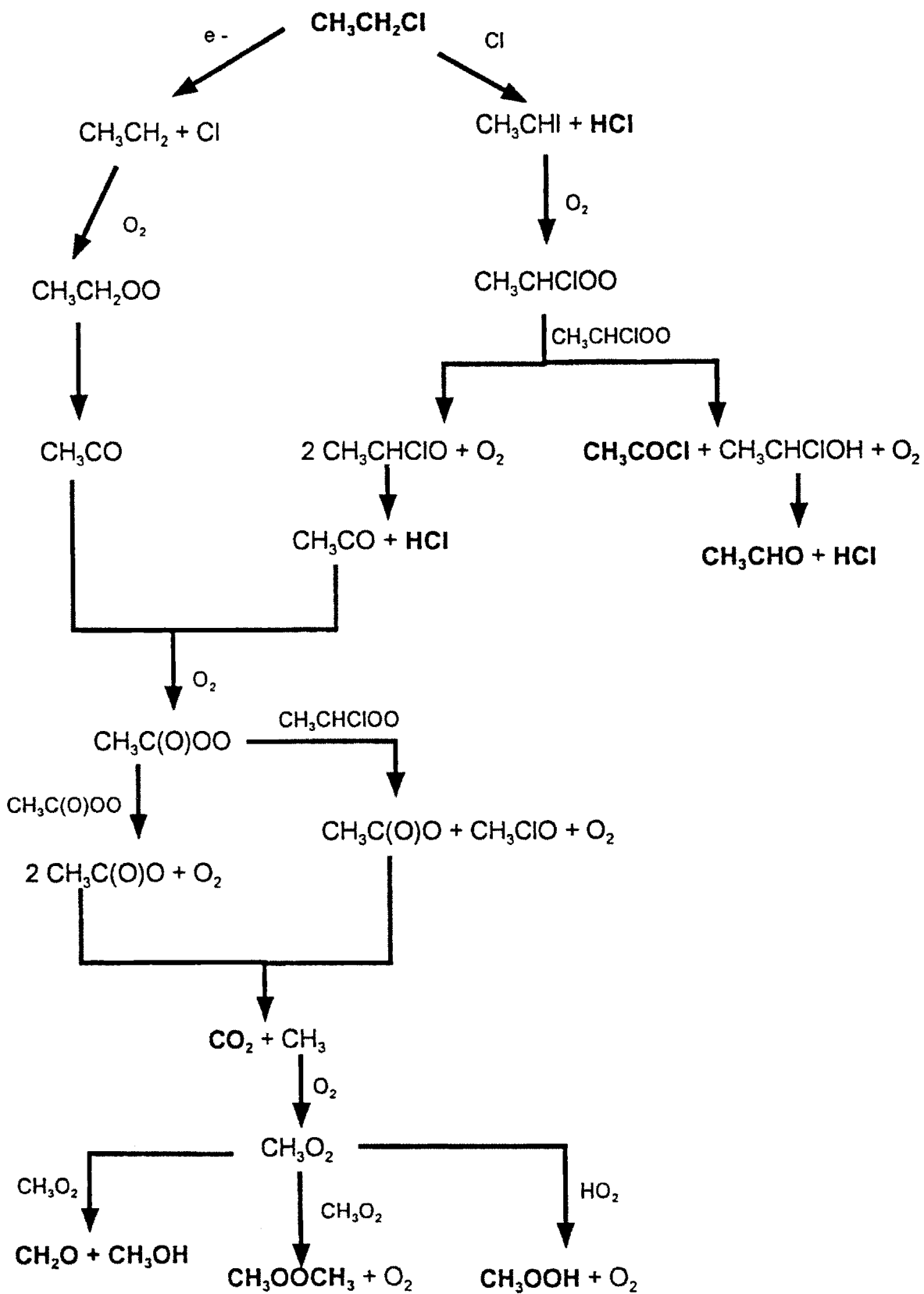
Figure 4.41: Schematic of reaction pathways of EC decomposition in the EBGPR.
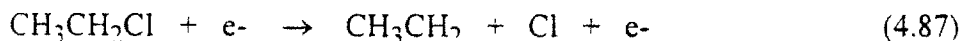
134

4.7.2. Reaction Pathways

The only major products of EC decomposition were carbon dioxide and hydrogen chloride. The ion abundances of these compounds as a function of electron beam dose is given in figure (4.39). At low electron beam dose, a small peak at $m/z = 43$ is present, which most likely corresponds to a small amount of acetyl chloride (CH_3CClO). The acetyl chloride probably decomposes very rapidly in the plasma, and thus is not seen at high electron beam doses. Figure 4.41 illustrates schematically the reaction pathways which will be outlined below.

There are two previous studies in the literature relating to ethyl chloride decomposition in the presence of both chlorine atoms and molecular oxygen. Knyazev[93] studied the reaction:

$$CH_3CHCl + O_2 \rightarrow CH_3CHClOO \rightarrow products \qquad (4.86)$$
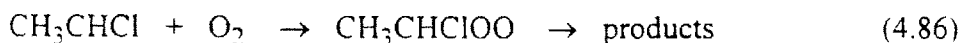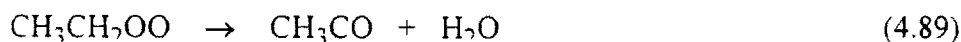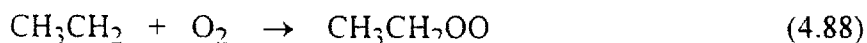
In this study, the major reaction product observed was vinyl chloride. However, no vinyl chloride was detected in the present work, and thus this pathway will be excluded from consideration.

Shi[94] studied the Cl atom induced oxidation of ethyl chloride in the presence of molecular oxygen. The following pathways are based on this study, with a few modifications. The initiation step is dissociative electron attachment on an EC molecule,

$$CH_3CH_2Cl + e- \rightarrow CH_3CH_2 + Cl + e- \qquad (4.87)$$

The ethyl radical can the be oxidized by molecular oxygen,

$$CH_3CH_2 + O_2 \rightarrow CH_3CH_2OO \qquad (4.88)$$

$$CH_3CH_2OO \rightarrow CH_3CO + H_2O \qquad (4.89)$$

The chlorine radical produced in reaction (4.87) can abstract a hydrogen from another EC molecule.

$$Cl + CH_3CH_2Cl \rightarrow CH_3CHCl + HCl \qquad (4.90)$$
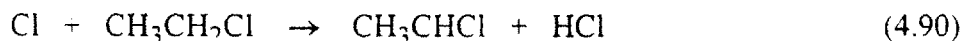
In reaction (4.90), the hydrogen abstraction takes place at the α position. Shi[94] has shown that abstraction at the α position is favored 82% of the time over abstraction at the β position. The chloroethyl radical decomposes through oxidation with molecular oxygen.

$$CH_3CHCl + O_2 \rightarrow CH_3CHClOO \tag{4.91}$$

$$2\,CH_3CHClOO \rightarrow 2\,CH_3CHClO + O_2 \tag{4.92}$$

$$2\,CH_3CHClOO \rightarrow CH_3COCl + CH_3CHClOH + O_2 \tag{4.92'}$$
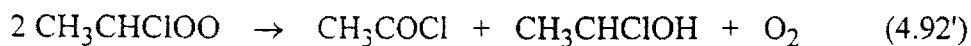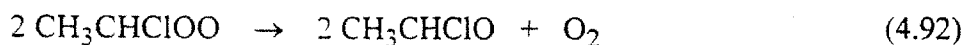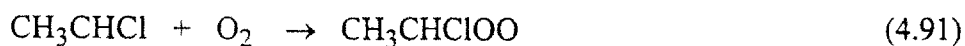
reaction (4.92') produces chloroacetyl chloride, which was a product observed in small quantity. The chlorinated alcohol produced in this reaction was not observed, and is believed by Shi to decompose spontaneously, producing more hydrogen chloride,

$$CH_3CHClOH \rightarrow CH_3CHO + HCl \tag{4.93'}$$
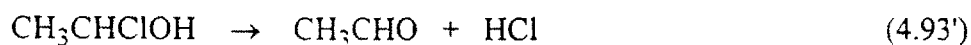
The other product of this reaction, acetaldehyde, was not observed. Thus primary pathway, is most likely through (4.92), which continues as follows:

$$CH_3CHClO \rightarrow CH_3CO + HCl \tag{4.93}$$

The CH_3CO radical is formed in reactions (4.89) and (4.93), and decomposes upon reaction with oxygen.

$$CH_3CO + O_2 \rightarrow CH_3C(O)OO \tag{4.94}$$

$$2\,CH_3C(O)OO \rightarrow 2\,CH_3C(O)O + O_2 \tag{4.95a}$$

$$CH_3C(O)OO + CH_3CHClOO \rightarrow CH_3C(O)O + CH_3CHClO + O_2 \tag{4.95b}$$

$$CH_3C(O)O \rightarrow CO_2 - CH_3 \tag{4.96}$$

$$CH_3 + O_2 \rightarrow CH_3O_2 \tag{4.97}$$

$$2\,CH_3O_2 \rightarrow CH_2O - CH_3OH \tag{4.98a}$$

$$2\,CH_3O_2 \rightarrow CH_3OOCH_3 + O_2 \tag{4.98b}$$

$$CH_3O_2 + HO_2 \rightarrow CH_3OOH \tag{4.98c}$$
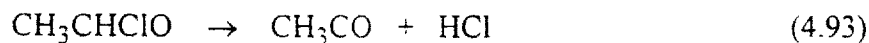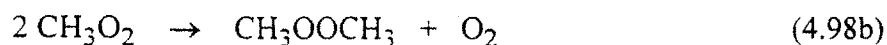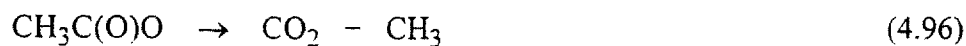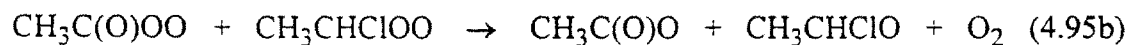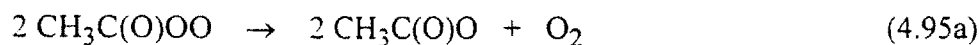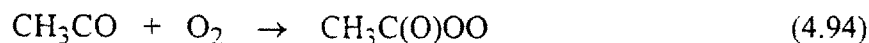
The pathway explains the formation of CO_2, HCl, and acetyl chloride. The peroxides produced in this mechanisms were not observed experimentally. This is not surprising since any peroxides formed would almost certainly decompose in the gas chromatograph to form water and oxygenated methanes.

4.8 Vinyl Chloride

4.8.1 Kinetic Analysis

A graph of outlet stream VC concentration versus electron beam dose is shown in figure 4.42 for several inlet stream concentrations. Greater than 99% decomposition of VC is achieved for the lower concentration streams at flow rates up to 3 liters/min. Fifty-three curves similar to those shown in figure 4.42 were generated at EC inlet concentrations from 100 to 3000 ppm. These curves were analyzed by the differential kinetic method. to determine the order with respect to time, n_t, and the order with respect to concentration. n_c.

Figure 4.43 shows the initial rates calculated from the curves as a function of initial concentration of VC. The results of the order with respect to concentration analysis are:

$$n_c = 0.50$$

and.

$$\ln k = 2.69 \quad \Rightarrow \quad k = 14.73 \; \text{Mrad}^{-1} \; \text{ppm}^{1/2}$$

The order with respect to time analysis was performed on each curve of VC concentration versus electron beam dose. A representative plot is shown in figure 4.44. The order with respect to time, n_t, and the rate constant. k. were calculated for each curve and the results averaged. to give:

$$n_t = 1.53 \pm 0.28$$

$$\ln k = -4.08 \pm 1.36 \quad \Rightarrow \quad k = 4.34 * 10^{-3} - 6.58 * 10^{-2} \quad \text{Mrad}^{-1} \; \text{ppm}^{-1/2}$$

As with all of the previous compounds, n_t is greater than n_c, showing that the kinetics are inhibited. Again rounding n_t to the nearest third or quarter integer, the final rate expression is:
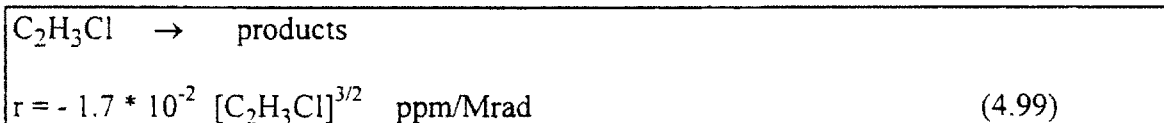
$C_2H_3Cl \quad \rightarrow \quad$ products	
$r = - 1.7 * 10^{-2} \; [C_2H_3Cl]^{3/2} \quad$ ppm/Mrad	(4.99)

This rate expression is used in conjunction with the ideal performance equation for the EBGPR derived in Section 2.2.2 to determine the reactor power needed to achieve a desired conversion of VC.

Using the INHIBIT model to calculate K and β' , as shown in figures 4.45a and 4.45b,

$$K = 0.06$$

$$\beta' = .000154 \, T_o + 1.00 \quad \text{Mrad}$$

Using the K and β' parameters again in equation (2.70), the energy expense, ε, was calculated as a function of the inlet concentration T_o, and the desired fractional decomposition η. The calculated curves are given in figure 4.48.

Rosocha β-values were calculated from the VC data up to 90% fractional decomposition, and the results are given in figure 4.46.

$$\beta = .00147 \, [T_o] \qquad \text{Mrad} \qquad (4.100)$$

The G-value for VC becomes.

$$G_{VC} = 23.5 \text{ molecules/ } 100 \text{ eV} \qquad (4.101)$$

Slater(5) reports $G_{VC} = 2.7 \pm 0.26$ for decomposition in air. This is a difference of a factor of ten from the results in this work. However, for VC decomposition in nitrogen, Slater reports G= 9.2. It seems unusual that the decomposition in nitrogen is more efficient than the decomposition in air, since oxygen most likely aids the oxidation of the molecule. Slater only considered very low concentrations of VC, 10 ppm and 100 ppm, whereas in this study a much larger range of concentration (100 ppm - 3000 ppm). Also, in the liner regression of the data. Slater did not force the curve to go through the initial concentration at zero dose. as was done in this study. This has a significant influence on the slope of the best fit line. and the resulting calculations. The difference in results is still significant however. and suggests that further work should be performed.
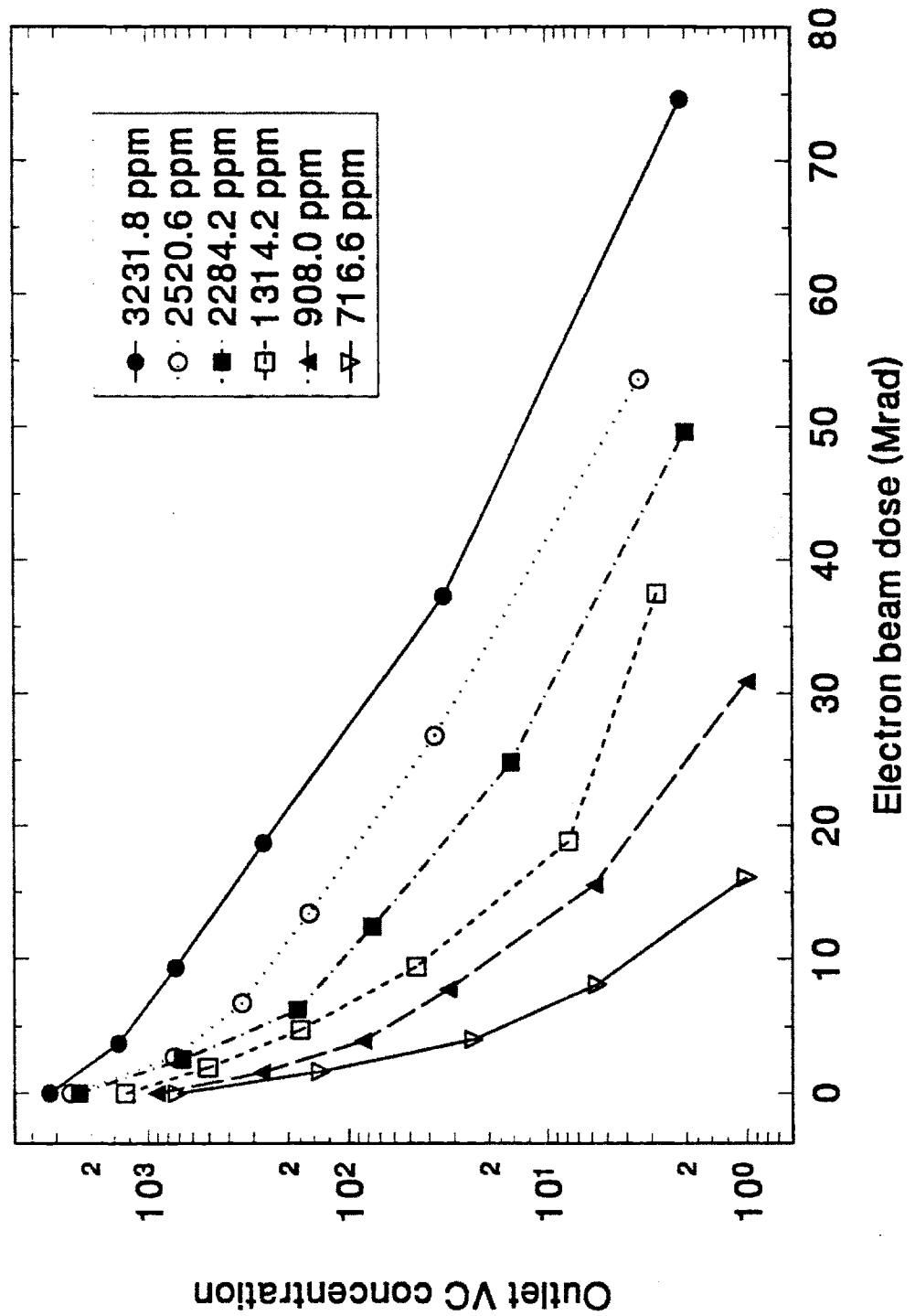
Figure 4.42: Vinyl Chloride outlet concentration as a function of electron beam dose.
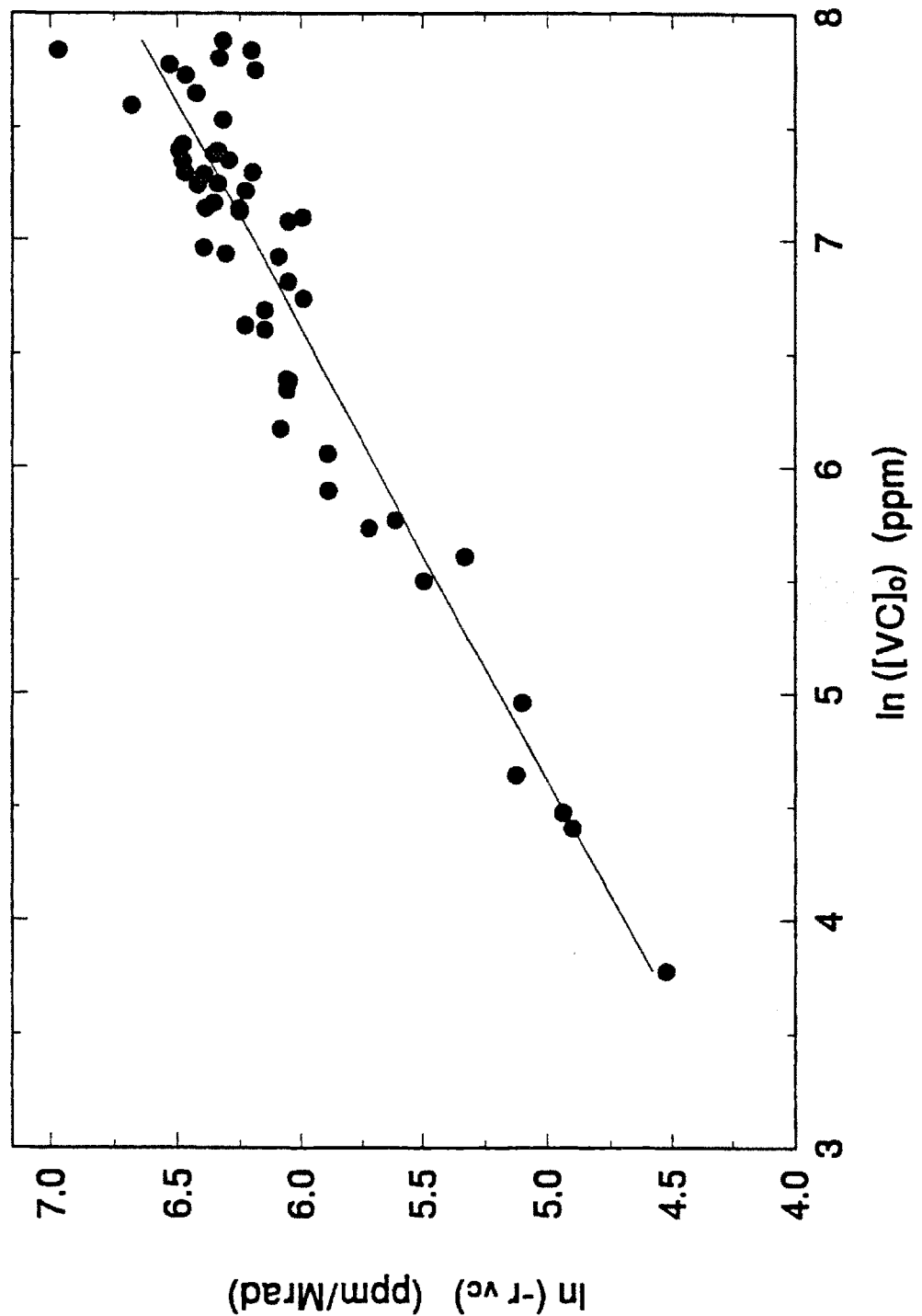
Figure 4.43: Differential kinetic analysis of VC decomposition. This graph shows the initial reaction rate. $-r = \dfrac{d[VC]}{dD}$, as a function of initial VC concentration. The slope of this line gives the order with respect to concentration, n_c, and the intercept with the Y-axis gives the rate constant, k.
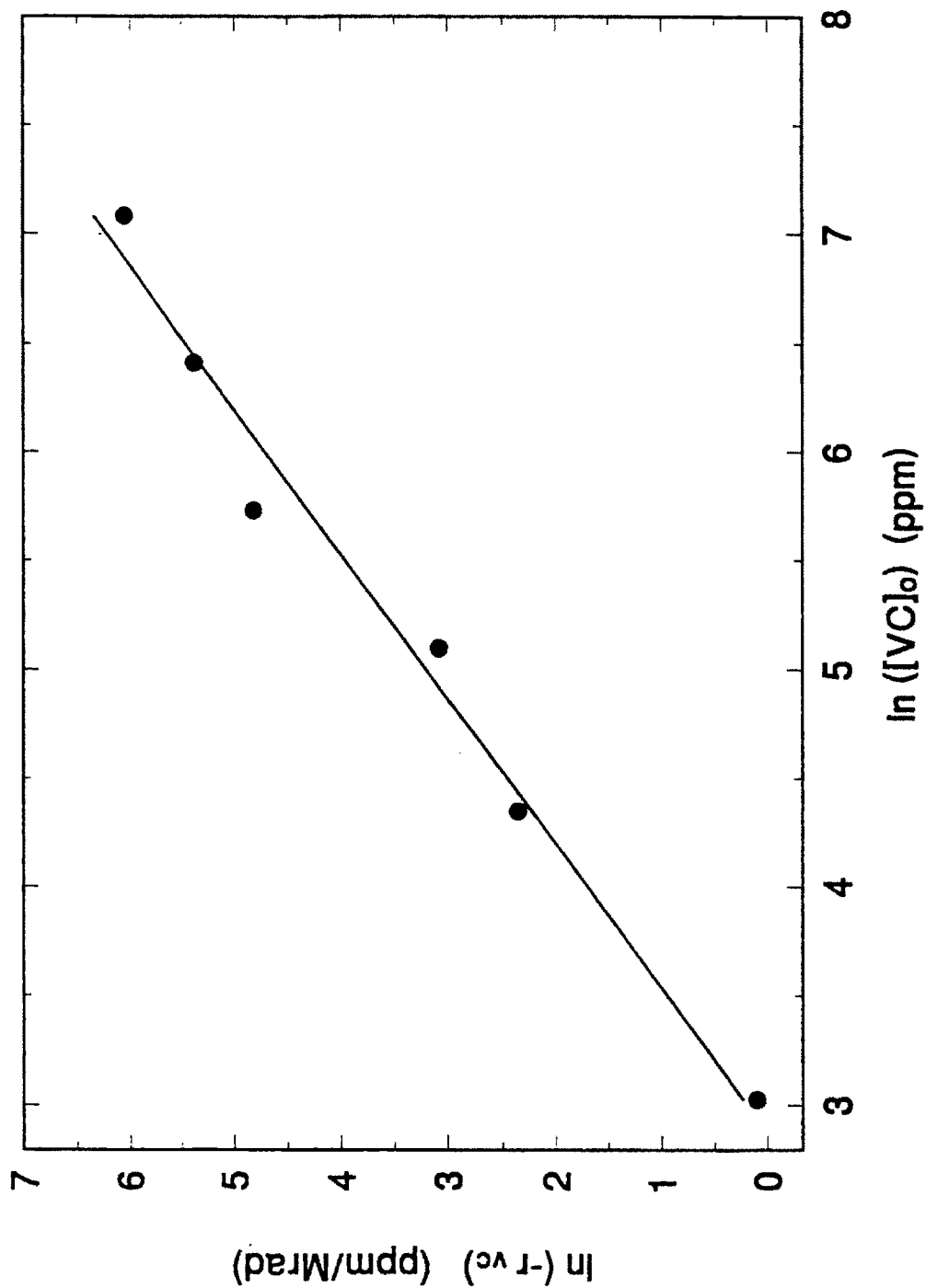
Figure 4.44: A representative graph of one run of VC, showing the actual reaction rate as a function of VC concentration, as the reaction proceeds. The slope of this line gives the order with respect to time, n_t, and the intercept with the Y-axis gives the rate constant, k.
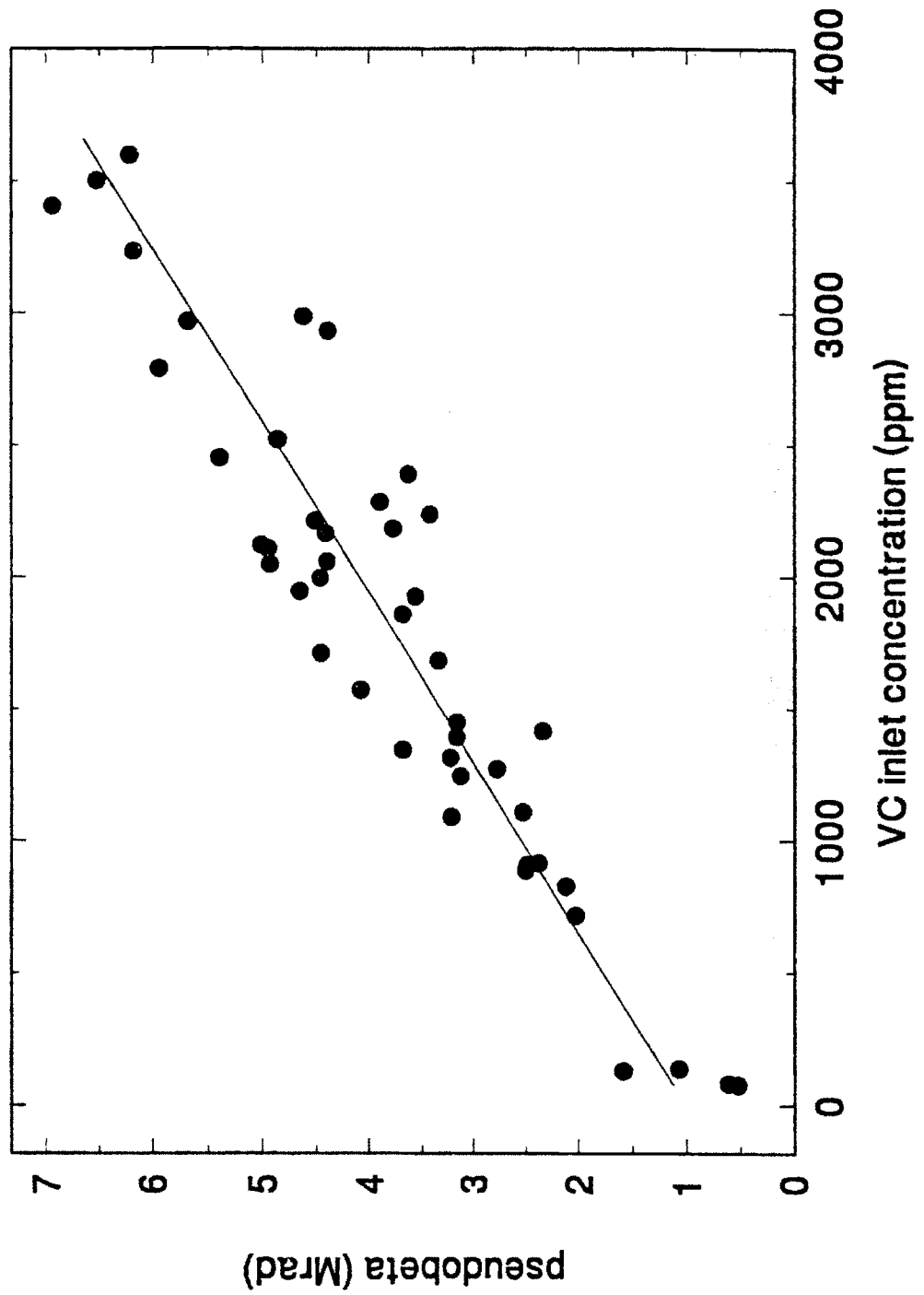
Figure 4.45a: Graph of pseudo-β, versus VC inlet concentration from INHIBIT model fit.
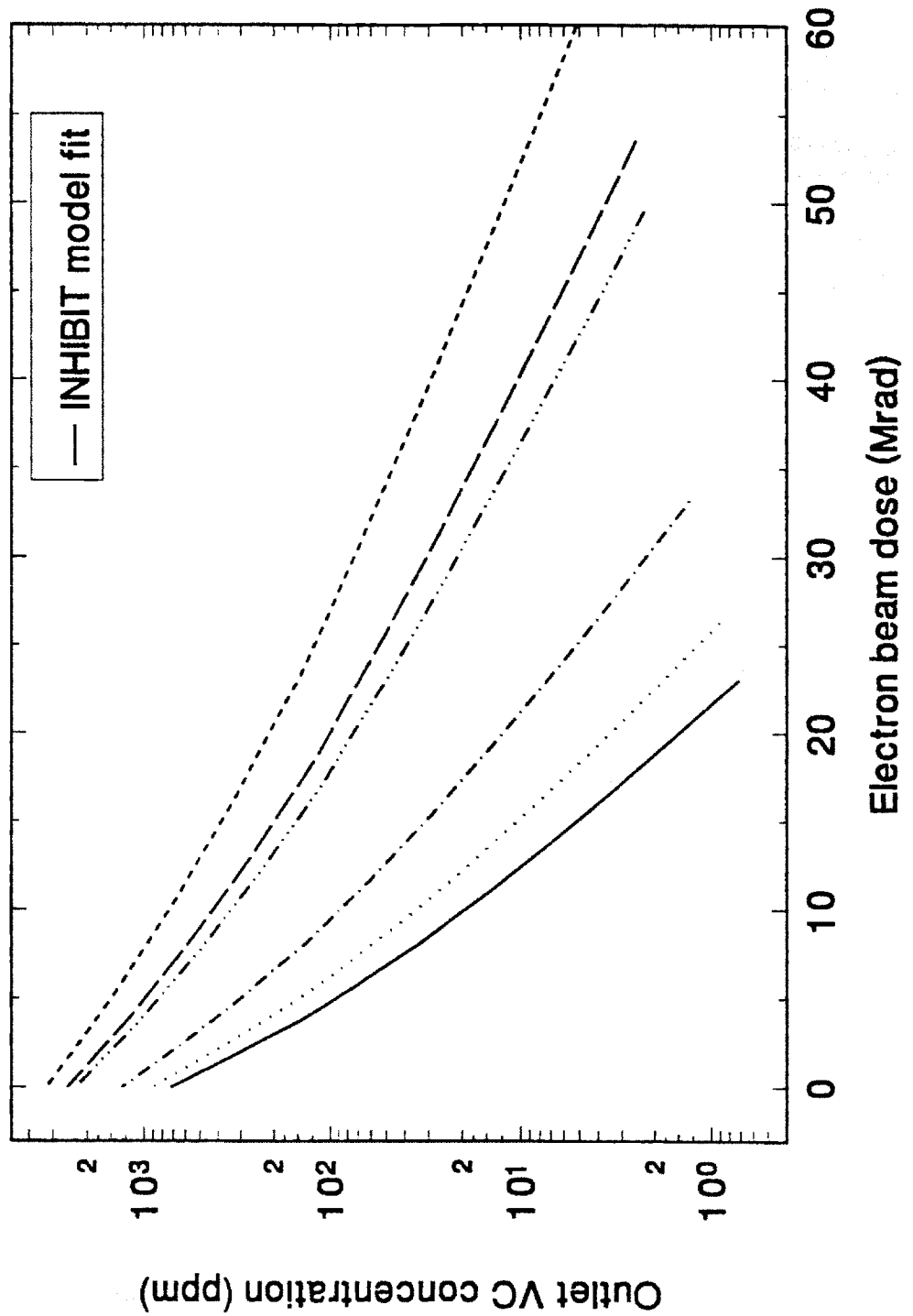
Figure 4.45b: Graph of calculated VC concentration versus electron beam dose curves from best fit INHIBIT model. The initial concentrations are the same as the experimental data given in figure 4.42 so the two graphs may be compared.

143
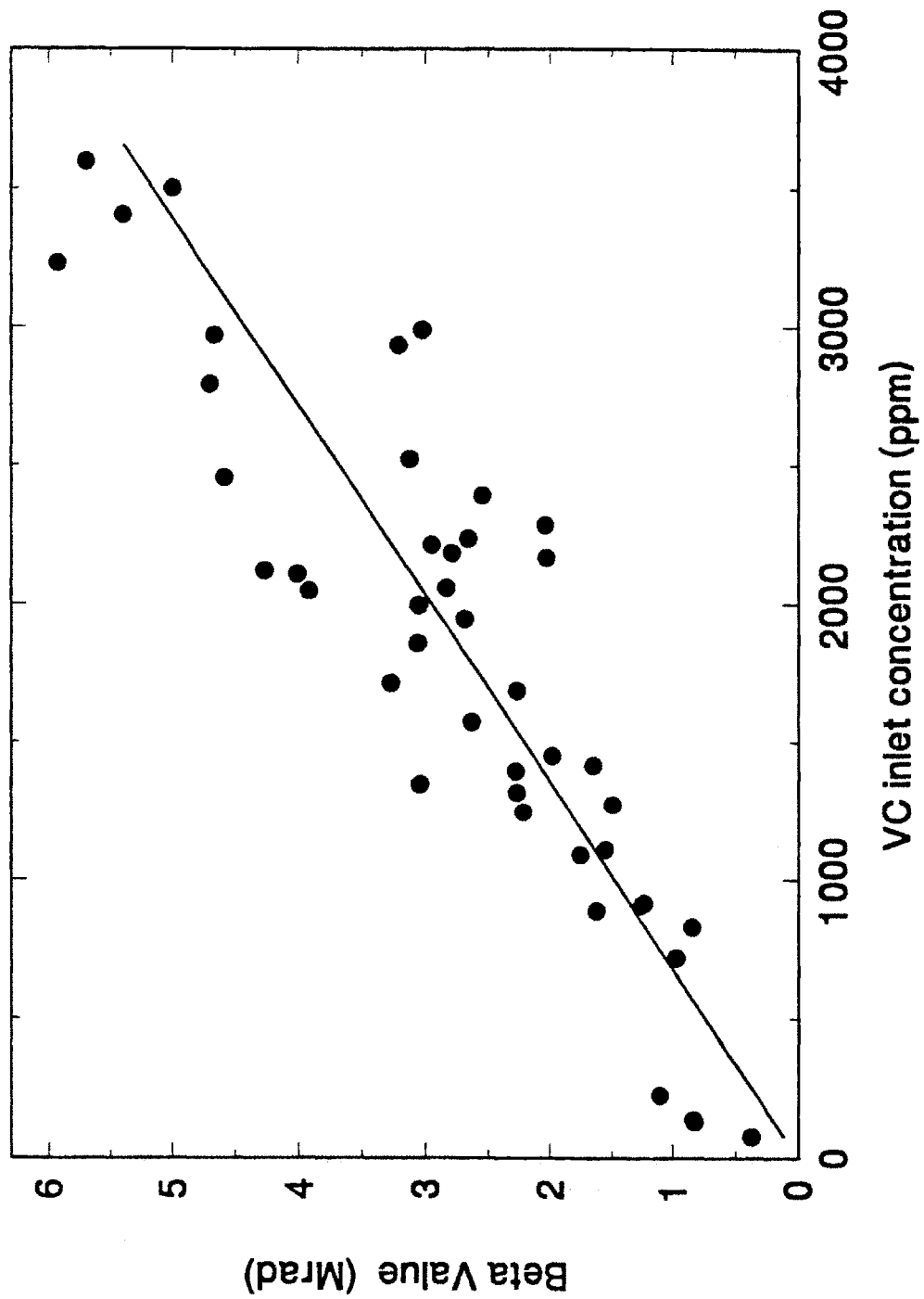
Figure 4.46: Graph of the Rosocha β-value versus inlet VC concentration
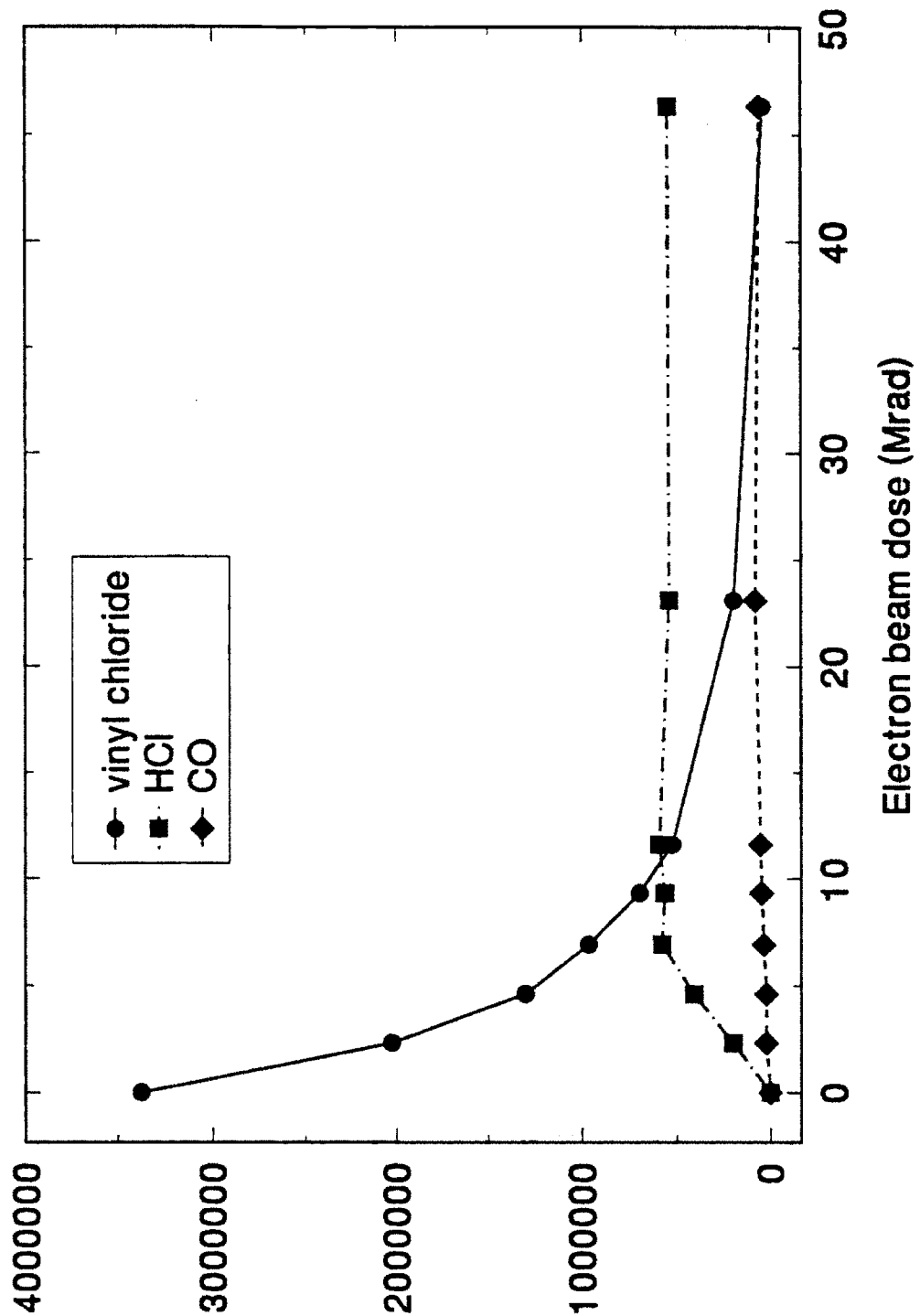
Figure 4.47: Major reaction products of VC decomposition. The ion abundances from the mass spectrometer peaks are given as a function of electron beam dose. The ion abundance is approximately linearly proportional to the concentration.

145
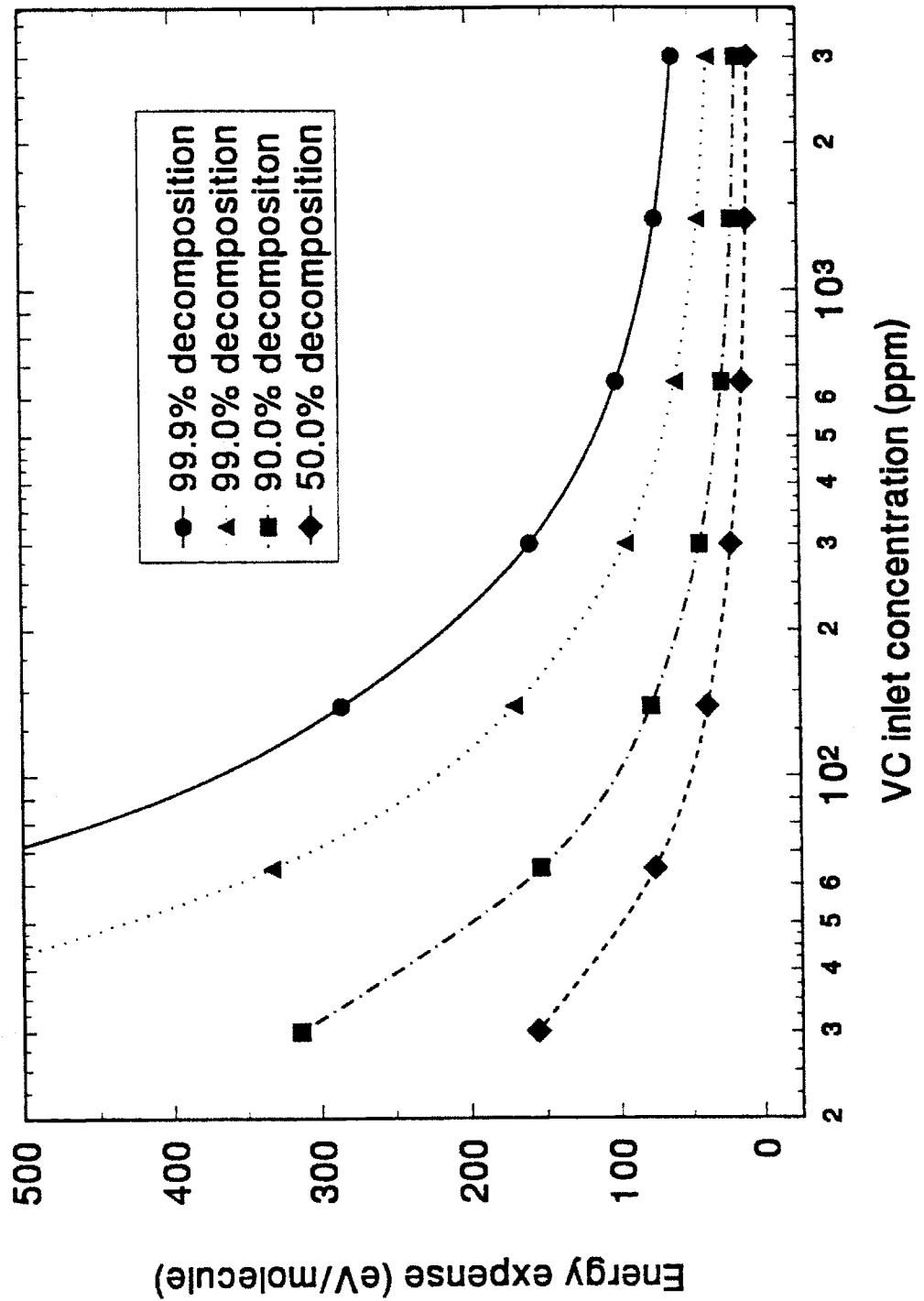
Figure 4.48: Specific energy, ε, required for VC decomposition, as a function of VC inlet concentration and desired fractional decomposition, η.

146
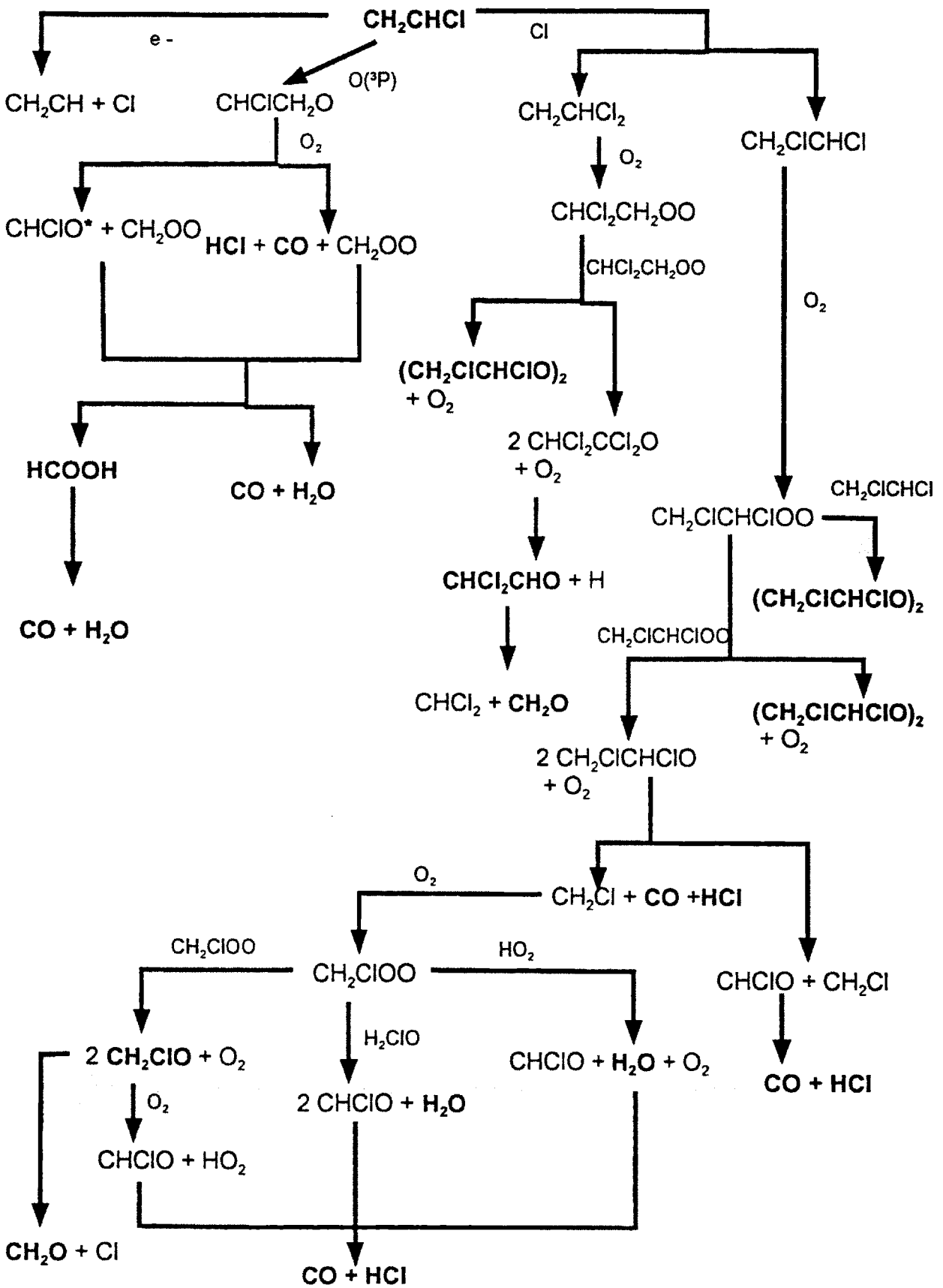
Figure 4.49: Schematic of reaction pathways of VC decomposition in the EBGPR.

4.8.2. Reaction Pathways

The only observed reaction products of VC decomposition were carbon monoxide and HCl, as shown in figure 4.47. The excess hydrogen was likely converted into water or molecular hydrogen, neither of which could be quantified wit the current analysis system. It is also possible that the hydrogen was present in an undetected product species, as explained below.

First and electron attachment induced dissociation mechanisms will be considered. This mechanisms follows closely that outlined by Sanheuza,[88]

$$e- + CH_2CHCl \rightarrow CH_2CH + Cl \qquad (4.102)$$
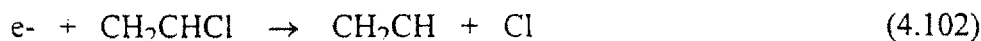
The C_2 radical formed may lose a hydrogen atom to forma carbene radical, which can polymerize or oxidize in some way. The chlorine radical then goes on to attack another VC molecule. this time at either the chlorinated or non-chlorinated carbon:

$$Cl + CH_2CHCl \rightarrow CH_2ClCHCl \qquad (4.03)$$

or

$$Cl + CH_2CHCl \rightarrow CH_2CHCl_2 \qquad (4.03')$$

Each of these species can be decomposed by reaction with oxygen molecules in the carrier gas.

$$CH_2ClCHCl + O_2 \rightarrow CH_2ClCHClOO \qquad (4.104)$$

$$2CH_2ClCHClOO \rightarrow 2 \textbf{CH}_2\textbf{ClCHClO} + O_2 \qquad (4.015a)$$

$$2CH_2ClCHClOO \rightarrow (\textbf{CH}_2\textbf{ClCHClO})_2 + O_2 \qquad (4.105b)$$

$$CH_2ClCHClOO + CH_2ClCHCl \rightarrow (\textbf{CH}_2\textbf{ClCHClO})_2 \qquad (4.105c)$$

$$CH_2ClCHClO \rightarrow \textbf{CHClO} + CH_2Cl \qquad (4.106a)$$

$$CH_2ClCHClO \rightarrow CH_2Cl + \textbf{CO} + \textbf{HCl} \qquad (4.106b)$$

$$CH_2Cl + O_2 \rightarrow CH_2ClOO \qquad (4.107)$$

$$2CH_2ClOO \rightarrow 2CH_2ClO + O_2 \qquad (4.108)$$

$$CH_2ClO \rightarrow \textbf{CH}_2\textbf{O} - Cl \qquad (4.109)$$

$$CH_2ClOO + CH_2ClO \rightarrow 2\textbf{CHClO} + \textbf{H}_2\textbf{O} \qquad (4.110a)$$

$$CH_2ClO + O_2 \rightarrow \textbf{CHClO} + HO_2 \qquad (4.110b)$$

$$CH_2ClOO + HO_2 \rightarrow \textbf{CHClO} + \textbf{H}_2\textbf{O} + O_2 \qquad (4.111b)$$

$$CH_2CHCl_2 + O_2 \rightarrow CHCl_2CH_2OO \qquad (4.104')$$

$$2CHCl_2CH_2OO \rightarrow 2CHCl_2CCl_2O + O_2 \qquad (4.105a')$$

$$2\,CHCl_2CH_2OO \rightarrow \textbf{(CHCl}_2\textbf{CH}_2\textbf{O)}_2 + O_2 \qquad (4.105b')$$

$$CHCl_2CH_2O \rightarrow CHCl_2CHO + H \qquad (4.106a')$$

$$CHCl_2CH_2O \rightarrow CHCl_2 + \textbf{CH}_2\textbf{O} \qquad (4.106b')$$

The second possible mechanisms for VC decomposition assumes that electron attachment is not important. and excited oxygen radicals initiate the decomposition process:

$$CHClCH_2 + O \rightarrow CHClCH_2O* \qquad (4.112)$$
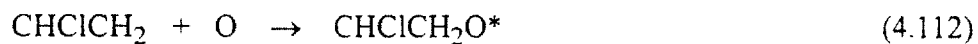
where the asterix denotes an excited species. This molecule decomposes by reaction with molecular oxygen.

$$CHClCH_2O* + O_2 \rightarrow \textbf{CHClO*} + CH_2OO \qquad (4.113a)$$

$$CHClCH_2O* + O_2 \rightarrow \textbf{HCl} + \textbf{CO} + CH_2OO \qquad (4.113b)$$

The CH_2OO radical can decompose by either of the following two rearrangements:

$$CH_2OO \rightarrow \textbf{HCOOH} \qquad (4.114a)$$

$$CH_2OO \rightarrow \textbf{CO} - \textbf{H}_2\textbf{O} \qquad (4.114b)$$

Both of these mechanisms can explain the formation of hydrogen chloride and carbon monoxide. The large amount of HCl observed experimentally, as well as the absence of any other chlorinated products seems to favor mechanism 2, $O(^3P)$ oxidation. However. other explanations for these results exists. The first mechanism, chlorine radical induced dissociation. predicts the production of several stable species which were not observed experimentally: CHClO, $(CH_2ClCHClO)_2$, and CH_2O (formaldehyde). It is not apparent how to construct a reasonable mechanisms based on dissociative electron attachment without the formation of at least one of these species. The second mechanism also produces unobserved products: CHClO and HCOOH (formic acid).

These mechanisms were produced from a compilation of reports in the literature, the most important here by Sanhueza.[88] In those experiments, no formaldehyde or $(CH_2ClCHClO)_2$ was observed either, so the reaction pathways to those species can be assumed to be insignificant. However both the $O(^3P)$ sensitized and the Cl sensitized reactions did produce CHClO, and the former produced formic acid. The fact that the products were not observed in the EBGPR experiments can be explained in several ways:

1. The major HCOOH and CHClO mass spectrometer peaks both occur at m/z = 29. These could easily have been overwhelmed by the large nitrogen isotope peak, and thus either or both of these species were formed but could not be detected.

2. HCOOH decomposes very rapidly in the energetic plasma to form water and carbon monoxide

$$HCOOH \rightarrow CO + H_2O \qquad (4.115)$$

3. CHClO decomposes very rapidly in the formula to form carbon monoxide and HCl:

$$CHClO \rightarrow CO + HCl \qquad (4.116)$$

Any of these explanations seem plausible, and so it is likely that the decomposition of VC in the reactor occurs by one or both of these two mechanisms. Further elucidation of the mechanism would require in-situ diagnostics such as plasma induced emission spectroscopy to examine the production of transient species. This is beyond the scope of the present work, and thus the two mechanisms above are left as equally likely though unconfirmed processes of VC decomposition in the EBGPR.

4.9 Other Compounds

In addition to the six main chemicals which make up the main focus of the study, five other chemicals were studied in the EBGPR:

1. Carbon tetrachloride (CCl_4)
2. 1,1,2 - Trichloroethane (1,1,2-$C_2H_3Cl_3$)
3. Perchloroethylene (C_2Cl_4)
4. Freon 113 ($C_2Cl_3F_3$)
5. Toluene (C_7H_8)

Graphs of outlet concentration versus electron beam dose for these compounds are given on the following pages. Rosocha β-values were also calculated for each compound, and graphs of these values as a function of concentration are also given. The best fits for the β-values and the corresponding G-values are given in table 4.1.

Due to the lack of sufficient data, it was not possible to perform any reaction pathway or quantitative kinetic analysis of these results. Nevertheless, for each compound, 99% decomposition was achieved in the reactor, showing the EBGPR may be useful for the study of a wide variety of chemical compounds, in addition to the chlorinated ethylenes and ethanes in this study.

Compound	β-value	G-value
CCl_4	$\beta=0.00585[T_o]$	G=5.91
1,1,2-TCA	$\beta=0.0338[T_o]$	G=1.02
PCE	$\beta=0.00808[T_o]$	G=4.28
Freon 113	$\beta=0.0389[T_o]$	G=0.89
Toluene	$\beta=0.0108[T_o]$	G=3.57

Table 4.1: β-values and G-values for several compounds. β-Values are given in Mrads when $[T_o]$ is in ppm. G is in molecules/100 eV.
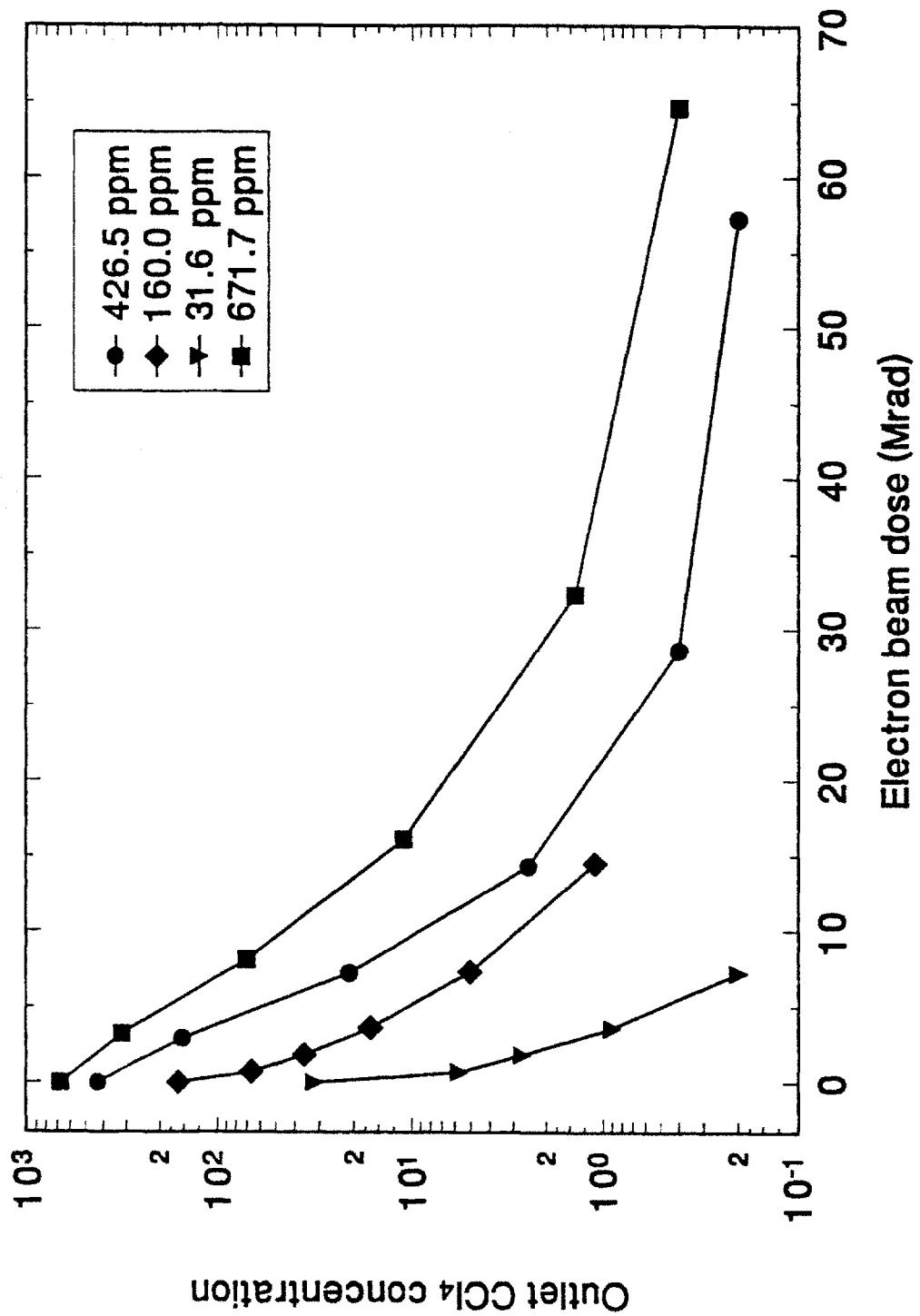
Figure 4.50: CCl$_4$ concentration versus electron beam dose

152
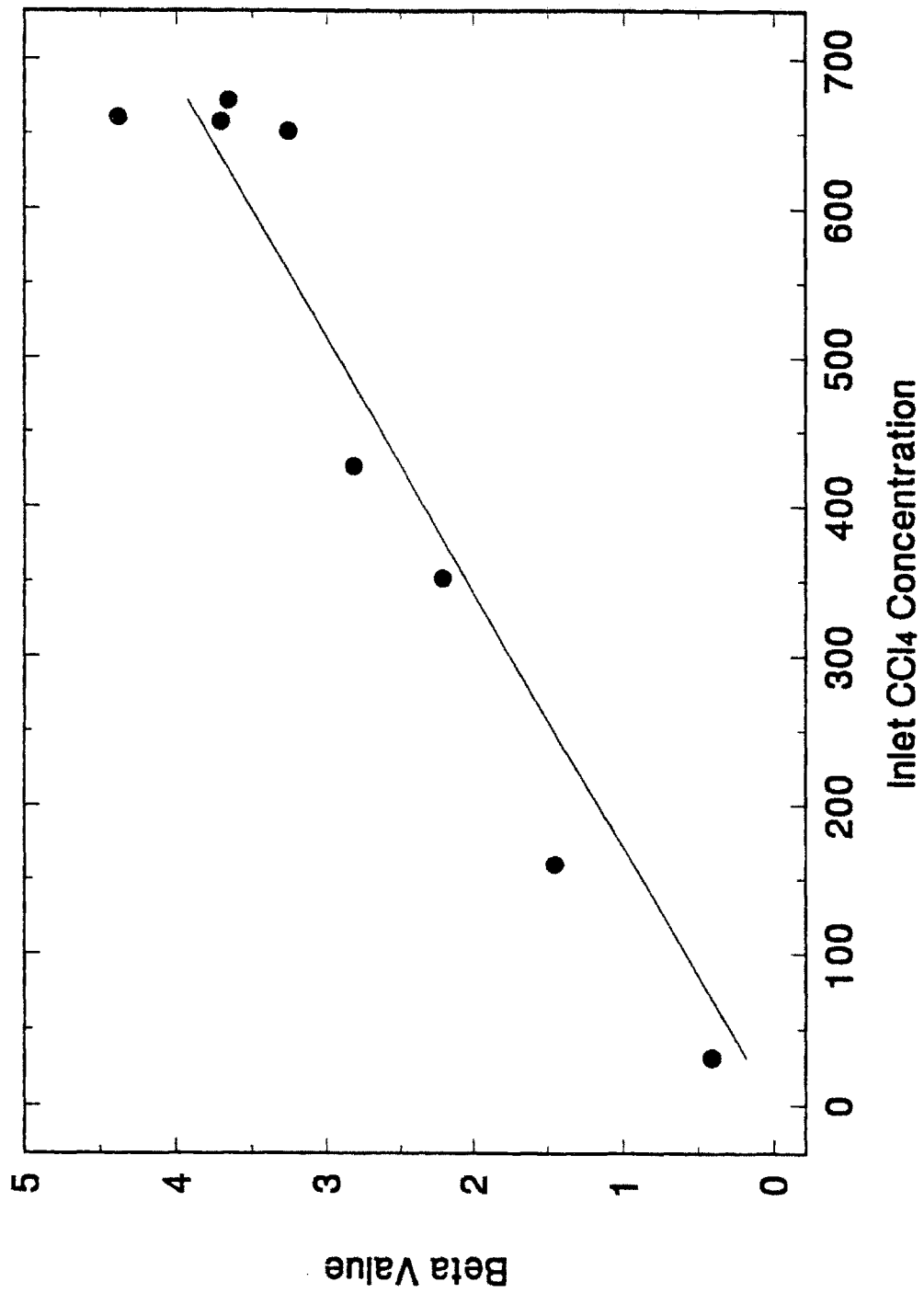
Figure 4.51: Rosocha β values for CCl₄ as a function of inlet concentration

153
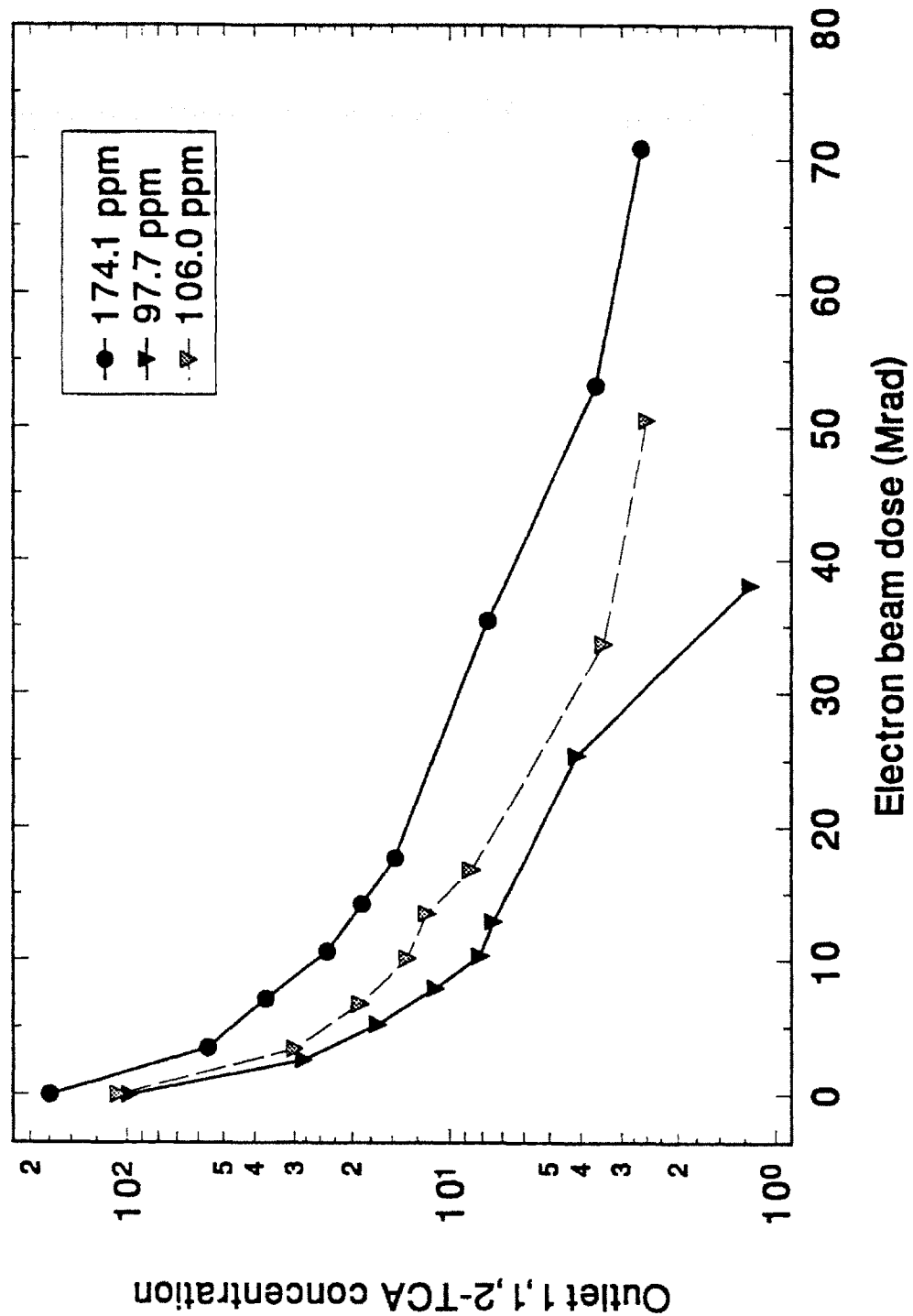
Figure 4.52: 1,1,2-TCA concentration versus electron beam dose

154
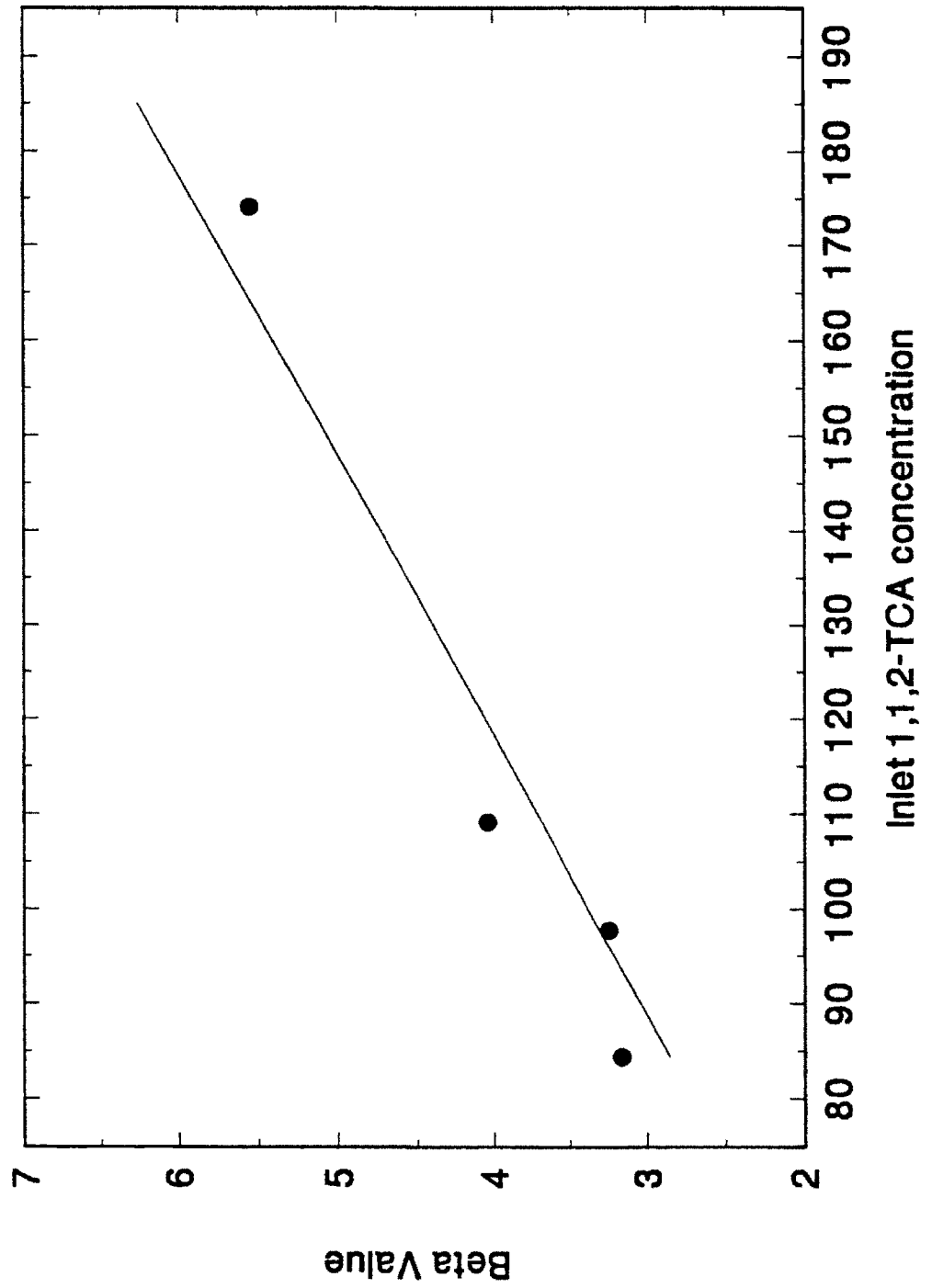
Figure 4.53: Rosocha β values for 1,1,2-TCA as a function of inlet concentration
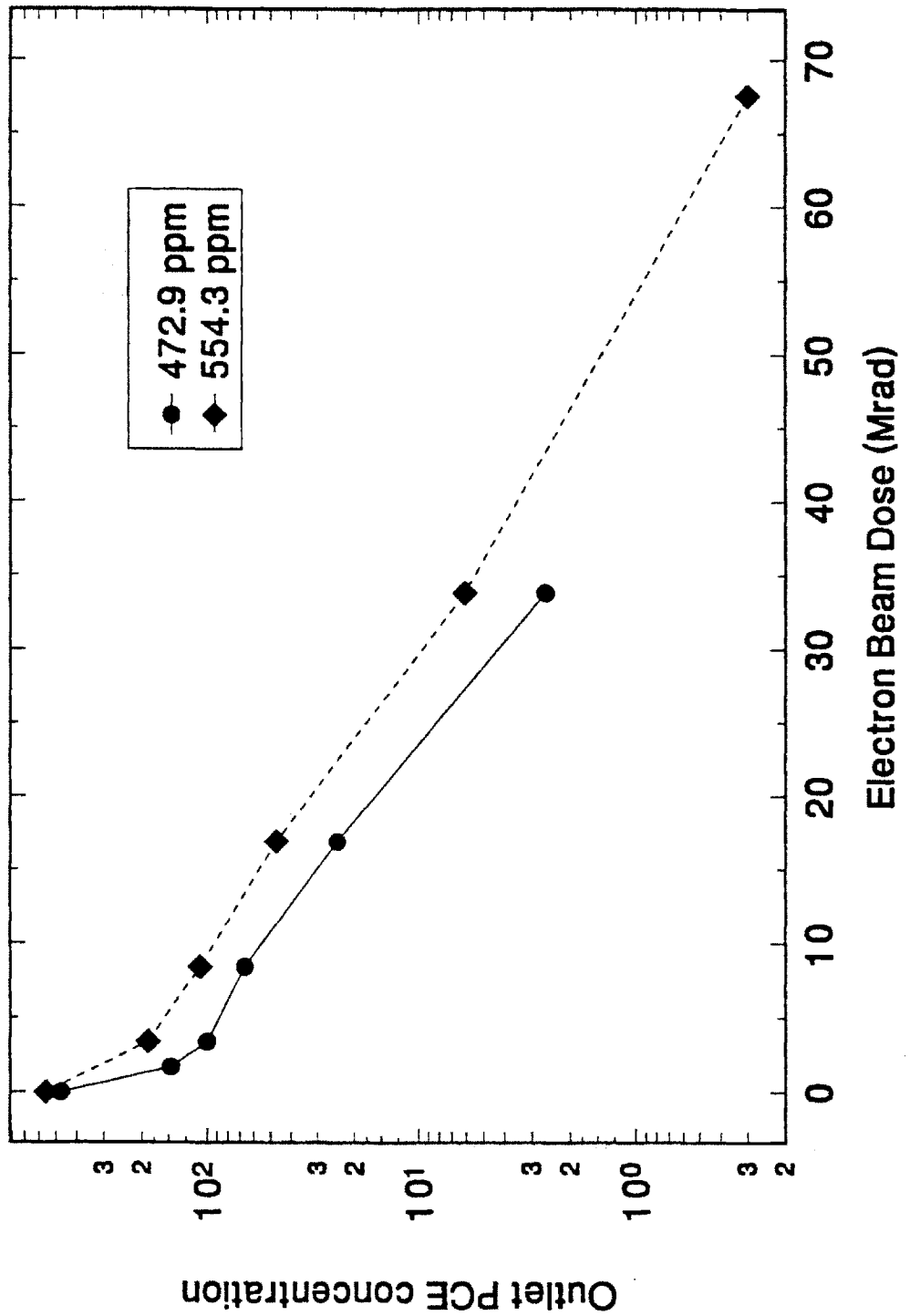
Figure 4.54: PCE concentration versus electron beam dose
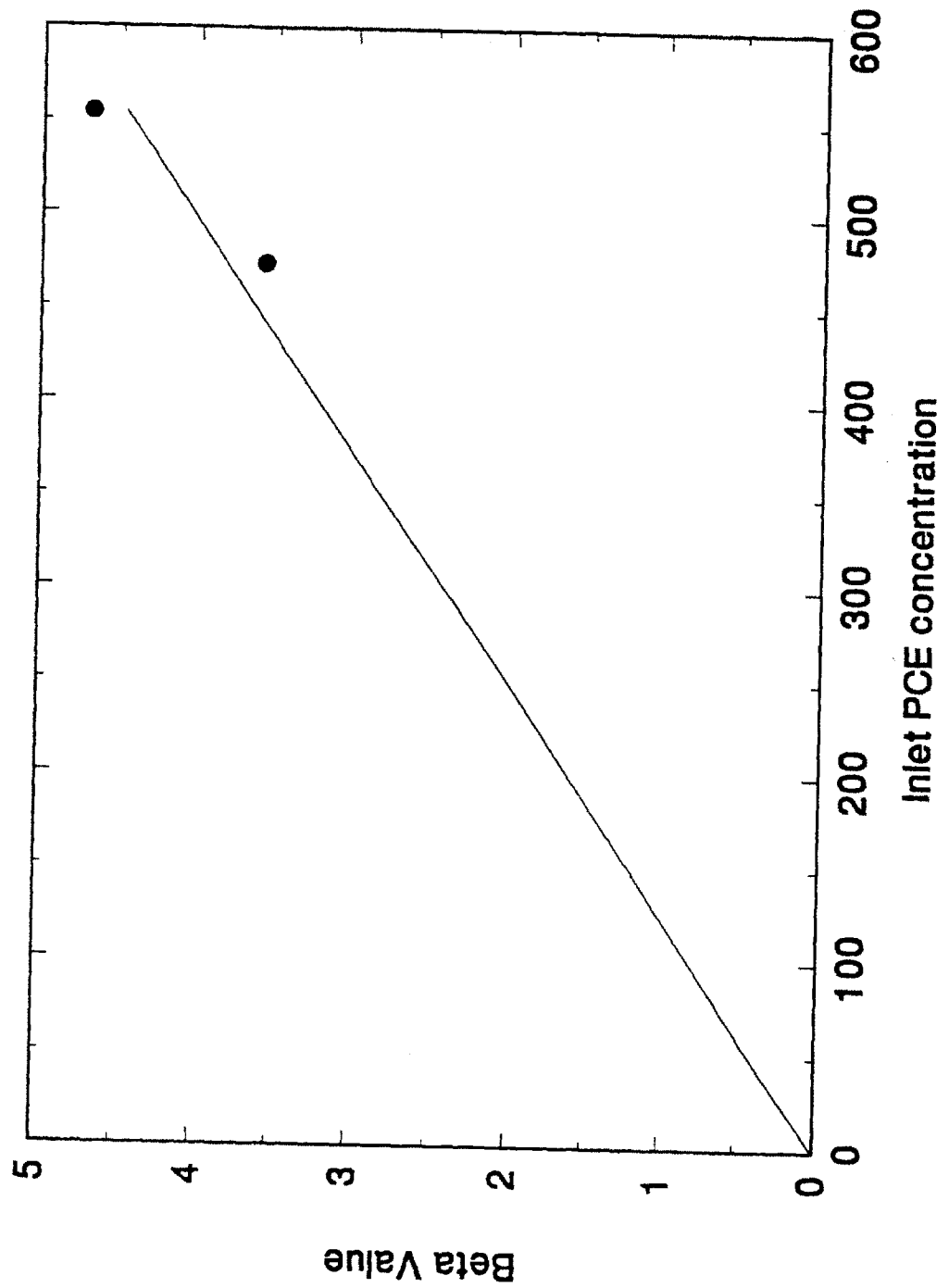
Figure 4.55: Rosocha β values for PCE as a function of inlet concentration
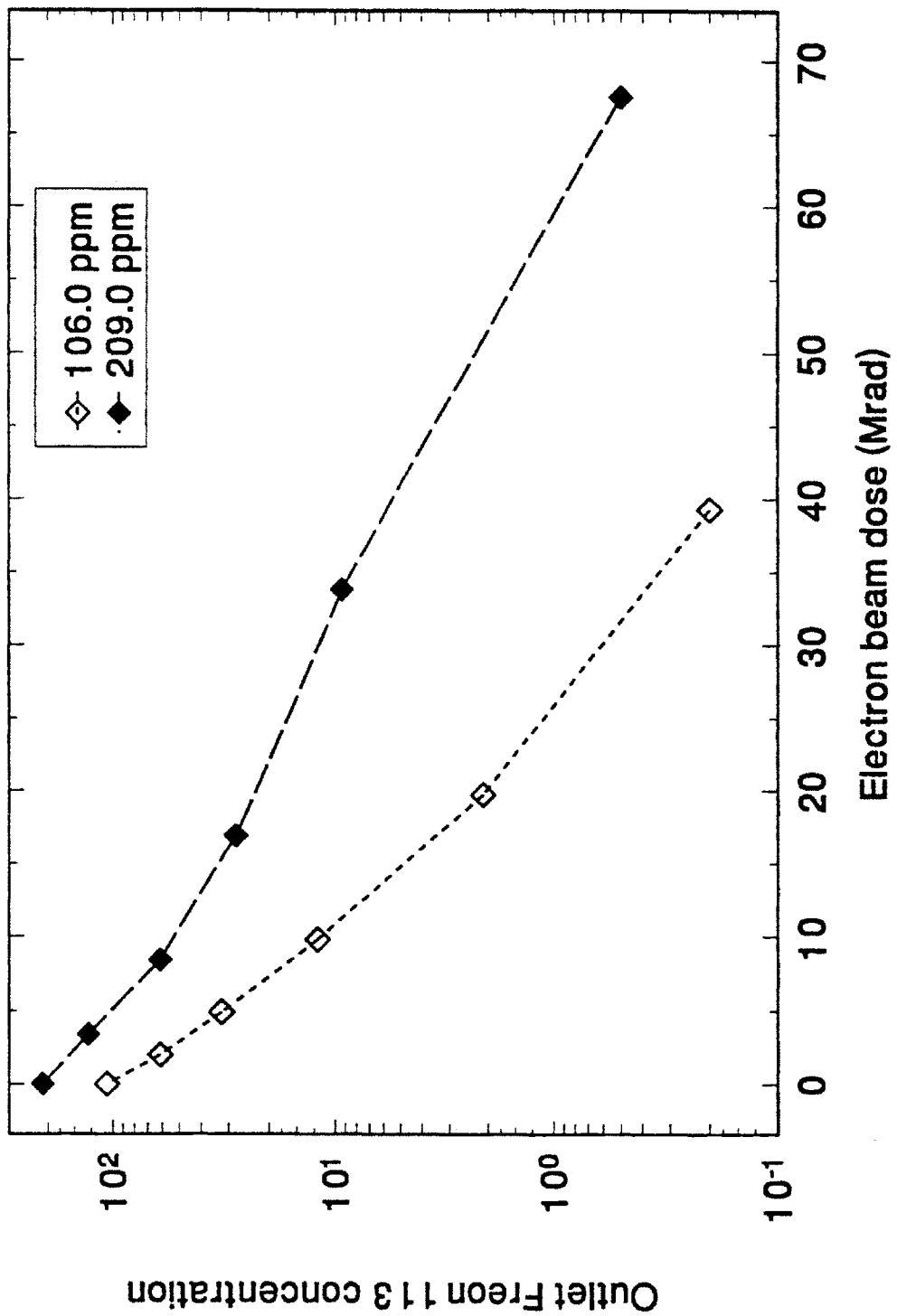
Figure 4.56: Freon 113 concentration versus electron beam dose

158
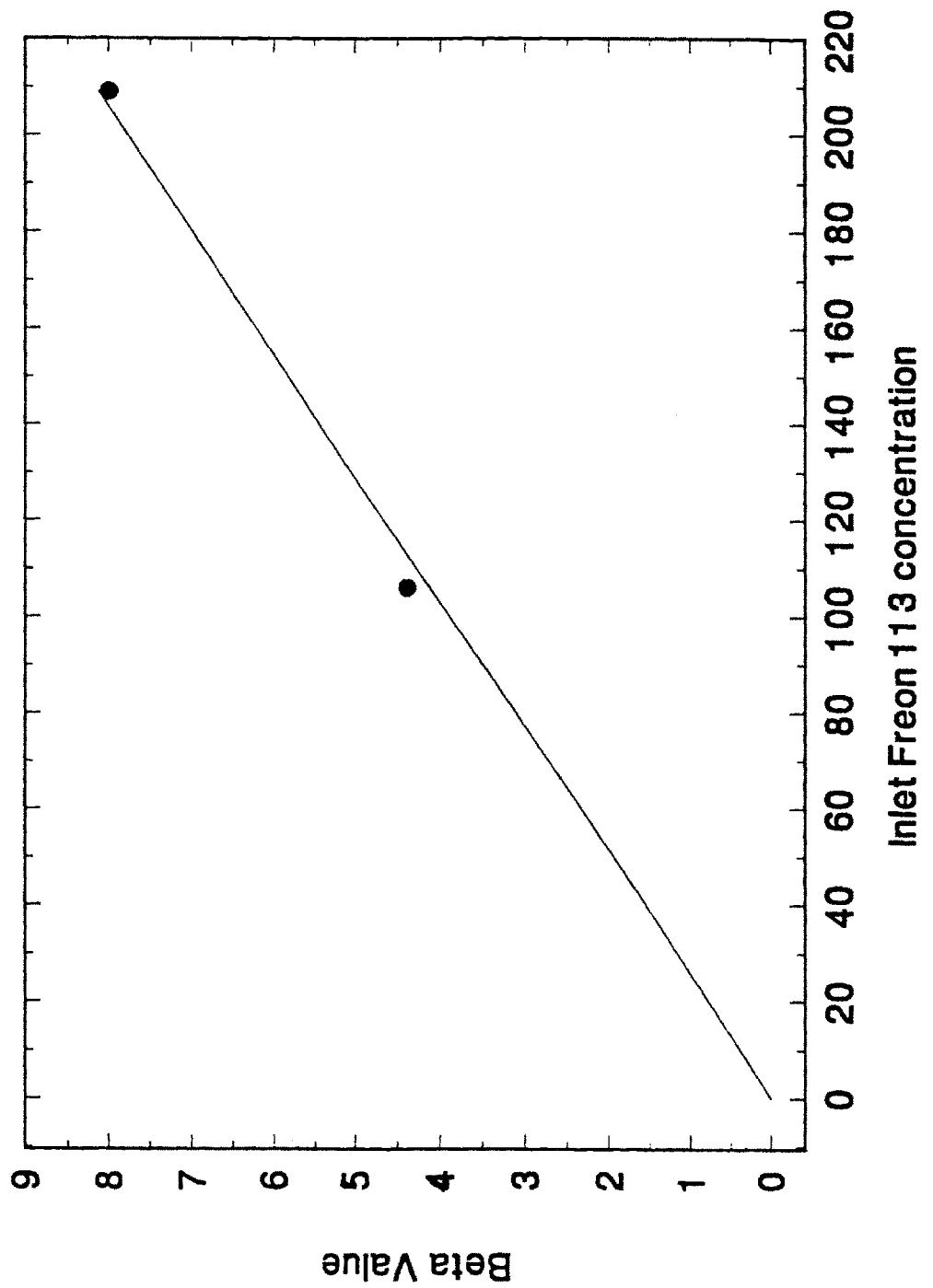
Figure 4.57: Rosocha β values for Freon 113 as a function of inlet concentration
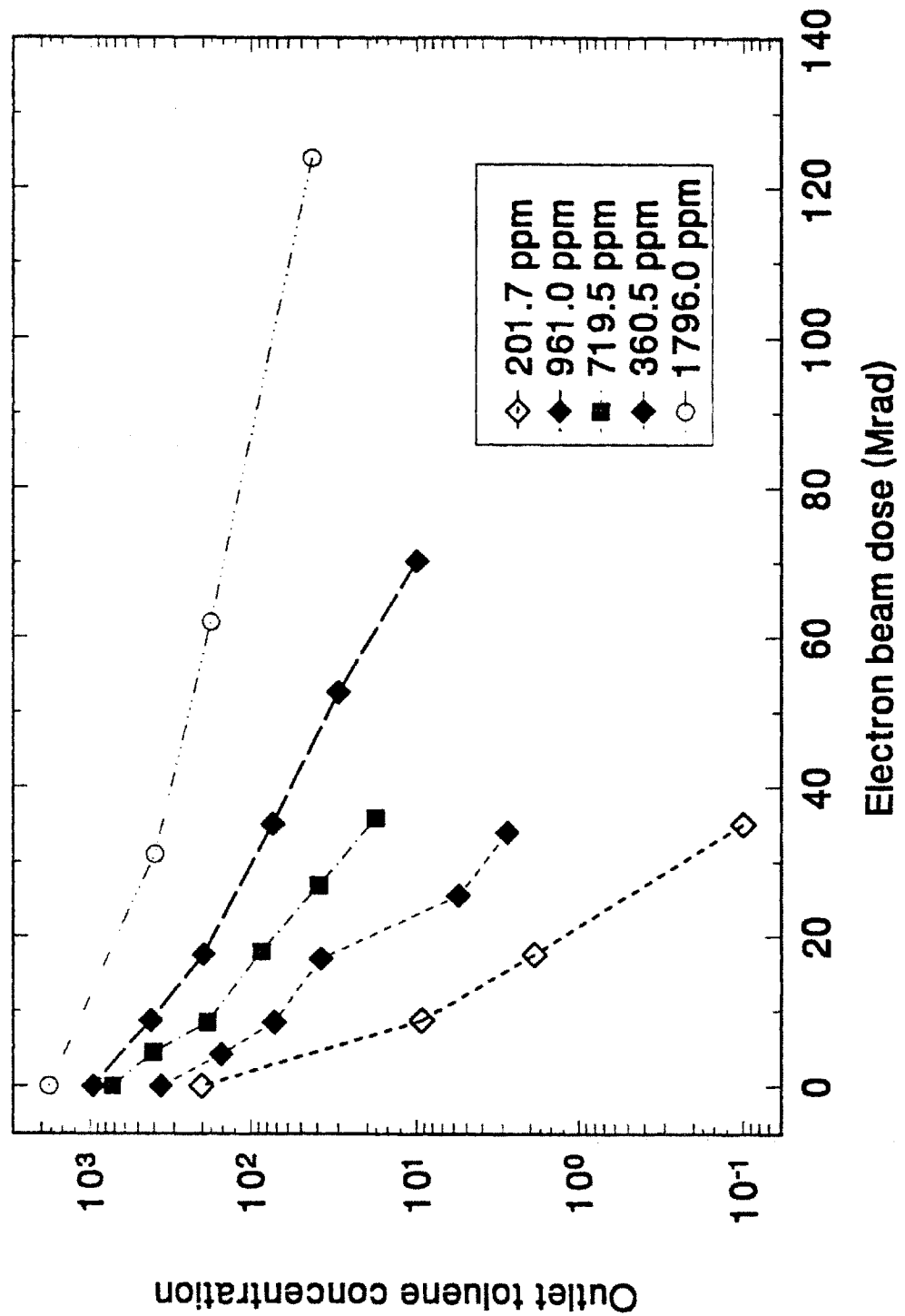
Figure 4.58: Toluene concentration versus electron beam dose

160
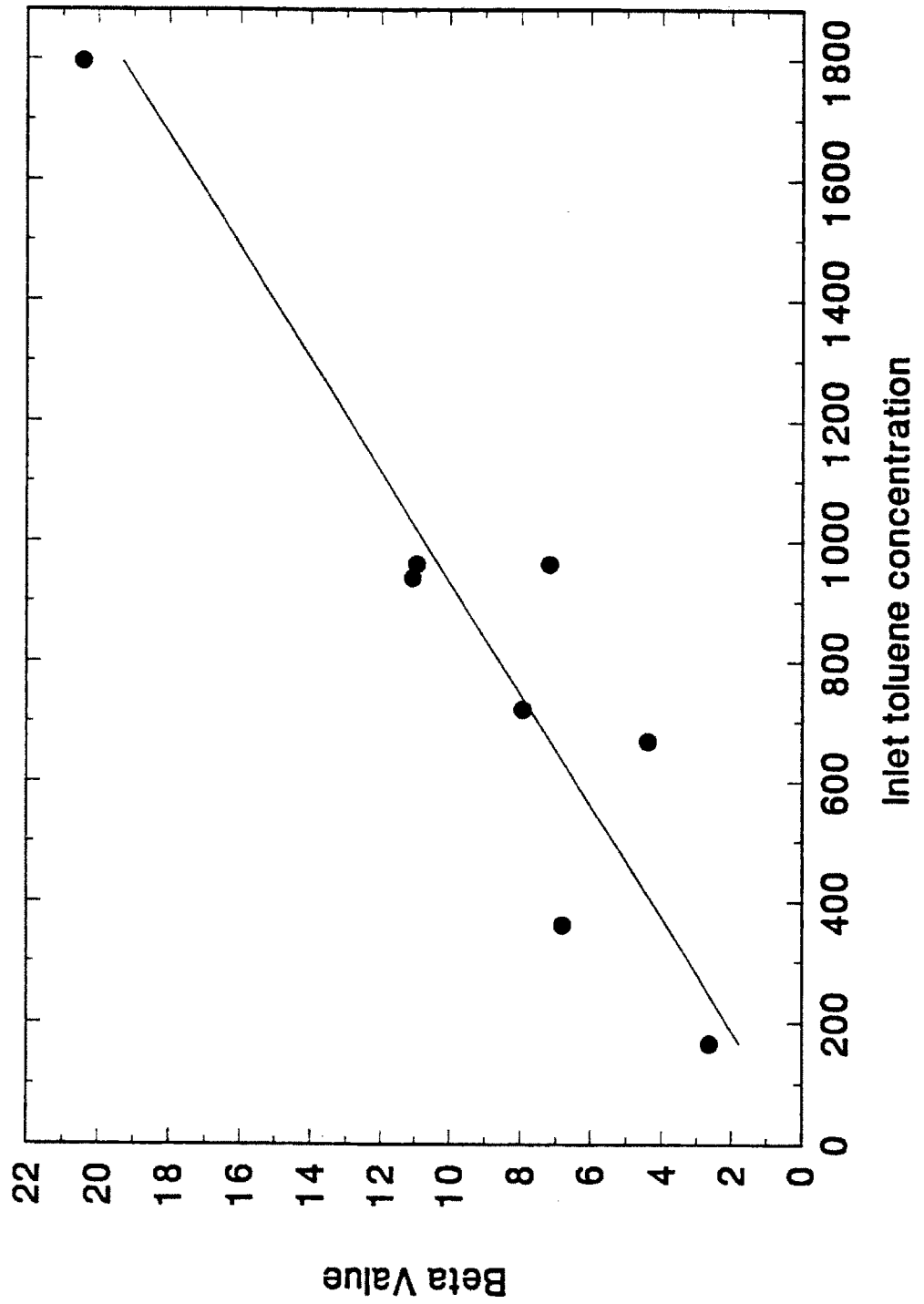
Figure 4.59: Rosocha β values for toluene as a function of inlet concentration

5. Discussion of the Hypothesis

Three processes of reaction initiation were discussed in section 4.2, dissociative recombination, electron attachment, and dissociative electron impact. All three of these mechanisms produce reactive radicals such as Cl• or O• which may then attack other VOC molecules, and further enhance the decomposition.

In a non-equilibrium plasma in which high temperature and energetic ionic reactions are assumed to be unimportant, the reaction initiation step is most likely one of these three mechanisms. The reactive radicals formed may be either chlorine from a VOC molecule, or oxygen from an oxygen molecule. The possible reaction chains are illustrated schematically in a flow diagram in figure 5.1.

This chart allows one to develop criteria to disprove the hypothesis presented in the *Introduction*, and repeated here:

The specific energy required for chlorinated VOC decomposition in the electron beam generated plasma reactor is determined by the electron attachment coefficient of the VOC and the susceptibility of the molecule to radical attack.

This hypothesis implies that a specific set of reaction pathways are predominant for chlorinated VOC decomposition the EBGPR. A general set of reaction pathways ways presented in Section 4.2, and these are repeated here for convenience.

initiation steps:

$$e\text{-} + O_2 \rightarrow 2O + e\text{-} \qquad k_{01} \qquad\qquad\qquad\qquad (R.01)$$

$$e\text{-} + T \rightarrow T^* + Cl\text{-} \qquad k_{02} \quad \text{dissociative electron attachment} \quad (R.02)$$

$$e\text{-} + T \rightarrow T^* + Cl + e\text{-} \quad k_{03} \quad \text{electron impact dissociation} \qquad (R.03)$$

$$e\text{-} + T^+ \rightarrow T^* + Cl \quad k_{04} \quad \text{dissociative recombination} \qquad (R.04)$$

decomposition steps

$$T^* \rightarrow P_{11} \qquad\qquad\qquad k_{11} \qquad (R.11)$$

$$\rightarrow P_{12} + I \qquad\qquad k_{12} \qquad (R.12)$$

$$\rightarrow P_{13} + Cl \qquad\qquad k_{13} \qquad (R.13)$$

162

$$Cl \;+\; T \;\rightarrow\; P_{21} \qquad\qquad k_{21} \qquad\qquad (R.21)$$

$$\rightarrow\; P_{22} \;+\; I \qquad\qquad k_{22} \qquad\qquad (R.22)$$

$$\rightarrow\; P_{23} \;+\; Cl \qquad\qquad k_{23} \qquad\qquad (R.23)$$

$$O \;+\; T \;\rightarrow\; P_{31} \qquad\qquad k_{31} \qquad\qquad (R.31)$$

$$\rightarrow\; P_{32} \;+\; I \qquad\qquad k_{32} \qquad\qquad (R.32)$$

$$\rightarrow\; P_{33} \;+\; Cl \qquad\qquad k_{33} \qquad\qquad (R.33)$$

inhibition steps

$$Cl \;+\; I \;\rightarrow\; ICl \qquad\qquad k_{41} \qquad\qquad (R.41)$$

$$O \;+\; I \;\rightarrow\; IO \qquad\qquad k_{42} \qquad\qquad (R.42)$$
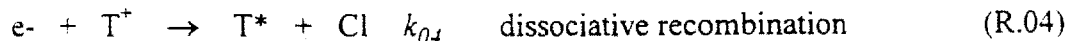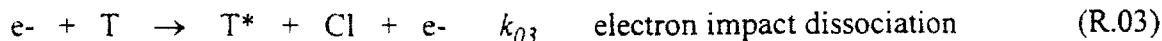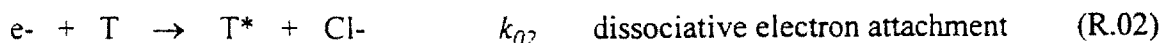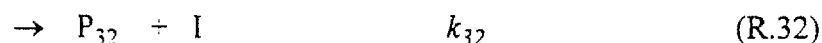
The hypothesis should hold true if the following criteria apply to this general set of reactions to determine the predominant pathways:

Criterion 1: The reaction is initiated by dissociative electron attachment, (R.04)

Criterion 2:. The decomposition is enhanced by radical reactions with the VOC (R.21 and R.31)

     The first criterion ensures that the electron attachment coefficient of the VOC is an important measure of how easily the molecule is decomposed in the reactor. The second criterion ensures that the susceptibility of the molecule to radical attack is an accurate measure of the enhancement of the decomposition by secondary radical mechanisms.

     On the other hand, the hypothesis will not be true if the following pathways of the reaction set are dominant:

1. The reaction is initiated by dissociative recombination, electron impact, or oxygen radical production (R.04, R.03, and R.01)

2. Inhibition reactions are much faster than radical attack on the VOCs. That is, if (R.41) and (R.42) are much faster then (R.21-R.33).

As a side note, the decomposition rate will be greatly enhanced (and the hypothesis also will still hold) if reaction (R.23) is important. This reaction regenerates the chlorine atom that is consumed, and thus will allow a chlorine radical chain reaction mechanism.

Now one must attempt to determine which reactions are important from the quantitative reaction rate data taken in the experiments and presented in Chapter 4. As discussed in the *Verification of the Hypothesis* section of the *Introduction* (Section 1.4.2), the six chlorinated VOCs in this study were chosen to compare their electron attachment coefficient and their chemical reactivity.

The electron attachment coefficients of TCA, TCA, DCA, DCE, EC, and VC are given in table 5.1. The more highly chlorinated compounds have higher electron attachment coefficients, as discussed in Section 1.4.2. If reaction (R.04) is important, the reaction rate should be proportional to the electron attachment coefficient. The reaction rate equations determined in Chapter 4 through the differential kinetic analysis are summarized in table 5.2.

In order to isolate the effect of electron attachment in these rate equations, one must consider only the rate constants in these expressions. This is because at low concentrations, the VOC molecules will not affect the decomposition of one another, and the reaction will proceed only through electron induced dissociation events. At very low concentrations, the order of the reaction has little effect, and the rate of reaction is determined predominantly by the rate constant k. Alternatively, one can realize that any dissociative electron-molecule interaction is necessarily a unimolecular decomposition reaction, so the order of this reaction whether electron attachment, impact, or dissociative recombination, must be unity. In any event, from table 5.2 it is evident that he orders of all of the reactions are the same, with the exception of TCE decomposition, so the order is unimportant in comparing the expressions. Thus by comparing the rate coefficients of the reactions, one can consider the "infinite dilution" reactions rate, which is the rate which would occur if the initiation steps in the above general mechanism occurred in isolation.

Considering the rate constants calculated by the differential kinetic method and given in table 5.2, one can see that for both the series of ethanes and the series of ethylenes, the reaction rate coefficients of the tri-chlorinated compounds are greater than those of the di-chlorinated compounds, which in turn are greater than that of the mono-chlorinated compounds. Thus the compounds with the higher electron attachment coefficients decompose more easily in the plasma than the compounds with low electron attachment coefficients. This suggests that reaction (R.04) is the predominant initiation step.

164

Chemical	Electron attachment rate coefficient using thermal electrons at 0.1 eV	Reference
1,1,1-Trichloroethane	6.5×10^{-9} cm^3/sec	80
Trichloroethylene	2.4×10^{-9} cm^3/sec	80
1,1-Dichloroethane	1×10^{-11} cm^3/sec	90
1,1-Dichloroethylene	2.7×10^{-11} cm^3/sec	80
Ethyl Chloride	10^{-15} cm^3/sec	estimated
Vinyl Chloride	10^{-15} cm^3/sec	estimated

Table 5.1: Electron Attachment Coefficients

$C_2H_3Cl_3$	$\rightarrow$ products	$r = -1.7 \times 10^{-2} [C_2H_3Cl_3]^{3/2}$
C_2HCl_3	$\rightarrow$ products	$r = -1.3 [C_2HCl_3]$
$C_2H_4Cl_2$	$\rightarrow$ products	$r = -1.01 \times 10^{-2} [C_2H_4Cl_2]^{1/2}$
$C_2H_2Cl_2$	$\rightarrow$ products	$r = -0.14 [C_2H_2Cl_2]^{3/2}$
C_2H_5Cl	$\rightarrow$ products	$r = -2.11 \times 10^{-3} [C_2H_5Cl]^{3/2}$
C_2H_3Cl	$\rightarrow$ products	$r = -1.7 \times 10^{-2} [C_2H_3Cl]^{3/2}$

Table 5.2: Reaction rates for decomposition determined by the differential kinetic method of Chapter 4. All reaction rates have units of ppm Mrad^{-1}.

This point will also be examined using the complementary treatment of the integral kinetic analysis also performed in Chapter 4. The energy expense. epsilon, was calculated for each compound through best fits to the integral INHIBIT model. The energy expense for 99% decomposition of each chlorinated ethane is given in figure 5.1 and for each chlorinated ethylene in figure 5.2. Once again, a trend is immediately apparent: the tri-chlorinated compounds require less energy for decomposition than the di-chlorinated compounds. which in turn require less energy than the monochlorinated compounds. The energy require for decomposition is inversely related to the electron capture coefficient of the molecule. in agreement with the differential kinetic results.

Both these treatments are consistent in showing that the energy required for decomposition is dependent upon the electron attachment coefficient of the molecule, Thus reaction (R.04) is likely the dominant initiation step, criterion 1 is justified, and the first part if the hypothesis is verified.

The second part of the hypothesis is that the energy required for decomposition is proportional to the susceptibility of the molecule to radical attack. This idea is somewhat more difficult to visualize and quantify than the first part of the hypothesis, so a brief discussion follows.

Ethanes are molecules with two carbons and a single bond (also called a sigma bond) between them. Ethylenes are molecules with two carbons and a double bond (also called a pi bond) between them. It is possible for a free radical to add to a carbon-carbon double bond. converting it to a single bond, as shown in reaction (5.1) below.

Theoretically. it could be possible for a free radical to add to a carbon-carbon single bond, thus rupturing the bond and creating two fragments. This is illustrated in reaction (5.2) below. However. it is well known in organic chemistry that the latter reaction almost never proceeds under standard conditions. Such combustion type reactions as reaction (5.2) can take place when the thermal temperature of the molecules is very high; this is the principle of incineration. However, recall that in the EBGPR, the plasma is assumed to be non-equilibrium, and the ions and molecules are cold. Thus high temperature reactions such as reaction (5.2) will not occur.

$$Cl + CHClCH_2 \rightarrow CHCl_2CH_2 \qquad \Delta H_{rxn} = -17.0 \text{ kcal/mol} \qquad (5.1)$$

$$Cl + CH_3CH_2Cl \rightarrow CH_3Cl + CH_2Cl \qquad \Delta H_{rxn} = 5.8 \text{ kcal/mol} \qquad (5.2)$$
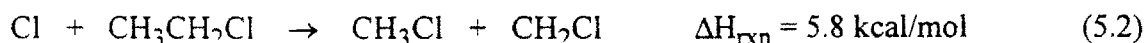
To make this statement somewhat more quantitative. the heats of reaction of these two reactions have been calculated. The details of the calculation by group additivity methods are given in Appendix C. Reaction (5.1) is seen to be exothermic, with ΔH_{rxn} = -17.0 kcal/mol. Reaction (5.2) is endothermic, with ΔH_{rxn} = 5.8 kcal/mol. Although this is not a definitive result. as the entropies of reaction and kinetic considerations are also important. one can say qualitatively that reactions which are more exothermic are more likely to proceed further to completion than reactions which are more endothermic.

Reaction (5.1) is chlorine radical addition to vinyl chloride, an ethylene. This reaction is allowed kinetically, is known to occur physically, and is exothermic. Reaction (5.2) is chlorine radical addition to ethyl chloride, an ethane. This reaction is not favorable from a chemistry point of view, since a carbon-carbon single bond is broken at low temperatures. and it is significantly more endothermic then the former reaction. The same qualitative results will hold true for all of the chlorinated ethylenes and ethanes in this study.

Therefore. the susceptibility of a molecule to radical attack, as given in the hypothesis. is related to these two reactions, and to their analogs for di- and tri-chlorinated compounds. Chlorinated ethylenes possess a carbon-carbon double bond, and thus they are susceptible to radical attack. Chlorinated ethanes have only a carbon-carbon single bond. and thus are not susceptible to radical attack.

Note here that attack at the carbon-hydrogen bond has not been considered. That is because the bond strength of the C-H bond is approximately 100 kcal/mol, while the C-C bond strength is approximately 88 kcal/mol. One must only consider here radical attack at the weakest bond. If that does not occur, attack at the stronger C-H bonds are also unlikely. Chlorine radical attack at the carbon chlorine bond would lead only to chlorine-chlorine substitution. and thus is not important.

Since chlorinated ethylenes are seen to be more susceptible to radical attack than chlorinated ethanes. than if the hypothesis is correct, the ethylenes should decompose more easily in the EBGPR than the chlorinated ethanes. Figure 5.3 compares the concentrations of TCA (an ethane) and TCE (an ethylene) versus electron beam dose. It is

seen that TCE decomposes much more rapidly than TCA. Figures 5.4 and 5.5 compare the concentration versus dose curves for DCA/DCE and EC/VC, respectively. In all cases, for a given number of chlorine atoms on the molecule (and thus a given electron attachment coefficient), the chlorinated ethylenes decompose more rapidly than the chlorinated ethanes.

The same results are apparent if one compares the reaction rate curves or the energy expense curves for TCA/TCE, DCA/DCE, or EC/VC. This is seen as confirmation of criterion 2, that the decomposition is enhanced by radical reactions with the VOC (R.21 and R.31). The second part of the hypothesis is thus verified.
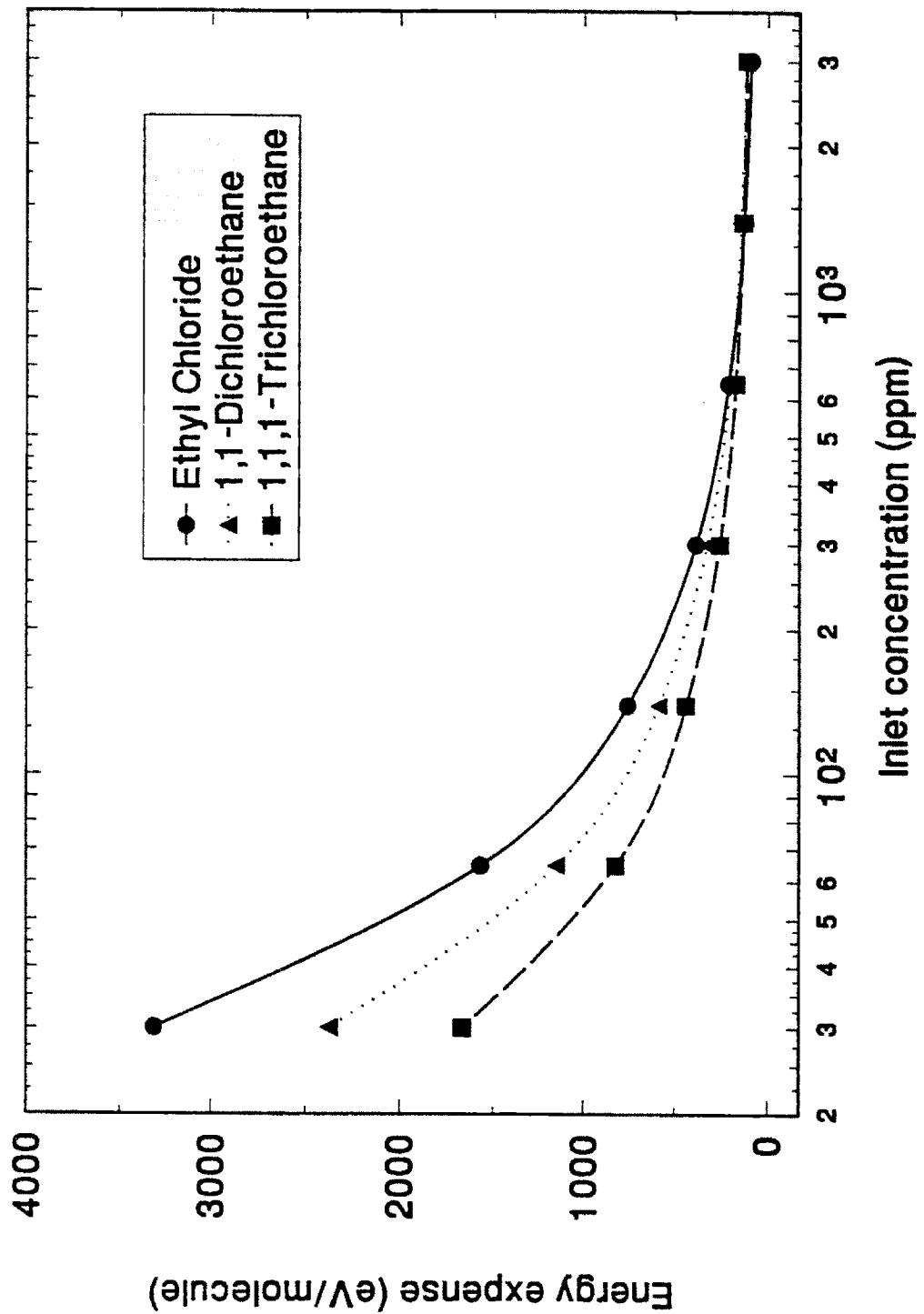
Figure 5.1: Energy expense in eV/molecule for 99% decomposition of three chlorinated ethanes. The more highly halogenated the compound, less energy is required for its decomposition.
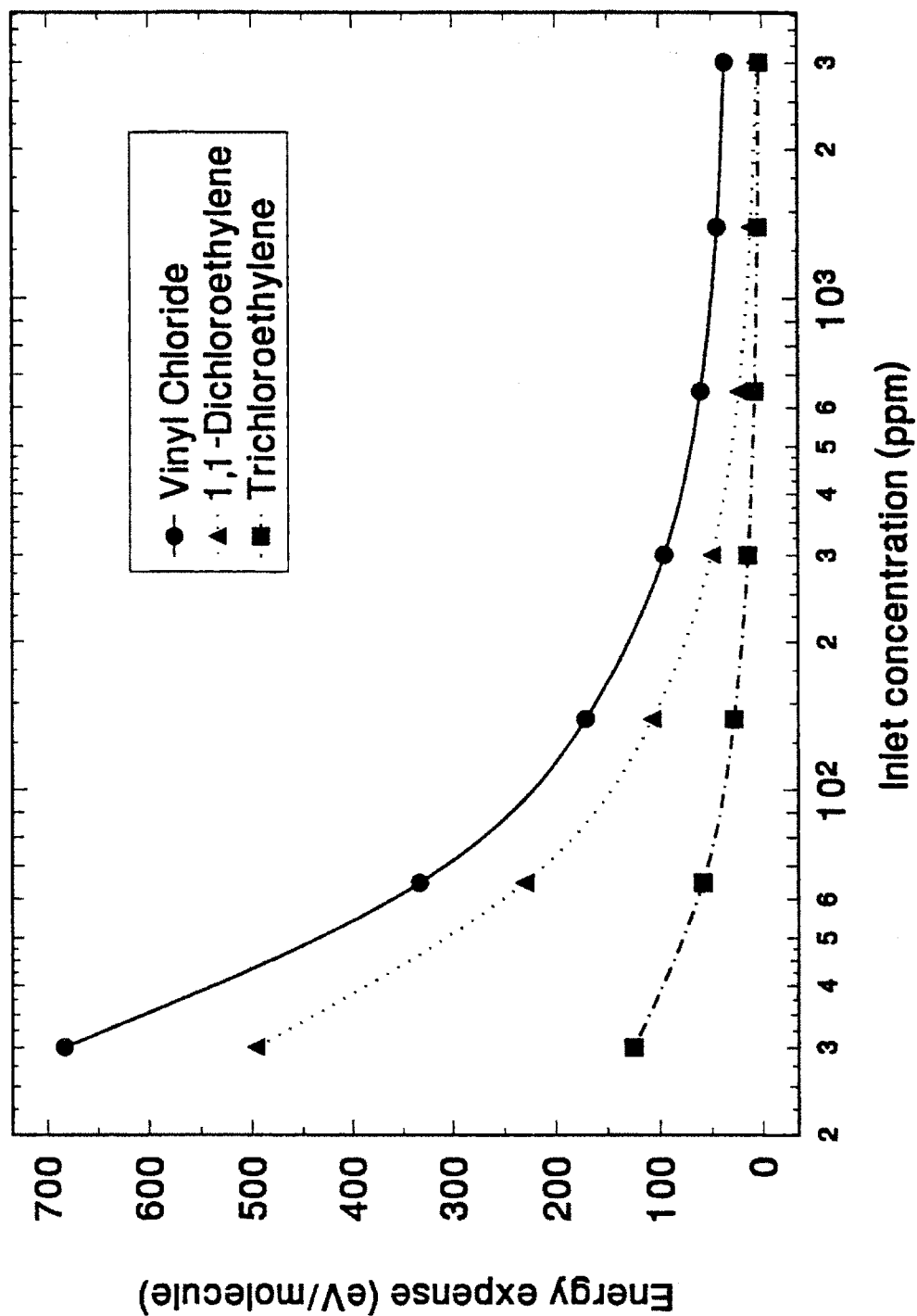
Figure 5.2: Energy expense in eV/molecule for 99% decomposition of three chlorinated ethylenes. The more highly halogenated the compound, less energy is required for its decomposition.
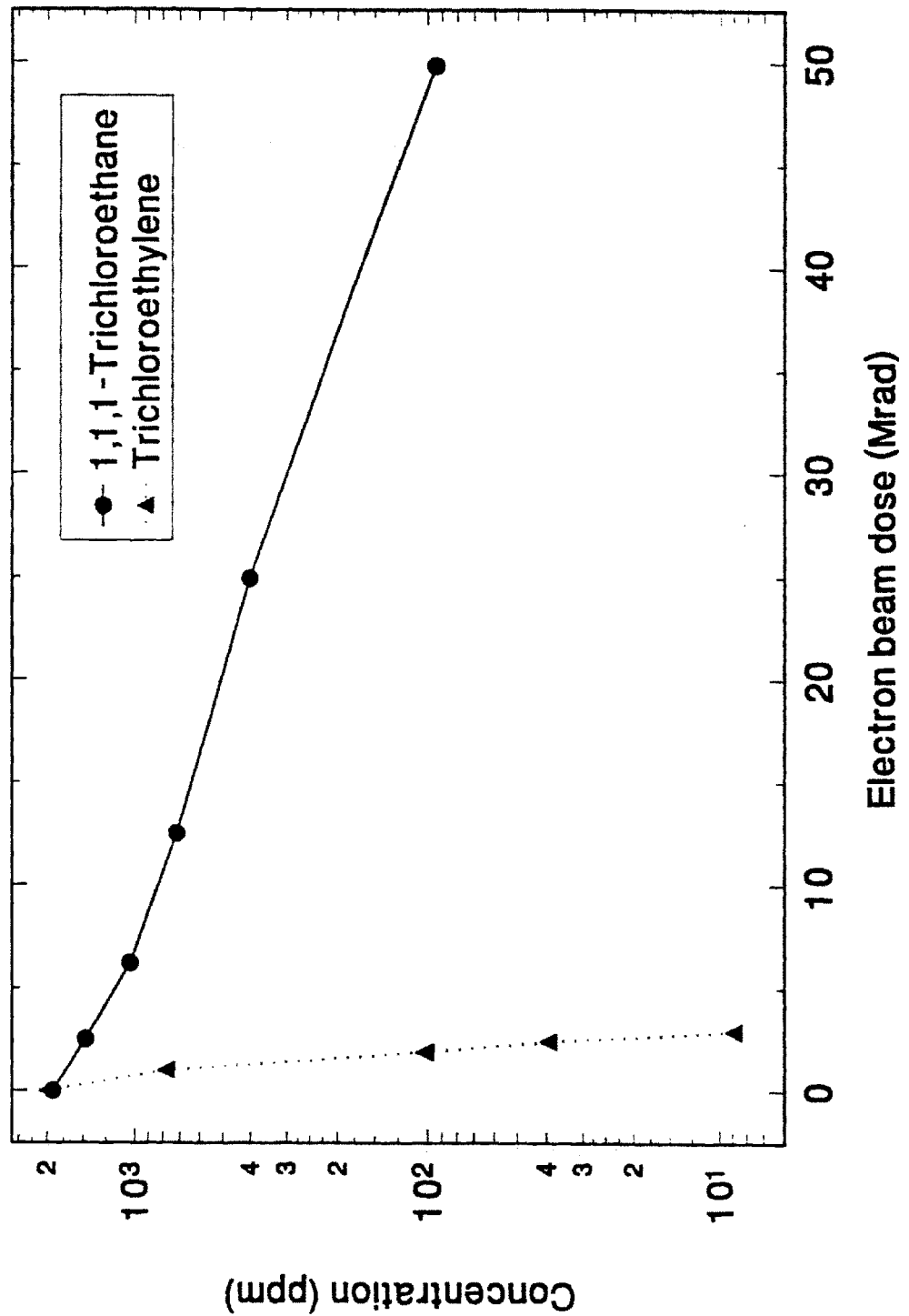
Figure 5.3: Concentrations of TCA and TCE versus electron beam dose. The ethylene concentration falls off much more rapidly.
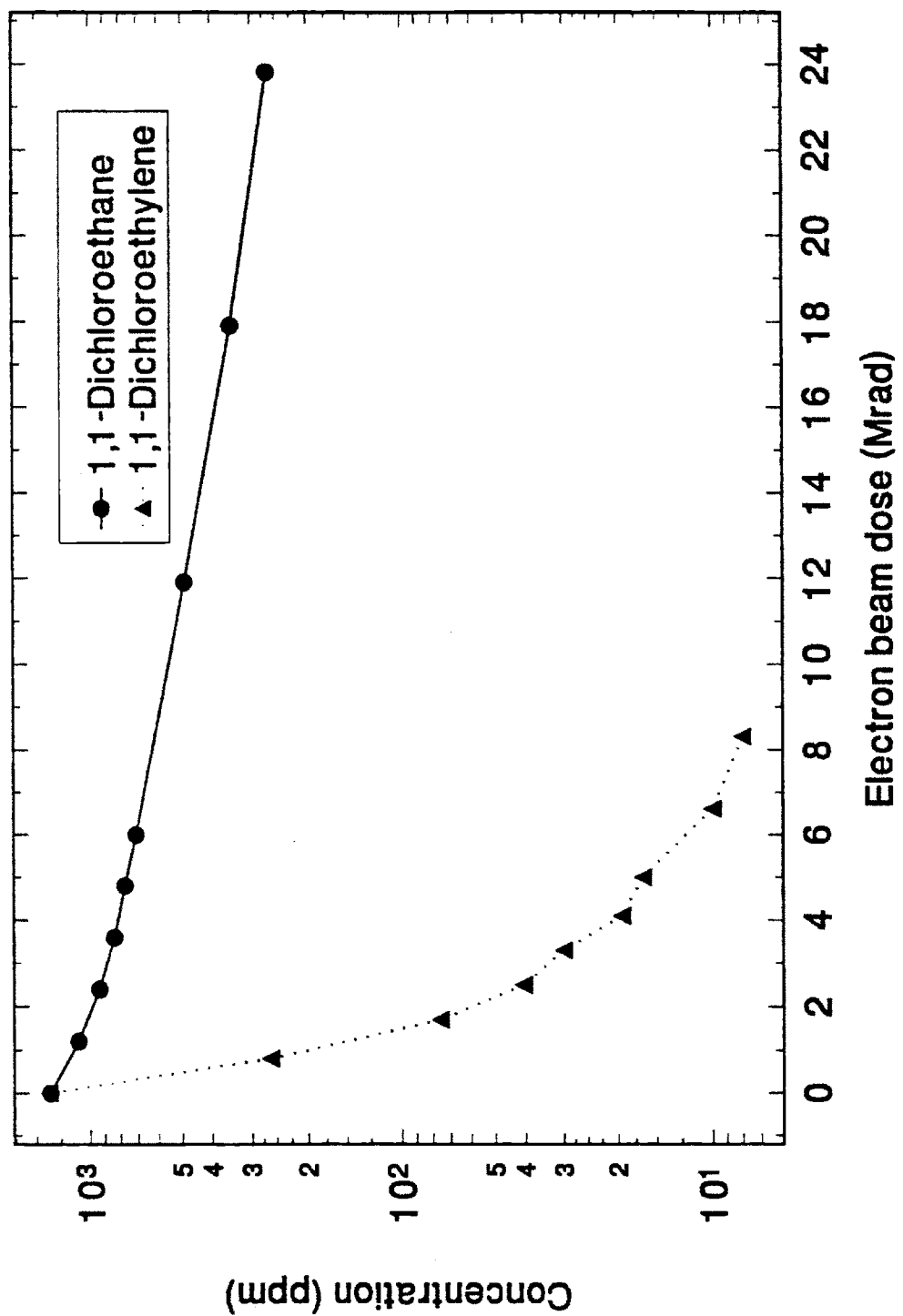
Figure 5.4: Concentrations of DCA and DCE versus electron beam dose. The ethylene concentration falls off much more rapidly.
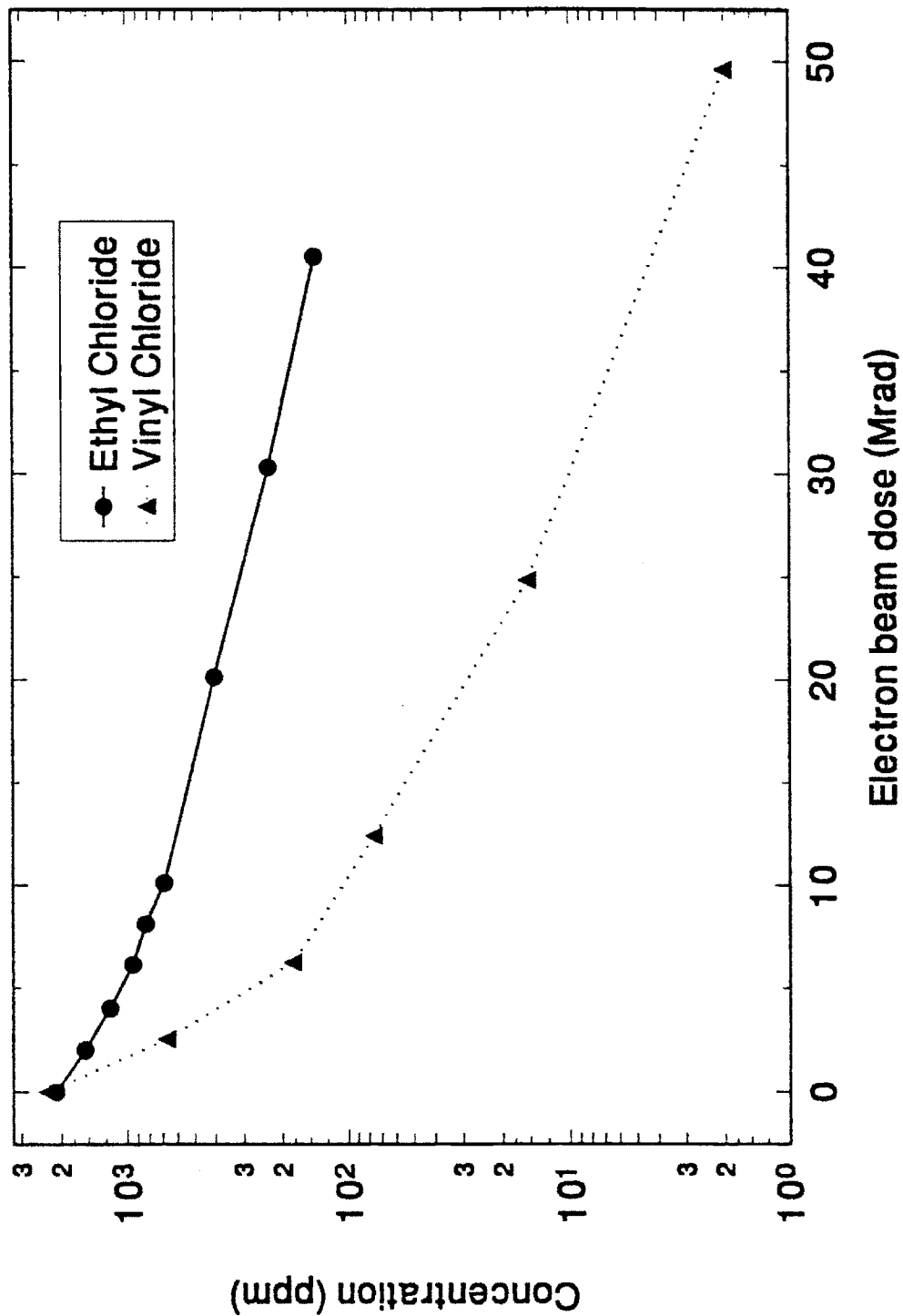
Figure 5.5: Concentrations of EC and VC versus electron beam dose. The ethylene concentration falls off much more rapidly.

6. Conclusion

The electron beam generated plasma reactor was successfully used as an instrument to determine the plasma chemistry kinetics, energetics and decomposition pathways of six chlorinated ethylenes and ethanes. A traditional chemical kinetic and chemical engineering analysis of the data from the EBGPR was performed, and the following hypothesis was verified:

The specific energy required for chlorinated VOC decomposition in the electron beam generated plasma reactor is determined by the electron attachment coefficient of the VOC and the susceptibility of the molecule to radical attack.

Several theoretical treatments were provided to aid in analyzing the data. A radiation chemistry approach was used to derive an expression to relate the VOC concentration to the electron beam dose through the G-value of the molecule, or equivalently, the β-value. The differential kinetic approach was explained, and the order with respect to time n_t and the order with respect to concentration, n_c, were discussed. It was shown how this kinetic method could be used wit the EBGPR data to generate reaction orders and rate constants. as well as to gain insight into inhibition mechanisms in the reactor. An integral kinetic model, the INHIBIT model, was derived analytically from a simplified set of chemical reactions. This model accounted for some of the inhibited quantities of the experimental data, but does not allow expression of the full non-linear nature of the problem.

A traditional chemical engineering analysis was applied to the EBGPR which was modeled as an ideal plug flow reactor. This allowed the derivation a modified performance equation relating the VOC outlet concentration from the reactor to the reactor power required, through the reaction rate expression:

$$\int_{C_{ko}}^{C_{kf}} \frac{dC_k}{-r} = -\frac{P}{\rho_0 F_0} \qquad (2.57)$$

This important formula determines the electron beam power which must be coupled to the plasma in order to decompose the VOC of interest to a specified outlet concentration at a given flow rate. The Reaction rate, r, was determined by the differential, order with respect to time analysis for TCA. TCE, DCA, DCE, EC, and VC. These rate expression have been summarized in table 5.2.

A modified reaction chamber was installed on the EBGPR to improve the reproducibility of the results. Unlike the previous design, the new reaction chamber is leak free within the detection limits of the instruments available. and it is constructed of

inexpensive. commercially available parts. Dosimetry calculations were performed with a Monte Carlo ACCEPT code to determine the electron beam dose to the plasma.

Nearly 4000 data points were collected with the EBGPR over the 15 month period of this study. These data points were used in conjunction with the differential and integral kinetic models described above to determine several quantities of interest for each of the six VOCs in this study. The rate constants, k, and unimolecular reaction orders, n_t, were determined. Best fits to the INHIBIT model gave values of K and β' which allowed a calculated analytic expression of the VOC concentration as a function of electron beam dose. The parameter K gives an indication of the importance of inhibition in the reaction mechanism: if K is near zero, then inhibition is unimportant, and the reaction follows first order exponential decay behavior. If K is non-zero, than the reaction appears to have inhibited kinetics. and the reaction follows a non-linear decay pattern.

Measurements were taken of all of the identifiable reaction product abundances. This information was used in conjunction with the kinetic analysis to determine possible reaction pathways for decomposition in the reactor. Reaction pathways for all six chlorinated ethylenes and ethanes were proposed. The mast important major reaction products in every case were carbon dioxide, carbon monoxide, and hydrogen chloride. Many other minor decomposition products were also observed.

Rosocha β-values and specific energies, ϵ. were determined for each VOC as a function of concentration. Unlike the efforts of previous research groups, in this study, β and ϵ. were allowed to vary with inlet concentration. For all most compounds, the two values did in fact have a marked dependence on inlet concentration. For cases where previous literature values for β were available at a known concentration, the results agreed very well with those from the EBGPR. This result is important to both the EBGPR study and the previous works, because it provides verification of the results of both studies. It also serves to show that the dosimetry calculation performed on the EBGPR have given reasonable values, since the beta values obtained are directly related to the knowledge of the electron beam dose.

6.1. Suggestions for Further Study

There are many areas which can still be explored using the electron beam generated plasma reactor. A much more complete model of the reaction mechanisms could be achieved through the use of an integrated kinetics modeling package such as CHEMKIN II. This would allow a better analysis of which reaction pathways are most important in each reaction mechanism proposed.

Other chemicals of commercial interest could be studied in the reactor. For example. hydrofluorocarbons are a likely choice to replace CFC's and PFC's as refrigerants. Commercial interest in these chemicals continues to grow, and new chemical processes will be needed to prevent emission of these compounds from chemical plants. The laboratory version of the EBGPR may be used to develop reaction rate expressions for these compounds. and to study their decomposition mechanisms and products.

Further work should probably be performed to verify the scaling equation given above. This equation should be able to predict the decomposition achieved in and EBGPR which satisfies the ideal PFR assumptions. If this turns out not to be the case, one should consider alternative scaling equations for the design of a commercial size reactor.

One aspect of the electron beam reactor which has not been dealt with at all in this study is the ability to change the mean electron temperature in the reaction chamber by an applied electric field. This is the *tunable* plasma reactor concept, and has not received any significant attention in this work, or in the studies of Koch. It is possible that by changing the electron energy distribution in the plasma, some chemicals may be more easily decomposed. This could occur by tuning the mean electron energy to match the peak of the dissociative electron capture cross section of a given chemical. This is a rather easy study to undertake, and may improve the energy efficiency of the reactor by a factor of two or more.

The amount of useful data taken with the EBGPR shows that it can be used as a tool for the study of plasma chemistry kinetics, as well as having use as a commercial unit operation for the decomposition of halogenated organic compounds. Much more advanced kinetic studies can be performed with the reactor is additional diagnostic devices are added which are common in chemical kinetic studies. These include laser-induced fluorescence and plasma emission spectroscopy devices, which allow measurements of transient species in the plasma, such as radicals and ions. Studies such as these are necessary to confirm any advanced kinetic study, as they allow direct observation of reaction intermediates which can only be assumed to exist in the present study.

References

1. M. Koch, "Decomposition of chlorinated organic compounds in gaseous hazardous waste using a tunable plasma reactor", Ph.D. Thesis, M.I.T. Department of Nuclear Engineering, 1994.

2. M. Koch, D.R. Cohn. R.M. Patrick, M.P. Scheutze, L. Bromberg, D. Reilly, K. Hadidi, P. Thomas, P. Falkos. "Electron beam atmospheric pressure cold plasma decomposition of tetrachloro methane CCl_4 and trichloro ethylene C_2HCl_3," submitted to *Environmental Science and Technology*, 1994.

3. M. Koch, D. R. Cohn. R. M. Patrick, M. P. Scheutze, L. Bromberg, D. Reilly, P. Thomas, "Electric field effects on decomposition of dilute concentrations of CHCl3 and CCl4 in electron beam generated air plasmas," *Physics Letters A*, **184**. 109, 1993.

4. M. Koch. "Prediction of electron beam cold plasma decomposition of CCl_4 on basis of G-value considerations." accepted by *Radiation Physics and Chemistry*, 1994.

5. R. C. Slater, D. H. Douglas-Hamilton, "Electron-beam-initiated destruction of low concentrations of vinyl chloride in carrier gases," *Journal of Applied Physics.*, **52**, 5820, 1981.

6. J. W. Bozzelli R. B. Barat. "Reactions of water vapor or molecular hydrogen with trichloroethylene in a microwave plasma reactor," *Plasma Chemistry and Plasma Processing*, **8**, 293. 1988.

7. J. W. Virden, W. O. Heath. S. C. Goheen, M.C. Miller, G. M. Mong, R. L. Richardson, "High energy corona for destruction of volatile organic compounds in process off-gases," SPECTRUM '92. Boise. Idaho, Pacific Northwest Laboratories. Richland, Washington, August 1992.

8. W. H. McCulla, L. A. Rosocha, W. C. Neely, E. J. Clothiaux, M. J. Kushner, M. J. Rood. "Treatment of hazardous organic wastes using wet air plasma oxidation," First Idaho National Engineering Laboratory Plasma Applications to Waste Treatment Workshop, Idaho National Engineering Laboratory, Idaho Falls. Idaho. January, 1991.

9. L. A. Rosocha. W. H. McCulla. F. B. Wampler, W. J. Cooper. C. N. Kurucz, T. D. Waite. W. C. Neely. E. J. Clothiaux, M. J. Kushner, M. J. Rood. "Two innovative advanced oxidation processes for waste treatment," Workshop on Environmentally Conscious Manufacturing. Albuquerque, New Mexico. Las Alamos National Laboratory, Los Alamos. New Mexico. LA-UR-91-1042, 1991.

10. L. A. Rosocha, W. H. McCulla, "Cold plasma destruction of air-based toxic compounds." presented at "Plasma Technologies for the Destruction of Air Toxics," Southern California Edison-Customer Technology Appreciation Center, San Diego, California, December 1991.

11. L.A. Rosocha, G. R. Allen, J. J. Coogan, M. Kang, J. D. Smith, W. H. McCulla, S. J. Buelow, R. B. Dyer, G. K. Anderson, F. B. Wampler, R. A. Tennant, P. J. Wantuck, "Advanced Chemical Processes for Hazardous Waste Destruction Study," Annual Report, Chemical and Laser Sciences Division, Los Alamos National Laboratory, Los Alamos, New Mexico, December 1991.

12. L. A. Rosocha, G. K. Anderson, L. A. Bechtold, J. J. Coogan, H. G. Heck, M. Kang, W. H. McCulla, R. A. Tennant, P. J. Wantuck, "Treatment of hazardous organic wastes using silent discharge plasmas," Proceedings of NATO Advanced Research Workshop on Non-Thermal Plasma Technologies for Pollution Control, Cambridge, England, LA-UR-92-3552, 1992.

13. S. M. Matthews, A.J. Boegel, S.F. Eccles, S. G. Homann, D.W. Rice, J. A. Loftis, M. C. Jovanovich, R. A. Caufield, B. J. Mincher, D. H. Meikrantz, R. J. Murphy, G. L. Gresham, M. J. Connoly, "High energy irradiation of chlorinated hydrocarbons," *Journal of Radioanalytical and Nuclear Chemistry*, **161**, 253, 1992.

14. S. M. Matthews, A. J. Boegel, D. W. Camp, R. A. Caufield, J. O. Cunnigham, P. F. Daley, J. J. Greci, M. C. Jovanovich, J. A. Loftis, P. D. Soran, "Remediation of a TCE groundspill using an electron accelerator," Proceedings of the International Topical Meeting on Nuclear and Hazardous Waste Management SPECTRUM '92, Boise, Idaho, August, 1992.

15. T. Oda, T. Takahashi, H. Ito, H. Yoshida, IEEE Transactions on Industry Applications, Vol. **28**, (3), 535-540, 1992.

16. G. H. Ramsey, N. Plaks, C. A. Vogel, W. A. Ponder, L. E. Hamel, "The destruction of volatile organic compounds by an innovative corona technology," Electric Power Research Institute Proceedings: Eighth Particulate Control Symposium, Vol. 1, "Electrostatic Precipitators," 1990, EPRI-GS-7050 pp. 9/1-9/15.

17. T. Yamamoto, P. A. Lawless, K. Ramanathan, D. S. Ensor, G. H. Ramsey, N. Plaks, "Application of corona-induced plasma reactors to decomposition of volatile organic compounds," Electric Power Research Institute Proceedings: Eighth Particulate Control Symposium, Vol. 1, "Electrostatic Precipitators," 1990, EPRI-GS-7050 pp. 10/1-10/11.

18. T. Yamamoto, K. Ramanathan, P. A. Lawless, D. S. Ensor, J. R. Newsome, N. Planks, G. H. Ramsey, "Control of volatile organic compounds by an AC energized ferroelectric pellet reactor and a pulsed corona reactor", *IEEE Transactions on Industry Applications*, **28**, (3), 528-534, 1992.

19. C. Nunez, G. Ramesey, "Corona destruction process for controlling VOCs and air toxics," presented at "Plasma Technologies for the Destruction of Air Toxics." Southern California Edison-Customer Technology Application Center, San Diego, California, December 1991.

20. A. Liu, W. A. Mulac, C. D. Jonah, "Pulse radiolysis study of the gas-phase reaction of OH radicals with vinyl chloride at 1 atm and over the temperature range 313-1173K," *Journal of Physical Chemistry*, **93**, 4092-4094, 1989.

21. N. G. Volkov, G. M. Gorbachenko, O. V. Lapidus, V. K. Lyapidevskii, "Role of ions in the radiation polymerization mechanism of vinyl chloride in the gas phase II. Investigation of electron attachment in vinyl chloride," *High Energy Chemistry*, **6**, 485, 1972.

22. M. C. Hsiao, B. T. Merritt, B. M. Penetrante, G. E. Vogtlin, P. H. Wallman, "Plasma assisted decomposition of methanol and trichloroethylene in atmospheric pressure air streams, by electrical discharge processing," *Journal of Applied Physics*, **78**, (5), 1-6, 1995.

23. H. Schyett, H. Esrom, L. Prager, R. Mehnert, C. Von Sonntag, in Non-Thermal Plasma Techniques for Pollution Control: Part B-Electron Beam and Electrical Discharge Processing, edited by B. M. Penetrante, and S. E. Scheultheis, (Springer, Heildberg, 1993) pp. 91-102.

24. S. M. Matthews, A. J. Boegel, J. A. Loftis, R. A. Caufield, B. J. Mincher, D. H. Meikrantz, R. J. Murphy, *Radiation Physics and Chemistry*, **42**, 689, 1993.

25. T. Yamamoto, P. A. Lawless, M. K. Owen, D. S. Ensor, C. Boss, in Non-Thermal Plasma Techniques for Pollution Control: Part B-Electron Beam and Electrical Discharge Processing, edited by B. M. Penetrante, and S. E. Scheultheis, (Springer, Heildberg, 1993) pp. 223-238.

26. D. Evans, L. A. Rosocha, G. K. Anderson, J. J. Coogan, M. J. Kushner, "Plasma remediation of trichloroethylene in silent discharge plasmas," *Journal of Applied Physics*, **74**, (9), 5378-5386, 1993.

27. L. A. Rosocha, G. K. Anderson, L. A. Bechtold, J. J. Coogan, H. G. Heck, M. Kang, W. H. McCulla, R. A. Tennant, P. J. Wantuck, in Non-Thermal Plasma Techniques for Pollution Control: Part B-Electron Beam and Electrical Discharge Processing, edited by B. M. Penetrante, and S. E. Scheultheis, (Springer, Heildberg, 1993) pp. 281-308.

28. W. C. Neely, E. I. Newhouse, E. J. Clothiaux, C. A. Gross, in Non-Thermal Plasma Techniques for Pollution Control: Part B-Electron Beam and Electrical Discharge

Processing, edited by B. M. Penetrante, and S. E. Scheultheis, (Springer, Heildberg, 1993) pp. 302-320.

29. E. I. Newhouse. W. C. Neely, E. J. Clothiaux, J. W. Rodgers, in ACS Symposium on Emerging Technologies in Hazardous Waste Management VI, pp. 207-210.

30. E. J. Clothiaux, J. A. Koropchak, R. R. Moore, *Plasma Chemistry and Plasma Processing*, 4, 15, 1984.

31. M. E. Fraser, D. A. Fee, R. S. Sheinson, *Plasma Chemistry and Plasma Processing*, 5, 163, 1985.

32. M. E. Fraser, R. S. Sheinson, *Plasma Chemistry and Plasma Processing*, 6, 27, 1986.

33. S. Masuda, in Non-Thermal Plasma Techniques for Pollution Control: Part B-Electron Beam and Electrical Discharge Processing, edited by B. M. Penetrante, and S. E. Scheultheis, (Springer, Heildberg, 1993) pp. 199-201.

34. T. Oda, T. Takahashi. H. Nakano, S. Masuda, in Proceedings of the 1991 IEEE Industrial Applications Society Meeting, Dearborn, MI, September/October 1991, pp. 734-739.

35. A. Czernichowski. T. Czech, in Proceedings of the 10th International Symposium on Plasma Chemistry, Bochum Germany, 1991.

36. A. Czernichowski. T. Czech, in Proceedings of the 3rd International Symposium on High-Pressure, Low-Temperature Plasma Chemistry, Strasbourg, France, 1991.

37. L. J. Bailin, M. E. Seilbert, L. A. Jonas, A. T. Bell, *Environmental Science and Technology*, 9, 254, 1975.

38. B. M. Penetrante. M. C. Hsiao, J. N. Bardsley, B. T. Merritt, G. E. Vogtlin, P. H. Wallman, "Electron beam and pulsed corona processing of carbon tetrachloride in atmospheric pressure gas streams," Submitted to *Physics Letters A*, 1995.

39. M. C. Hsiao, B. T. Merritt, B. M. Penetrante, G. E. Vogtlin, P. H. Wallman, "Effect of gas temperature and oxygen content on pulsed corona discharge processing of methylene chloride." Submitted to *Chemical Physics Letters*, 1995.

40. B. M. Penetrante. M. C. Hsiao, J. N. Bardsley, B. T. Merritt, G. E. Vogtlin, P. H. Wallman, "Electron beam and pulsed corona processing of volatile organic compounds in gas streams." Submitted to *Pure and Applied Chemistry*, 1995.

41. J. S. Chang, F. Kaufman, "Kinetics of the reactions of hydroxyl radicals with some halocarbons: $CHFCl_2$, CH_2Cl, CH_3CCl_3, C_2HCl_3, and C_2Cl_4," *Journal of Chemical Physics*, **66**, (11), 4989-4994, 1977.

42. T. R. Krause, J. E. Helt, "Chemical detoxification of trichloroethylene and 1,1,1-trichloroethane in a microwave discharge plasma reactor at atmospheric pressure," Chapter 19 in Emerging Technologies in Hazardous Waste Management III, edited by W. D. Tedder and F. G. Pohland, ACS, Washington D. C., (1993).

43. R. B. Barat, J. W. Bozelli, "Reactions of chlorocarbons to HCl and hydrocarbons in a hydrogen-rich microwave -induced plasma reactor," *Journal of Environmental Science and Technology*, **23**, 666-671, 1989.

44. M. J. Kushner, "Modeling of plasma remediation of SO_2, N_xO_y, and VOCs: progress report and databases." Presented at conference. March 1995.

45. N. L. Aleksandrov, S. V. Dobkin, A. M. Konchakov, D. A. Novitskii, "Catalytic decomposition of Freons in microwave discharge afterglow," *Plasma Physics Reports*, **20**, (5), 442-448, 1994.

46. H. Sekiguchi, T. Honda, A. Kanzawa, "Thermal plasma decomposition of chlorofluorocarbons." *Plasma Chemistry and Plasma Processing*, **13**, (3), 463-478, 1993.

47. A. Besson, L. Fournier, "Action of the silent discharge on chloroform, carbon tetrachloride, and methyl chloride." *Compt.rend.*, **150**, 1118, 1910.

48. P. N. Ghosh, B. D. Chatterjee, "Investigation of high frequency discharge. Methane, methyl chloride, dichloromethane, chloroform, carbon tetrachloride," *Z. Physik*, **65**, 102, 1930.

49. N. V. Thornton, A. B. Burg, H. I. Schelisinger, "The behavior of dichlorodifluoromethane and chlorotrifluoromethane in the electric discharge," *Journal of the American Chemical Society*, **55**, 3177, 1933.

50. M. Nakajima, "Synthesis of benzene hexachloride by silent discharge," *Botyu Kagaku*, **17**, 6, 1952.

51. H. Schueler, L. Reinebeck, "Chlorobenzene in a glow discharge," *Naturw.*, **39**, 445, 1952.

52. M. Nakajima, "Synthesis of some organic compounds in the electric discharge. II. Synthesis of benzene hexachloride by the silent discharge," *Society of Organic Synthesis Chemistry (Japan)*, **11**, 294, 1953.

53. S. Nakoka, S. Nishio. J. Yamataya, "Silent discharge applied to photochemical synthesis of benzene hexachloride." Reports of the Research Laboratory Asahi. Glass Co.. **3**, 65, 1953.

54. D. N. Andreev, "Condensation of methylthrichlorosilane in the silent discharge," *Doklady Akad. Nauk. SSSR.*, **100**. 697, 1955.

55. D. N. Andreev, "Condensation of methylthrichlorosilane in a silent discharge," *Acad. Nauk. SSSR. Izv. Otel Khin Nauk.*, 7, 818, 1957.

56. M. Nishi, S. Hamamura. "Glow discharge through the vapors of benzene, toluene, and chlorobenzene," *Journal of Science Hiroshima University*, **23**, 201, 1959.

57. H. Schueler, M. Stockberger, "Dissociation processes of benzene and benzene derivatives in a corona discharge," *Z. Naturforsch.*, **14a**, 229, 1959.

58. D. N. Andreev, "Condensation of methyltrichlorosilane in a silent discharge," *Izvest. Akad. Nauk. SSSR. Odtel Khin Nauk.*, 273, 1960.

59. M. Nishi, S. Hamamura. "Emission spectra from the positive column in the glow discharge through the vapors of monohalogenbenzenes," *Journal of Science Hiroshima University Ser. A-II.* **25**. (1). 13, 1961.

60. H. Suhr, G. Rolle. B. Schrader, "Organic synthesis in discharge plasmas," *Naturw.*, **55**, (4), 160, 1962.

61. D. N. Andreev, V. B. Lyutyi, "Synthesis of phenyltrichlorosilane in a glow discharge," *Zh. Prikl. Khim.*, **36**, (9), 2096, 1963.

62. F. Swift, R. L. Sung. J. Doyle, J. K. Stille, "Reaction of carbon tetrachloride in a r-f glow discharge," *Journal of Organic Chemistry*, **30**, 3114, 1965.

63. C. E. Rix, "Reactions of halobenzenes in a r.f. glow discharge," *Dissertation Abstracts*, **27B**, 418. 1966.

64. J. K. Stille, C. E. Rix. "Reaction of halobenzene in a r.f. glow discharge," *Journal of Organic Chemistry*, **31**. 1591, 1966.

65. L. Tokarzewski. A. Dynarowicz. "The effect of silent discharge on vinyl chloride," *Roczniki Chem.*, **40**. 657. 1966.

66. N. L. Volodin. F. B. Vurzel, L. S. Polak, Y. I. Schmykov, P. N. Endyuskin, "Formation of acetylene and hydrogen chloride by the pyrolysis of chlorinated hydrocarbons in a plasma jet," *Khim. Vys Enrg.*, **5**, (4), 302, 1971.

67. J. E. Nicholas, A. I. Spiers, "Kinetics and mechanism in the decomposition of CCl_4 in a radio frequency pulse discharge," *Plasma Chemistry and Plasma Processing*, **5**, (3), 263-273, 1985.

68. T. Wakabayshi, "Decomposition of halogenated organic compounds by r.f. plasma at atmospheric pressure," presented at the 9th International Symposium on Plasma Chemistry, Pugnochiuso, Italy, September 4-9, 1989.

69. F.W. Breitbarth, S. Rottmayer, "Investigation of radical reactions in C_2Cl_4 and $C_2Cl_4O_2$ discharges by EPR, mass, and emission spectroscopy," *Plasma Chemistry and Plasma Processing*, **6**, (4), 381, 1986.

70. L. A. Rosocha, J. J. Coogan, "Processing of pollutants in dielectric-barrier plasma reactors," In Proceedings of the 12th International Symposium on Plasma Chemistry, vol. 2, edited by J. V. Heberlein, D. W. Ernie, J. T. Roberts, pp. 665-670, 1995.

71. I. Borger, J. Lachmann, B. G. Trusov, "Kinetical Modeling of Chemical Processes during conversion of chlorinated hydrocarbons in a thermal plasma," In Proceedings of the 12th International Symposium on Plasma Chemistry, vol. 2, edited by J. V. Heberlein, D. W. Ernie, J. T. Roberts, pp. 695-800, 1995.

72. B. Lerner, J. Biringham, R. Tonkyn, S. Barlow, T. Orlando, "Decomposition of trichloroethylene by a large scale, high flow packed-bed gas phase corona reactor," In Proceedings of the 12th International Symposium on Plasma Chemistry, vol. 2, edited by J. V. Heberlein, D. W. Ernie, J. T. Roberts, pp. 697-702, 1995.

73. G. Schultz, G. Birkhahn, I. Borger, J. Lachmann, "Decomposition of 1,1-dichloroethane in hydrogen by non-equilibrium rf plasma," In Proceedings of the 12th International Symposium on Plasma Chemistry, vol. 2, edited by J. V. Heberlein, D. W. Ernie, J. T. Roberts, pp. 1119-1124, 1995.

74. S. A. Vitale, K. Hadidi, D. Cohn, L. Bromberg, P. Falkos, "Electron Beam Generated Plasma Decomposition of 1,1,1-Trichloroethane," Submitted to *Plasma Chemistry and Plasma Processing*, August 1995.

75. K. J. Laidler, Chemical Kinetics, 3rd. Edition, Harper Collins Publisher, 1987, p. 18-20.

76. W. L. Miller, *Tran. R. Soc. Can.*, **11**, ser. 3, sec. 3, 245, 1908.

77. Alfa Catalog, Research Chemicals and Accessories, Johnson Matthey Catalog Company, Ward Hill, MA, 1993-1994.

78. L. G. Christoporou, Electron-Molecule Interactions and Their Applications, Volume 1, Academic Press, Inc., pp. 335-397, 478-569, 1984.

79. W. D. Chang, S. M. Senkan, Environmental Science and Technology, **23**, 442 (1989).

80. M. J. Thomson, B. S. Higgins, D. Lucas, C. P. Koshland and R. F. Sawyer, *Combustion and Flame*, **98**, 350 (1994).

81. Z. Jiang, P. H. Taylor and B. Dellinger, *J. Phys. Chem.*, **96**, 8961 (1992).

82. L. Nelson, I. Shanahan, H. W. Sidebottom, J. Treacy and O.J. Nielsen, *Int J of Chem Kinetics*, **22**, 577 (1990).

83. M. J. Thomson, D. Lucas, C. P. Koshland, R.F. Sawyer, Y. Wu and J. W. Bozzelli, *Combustion and Flame*. **98**, 155 (1994).

84. J. S. Chang and F. Kaufman, *J. Chem. Phys.*, **66**, 4989 (1977).

85. R. B. Barat and J. W. Bozzelli, *Environ Sci and Tech*, **23**, 666 (1989).

86. P. G. Blystone, M. D. Johnson, R. H. Werner, P. F. Daley, "Advanced Ultraviolet Flash Lamps for the Destruction of Organic Contaminants in Air," Chapter 18 in Emerging Technologies in Hazardous Waste Management III, edited by W. D. Tedder, F. G. Pohland, ACS, Washington D. C., 1993.

87. C. J. Howard, *Journal of Chemical Physics*, Vol. 65, No. 11, p. 4771-4777, (1976).

88. E. Sanhueza, I.C. Hisatsune, J. Heicklen, *Chemical Reviews*, 76:801 (1976).

89. J. R. Hollahan, A. T. Bell, Techniques and Applications of Plasma Chemistry, John Wiley and Sons, NY p. 29 (1974).

90. L. G. Christophorou, Atomic and Molecular Radiation Physics, Wiley-Interscience, p.483.

91. S. W. Benson, Thermochemical Kinetics, 2nd edition, John Wiley & Sons, 1976, pp.53-77.

92. R. C. Weast, Handbook of Chemistry and Physics, 57th edition, CRC Press, 1976, pp.F231-F240.

93. V. D. Knyazev, A. Bencsura, I. A. Dubinsky, D. Gutman, C. F. Melius, S. M. Senkan, "Kinetics and thermochemistry of the reaction of 1-chloroethyl radical with molecular oxygen," Journal of Physical Chemistry, **99**, pp.230-238 (1995).

94. J. Shi, T. J. Wallington, E. W. Kaiser, "FTIR product study of the Cl-initiated oxidation of C_2H_5Cl: reactions of the alkoxy radical CH_3CHClO," Journal of Physical Chemistry, **97**, pp.6184-6192, (1993).

95. C. Sotowa, Y. Korai, I. Mochida, K. Higuchi, "Coking phenomena in the pyrolysis of ethylene dichloride into vinyl chloride," *Preprints, Journal of Petroleum Chemistry*, pp.622-624, (1995).

96. Z. Jiang, P. H. Taylor, B. Dellinger, "Laser photolysis/laser-induced fluorescence studies of the reaction of OH with 1,1-dichloroethane over an extended temperature range," *Journal of Physical Chemistry*, **96**, pp.8964-8966, (1992).

97. K. Ramanathan, J. J. Spivey, "Catalytic oxidation of 1,1-dichloroethane," *Combustion Science and Technology*, **63**, pp. 247-255, (1989).

APPENDIX A: Derivation of INHIBIT model equation

A chemical kinetic method of arriving at a relation between electron beam dose and reactant concentration will be derived on the basis of an inhibitor species model in which other species in the plasma compete with the VOC molecules for the energy deposited by the electron beam.[5.74] The model assumes that chlorine and oxygen radicals formed in the plasma initiate the halogenated VOC decomposition reaction, and will be referred to as the VOC removal agent X_1. This reaction proceeds with rate constant k_1,

$$X_1 + T \rightarrow P_1 + X_2 \qquad\qquad k_1 \qquad\qquad (A.1)$$

where T represents a generic VOC, P_1 is some stable decomposition product, and X_2 is a byproduct. either a radical or a molecule. X_2 will further react with other VOC molecules, and thus enhance the decomposition rate,

$$X_2 + T \rightarrow P_2 \qquad\qquad k_2 \qquad\qquad (A.2)$$

or X_2 could be scavenged by some other species in the plasma, M, which could be an oxygen molecule or radical. or a decomposition product of the VOC,

$$X_2 + M \rightarrow P_3 \qquad\qquad k_3 \qquad\qquad (A.3)$$

The rate equations for reactions for species X_1. X_2. and T are given by,

$$\frac{d[T]}{dt} = -k_1 [X_1] [T] - k_2 [X_2][T] \qquad\qquad (A.4)$$

$$\frac{d[X_1]}{dt} = S - k_1 [X_1] [T] \qquad\qquad (A.5)$$

$$\frac{d[X_2]}{dt} = -k_1 [X_1][T] - k_2 [X_2][T] - k_3 [M][X_2] \qquad\qquad (A.6)$$

Where S is the X_1 formation rate. To solve these equations analytically, several assumptions must be made. First, it is assumed that the concentration initial VOC removal species X_1 is constant. This is probably a good assumption, since the initiating species is likely either oxygen radicals or electrons, both of which are present in great excess. Second. a pseudo-steady state assumption is placed on species X_2. This is common practice for a chemical kinetic analysis in which a transient species can be assumed to be in low concentration since it is removed by some mechanism very soon after it is formed. Finally the assumption is made that the inhibitor species concentration, [M]. is constant. With these assumptions, we have

$$0 = -k_1[X_1][T] - k_2[X_2][T] - k_3[M][X_2]$$

solving for X_2,

$$X_2 = \frac{k_1 X_1 T}{k_2 T + k_3 M}$$

substituting for X_2 in (A.5),

$$\frac{dT}{dt} = -k_1 X_1 \left[T \left(1 + \frac{k_2 T}{k_2 T + k_3 M} \right) \right]$$

separating variables,

$$\frac{k_2 T + k_3 M}{T(k_3 M + 2k_2 T)} dT = -k_1 x_1 dt$$

integrating this expression using the boundary condition $T = T_0$ when $t=0$. one obtains

$$\frac{T}{T_0} \sqrt{\frac{k_3 M + 2k_2 T_0}{k_3 M + 2k_2 T}} = \exp(-k_1 X_1 \cdot t$$

and defining,

$$K = \frac{k_3[M]}{2 \cdot k_2 \cdot [T_0]} = \text{constant}$$

the INHIBIT model equation is obtained.

$$\frac{[T]}{[T_0]} \cdot \sqrt{\frac{K+1}{K + [T]/[T_0]}} = \exp(-k_1[X_1] \cdot t) \qquad (A.7)$$

186

APPENDIX B: Derivation of the electron beam dose equation

The electron beam dose to the gas is defined as the energy depostied per unit mass of gas,

$$D = \frac{E}{m} \qquad (B.1)$$

or equivalently in dynamic units, the power depositied i the gas, divided by the mass flow rate.

$$D = \frac{P}{\dot{m}} \qquad (B.2)$$

The power deposited is equal to the energy deposited times electron beam curent which enters the chamber.

$$P = V \cdot I = \Delta E \cdot I \qquad (B.3)$$

The current which enters the chamber is equal to the measured current, minus the fraction which is intercepted by the copper plate due to beam spreading, and minus the current which is intercepted by the foil support structure,

$$I = I_o(1 - f_1 - f_2) = \tau \cdot \tau^* \cdot I_o \qquad (B.4)$$

where τ is the percentage of electrons which are not intercepted by the copper plate, and τ^* is the percentage of electrons which are not intercepted by the support grid.

The mass flow rate of the gas is difficult to measure, but assuming that the VOC is in low concentration. the mass flow rate of the gas is related to the volumetric flow rate through the density of air.

$$\dot{m} = \rho_c \dot{V} \qquad (B.5)$$

combining equations (B.2-B.5),

$$D = \frac{\Delta E \cdot \left(\tau \cdot \tau^* \cdot I_o\right)}{\rho_c \cdot \dot{V}} \qquad (B.6)$$

now using $\tau = 0.50$ and $\tau^* = 0.73$ as measured by Koch, with the density of air $\rho_c = 1.18$ kg/m^3.

$$D = 0.287 \cdot \frac{\Delta E \cdot (I_o)}{\dot{V}}$$

using the following conversions to get $\dot{V}$, I_o, and D in the desired units,

$$\dot{V}\left(\frac{m^3}{sec}\right) = \frac{1}{6 \times 10^7} \cdot \dot{V}\left(\frac{ml}{min}\right)$$

$$D\left(\frac{J}{kg\ air}\right) = 10^4 \cdot D(Mrad)$$

$$I_o\ (Amps) = 1000 \times I_o\ (mA)$$

one obtains.

$$D = 1.722 \times 10^6 \cdot \frac{\Delta E \cdot (I_o)}{\dot{V}} \qquad Mrad \qquad\qquad (B.7)$$

with $\Delta E\ [=]\ eV$, $I_o\ [=]\ mA$, and $\dot{V}\ [=]\ ml/min$

Now for the rectangular reaction chamber. Koch found that the average electron energy deposition. ΔE. was 17 keV. Using this in equation (B.7), one obtains the equation for the electron beam dose as a function of measured electron beam current and volumetric flow rate.

$$D = 3.14 \times 10^{10} \cdot \frac{\Delta E \cdot (I_o)}{\dot{V}} \qquad Mrad \qquad\qquad (B.8)$$

In the present study, the average energy deposition in the cylindrical reaction chamber was determined to be 18.8 keV, giving

$$D = 3.47 \times 10^{10} \cdot \frac{\Delta E \cdot (I_o)}{\dot{V}} \qquad Mrad \qquad\qquad (B.9)$$

APPENDIX C: Heats of reaction calculation

To determine the heats of reaction, ΔH_r, of the following reactions, one must know the heats of formation, ΔH_f, of each species.
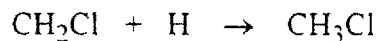
$$Cl + C_2H_5Cl \rightarrow CH_3Cl + CH_2Cl \qquad\qquad (C.1)$$

$$Cl + C_2H_3Cl \rightarrow CHCl_2CH_2 \qquad\qquad (C.2)$$

The following heats of formation are available in the literature:

$\Delta H_f (Cl) = 28.9$ kcal/mol[91]

$\Delta H_f (C_2H_5Cl) = -26.7$ kcal/mol[91]

$\Delta H_f (C_2H_3Cl) = 5.0$ kcal/mol[91]

to find $\Delta H_f (CH_2Cl)$, a radical species, the bond dissociation energy of $D(H\text{-}CH_2Cl)$ can be used,

$$CH_2Cl + H \rightarrow CH_3Cl$$

$$D(H\text{-}CH_2Cl) = \Delta H_f(H) + \Delta H_f(CH_2Cl) - \Delta H_f(CH_3Cl)$$

$\Delta H_f(H) = 52$ kcal/mol[92]

$\Delta H_f(CH_3Cl) = -19.6$ kcal/mol[92]

$D(H\text{-}CH_2Cl) = 100.9$ kcal/mol[92]

which gives,

$\Delta H_f(CH_2Cl) = 29.3$ kcal/mol

to find $\Delta H_f (CHCl_2CH_2)$, another radical species, Benson group additivity methods will be used.

$$\Delta H_f(CHCl_2CH_2) = \Delta H_f(C\bullet - (C)(H)_2) + \Delta H_f(C - (C\bullet)(H)(Cl)_2)$$

$$\Delta H_f\,(C\bullet - (C)(H)_2) \;=\; 35.82\ \text{kcal/mol}^{(91)}$$

$$\Delta H_f\,(C - (C\bullet)(H)(Cl)_2) \;\approx\; \Delta H_f\,(C - (C)(H)(Cl)_2) \;=\; -18.9\ \text{kcal/mol}^{(91)}$$

which gives,

$$\Delta H_f\,(CHCl_2CH_2) \;=\; 16.92\ \text{kcal/mol}$$

The heats of reaction can now be calculated,

$$\Delta H_{r1} \;=\; \Delta H_f\,(CH_3Cl) \;+\; \Delta H_f\,(CH_2Cl) \;-\; \Delta H_f\,(Cl) \;-\; \Delta H_f\,(C_2H_5Cl) \;=\; 5.8\ \text{kcal/mol}$$

$$\Delta H_{r2} \;=\; \Delta H_f\,(CHCl_2CH_2) \;-\; \Delta H_f\,(Cl) \;-\; \Delta H_f\,(C_2H_3Cl) \;=\; -17.08\ \text{kcal/mol}$$